frontiers | Research Topics

Application of innovative techniques in genetic and cellular therapies

Edited by
Yuan Xiong, Jingfeng Li and Yori Endo

Published in
Frontiers in Bioengineering and Biotechnology

ISSN 1664-8714
ISBN 978-2-8325-3650-6
DOI 10.3389/978-2-8325-3650-6

About Frontiers

Frontiers is more than just an open access publisher of scholarly articles: it is a pioneering approach to the world of academia, radically improving the way scholarly research is managed. The grand vision of Frontiers is a world where all people have an equal opportunity to seek, share and generate knowledge. Frontiers provides immediate and permanent online open access to all its publications, but this alone is not enough to realize our grand goals.

Frontiers journal series

The Frontiers journal series is a multi-tier and interdisciplinary set of open-access, online journals, promising a paradigm shift from the current review, selection and dissemination processes in academic publishing. All Frontiers journals are driven by researchers for researchers; therefore, they constitute a service to the scholarly community. At the same time, the *Frontiers journal series* operates on a revolutionary invention, the tiered publishing system, initially addressing specific communities of scholars, and gradually climbing up to broader public understanding, thus serving the interests of the lay society, too.

Dedication to quality

Each Frontiers article is a landmark of the highest quality, thanks to genuinely collaborative interactions between authors and review editors, who include some of the world's best academicians. Research must be certified by peers before entering a stream of knowledge that may eventually reach the public - and shape society; therefore, Frontiers only applies the most rigorous and unbiased reviews. Frontiers revolutionizes research publishing by freely delivering the most outstanding research, evaluated with no bias from both the academic and social point of view. By applying the most advanced information technologies, Frontiers is catapulting scholarly publishing into a new generation.

What are Frontiers Research Topics?

Frontiers Research Topics are very popular trademarks of the *Frontiers journals series*: they are collections of at least ten articles, all centered on a particular subject. With their unique mix of varied contributions from Original Research to Review Articles, Frontiers Research Topics unify the most influential researchers, the latest key findings and historical advances in a hot research area.

Find out more on how to host your own Frontiers Research Topic or contribute to one as an author by contacting the Frontiers editorial office: frontiersin.org/about/contact

Application of innovative techniques in genetic and cellular therapies

Topic editors

Yuan Xiong — Huazhong University of Science and Technology, China

Jingfeng Li — Wuhan University, China

Yori Endo — Brigham and Women's Hospital, Harvard Medical School, United States

Citation

Xiong, Y., Li, J., Endo, Y., eds. (2023). *Application of innovative techniques in genetic and cellular therapies*. Lausanne: Frontiers Media SA.

doi: 10.3389/978-2-8325-3650-6

Table of contents

frontiers | Frontiers in Bioengineering and Biotechnology

TYPE Editorial
PUBLISHED 14 December 2023
DOI 10.3389/fbioe.2023.1336900

OPEN ACCESS

EDITED AND REVIEWED BY
Andrea Banfi,
University of Basel, Switzerland

*CORRESPONDENCE
Yori Endo,
yoriendo1010@gmail.com

RECEIVED 11 November 2023
ACCEPTED 08 December 2023
PUBLISHED 14 December 2023

CITATION
Endo Y (2023), Editorial: Application of innovative techniques in genetic and cellular therapies.
Front. Bioeng. Biotechnol. 11:1336900.
doi: 10.3389/fbioe.2023.1336900

Editorial: Application of innovative techniques in genetic and cellular therapies

Yori Endo*

Brigham and Women's Hospital, Harvard Medical School, Boston, MA, United States

KEYWORDS

cell therapy, gene therapy, exosome, miRNA, degenerative diseases

Editorial on the Research Topic
Application of innovative techniques in genetic and cellular therapies

Cellular and gene therapies aim to restore or enhance cellular functionalities lost in disease or injuries. Cellular therapies, however are limited by both practical and legislative challenges. The current Research Topic covers some of the alternative avenues, such as the use of exosome as a surrogate for cellular autocrine/paracrine functions and how they may replace, supplement or even supplant cellular therapies in some aspects. It also explores various methods for improving targeted deliveries of drugs/nucleic acids beyond the use of viral vectors such as engineered exosomes and electroporation.

Cellular therapies have become one of the most explored avenues for treating degenerative diseases and injuries in the past few years. For some cases, cell transplantation is the only feasible alternative to tissue grafting or replacement, mitigation of which is desired for a number of reasons, including a requirement for invasive surgeries, donor site morbidities, and complications. Transplantation of cells allows harnessing of their functions, particularly that of regenerative functions. Their ability to respond to the environment at the transplant site through differentiation, release of factors etc., give them unique advantages during the whole course of regeneration (Sánchez et al., 2012; El-Kadiry et al., 2021). Poor cell survival, however, has been a major obstacle in achieving sufficient regenerative outcomes. In addition, the status of the cells at the time of transplantation seems to alter the cellular behavior post-transplantation and the subsequent clinical outcomes. Much of the recent innovation has therefore focused on the process of "priming." In the context of priming, the induction of cellular quiescence has gained much attention due to its close relationship with the regenerative capacity of cells. Indeed, finding the appropriate method of inducing quiescence in progenitor cells has made a significant difference to the regenerative outcomes in skeletal muscle injuries (Xie et al., 2018; Endo et al., 2023). Similarly, Chen et al. described how quiescence preconditioning augmented the proliferation of the transplanted nucleus pulposus stem cells and improved the overall intervertebral disc regeneration. Priming, particularly the induction of quiescence, seems to be an innovative and effective method for maximizing the attainable regenerative functions in cellular therapies and therefore deserves continued research interest.

Exosome-based therapies are an attractive alternative to transplanting whole cells. Exosomes isolated from cells can perform some aspects of the complex paracrine/endocrine functions of the cells of origin, thus acting as their functional surrogates. The

use of exosome has some potential commercial and clinical advantages, namely scalability, stability, (less) immunogenicity and accessibility to certain tissues across physiological barriers. In this Issue, Wang et al. reviewed recent findings showing that exosomes derived from different cell types found in bones perform unique functions by regulating gene expressions of the recipient cells, and suggested a potential therapeutic method based on selective utilization of such exosome for treating metabolic disorders of the bones.

Another innovative approach is to engineer exosomes as a vehicle for targeted delivery of various therapeutic agents, such as drugs and nucleic acids. One of the challenges that has prevented wider clinical applications of (natural) exosome has been their poor targeting ability. In this Issue, Jin et al. summarize some of the recently developed methods that allow exosomes delivery to specific targets that may otherwise be unreachable. Linking of exosomes with an anti-GAP43 monoclonal antibody or glycation end-products (RAGE)-binding-peptide allowed successful delivery of drugs or oligonucleotides to the brain in ischemic stroke treatment. The use of engineered exosomes may therefore become one of the optimal options in cases where tissue accessibility through physiological barriers and superior stability are necessary.

Similarly, the use of viral vector can achieve excellent topology and specificity for drug/nucleic acid deliveries. One exemplary such use explored in this Issue is for the delivery of miRNA inhibitors to regulate a group of gene expressions and subsequently the target cell activities. Wang et al. reported improved bone metabolism and slowed osteoporosis progression using adeno-associated virus expressing a miRNA-214 inhibitor. There is a strong collective evidence indicating efficacy of viral vectors. However, there remains a need for improved production efficiency for larger scale production in order to widen its clinical applications. Heuvel et al. argue that production of stable viral packaging cell suspensions holds the key to this. Their findings strongly indicate that the use of transposon-encoding mRNA is superior to plasmid-based transposase, and that this strategy should help establish virus VPCs producing vectors with a broadened host cell range. The use of virus as a vaccine platform is another innovative avenue explored and exploited in particular with an effort to combat COVID-19, including Alkayyal et al. The VSVΔ51M oncolytic virus platform was repurposed to express the SARS-CoV-2 spike receptor-binding domain antigen, and successfully induced a humoral immune response in mice.

While others looked into developing biological vectors, there is a branch of research that is looking into physical methodologies to achieve localized drug/nucleic acid delivery. Electroporation is a method used for permeabilization of plasma membranes of biological cells, and its use is now is being explored for targeted drug/DNA delivery into living cells. Gene electro-transfer allows for delivery of DNA encoding therapeutic transgenes and its use is tested in cancer therapies and infectious diseases vaccines (Heller and Heller, 2015). While it is an attractive method with many practical advantages, Malyško-Ptašinskė et al. argue that establishment of optimal pulsing protocols is still necessary, and the treatment planning steps should include simulation of spatial electric field distribution and possible thermal effects.

In parallel with the development of delivery methods for drugs and nucleic acids, much effort has been made in discoveries of novel therapeutic targets for the treatment of degenerative conditions. The regulation of RNA modifications has attracted much research interest in the recent years as a potential therapeutic target for treating various conditions. In particular, m6A methylation has been extensively studied as it is the most common post-transcriptional modification of eukaryotic mRNAs and long non-coding RNAs. The exact roles of this particular RNA methylation in various physiological and pathological conditions seem complex, and a better understanding would most certainly benefit pioneering of a novel therapeutic avenue. In this Issue, Luo et al. and Wen et al. explored the roles of m6A methylation in wound healing and bone and intervertebral disc degeneration (IVDD), respectively. While both described that RNA methylation is a major regulatory pathway of cellular processes such as autophagy/apoptosis and proliferation, the effects reported are contradictory, highlighting the need for further research to establish viable therapeutic strategies. Aside from RNA modification, Wei et al., explained the roles of inflammatory and oxidative responses in IVDD pathogenesis and described the potential therapeutic values of anti-oxidant and anti-inflammatory therapies. While these avenues provide some promising prospects in developing novel therapies for IVDD, it was concluded that there has been too little evidence yet for comprehensive understanding of their therapeutic values. PI3K/AKT pathway regulates broad physiological and pathological processes, and Guo et al. suggest that its regulation may be an important factor in the development acute compartment syndrome that commonly occurs following severe fractures.

Author contributions

YE: Writing–original draft.

Funding

The author(s) declare that no financial support was received for the research, authorship, and/or publication of this article.

Conflict of interest

The author declares that the research was conducted in the absence of any commercial or financial relationships that could be construed as a potential conflict of interest.

Publisher's note

References

El-Kadiry, A. E., Rafei, M., and Shammaa, R. (2021). Cell therapy: types, regulation, and clinical benefits. *Front. Med. (Lausanne)* 8, 756029. PMID: 34881261; PMCID: PMC8645794. doi:10.3389/fmed.2021.756029

Endo, Y., Zhu, C., Giunta, E., Guo, C., Koh, D. J., and Sinha, I. (2023). The role of hypoxia and hypoxia signaling in skeletal muscle physiology. *Adv. Biol.*, e2200300. Advance online publication. doi:10.1002/adbi.202200300

Heller, R., and Heller, L. C. (2015). Gene electrotransfer clinical trials. *Adv. Genet.* 89, 235–262. Epub 2014 Dec 4. PMID: 25620013. doi:10.1016/bs.adgen.2014.10.006

Sánchez, A., Schimmang, T., and García-Sancho, J. (2012). Cell and tissue therapy in regenerative medicine. *Adv. Exp. Med. Biol.* 741, 89–102. PMID: 22457105. doi:10.1007/978-1-4614-2098-9_7

Xie, L., Yin, A., Nichenko, A. S., Beedle, A. M., Call, J. A., and Yin, H. (2018). Transient HIF2A inhibition promotes satellite cell proliferation and muscle regeneration. *J. Clin. Investigation* 128, 2339–2355. doi:10.1172/JCI96208

frontiers | Frontiers in Bioengineering and Biotechnology

TYPE Review
PUBLISHED 22 July 2022
DOI 10.3389/fbioe.2022.953916

OPEN ACCESS

EDITED BY
Yuan Xiong,
Huazhong University of Science and Technology, China

REVIEWED BY
Zeming Liu,
Huazhong University of Science and Technology, China
Yan Xu,
Huazhong University of Science and Technology, China

*CORRESPONDENCE
Bo Gao,
gaobofmmu@hotmail.com
Lingli Zhang,
lingliwdc@163.com

SPECIALTY SECTION
This article was submitted to Preclinical Cell and Gene Therapy, a section of the journal Frontiers in Bioengineering and Biotechnology

RECEIVED 26 May 2022
ACCEPTED 29 June 2022
PUBLISHED 22 July 2022

CITATION
Wang Z, Zhao Z, Gao B and Zhang L (2022), Exosome mediated biological functions within skeletal microenvironment. *Front. Bioeng. Biotechnol.* 10:953916. doi: 10.3389/fbioe.2022.953916

Exosome mediated biological functions within skeletal microenvironment

Zhikun Wang[1], Zhonghan Zhao[1], Bo Gao[2]* and Lingli Zhang[3]*

[1]School of Kinesiology, Shanghai University of Sport, Shanghai, China, [2]Institute of Orthopedic Surgery, Xijing Hospital, Fourth Military Medical University, Xi'an, China, [3]College of Athletic Performance, Shanghai University of Sport, Shanghai, China

Exosomes are membranous lipid vesicles fused with intracellular multicellular bodies that are released into the extracellular environment. They contain bioactive substances, including proteins, RNAs, lipids, and cytokine receptors. Exosomes in the skeletal microenvironment are derived from a variety of cells such as bone marrow mesenchymal stem cells (BMSCs), osteoblasts, osteoclasts, and osteocytes. Their biological function is key in paracrine or endocrine signaling. Exosomes play a role in bone remodeling by regulating cell proliferation and differentiation. Genetic engineering technology combined with exosome-based drug delivery can therapy bone metabolic diseases. In this review, we summarized the pathways of exosomes derived from different skeletal cells (i.e., BMSCs, osteoblasts, osteocytes, and osteoclasts) regulate the skeletal microenvironment through proteins, mRNAs, and non-coding RNAs. By exploring the role of exosomes in the skeletal microenvironment, we provide a theoretical basis for the clinical treatment of bone-related metabolic diseases, which may lay the foundation to improve bone tumor microenvironments, alleviate drug resistance in patients.

KEYWORDS

skeletal related exosomes, bone marrow mesenchymal stem cell, osteoblast, osteoclast, skeletal microenvironment, osteocyte

1 Introduction

Although seemingly simple and inert, bones are surprisingly complex and busy tissue. It has been found that abnormal proliferation and differentiation of bone marrow mesenchymal stem cells (BMSCs), osteoblasts, osteocytes and osteoclasts can lead to a variety of bone diseases such as osteoporosis, osteoarthritis, spinal tuberculosis, bone tumors, and osteosclerosis (Zhou et al., 2019). Osteoporosis is a common systemic metabolic bone disease in the elderly, mainly characterized by decreased bone mass, increased bone fragility and bone microstructure destruction (Johnston and Dagar, 2020). Osteoarthritis is the most common chronic degenerative joint disease and a leading cause of pain and disability. The incidence of the disease grows as people age, and its prevalence is steadily increasing and is projected to become the largest cause of disability by 2030 (Cross et al., 2014). The main pathological feature of spinal tuberculosis is progressive

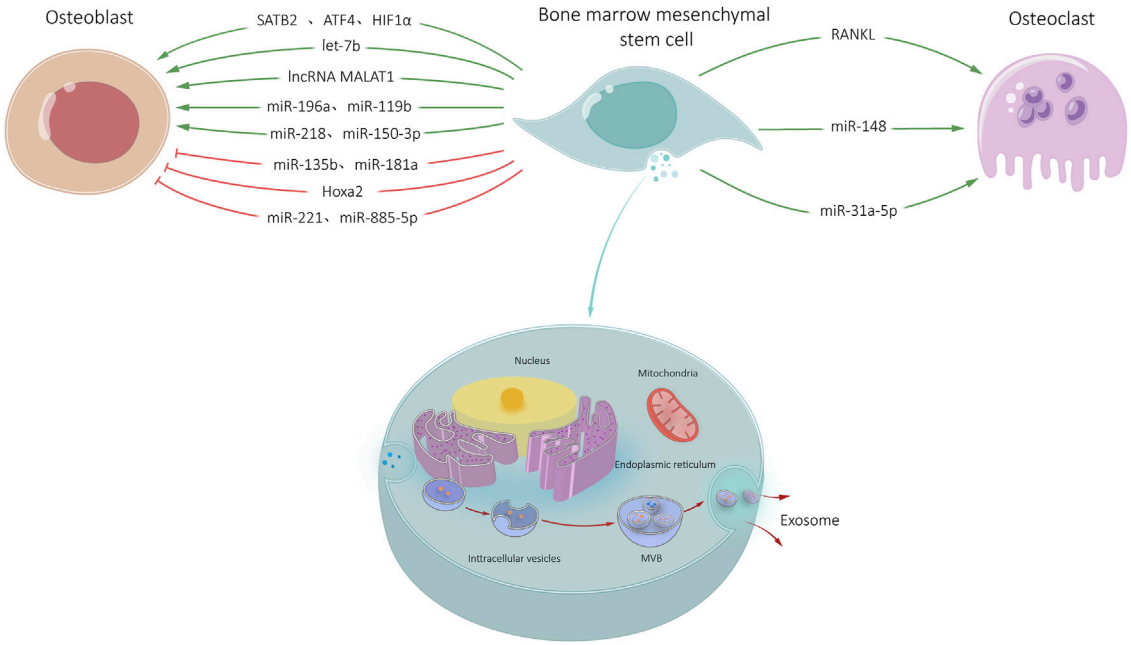

FIGURE 1
BMSC-Exos-mediated communication within the skeletal micro-environment. BMSC-Exos promoted osteoblast differentiation by SATB2, ATF4, HIF1α, let-7b, lncRNA MALAT1, and miRNAs (i.e., miR-196a, miR-119b, miR-218, miR-150-3p). BMSC-Exos inhibitied osteogenic differentiation through miR-135b, miR-181a, Hoax2, miR-221, and miR-885-5p. BMSC-Exos promoted osteoclast differentiation through RANKL, miR-148, and miR-31a-59.

bone destruction. The prevalence rate of spinal tuberculosis is the number one in all bone and joint tuberculosis. Bone is one of the most common sites of systemic metastases, accounting for 15–20% of metastatic tumors. Spinal metastases occur in approximately 36% of patients who die of malignancy, while primary bone and soft tissue tumors account for 2–3% of systemic tumors. Malignant bone tumors can either originate from other tissues or organs in the body and metastasize to the bone or directly invade the bone through blood circulation and lymphatic system. Malignant bone tumors develop rapidly with high mortality (Lambert et al., 2017; Chen et al., 2021). Rickets is a metabolic bone disease in children characterized by the failure to mineralize growth plates and an osteoid matrix (Munns et al., 2016). Osteosclerosis is complications of myeloproliferative tumors. These diseases lead to excessive growth of bone trabeculae and collagen fibers that replace hematopoietic cells, resulting in abnormal bone marrow function (Mankar et al., 2020). Bone disorders are caused by congenital or acquired factors that destroy and interfere with normal bone metabolism and biochemical status, resulting in bone biochemical metabolism disorders. To meet the clinical needs of orthopedic diseases, exosomes become a new therapeutic strategy.

Current treatments for bone-related metabolic diseases are limited by poor therapeutic effects, adverse events, failure to improve bone absorption, abnormal bone growth and mineral deposition, and difficulty in reversing the bone disease (Tsai et al., 2019). Stem cell transplantation for osteoporosis treatment has shown preliminary feasibility and efficacy results in mice models; however, there were issues with immune rejection, increased risk of cell malignancy, and stem cell homing limit the adoption of such treatment (Aghebati-Maleki et al., 2019). Therefore, it is necessary to find a targeted treatment for bone metabolic diseases that can minimize the potential harm caused by long-term drug exposure.

Exosomes are nanoscale vesicle particles secreted by cells, which have biological activities similar to those of the source cells and play an important role in intercellular communication (Tkach and Thery, 2016). Studies have found that exosomes derived from skeletal cells participate in skeletal cell proliferation and differentiation (Chen et al., 2017; Song et al., 2019; Xie et al., 2020). Exosomes have high stability, no immunogenicity and strong targeting ability, which make up for the deficiency of traditional drugs and stem cell therapy. A variety of inclusions carried by exosomes can directly act on these skeletal cells. Therefore, the study on the involvement of exosomes derived from various skeletal cells in the regulation of skeletal cell proliferation and differentiation can provide a theoretical basis for the study of bone diseases, and has certain clinical significance for the diagnosis and treatment of bone diseases.

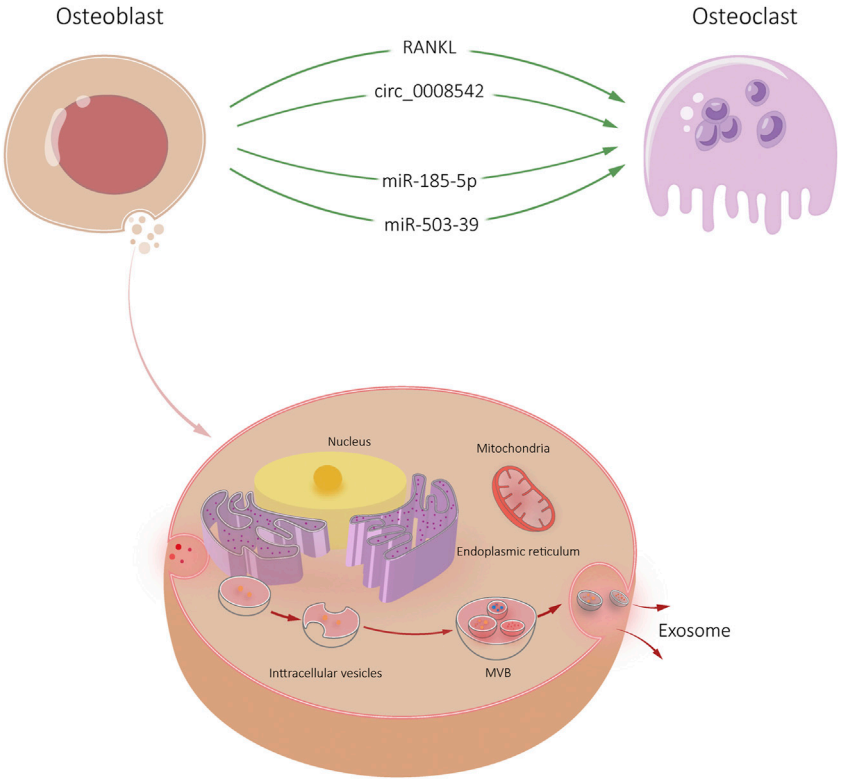

FIGURE 2
Osteoblast-Exos-mediated communication within the skeletal micro-environment. Osteoblast-Exos promoted osteoclast differentiation by RANKL, circ_0008542, miR-185-5p, and miR-503-39.

2 Characteristics of skeleton-derived exosomes

Exosome is a vesicle with a double-layer lipid membrane structure. It is spherical or cup-shaped, with a diameter of about 40–100 nm and a density of about 1.13–1.21 g/ml (Tkach and Thery, 2016). Exosome contains nucleic acids, which regulate physiological and pathological processes (Zhang et al., 2015; Tkach and Thery, 2016). Non-specific expression proteins found in the exosomes can be used as the protein marker to identify exosomes, including heat shock protein, tumor susceptibility gene101 (TSG101), four-molecule cross-linked transmembrane protein superfamily (CD9, CD63, CD81, CD82), and ALG-2-interacting protein (Alix) (Tkach and Thery, 2016). Moreover, some specific expression proteins are cell-derived and related to cell signal transduction (Zhong et al., 2021).

Exosome play a key role in paracrine or endocrine signaling. The proteins, lipids and nucleic acids contained inside the exosomes have specific biological functions. Exosome transmits information acts on target cells by either targeting cells *via* their receptors (Mathivanan et al., 2010) or entering the target cell *via* endocytosis. The exosomes carry proteins, lipids and nucleic acids into the target cell and activate relevant signaling pathways (Mathivanan et al., 2010).

Exosome are involved in cell proliferation and differentiation, therefore play an important role in bone tissue engineering. The composition of bone-derived exosomes differs from exosomes originated from other sources. During bone reconstruction, bone-derived exosomes may release proteins involved in bone formation, such as alkaline protease (ALP), bone morphogenetic protein (BMP), eukaryotic translation initiation factor2 (elF2), osteopontin (OPN), bone sialoprotein (BSP), and osteocalcin (OCN). Bone-derived exosomes also contain osteoclast differentiation-related proteins such as the receptor activator of nuclear factor κB–ligand (RANKL) and RANK (Huynh et al., 2016). In addition, microRNAs (miRNAs)-related to bone remodeling, such as miR-24, let-7, miR-143-3p, miR-10b-5p, miR-199b, miR-218, and miR-214-3p were also found in bone-derived exosomes (Huynh et al., 2016; Li et al., 2016). These miRNAs have a crucial role in bone formation and resorption. Bone-associated exosomes can selectively transport specific information, depending on the proteins or factors within the exosomes. Pathological conditions, such as inflammation, hypoxia, and pH changes (Deng et al., 2017), can affect exosome release.

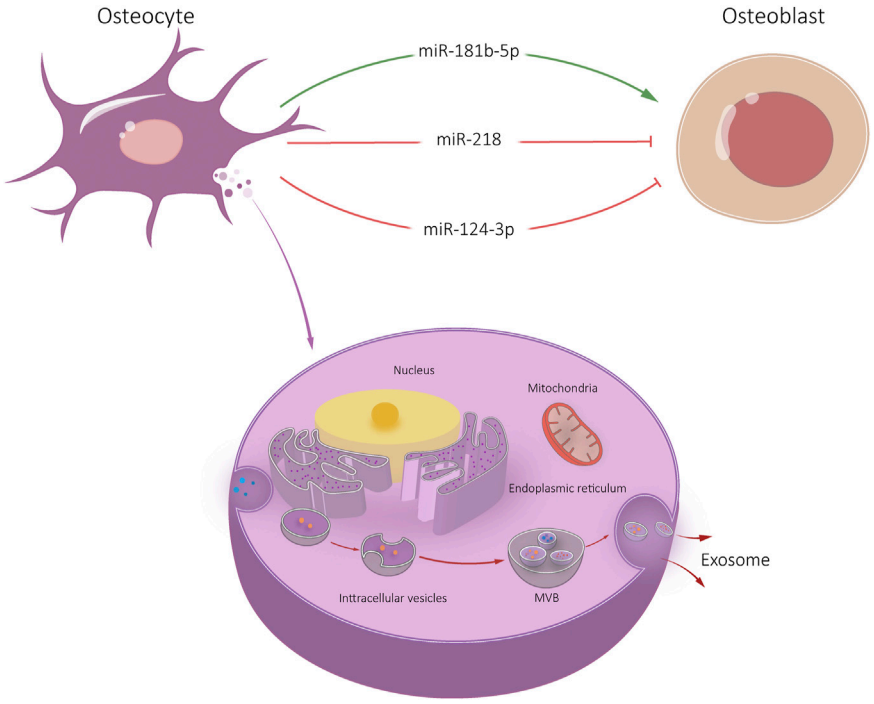

FIGURE 3
Osteocyte-Exos-mediated communication within the skeletal micro-environment. Osteocyte-Exos promoted osteoblast differentiation through miR-181b-5p, and inhibited osteoblast differentiation through miR-218 and miR-124-3p.

3 BMSC-Exos-mediated communication within the skeletal micro-environment

BMSCs are stem cells derived from the mesoderm that play an important role in bone regeneration and repair. They also have paracrinal function (Eirin et al., 2017). We previously introduced the characteristics and functions of exosomes derived from BMSC (BMSC-Exos) in detail (Wang Z. et al., 2021). BMSC-Exos enter target cells through endocytosis and plays a bioactive role, showing tissue repair ability similar to BMSCs (van der Pol et al., 2012). Moreover, due to its low immunogenicity and low cellular activity, it is safer than transplantation of stem cells (Liu et al., 2015).

3.1 Effects of BMSC-Exos on osteoblasts

Osteoblasts are functional cells that secrete bioactive substances regulating bone formation and remodeling. To detect the effect of BMSC-Exos on osteoblast proliferation, the proliferation curves of osteoblasts stimulated by different concentrations of BMSC-Exos were plotted. Osteoblast proliferation rates were significantly increased after BMSC-Exos were added and were proportional to the concentration of BMSC-Exos (Zhang et al., 2021). These results suggest that BMSC-Exos effectively promote osteoblast proliferation in a dose- and time-dependent manner.

Early differentiation of BMSC into osteoblasts, and mature osteoblasts undergo further mineralization, are both important evaluation indicators of osteogenic differentiation. ALP activity is a marker of early differentiation in osteoblasts (Osugi et al., 2012). OCN is essential in regulating bone conversion and mineralization, and often used as a marker of bone formation in late stage (Tsao et al., 2017). Both runt-related transcription factor 2 (Runx2) and osterix (OSX) are important transcription factors in osteoblast differentiation and control the expression of bone-related genes such as OPN, BSP, and OCN (Okamura et al., 2013). BMSC-Exos up-regulates the expression of Runx2, OSX, OCN and other osteogenic genes (Yang et al., 2013; Tsao et al., 2017).

3.1.1 Effects of BMSC-Exos on osteoblasts by protein

The expression of DNA-binding protein SATB2 (SATB2) in osteoblasts is beneficial for osteoblast differentiation (Gong et al., 2014). Wang et al. (Yang et al., 2019) treated osteoblasts with BMSC-Exos. It was found that the protein expression of SATB2 and cyclic AMP-dependent transcription factor 4 (ATF4) increased significantly. However, the expression of

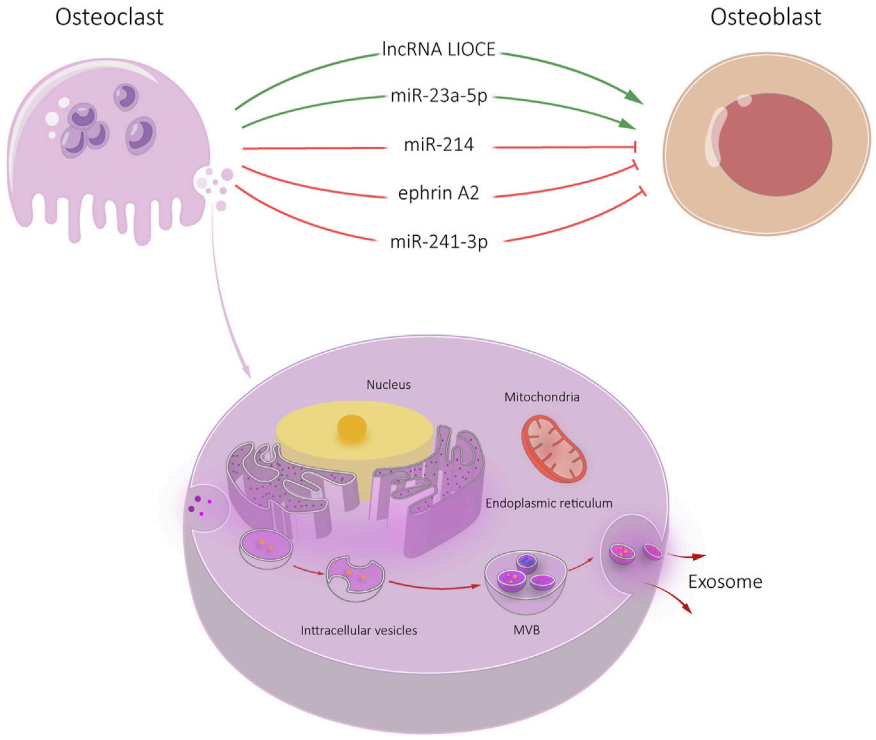

FIGURE 4
Osteoclast-Exos-mediated communication within the skeletal micro-environment. Osteoclast-Exos promoted osteoblast differentiation by lncRNA LIOCE and miR-23a-5p, and inhibited osteoblast activity by miR-214, ephrin A2 and miR-241-3p.

homeobox protein Hox-A2 (Hoxa2) was significantly decreased. The results showed that the changes in the expression of these proteins promoted osteoblast differentiation and bone regeneration. In a study on the effect of hypoxia-inducible factor 1α in BMSC-Exos (BMSC-Exos-HIF1α) on repairing critical bone defects in rats, it was found that BMSC-Exos-HIF1α stimulated osteogenic proliferation and differentiation of BMSCs (Ying et al., 2020). The combination of BMSC-Exos-HIF1α and beta-tricalcium phosphate (β-TCP) artificial bone can repair bone defects by promoting new bone regeneration and new blood vessel formation (Ying et al., 2020).

In summary, BMSC-Exos affects osteogenic differentiation and proliferation by targeting osteoblast delivery of carried proteins.

3.1.2 Effects of BMSC-Exos on osteoblasts by non-coding RNA

MiRNA regulates about one third of the protein coding genes in human body, which has attracted extensive attention in terms of molecular regulation of gene expression (Zhang et al., 2015). The proportion of miRNA in exosomes is higher than that in metrocyte. Exosomes regulate osteoblast proliferation through miRNA, and affect mRNA expression. MiRNA-mediated dysregulation is an important pathological factor in osteoporosis and other bone related diseases (Wei et al., 2021).

In recent years, exosomes have been found to play an important role in regulating BMSCs osteogenic differentiation through miRNA. Xu et al. (2014) studied miRNA expression profiles in exosomes during BMSCs osteogenic differentiation and found that nine miRNAs significantly increased in BMSC-Exos, including let-7a, miR-218, miR-199b, miR-135b, miR-148a, miR-203, miR-299-5p, miR-302b and miR-219, etc. MiRNAs were found in exosomes during BMSC osteogenic differentiation. MiR-199b may regulate osteoblast differentiation through Runx2. Let-7b enhances osteogenesis and bone formation by regulating high mobility group protein A2, while inhibiting adipogenesis in human mesenchymal stem cells (hMSCs). MiR-218 promotes osteogenic differentiation of human adipose-derived mesenchymal stem cells through Wnt/β-catenin signaling pathway. MiR-135b regulates the mineralization of human stem cell osteogenic differentiation, which is up-regulated by impaired osteogenic differentiation of mesenchymal stem cells (MSCs) derived from multiple myeloma patients (Xu et al., 2014). Therefore, these results may indicate that exosomes miRNAs play a regulatory role in osteogenic differentiation through networking with cellular signaling pathways. Xu et al. (2014) also found that miR-221, miR-155,

miR-885-5p, miR-181A and miR-320c were significantly decreased in the expression of BMSC-Exos. Down-regulation of miR-221 may lead to osteogenic differentiation of hMSCs. MiR-885-5p and miR-181a inhibited osteoblast differentiation Runx2 and TβR-I/Alk5, respectively. Therefore, down-regulation of miR-885-5p and miR-181a can promote the proliferation and activation of osteoblasts, thus becoming negative regulators of BMSCs osteogenic differentiation (Bhushan et al., 2013). In animal experiments, miR-196a enriched in BMSC-Exos promoted bone formation in Sprague-Dawley rats (SD rats) with skull defects (Qin et al., 2016). This study provides new directions for the research and treatment of exosomes secreted by BMSCs in the field of bone related diseases in the future.

Long non-coding RNA (lncRNA) is important in regulating various cellular physiological activities such as cell proliferation, differentiation, maturation and apoptosis. Yang et al. (2019) found that lncRNA Metastasis associated lung adenocarcinoma transcript 1 (MALAT1) in BMSC-Exos can be transferred to osteoblasts. Moreover, transfer-related lncRNA MALAT1 up-regulates the expression of SATB2 in osteoblasts by sponging miR-34c, thus regulating osteoblast differentiation.

Circular RNA (circRNA) was discovered in plant viruses in 1976 and has been considered as a byproduct of transcription without any other biological functions. However in recent years, circRNA has been found to widely exist in the cytoplasm of different organisms with high stability and play an important role in eukaryotic cells (Danan et al., 2012). In malignant tumors, circRNA binds to corresponding miRNA through miRNA response elements and inhibits gene expression, thus affecting the tumor development (Alimirzaie et al., 2019). However, there have been no reports on circRNA in BMSC-Exos for osteoblasts, suggesting a potential area for future research (Figure 1).

3.2 Effects of BMSC-Exos on osteoclasts

Osteoclasts are closely related to bone resorption and are mainly differentiated from macrophages and peripheral monocytes under the combined stimulation of multiple signaling factors. Exosomes are an important regulator of paracrine secretion of osteoclasts. RANKL plays a key role in osteoclast differentiation. RANK is abundantly expressed by exosomes in osteoclasts (Xu et al., 2018) and binds to RANKL to competitively inhibits the RANK pathway.

MiR-148a and miR-31a-5p in BMSC-Exos play an important role in osteoclast differentiation. MiR-148a promotes osteoclast differentiation by controlling transcription factor MAFB (MAFB) (Cheng et al., 2013). MiR-31a-5p regulates osteogenic differentiation of BMSCs and inhibits transforming protein RhoA (RhoA) expression by binding non-coding regions. MiR-31a-5p has been found to target regulatory coupling points between osteoclasts and osteoblasts (Xu et al., 2018). Inhibiting miR-31a-5p reduces bone resorption in osteoclasts, while enhancing bone structure (Xu et al., 2018). Therefore, inhibiting miR-31a-5p can alleviate bone metabolism imbalance in osteoporosis. However, no detailed reports have been reported on the regulation of lncRNA and circRNA in BMSC-Exos on osteoclasts. In a word, the results demonstrate the efficiency of BMSC-Exos in targeting osteoclasts to regulate bone resorption to promote bone regeneration, providing a novel approach for the treatment of osteoporosis (Figure 1).

4 Osteoblast-Exos-mediated communication within the skeletal micro-environment

BMSCs can differentiate and mineralize osteoblasts (MOB). BMSCs differentiate into bone progenitor cells, osteoblast precursors, and then form osteoblasts. Osteoblasts migrate to the absorbed site and secrete bone matrix. The bone matrix then mineralizes to form new bone. However, the role of MOBs in regulating MSCs remains unclear.

4.1 Effect of osteoblast-Exos on BMSCs

Exosome mRTNA translation into functional proteins control the fate of BMSCs. BMSCs co-cultured with MOB showed increased osteogenic ability *in vitro*, indicating the presence of soluble osteogenic factors released by MOB (Heino et al., 2004; Csaki et al., 2009; Birmingham et al., 2012; Tsai et al., 2012). In permineralized osteoblast cell line MC3T3-E1, exosomes promote the differentiation of BMSCs into osteoblasts (Cui et al., 2016). The activation of wnt/β-catenin signaling pathway promotes bone differentiation of mouse BMSCs. Exosomes isolated from osteoblasts contain key transcription factors involved in osteogenesis (Runx2 and OSX) (Narayanan et al., 2018). Extracellular matrix (ECM)-mediated BMSCs differentiation is enhanced by specific transcription factors and miRNA in osteoblast-Exos (Narayanan et al., 2018). SiRNA-mediated Runx2 knockdown further confirms the importance of exosomes RNA in lineage specific promoter activation (Mishima et al., 2021).

4.2 Effect of osteoblast-Exos on osteoclasts

Spinal tuberculosis is the main pathological feature of progressive bone destruction, and has the highest incidence rate in osteoarticular tuberculosis (Khanna and Sabharwal, 2019). Abnormal proliferation and activation of osteoclasts in spinal tuberculosis trigger pathological bone destruction.

Osteoblasts and osteoclasts work together to promote the healthy bone growth.

The bone (reconstruction) model is characterized by alternating stages of osteoclast destruction and osteoblast formation (Ducy et al., 2000). Bone is constantly renewing itself through remodeling, a coordinated system in which osteoclasts absorb equal amounts of ECM and are deposited by osteoblasts (Wei and Ducy, 2010). Under normal circumstances, osteoblasts form new bone and osteoclasts absorb old bone. In the skeletal microenvironment, osteoblasts and osteoclasts interact with each other through cytokines, chemical transmitters, and cell contact (Tamma and Zallone, 2012; Yuan et al., 2018). Osteoblasts and osteoclasts maintain a dynamic balance to ensure the healthy bone growth (Chen et al., 2018). In pathological conditions, this dynamic balance is disrupted, affecting both bone structure and function (Tamma and Zallone, 2012). The interaction between osteoblasts and osteoclasts has been gradually recognized.

Exosomes is the medium of intercellular communication that has attracted recent attention from research. While osteoclast exosomes can transport miRNA and inhibit osteoblast function (Li et al., 2016; Sun et al., 2016; Yang et al., 2020), osteoblasts exosomes can also induce osteoclast formation (Deng et al., 2015). This exosome-mediated intercellular communication between osteoblasts and osteoclasts may represent a new mechanism for bone modeling and remodeling.

Bone homeostasis is largely maintained by the cellular communication between osteoclasts and osteoblasts. *Mycobacterium tuberculosis* lysate (MTL) stimulates mouse osteoblasts. Osteoblast-derived exosomes induced by MTL (MTL-OB-Exos) were isolated and extracted. Osteoclast precursor RAW264.7 cells were induced by MTL-OB-Exos. It was found that MTL-OB-Exos enhanced the osteoclast formation abilities of RAW264.7 (Yuan et al., 2018; Khanna and Sabharwal, 2019). Exosomes derived from osteoblasts contain RANKL protein, which can specifically bind to RANK on osteoclast precursor cells and participate in the RANKL-RANK-OPG regulatory axis to enhance osteoclast differentiation and function (Deng et al., 2015).

Exosomes-derived miRNAs have a role in dynamic bone homeostasis (Xie et al., 2017). It has been reported that mineralized osteoblasts release exosomes containing miR-503-3p. The molecular mechanism of miR-503-3p in osteoclasts remains unclear. It was found that the isolation of exosomes and miR-503-3p from osteoblast supernatant inhibited the differentiation of osteoclast progenitors (Wang Q. et al., 2021). Meanwhile, Heparinase gene (Hpse), the target gene of miR-503-3p, inhibited osteoclast differentiation by down-regulating Hpse expression. Osteoblast-derived exosomes inhibit osteoclast differentiation through miR-503-3p/Hpse axis (Wang Q. et al., 2021).

Current research on circRNA focuses on regulating cell transcription and translation, encoding proteins and molecular sponge activity of miRNA (Hansen et al., 2013; Memczak et al., 2013; Ashwal-Fluss et al., 2014). In skeletal system, circRNAs participate in the regulation of bone remodeling through the miRNA-mRNA axis in the form of molecular sponge (Qian et al., 2017; Li et al., 2018; Chen et al., 2019). The exosomes of MC3T3-E1 contain circ_0008542, which can increase tensile stimulation and promote osteoclast differentiation and bone resorption. Circ_0008542 upregulates Tnfrsf11a (RANK) gene expression by acting as miR-185-5p sponge. Specifically, circ_0008542 exerts a molecular sponge effect in osteoclasts through the miR-185-5p/RANK axis and gradually upregulates osteoclast differentiation (Wang W. et al., 2021). Meanwhile, circ_0008542 1916-1992bp fragment increased m6A methylation levels, inhibited RNA methylase METTL3, all of which induced osteoclasts differentiation and bone resorption. Injection of circ_0008542 + ALKBH5 into the tail vein of mice reversed the same effect *in vivo*. Site-directed mutagenesis showed that the 1956bp on circ_0008542 was the m6A functional site with the above biological functions (Wang W. et al., 2021). The RNA methylase METTL3 acts on the m6A functional site of 1956bp in circ_0008542, which promotes competitive binding of circ_0008542 to miR-185-5p. This binding results in increased expression of the target gene RANK and the initiation of osteoclast bone resorption. In contrast, the RNA demethylase ALKBH5 inhibits circ_0008542 binding to miR-185-5p, thereby correcting the bone resorption process (Figure 2).

5 Osteocyte-Exos-mediated communication within the skeletal micro-environment

Exosomes secreted by osteoblasts, osteocytes, osteoclasts, and other cells in the skeletal microenvironment influence bone formation and reabsorption. Also, exosomes affect bone tumor and lesion (Xie et al., 2017; Wang Q. et al., 2021; Hu et al., 2021). Osteocytes can regulate the functions of osteoblasts and osteoclasts by sensing systemic or local stimuli and secreting various cytokines and signaling molecules. Osteocytes derived exosomes contain many osteogenic factors, which can significantly enhance the targeted recruitment and osteogenesis of BMSCs.

It was found that miR-218 expression was significantly down-regulated in exosomes released by myostatin treated osteocytes (Qin et al., 2017). After endocytosis by osteocytes, Runx2 expression was down-regulated through the Wnt signaling pathway, thus inhibiting osteoblast differentiation. However, there was no significant change osteoclast activity of osteoclasts after exosome endocytosis (Qin et al., 2017). Sato et al. (2017) reported that the levels of 12 miRNAs, including miR-3473a, miR-6244, miR-5621-5p and miR-6239, in plasma exosomes of mice with reduced bone cells were significantly reduced. It is suggested that specific miRNA derived from

osteocyte-Exos plays a biological role in bone remodeling. In addition, osteocyte-Exos carrying miR-124-3p can inhibit galectin-3 expression in osteoblasts under high glucose conditions, thereby reducing periodontal bone mass in diabetic periodontitis mice (Li et al., 2020). Whether this relevant mechanism is applicable in the treatment of diabetic OP still needs further experimental verification.

Osteocytes are mechanically sensitive cells that respond to external stimuli by regulating their secretion groups. Exosomes exposed to mechanical strain facilitate proliferation and osteogenic differentiation of human periodontal ligament stem cells (HPDLSC). High-throughput miRNA sequencing showed that miR-181b-5p was upregulated in exosomes exposed to mechanical strain. It may inhibit phosphatase and tensin homolog (PTEN). Meanwhile, protein kinase B (Akt) was enhanced (Lv et al., 2020). However, the research on osteocyte is still relatively new. Further research on osteocyte-Exos can provide a foundation for understanding bone remodeling and bone diseases (Figure 3).

6 Osteoclast-Exos-mediated communication within the skeletal micro-environment

Inflammatory bone disease is caused by bone loss caused by abnormally activated osteoclasts. Osteoclasts phenotypes and functions vary based on precursor cell origin, cytokine expression, and microenvironment-dependent factors. Inflammatory osteoclasts (iOCLs) lose their immunosuppressive effect relative to OCL under physiological conditions, which induces TNF-α-producing $CD4^+$T cells in an antigen-dependent manner. This change ultimately leads to iOCL cascade amplification.

Osteoclasts-derived exosomes have been shown to modulate OCL-osteoblast communication (Yuan et al., 2018). iOCL-derived and OCL-derived exosomes promote osteoblast activity. We found that iOCL exosomes specifically target osteoblasts through ephrinA2/EphA2 (Ren et al., 2022). IOCL exosomes were rich in lncRNA from iOCL-derived exosome (lncRNA LIOCE), which promoted osteoblast activity after incorporation into osteoblasts. In addition, exosomes from lncRNA LIOCE stabilized osteogenic transcription factor OSX by reducing ubiquitination levels of OSX. Bone loss in a mouse model of inflammatory osteolysis was alleviated after injection of iOCL exosomes coated with lncRNA LIOCE. The role of lncRNA LIOCE-coated exosomes in promoting bone formation has been confirmed in rat bone repair models (Ren et al., 2022). IOCL-derived exosomes lncRNA LIOCE promote bone formation by upregulating OSX expression (Ren et al., 2022). Therefore, lncRNA LIOCE-coated exosomes may be an effective strategy for the treatment of osteoporosis and other bone metabolic diseases.

Osteoclasts secrete microRNA-rich exosomes through which miR-214 is transferred to osteoblasts to inhibit their function. MiR-214 and ephrinA2 levels are upregulated in serum exosomes of both patients with osteoporosis and transgenic mice models (Sun et al., 2016). These exosomes significantly inhibit osteoblast activity. Li et al. (2016) found that increased levels of osteoclast miR-214-3p and serum exosome miR-214-3p were associated with decreased bone formation in older women with fractures and ovariectomized mice. Osteoclast-specific miR-214-3p in knockout mice showed increased and bone formation decreased, suggesting that osteoclast exosomes affect osteoblast bone formation (Li et al., 2016).

Osteoclast targeting antagomir-214-3p therapy can rescue bone formation. Sun et al. (2016) found that exosomes of OCL recognized osteoblasts by ephrin A2/EphA2 and released miR-214/miR-214-3p into osteoblasts, inhibiting osteoblast differentiation. Yang et al. (2020) found that miR-23a-5p was highly expressed in the exosomes of RANKL induced RAW 264.7 cells. ALP staining showed that miR-23a-5p inhibits osteoblast activity.

Osteoclast-derived exosomes containing miR-23a-5p can effectively inhibit osteogenic differentiation by inhibiting Runx2 and promoting transcriptional coactivator YAP (YAP)-mediated MT1DP. Runx2 is the target gene of miR-23a-5p, which interacts with YAP. Runx2 and YAP suppress putative metallothionein MT1DP (MT1DP) expression, which to promotes osteogenic differentiation by regulating Hepatocyte nuclear factor 3-α (FoxA1) and Runx2 (Yang et al., 2020) (Figure 4).

7 Summary

With the development of biomedicine, exosomes as drug carriers have attracted extensive attention of researchers (Yeo et al., 2013). Several exosome-based drug formulations are currently undergoing clinical trials, and some have recently been approved for clinical use. Exosomes have successfully encapsulated bioactive molecules such as curcumin, paclitaxel, neurotoxin-I, and dexamethasone, all of which improve biodistribution and controlled release (Chen et al., 2009; Hines and Kaplan, 2013). Exosomes can promote cell signaling *via* the endocrine or paracrine systems. Depending on the content within the exosomes (such as RNA, lipids, functional proteins and other active substances attached to them), exosomes can regulate the biological behavior of cells.

Transplantation of BMSC-Exos showed similar biological functions to BMSCs. BMSC-Exos can up-regulate the osteogenic gene expression and promote osteoblast proliferation and differentiation as well as bone regeneration. In BMSC-Exos, miRNA plays an important role in osteoclast differentiation. MiRNA can promote or inhibit osteoclast differentiation by binding specific non-coding regions. It is also a targeted regulatory point for coupling of osteoclasts and osteoblasts. Regulating miRNA in BMSC-Exos may be a potential method to attenuate the imbalance of bone metabolism in osteoporosis.

Osteoblast-Exos can promote bone differentiation of BMSCs by activating Wnt/β-catenin signaling pathway. Specific transcription factors and miRNA in osteoblast-Exos enhance BMSCs differentiation. Osteoblast-Exos also serve as a medium for communication between osteoblasts and osteoclasts. Related lncRNA in osteoclast-Exos promote bone formation by up-regulating the expression of osteogenic genes. Related miRNAs in osteoclast-Exos are transferred into osteoblasts and affect osteoblast differentiation and bone formation. It is believed that the future studies on exosome of bone cells will play an important role in the occurrence and development of bone metabolic diseases and provide new ideas for fundamental research and clinical diagnosis of bone related diseases.

Author contributions

LZ gave the brief introduction of this article. ZW, ZZ, and LZ were responsible for manuscript writing. BG revised the manuscript. All authors approved the final version of this manuscript.

Funding

The work was supported by Youth Program of National Natural Science Foundation of China (81902298); Shanghai Frontiers Science Research Base of Exercise and Metabolic Health, Shanghai University of Sport, Shanghai 200438, China; Shanghai Key Lab of Human Performance (Shanghai University of sport) (11DZ2261100).

Acknowledgments

We appreciate the time and effort of the participants in this study.

Conflict of interest

The authors declare that the research was conducted in the absence of any commercial or financial relationships that could be construed as a potential conflict of interest.

Publisher's note

References

Aghebati-Maleki, L., Dolati, S., Zandi, R., Fotouhi, A., Ahmadi, M., Aghebati, A., et al. (2019). Prospect of mesenchymal stem cells in therapy of osteoporosis: A review. *J. Cell. Physiol.* 234 (6), 8570–8578. doi:10.1002/jcp.27833

Alimirzaie, S., Bagherzadeh, M., and Akbari, M. R. (2019). Liquid biopsy in breast cancer: A comprehensive review. *Clin. Genet.* 95 (6), 643–660. doi:10.1111/cge.13514

Ashwal-Fluss, R., Meyer, M., Pamudurti, N. R., Ivanov, A., Bartok, O., Hanan, M., et al. (2014). circRNA biogenesis competes with pre-mRNA splicing. *Mol. Cell* 56 (1), 55–66. doi:10.1016/j.molcel.2014.08.019

Bhushan, R., Grunhagen, J., Becker, J., Robinson, P. N., Ott, C. E., and Knaus, P. (2013). miR-181a promotes osteoblastic differentiation through repression of TGF-β signaling molecules. *Int. J. Biochem. Cell Biol.* 45 (3), 696–705. doi:10.1016/j.biocel.2012.12.008

Birmingham, E., Niebur, G. L., McHugh, P. E., Shaw, G., Barry, F. P., and McNamara, L. M. (2012). Osteogenic differentiation of mesenchymal stem cells is regulated by osteocyte and osteoblast cells in a simplified bone niche. *Eur. Cell. Mat.* 23, 13–27. doi:10.22203/ecm.v023a02

Chen, C., Johnston, T. D., Jeon, H., Gedaly, R., McHugh, P. P., Burke, T. G., et al. (2009). An *in vitro* study of liposomal curcumin: Stability, toxicity and biological activity in human lymphocytes and Epstein-Barr virus-transformed human B-cells. *Int. J. Pharm. X.* 366 (1-2), 133–139. doi:10.1016/j.ijpharm.2008.09.009

Chen, C., Wang, D., Moshaverinia, A., Liu, D., Kou, X., Yu, W., et al. (2017). Mesenchymal stem cell transplantation in tight-skin mice identifies miR-151-5p as a therapeutic target for systemic sclerosis. *Cell Res.* 27 (4), 559–577. doi:10.1038/cr.2017.11

Chen, F., Han, Y., and Kang, Y. (2021). Bone marrow niches in the regulation of bone metastasis. *Br. J. Cancer* 124 (12), 1912–1920. doi:10.1038/s41416-021-01329-6

Chen, X., Ouyang, Z., Shen, Y., Liu, B., Zhang, Q., Wan, L., et al. (2019). CircRNA_28313/miR-195a/CSF1 axis modulates osteoclast differentiation to affect OVX-induced bone absorption in mice. *RNA Biol.* 16 (9), 1249–1262. doi:10.1080/15476286.2019.1624470

Chen, X., Wang, Z., Duan, N., Zhu, G., Schwarz, E. M., and Xie, C. (2018). Osteoblast–osteoclast interactions. *Connect. Tissue Res.* 59 (2), 99–107. doi:10.1080/03008207.2017.1290085

Cheng, P., Chen, C., He, H. B., Hu, R., Zhou, H. D., Xie, H., et al. (2013). miR-148a regulates osteoclastogenesis by targeting V-maf musculoaponeurotic fibrosarcoma oncogene homolog B. *J. Bone Min. Res.* 28 (5), 1180–1190. doi:10.1002/jbmr.1845

Cross, M., Smith, E., Hoy, D., Nolte, S., Ackerman, I., Fransen, M., et al. (2014). The global burden of hip and knee osteoarthritis: Estimates from the global burden of disease 2010 study. *Ann. Rheum. Dis.* 73 (7), 1323–1330. doi:10.1136/annrheumdis-2013-204763

Csaki, C., Matis, U., Mobasheri, A., and Shakibaei, M. (2009). Co-culture of canine mesenchymal stem cells with primary bone-derived osteoblasts promotes osteogenic differentiation. *Histochem. Cell Biol.* 131 (2), 251–266. doi:10.1007/s00418-008-0524-6

Cui, Y., Luan, J., Li, H., Zhou, X., and Han, J. (2016). Exosomes derived from mineralizing osteoblasts promote ST2 cell osteogenic differentiation by alteration of microRNA expression. *FEBS Lett.* 590 (1), 185–192. doi:10.1002/1873-3468.12024

Danan, M., Schwartz, S., Edelheit, S., and Sorek, R. (2012). Transcriptome-wide discovery of circular RNAs in Archaea. *Nucleic Acids Res.* 40 (7), 3131–3142. doi:10.1093/nar/gkr1009

Deng, L., Wang, Y., Peng, Y., Wu, Y., Ding, Y., Jiang, Y., et al. (2015). Osteoblast-derived microvesicles: A novel mechanism for communication between osteoblasts and osteoclasts. *Bone* 79, 37–42. doi:10.1016/j.bone.2015.05.022

Deng, L. L., Peng, Y., Jiang, Y. H., Wu, Y., Ding, Y., Wang, Y., et al. (2017). Imipramine protects against bone loss by inhibition of osteoblast-derived microvesicles. *Int. J. Mol. Sci.* 18 (5), 1013. doi:10.3390/ijms18051013

Ducy, P., Schinke, T., and Karsenty, G. (2000). The osteoblast: A sophisticated fibroblast under central surveillance. *Science* 289 (5484), 1501–1504. doi:10.1126/science.289.5484.1501

Eirin, A., Zhu, X. Y., Puranik, A. S., Tang, H., McGurren, K. A., van Wijnen, A. J., et al. (2017). Mesenchymal stem cell–derived extracellular vesicles attenuate kidney inflammation. *Kidney Int.* 92 (1), 114–124. doi:10.1016/j.kint.2016.12.023

Gong, Y., Xu, F., Zhang, L., Qian, Y., Chen, J., Huang, H., et al. (2014). MicroRNA expression signature for Satb2-induced osteogenic differentiation in bone marrow stromal cells. *Mol. Cell. Biochem.* 387 (1-2), 227–239. doi:10.1007/s11010-013-1888-z

Hansen, T. B., Jensen, T. I., Clausen, B. H., Bramsen, J. B., Finsen, B., Damgaard, C. K., et al. (2013). Natural RNA circles function as efficient microRNA sponges. *Nature* 495 (7441), 384–388. doi:10.1038/nature11993

Heino, T. J., Hentunen, T. A., and Vaananen, H. K. (2004). Conditioned medium from osteocytes stimulates the proliferation of bone marrow mesenchymal stem cells and their differentiation into osteoblasts. *Exp. Cell Res.* 294 (2), 458–468. doi:10.1016/j.yexcr.2003.11.016

Hines, D. J., and Kaplan, D. L. (2013). Poly(lactic-co-glycolic) acid-controlled-release systems: Experimental and modeling insights. *Crit. Rev. Ther. Drug Carr. Syst.* 30 (3), 257–276. doi:10.1615/critrevtherdrugcarriersyst.2013006475

Hu, Y., Wang, Y., Chen, T., Hao, Z., Cai, L., and Li, J. (2021). Exosome: Function and application in inflammatory bone diseases. *Oxid. Med. Cell. Longev.* 2021, 1–17. doi:10.1155/2021/6324912

Huynh, N., VonMoss, L., Smith, D., Rahman, I., Felemban, M., Zuo, J., et al. (2016). Characterization of regulatory extracellular vesicles from osteoclasts. *J. Dent. Res.* 95 (6), 673–679. doi:10.1177/0022034516633189

Johnston, C. B., and Dagar, M. (2020). Osteoporosis in older adults. *Med. Clin. North Am.* 104 (5), 873–884. doi:10.1016/j.mcna.2020.06.004

Khanna, K., and Sabharwal, S. (2019). Spinal tuberculosis: A comprehensive review for the modern spine surgeon. *Spine J.* 19 (11), 1858–1870. doi:10.1016/j.spinee.2019.05.002

Lambert, A. W., Pattabiraman, D. R., and Weinberg, R. A. (2017). Emerging biological principles of metastasis. *Cell* 168 (4), 670–691. doi:10.1016/j.cell.2016.11.037

Li, D., Liu, J., Guo, B., Liang, C., Dang, L., Lu, C., et al. (2016). Osteoclast-derived exosomal miR-214-3p inhibits osteoblastic bone formation. *Nat. Commun.* 7, 10872. doi:10.1038/ncomms10872

Li, J., Guo, Y., Chen, Y. Y., Liu, Q., Tan, L., Zhang, S. H., et al. (2020). miR-124-3p increases in high glucose induced osteocyte-derived exosomes and regulates galectin-3 expression: A possible mechanism in bone remodeling alteration in diabetic periodontitis. *FASEB J.* 34 (11), 14234–14249. doi:10.1096/fj.202000970rr

Li, X., Zheng, Y., Zheng, Y., Huang, Y., Zhang, Y., Jia, L., et al. (2018). Circular RNA CDR1as regulates osteoblastic differentiation of periodontal ligament stem cells via the miR-7/GDF5/SMAD and p38 MAPK signaling pathway. *Stem Cell Res. Ther.* 9 (1), 232. doi:10.1186/s13287-018-0976-0

Liu, S., Liu, D., Chen, C., Hamamura, K., Moshaverinia, A., Yang, R., et al. (2015). MSC transplantation improves osteopenia via epigenetic regulation of notch signaling in lupus. *Cell Metab.* 22 (4), 606–618. doi:10.1016/j.cmet.2015.08.018

Lv, P. Y., Gao, P. F., Tian, G. J., Yang, Y. y., Mo, F. f., Wang, Z. h., et al. (2020). Osteocyte-derived exosomes induced by mechanical strain promote human periodontal ligament stem cell proliferation and osteogenic differentiation via the miR-181b-5p/PTEN/AKT signaling pathway. *Stem Cell Res. Ther.* 11 (1), 295. doi:10.1186/s13287-020-01815-3

Mankar, R., Bueso-Ramos, C. E., Yin, C. C., Hidalgo-Lopez, J. E., Berisha, S., Kansiz, M., et al. (2020). Automated osteosclerosis grading of clinical biopsies using infrared spectroscopic imaging. *Anal. Chem.* 92 (1), 749–757. doi:10.1021/acs.analchem.9b03015

Mathivanan, S., Ji, H., and Simpson, R. J. (2010). Exosomes: Extracellular organelles important in intercellular communication. *J. Proteomics* 73 (10), 1907–1920. doi:10.1016/j.jprot.2010.06.006

Memczak, S., Jens, M., Elefsinioti, A., Torti, F., Krueger, J., Rybak, A., et al. (2013). Circular RNAs are a large class of animal RNAs with regulatory potency. *Nature* 495 (7441), 333–338. doi:10.1038/nature11928

Mishima, S., Takahashi, K., Kiso, H., Murashima-Suginami, A., Tokita, Y., Jo, J. I., et al. (2021). Local application of Usag-1 siRNA can promote tooth regeneration in Runx2-deficient mice. *Sci. Rep.* 11 (1), 13674. doi:10.1038/s41598-021-93256-y

Munns, C. F., Shaw, N., Kiely, M., Specker, B. L., Thacher, T. D., Ozono, K., et al. (2016). Global consensus recommendations on prevention and management of nutritional rickets. *J. Clin. Endocrinol. Metab.* 101 (2), 394–415. doi:10.1210/jc.2015-2175

Narayanan, K., Kumar, S., Padmanabhan, P., Gulyas, B., Wan, A. C., and Rajendran, V. M. (2018). Lineage-specific exosomes could override extracellular matrix mediated human mesenchymal stem cell differentiation. *Biomaterials* 182, 312–322. doi:10.1016/j.biomaterials.2018.08.027

Okamura, H., Yoshida, K., Yang, D., and Haneji, T. (2013). Protein phosphatase 2A Cα regulates osteoblast differentiation and the expressions of bone sialoprotein and osteocalcin via osterix transcription factor. *J. Cell. Physiol.* 228 (5), 1031–1037. doi:10.1002/jcp.24250

Osugi, M., Katagiri, W., Yoshimi, R., Inukai, T., Hibi, H., and Ueda, M. (2012). Conditioned media from mesenchymal stem cells enhanced bone regeneration in rat calvarial bone defects. *Tissue Eng. Part A* 18 (13-14), 1479–1489. doi:10.1089/ten.tea.2011.0325

Qian, D. Y., Yan, G. B., Bai, B., Chen, Y., Zhang, S. J., Yao, Y. C., et al. (2017). Differential circRNA expression profiles during the BMP2-induced osteogenic differentiation of MC3T3-E1 cells. *Biomed. Pharmacother.* 90, 492–499. doi:10.1016/j.biopha.2017.03.051

Qin, Y., Peng, Y., Zhao, W., Pan, J., Ksiezak-Reding, H., Cardozo, C., et al. (2017). Myostatin inhibits osteoblastic differentiation by suppressing osteocyte-derived exosomal microRNA-218: A novel mechanism in muscle-bone communication. *J. Biol. Chem.* 292 (26), 11021–11033. doi:10.1074/jbc.m116.770941

Qin, Y., Wang, L., Gao, Z., Chen, G., and Zhang, C. (2016). Bone marrow stromal/stem cell-derived extracellular vesicles regulate osteoblast activity and differentiation *in vitro* and promote bone regeneration *in vivo*. *Sci. Rep.* 6, 21961. doi:10.1038/srep21961

Ren, L., Zeng, F., Deng, J., Bai, Y., Chen, K., Chen, L., et al. (2022). Inflammatory osteoclasts-derived exosomes promote bone formation by selectively transferring lncRNA LIOCE into osteoblasts to interact with and stabilize Osterix. *FASEB J.* 36 (2), e22115. doi:10.1096/fj.202101106rr

Sato, M., Suzuki, T., Kawano, M., and Tamura, M. (2017). Circulating osteocyte-derived exosomes contain miRNAs which are enriched in exosomes from MLO-Y4 cells. *Biomed. Rep.* 6 (2), 223–231. doi:10.3892/br.2016.824

Song, H., Li, X., Zhao, Z., Qian, J., Wang, Y., Cui, J., et al. (2019). Reversal of osteoporotic activity by endothelial cell-secreted bone targeting and biocompatible exosomes. *Nano Lett.* 19 (5), 3040–3048. doi:10.1021/acs.nanolett.9b00287

Sun, W., Zhao, C., Li, Y., Wang, L., Nie, G., Peng, J., et al. (2016). Osteoclast-derived microRNA-containing exosomes selectively inhibit osteoblast activity. *Cell Discov.* 2, 16015. doi:10.1038/celldisc.2016.15

Tamma, R., and Zallone, A. (2012). Osteoblast and osteoclast crosstalks: From OAF to ephrin. *Inflamm. Allergy Drug Targets* 11 (3), 196–200. doi:10.2174/187152812800392670

Tkach, M., and Thery, C. (2016). Communication by extracellular vesicles: Where we are and where we need to go. *Cell* 164 (6), 1226–1232. doi:10.1016/j.cell.2016.01.043

Tsai, J. N., Lee, H., David, N. L., Eastell, R., and Leder, B. Z. (2019). Combination denosumab and high dose teriparatide for postmenopausal osteoporosis (DATA-HD): A randomised, controlled phase 4 trial. *Lancet Diabetes Endocrinol.* 7 (10), 767–775. doi:10.1016/s2213-8587(19)30255-4

Tsai, M. T., Lin, D. J., Huang, S., Lin, H. T., and Chang, W. H. (2012). Osteogenic differentiation is synergistically influenced by osteoinductive treatment and direct cell–cell contact between murine osteoblasts and mesenchymal stem cells. *Int. Orthop.* 36 (1), 199–205. doi:10.1007/s00264-011-1259-x

Tsao, Y. T., Huang, Y. J., Wu, H. H., Liu, Y. A., Liu, Y. S., and Lee, O. (2017). Osteocalcin mediates biomineralization during osteogenic maturation in human mesenchymal stromal cells. *Int. J. Mol. Sci.* 18 (1), 159. doi:10.3390/ijms18010159

van der Pol, E., Böing, A. N., Harrison, P., Sturk, A., and Nieuwland, R. (2012). Classification, functions, and clinical relevance of extracellular vesicles. *Pharmacol. Rev.* 64 (3), 676–705. doi:10.1124/pr.112.005983

Wang, Q., Shen, X., Chen, Y., Chen, J., and Li, Y. (2021). Osteoblasts-derived exosomes regulate osteoclast differentiation through miR-503-3p/Hpse axis. *Acta Histochem.* 123 (7), 151790. doi:10.1016/j.acthis.2021.151790

Wang, W., Qiao, S. C., Wu, X. B., Sun, B., Yang, J. G., Li, X., et al. (2021). Circ_0008542 in osteoblast exosomes promotes osteoclast-induced bone resorption through m6A methylation. *Cell Death Dis.* 12 (7), 628. doi:10.1038/s41419-021-03915-1

Wang, Z., Wu, Y., Zhao, Z., Liu, C., and Zhang, L. (2021). Study on transorgan regulation of intervertebral disc and extra-skeletal organs through exosomes derived from bone marrow mesenchymal stem cells. *Front. Cell Dev. Biol.* 9, 741183. doi:10.3389/fcell.2021.741183

Wei, J., and Ducy, P. (2010). Co-dependence of bone and energy metabolisms. *Arch. Biochem. Biophys.* 503 (1), 35–40. doi:10.1016/j.abb.2010.05.021

Wei, Y., Ma, H., Zhou, H., Yin, H., Yang, J., Song, Y., et al. (2021). miR-424-5p shuttled by bone marrow stem cells-derived exosomes attenuates osteogenesis via regulating WIF1-mediated Wnt/β-catenin axis. *Aging (Albany NY)* 13 (13), 17190–17201. doi:10.18632/aging.203169

Xie, X., Xiong, Y., Panayi, A. C., Hu, L., Zhou, W., Xue, H., et al. (2020). Exosomes as a novel approach to reverse osteoporosis: A review of the literature. *Front. Bioeng. Biotechnol.* 8, 594247. doi:10.3389/fbioe.2020.594247

Xie, Y., Chen, Y., Zhang, L., Ge, W., and Tang, P. (2017). The roles of bone-derived exosomes and exosomal microRNAs in regulating bone remodelling. *J. Cell. Mol. Med.* 21 (5), 1033–1041. doi:10.1111/jcmm.13039

Xu, J. F., Yang, G. H., Pan, X. H., Zhang, S. J., Zhao, C., Qiu, B. S., et al. (2014). Altered MicroRNA expression profile in exosomes during osteogenic differentiation of human bone marrow-derived mesenchymal stem cells. *Plos One* 9 (12), e114627. doi:10.1371/journal.pone.0114627

Xu, R., Shen, X., Si, Y., Fu, Y., Zhu, W., Xiao, T., et al. (2018). MicroRNA-31a-5p from aging BMSCs links bone formation and resorption in the aged bone marrow microenvironment. *Aging Cell* 17 (4), e12794. doi:10.1111/acel.12794

Yang, D., Okamura, H., Nakashima, Y., and Haneji, T. (2013). Histone demethylase Jmjd3 regulates osteoblast differentiation via transcription factors Runx2 and osterix. *J. Biol. Chem.* 288 (47), 33530–33541. doi:10.1074/jbc.m113.497040

Yang, J. X., Xie, P., Li, Y. S., and Wen, T. (2020). Osteoclast-derived miR-23a-5p-containing exosomes inhibit osteogenic differentiation by regulating Runx2. *Cell. Signal.* 70, 109504. doi:10.1016/j.cellsig.2019.109504

Yang, X., Yang, J., Lei, P., and Wen, T. (2019). LncRNA MALAT1 shuttled by bone marrow-derived mesenchymal stem cells-secreted exosomes alleviates osteoporosis through mediating microRNA-34c/SATB2 axis. *Aging* 11 (20), 8777–8791. doi:10.18632/aging.102264

Yeo, R. W., Lai, R. C., Zhang, B., Tan, S. S., Yin, Y., Teh, B. J., et al. (2013). Mesenchymal stem cell: An efficient mass producer of exosomes for drug delivery. *Adv. Drug Deliv. Rev.* 65 (3), 336–341. doi:10.1016/j.addr.2012.07.001

Ying, C., Wang, R., Wang, Z., Tao, J., Yin, W., Zhang, J., et al. (2020). BMSC-exosomes carry mutant HIF-1α for improving angiogenesis and osteogenesis in critical-sized calvarial defects. *Front. Bioeng. Biotechnol.* 8, 565561. doi:10.3389/fbioe.2020.565561

Yuan, F. L., Wu, Q. Y., Miao, Z. N., Xu, M. H., Xu, R. S., Jiang, D. L., et al. (2018). Osteoclast-derived extracellular vesicles: Novel regulators of osteoclastogenesis and osteoclast–osteoblasts communication in bone remodeling. *Front. Physiol.* 9, 628. doi:10.3389/fphys.2018.00628

Zhang, J., Li, S., Li, L., Li, M., Guo, C., Yao, J., et al. (2015). Exosome and exosomal MicroRNA: Trafficking, sorting, and function. *Genomics Proteomics Bioinforma.* 13 (1), 17–24. doi:10.1016/j.gpb.2015.02.001

Zhang, Y., Cao, X., Li, P., Fan, Y., Zhang, L., Ma, X., et al. (2021). microRNA-935-modified bone marrow mesenchymal stem cells-derived exosomes enhance osteoblast proliferation and differentiation in osteoporotic rats. *Life Sci.* 272, 119204. doi:10.1016/j.lfs.2021.119204

Zhong, Y., Li, X., Wang, F., Wang, S., Wang, X., Tian, X., et al. (2021). Emerging potential of exosomes on adipogenic differentiation of mesenchymal stem cells. *Front. Cell Dev. Biol.* 9, 649552. doi:10.3389/fcell.2021.649552

Zhou, M., Li, S., and Pathak, J. L. (2019). Pro-inflammatory cytokines and osteocytes. *Curr. Osteoporos. Rep.* 17 (3), 97–104. doi:10.1007/s11914-019-00507-z

frontiers | Frontiers in Bioengineering and Biotechnology

TYPE Original Research
PUBLISHED 11 August 2022
DOI 10.3389/fbioe.2022.946261

OPEN ACCESS

EDITED BY
Jingfeng Li,
Zhongnan Hospital, Wuhan University, China

REVIEWED BY
Tao Yu,
Tongji University, China
Xiangyu Chu,
Huazhong University of Science and Technology, China
Yiqiang Hu,
Huazhong University of Science and Technology, China

*CORRESPONDENCE
Zhiyong Hou,
drzyhou@gmail.com
Yingze Zhang,
yzling_liu@163.com

†These authors have contributed equally to this work

SPECIALTY SECTION
This article was submitted to Preclinical Cell and Gene Therapy, a section of the journal Frontiers in Bioengineering and Biotechnology

RECEIVED 17 May 2022
ACCEPTED 04 July 2022
PUBLISHED 11 August 2022

CITATION
Guo J, Chen X, Lin Z, Jin L, Hou Z, Dong W and Zhang Y (2022), Tight junction disruption through activation of the PI3K/AKT pathways in the skin contributes to blister fluid formation after severe tibial plateau fracture. *Front. Bioeng. Biotechnol.* 10:946261. doi: 10.3389/fbioe.2022.946261

Tight junction disruption through activation of the PI3K/AKT pathways in the skin contributes to blister fluid formation after severe tibial plateau fracture

Jialiang Guo[1,2†], Xiaojun Chen[2†], Zhe Lin[2], Lin Jin[2], Zhiyong Hou[2*], Weichong Dong[3] and Yingze Zhang[2,4,5*]

[1]The School of Medicine, Nankai University, Tianjin, China, [2]Department of Orthopaedics, The Third Hospital of Hebei Medical University, Shijiazhuang, China, [3]Department of Pharmacy, The Second Hospital of Hebei Medical University, Shijiazhuang, China, [4]Chinese Academy of Engineering, Beijing, China, [5]NHC Key Laboratory of Intelligent Orthopeadic Equipment (The Third Hospital of Hebei Medical University), Shijiazhuang, China

Background: Acute compartment syndrome (ACS) is an orthopedic emergency that commonly occurs after severe tibial plateau fracture. Fracture blisters form on the skin, and it was found in our previous study that when blisters form, the compartment pressure significantly decreases. However, the potential mechanism underlying this pressure decrease has not yet been elucidated.

Methods: To obtain a comprehensive understanding of the changes that occur after blister formation on the skin, the changes in tight junction expression in the skin after tibial plateau fracture were observed. Blister samples and normal skin were collected from patients with bicondylar tibial plateau fractures with or without blisters. The epidermis thickness was measured, and the difference in the levels of K1, K5, K10, and skin barrier proteins such as claudin 1, claudin 2, and occludin between the two groups was evaluated by immunochemistry analysis, immunofluorescence, Western blotting, and qPCR.

Results: The skin was thinner and the levels of K1, K5, and K10 were significantly decreased in blistered skin. Furthermore, the PI3K/AKT pathway was found to be activated, and the tight junction expression was significantly decreased in blistered skin. This indicates that the paracellular pathway, which is essential for accelerating fluid accumulation in blisters and indirectly decreases compartment pressure, was activated.

Conclusion: Changes in the tight junction expression after blister formation may underlie blister fluid formation and indirectly explain the decrease in compartment pressure under blistered skin after severe tibial plateau fracture.

KEYWORDS

tibial plateau fracture, fracture blisters, tight junctions, acute compartment syndrome, paracellular pathway

Introduction

The treatment of severe tibial plateau fractures after high-energy trauma in adults is challenging. Acute compartment syndrome (ACS) is always considered an orthopedic emergency that is commonly encountered in severe tibial plateau fractures. Among the numerous physical signs after fracture, blisters on the skin have been reported to be a common indicator found in approximately 2.9% of all fractures requiring hospitalization (Uebbing et al., 2011). Two types of fracture blisters have been observed: one is a blood-filled blister, which represents more severe injury to the skin with complete separation of the dermo-epidermal junction; and the other is the serous-filled blister that exhibits only partial separation of the dermo-epidermal junction (Strebel et al., 2020).

A fracture blister is a phenomenon observed on the skin, and its importance has generally been ignored in orthopedic and dermatologic studies. The presence of these blisters frequently alters the proposed treatment or timing of surgery. The reason for these changes is the fear of wound breakdown or surgical site infection when an incision is made through a blister bed. In our previous research, it was found that when blisters appeared, the compartment pressure was lower than when they did not appear (Guo et al., 2021). It was therefore assumed that the formation of skin blisters might be a potential method of myofascial pressure release (Guo et al., 2019). However, whether the skin can release or transmit the abnormally increased tension or pressure originating from the compartment through its own regulation is still unknown. Therefore, an exploration or observation of the changes after blister formation on the skin would be beneficial to explain the reason for the decreased compartment pressure.

The skin, which comprises the epidermis, dermis, and hypodermis, can protect our body from harmful or poisonous external environments. The epidermis is the outermost layer composed of multilayered epithelial tissue, and the barrier function of the skin is mainly provided by the corneocytes that are connected through corneodesmosomes and lamellar lipids in the stratum corneum (Jung et al., 2019). Furthermore, tight, gap, and adherens junctions also contribute to the protective skin barrier (Draelos, 2012). Among them, tight junctions (TJs) create an intercellular barrier limiting the paracellular movement of solutes and material across epithelia. In general, the architecture can be conceptualized into compartments with transmembrane barrier proteins (claudins, occludin, etc.), linked to peripheral scaffolding proteins. Furthermore, there has been gradual recognition among physiologists studying epithelial transport that TJs, which have been considered to be impermeable structures, are actually variably permeable to ions and solutes (Frömter and Diamond, 1972). Many studies have focused on TJs and their regulators as therapeutic targets (Gamero-Estevez et al., 2019; Lobo de Sa et al., 2019; He et al., 2020). Quercetin, a common flavonoid was reported to improve the intestinal TJ barrier and reduce the rate of kidney stone formation by inducing phosphatidylinositol-3-kinase (PI3K)/protein kinase B (AKT)-regulated claudin expression changes (Gamero-Estevez et al., 2019).

It was previously reported that there are three distinguishable processes when blisters occur: the loosening of the structure, a phase of discontinuity, and fluid accumulation (Bork, 1978). However, no experiments on TJ changes in blistered skin in tibial plateau fractures have been conducted, and the pathways for fluid migration or accumulation remain unknown. To obtain a comprehensive understanding of the TJ changes in blistered skin in tibial plateau fractures, this research collected the patient skin from bicondylar tibial plateau fractures and explored the TJ changes in the blistered skin with the objective of explaining the reasons for the potential ability to release or transmit the abnormally increased tension or pressure originating from the fractured compartment.

Materials and methods

Demographic data

The medical records for severe tibial plateau fractures with or without ACS (Schatzker V and VI) in our department were included in this research. This study was approved by the Regional Ethics Committee of the Third Hospital of Hebei Medical University (S2020-022-1) and was performed in accordance with the ethical standards in the 1964 Declaration of Helsinki. The clinical trial number of this research was NCT04529330. The inclusion criteria were as follows: fracture patients with Schatzker V or VI who were older than 18 years. The exclusion criteria were pathologic or extra-articular proximal tibial fracture and those patients with 18 years of age or younger. Normal skin (10 samples from individuals with tibial plateau fractures who did not have blisters, control group, CG) and blistered skin (12 samples from individuals with tibial plateau fractures who had blisters, blister group, BG) were collected from the operation procedure (Figures 1, 2), and informed written consent was obtained from all of the enrolled patients. There were no significant differences in demographic data between the two groups (Table 1). The blister and normal tissues were collected around the main fracture line position, and the size of each sample was approximately 1 cm^2. Each tissue sample was divided for use in various assays.

Histopathology

A 4% paraformaldehyde PBS (pH 7.4) solution was utilized to fix the skin for 1 day at 4°C. The skins were then

FIGURE 1
(A) Anterior-posterior X-rays of a Schatzker VI tibial plateau fracture. **(B)** Lateral view of this fracture. **(C)** Fracture appearance with a serous-filled blister observed on the skin around the fracture site (proximal tibia) after admission. **(D)** Blister became larger after 1 day, and the patients were not subjected to fasciotomy. When a blister was observed, the intracompartmental pressure decreased significantly.

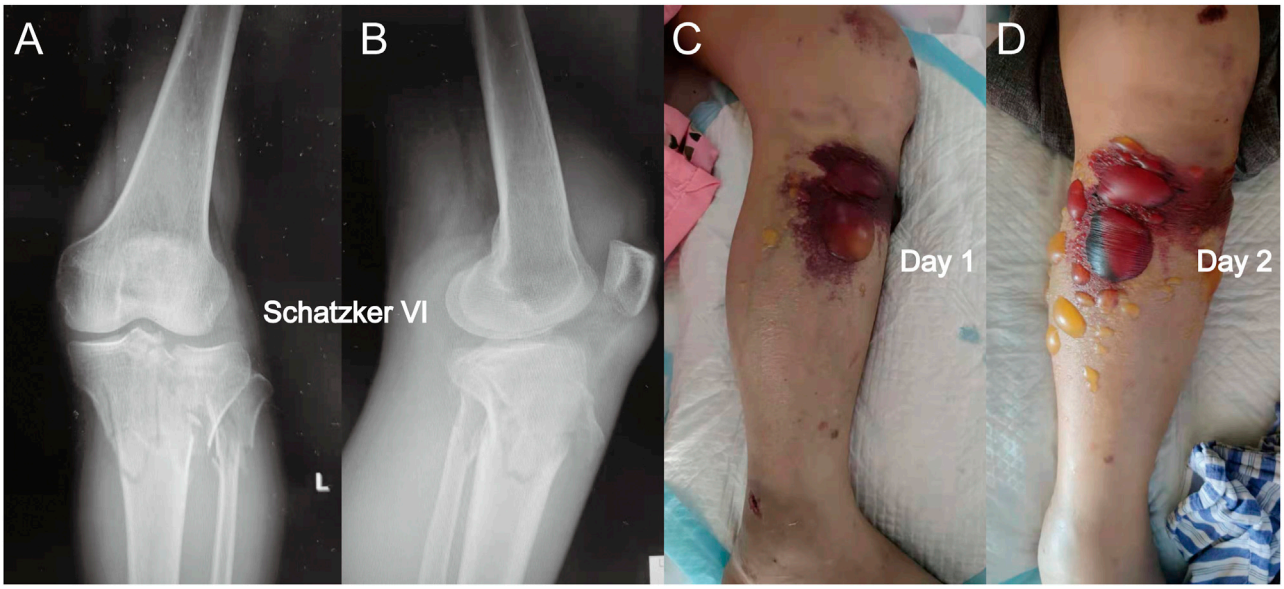

FIGURE 2
(A) Anterior-posterior X-rays of another Schatzker VI tibial plateau fracture. **(B)** Lateral view of this fracture. **(C)** Fracture appearance with a blood-filled blister. The blood-filled blister was larger than the serous blister observed in Figure 1. **(D)** Blister became larger after 1 day, and a similar phenomenon in which the intracompartmental pressure decreased after the appearance of the blood-filled blister was observed.

processed for standard dehydration in graded alcohol and embedding in paraffin. Sagittal 3 μm sections were cut (Microm HM360, Waldorf, Germany), and hematoxylin and eosin (HE) staining was used for histological evaluation with standard methods. Light microscopy (Nikon eclipse C1, Nikon, Japan) was used to obtain histological images, which were processed with built-in software (Nikon DS-U3).

TABLE 1 The demographic data in CG and BG.

	CG	BG	*P*
Gender			
Male	7	10	—
Female	3	2	0.406
Age	46.3 ± 7.6	45.9 ± 7.0	0.821
Fracture Type			
Schatzker V	4	7	—
Schatzker VI	6	5	0.392
Chronic Disease			
Normal	5	7	—
Hypertension	3	4	—
Diabetes	2	1	0.729
Acute complications			
Artery injury	0	0	—
VTE	3	1	0.293
Open injury	0	0	—

Immunohistochemical staining

Normal or blister human skin samples were cut into 3 μm slices, and a rehydration procedure was sequentially applied with a descending ethanol series. Next, a high-pressure cooker was used to conduct antigen retrieval (pH 8.0, Servicebio, G1106, Wuhan, China) for 20 min, followed by three cooling phases over 5 min. To block endogenous peroxidase activity, the sections were placed in 3% hydrogen peroxide and incubated at room temperature in the dark for 25 min. The sections were placed in PBS (pH 7.4) and shaken on a decolorizing shaker 3 times for 5 min each time. Bovine serum albumin (BSA; 3%) was added to the circle to evenly cover the tissue, and the tissues were sealed for 30 min at room temperature. Anti-keratin1 (Servicebio, GB14050, 1:100, Wuhan, China), anti-keratin 5 (Servicebio, GB14016, 1:100, Wuhan, China), and anti-keratin 10 (Servicebio, GB14051, 1:100, Wuhan, China) antibodies were used to evaluate the difference between the two groups. After incubation with the primary antibodies, the sections were placed in PBS (pH 7.4), washed by shaking on a decolorizing shaker three times (5 min each time), and incubated with secondary antibody (HRP-labeled) at room temperature for 5′ minutes. Hematoxylin (Sigma, St. Louis, MO, United States) was used for nuclear staining. All immunohistochemistry images were obtained and analyzed by microscopy and with a relative imaging system (Nikon E100).

Immunofluorescence staining

Commercial primary antibodies, including anti-occludin (Servicebio, GB-111401, 1:500, Wuhan, China), anti-claudin 1 (Servicebio, GB14066, 1:100, Wuhan, China), anti-claudin 2 (Servicebio, GB14068, 1:100, Wuhan, China), anti-keratin 1 (Servicebio, GB14050, 1:100, Wuhan, China), anti-keratin 5 (Servicebio, GB14061, 1:100, Wuhan, China), and anti-keratin 10 (Servicebio, GB14051, 1:100, Wuhan, China) were diluted. After incubation with the primary antibodies, the samples were washed with PBS three times (5 min each time). Next, the samples were incubated with secondary antibodies at room temperature for 5′ min in darkness. After three washes with PBS (5 min each time), DAPI (Sigma, St. Louis, MO, United States) was used for nuclear staining. All IF images were obtained by microscopy and with a relative imaging system (Nikon Eclipse C1). To quantify the level of protein expression, ImageJ software was utilized to generate a mask, which was applied to each corresponding protein channel being quantified (occludin, claudin 1, claudin 2). The mean pixel intensity was used to quantify each region that overlapped with occludin labeling.

Western blotting

Fresh human skin tissues were cut into very small pieces. The appropriate amount of cytoplasmic protein extract was then mixed in. The tissue was homogenized in RIPA buffer (Servicebio). The protein concentrations were determined with a BCA protein concentration measurement kit. The skin samples were then separated by SDS–PAGE and electrotransferred to polyvinylidene fluoride (PVDF; 0.45 μm) membrane (Roche, Basel, Switzerland) at 300 mA for 30 min. The membrane was then blocked in a TBS buffer containing 3% BSA for 30 min at 37°C. Then, the membrane was incubated with primary antibodies at 4°C overnight and HRP-conjugated secondary antibodies for 30 min. The results from the two groups were compared within the software ImageJ.

RNA preparation and quantitative real-time PCR

Real-time PCR was used to investigate the total amount of RNA isolated from the normal and blistered skin samples. The isolated RNA was quantified, reverse transcribed, and analyzed by qRT–PCR (Stepone plus, ABI, United States). The PCR primer sequences for occludin were 5′-TTCCTATAAATC CACGCCGG-3′ (forward) and 5′-TGTCTCAAAGTTACC ACCGCTG-3′ (reverse); those for claudin 1 were 5′-CTGTGG ATGTCCTGCGTGTC-3′ (forward) and 5′-ACTGGGGTCATA GGGTCATAGAAT (reverse); those for claudin 2 were 5′- TTG GGCTTGGTAGGCATCGT-3′ (forward) and 5′- CAGGAA TCCCGAGCCAAAGA (reverse); and those for β-actin were 5′- CACCCAGCACAATGAAGATCAAGAT-3′ (forward) and 5′- CCAGTTTTTAAATCCTGAGTCAAGC-3′ (reverse). The cycling conditions were set as follows: 25°C for 5 min, 42°C for 30 min, and 45 cycles of 85°C for 5 s. The mRNA levels were normalized to the corresponding β-actin levels in human skin.

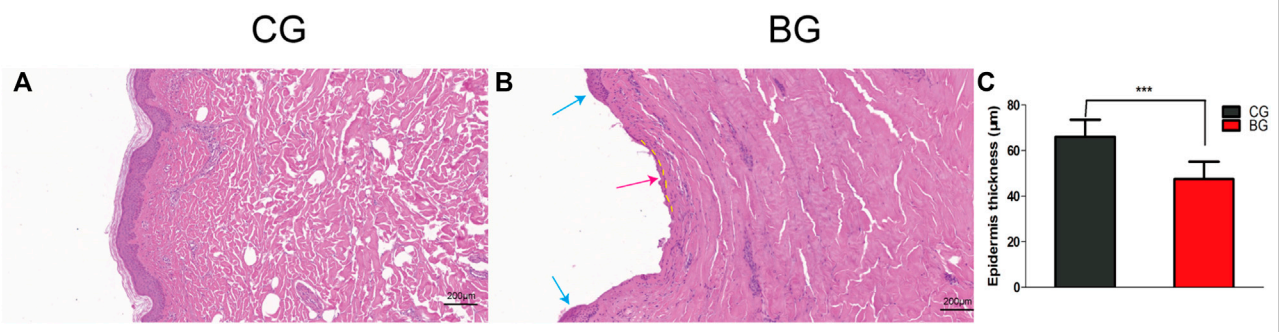

FIGURE 3
(A) Normal skin was stained with HE, and the cornified layer in the epidermal layer was intact. **(B)** Blistered skin was stained with HE and observed by light microscopy. The epidermal layer was disrupted (blue arrow) and separated from the dermis, with a small portion of the stratum basale retained (dotted yellow line), which explained the quick recovery of the blistered skin (red arrow). **(C)** Comparison of skin thicknesses in the two groups. CG: control group; BG: blister group.

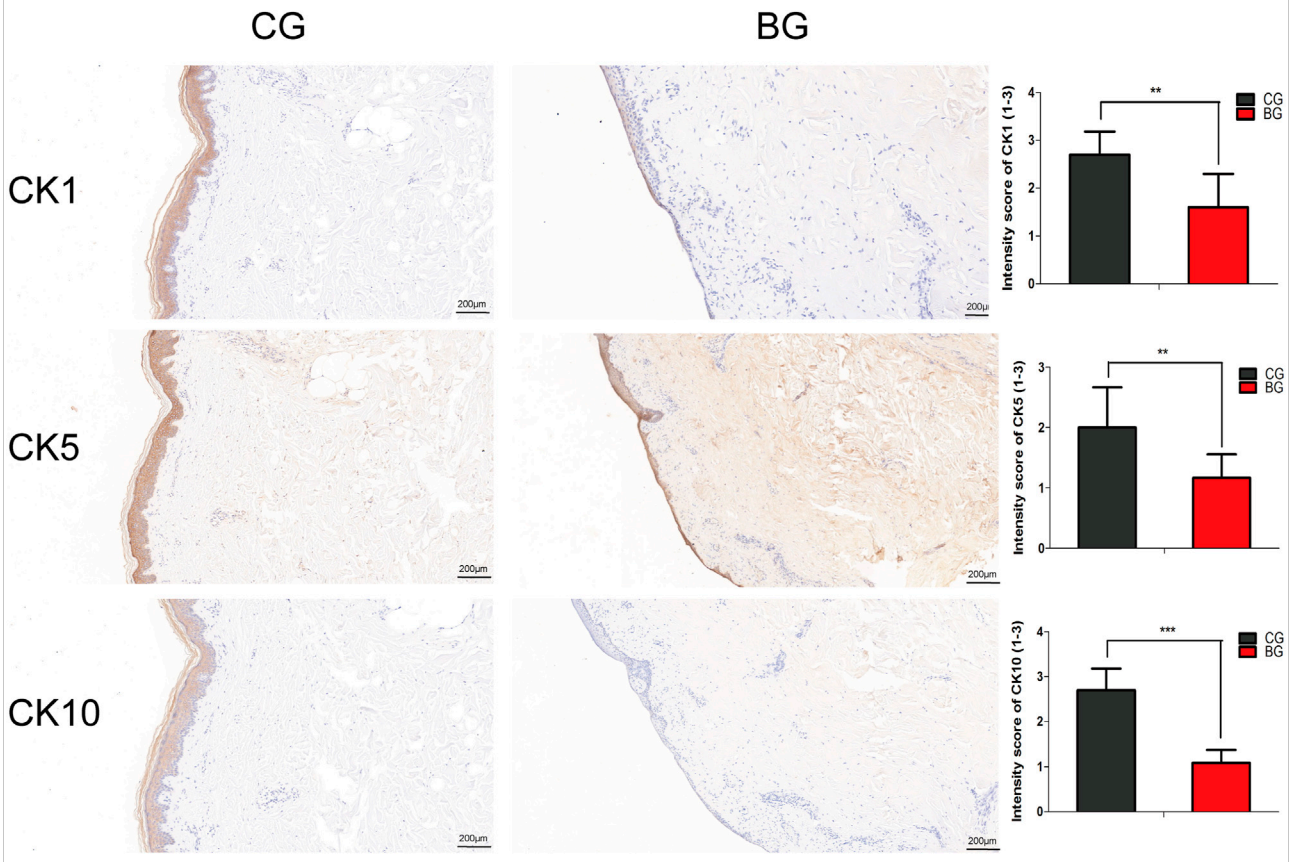

FIGURE 4
Immunohistochemical images of the two groups with antibodies against cytokeratins K1, K5, and K10. The epidermal layer was disrupted and separated from the dermis, while a small portion of the stratum basale was retained in the BG. The cytokeratins were distributed nonhomogeneously in the residual middle layer of the epidermis. The intensity scores for K1, K5, and K10 in the two groups were compared, and the expressions of K1, K5, and K10 were significantly decreased in the BG. K1: cytokeratin 1, K5: cytokeratin 5, K10: cytokeratin 10. (Bars = 200 μm, *: $p < 0.05$, **: $p < 0.01$, and ***: $p < 0.001$).

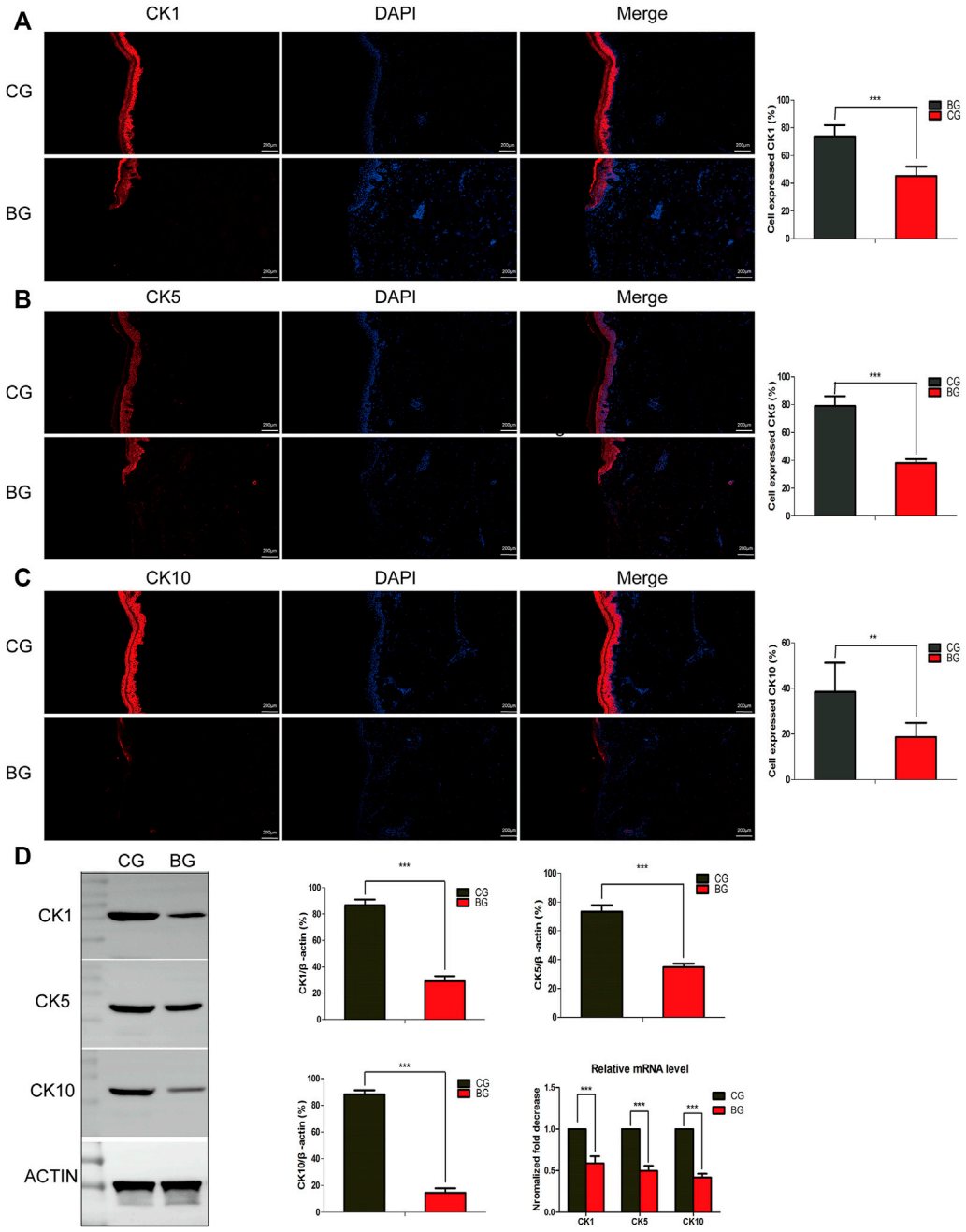

FIGURE 5
(A–C) Immunofluorescence analysis of normal and blistered skin. Images of immunofluorescence staining of the cytokeratins K1, K5, and K10 in the two groups. In accordance with the immunohistochemical results, the number of positively expressing cells was compared for K1, K5, and K10, and the positive expression rate was significantly decreased in the BG. **(D)** Representative Western blots of cytokeratins K1, K5, and K10 in control and blistered human skin. It was observed that the expression of the three cytokeratins was significantly decreased in the BG group. *: $p < 0.05$, **: $p < 0.01$, and ***: $p < 0.001$).

Statistical analysis

Continuous data are presented as the means with standard deviation. Mann–Whitney U tests were conducted for comparisons between the two independent groups, and Kruskal–Wallis H tests were used to conduct comparisons among three independent groups. Homogeneity of variance for continuous variables was evaluated using the

10.3389/fbioe.2022.946261

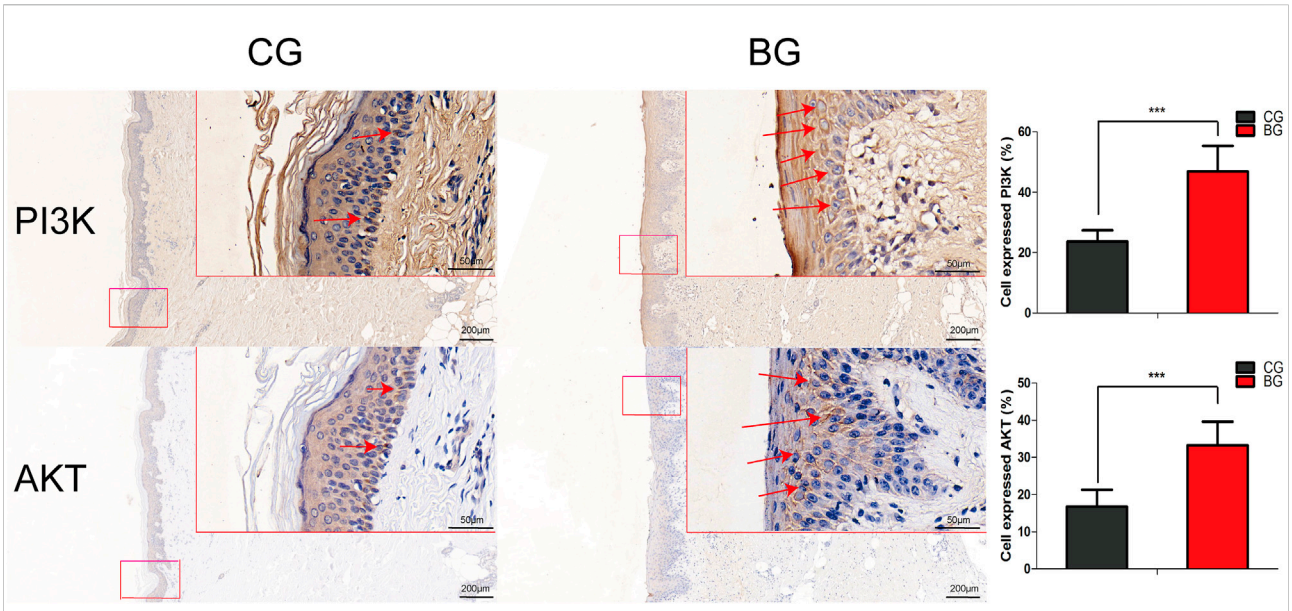

FIGURE 6
Immunohistochemical images of PI3K and AKT in normal and blistered skin. The number of cells expressing PI3K or AKT in the two groups was compared, and the expression of PI3K or AKT increased significantly in blister skin compared with normal skin. (Bars = 200 and 50 μm, *: $p < 0.05$, **: $p < 0.01$, and ***: $p < 0.001$).

Levene test for equality of variances. For all analyses in this research, significance was set at the $p < 0.05$ level. All analyses were conducted using SPSS version 22.0 (IBM Corp, Armonk, NY).

Results

Human blistered skin demonstrated a decrease in epidermal differentiation markers

Compared with the normal corneum stratum in the normal skin, the cornified layer was completely disrupted and disappeared in blistered skin, as observed by the histology of HE-stained skin. The epidermis was separated from the dermis, and a portion of the stratum basale was retained (Figure 3). The thickness of the epidermis was significantly decreased in the BG compared with that in the CG ($p < 0.001$).

To further analyze the changes after blister observation, normal and blistered skin were analyzed with immunohistochemistry against cytokeratin 1 (K1), 5 (K5), and 10 (K10). It was demonstrated that in blistered skin, K1, K5, and K10 were distributed nonhomogeneously in the residual middle layer of the epidermis, namely, the spinous layer and granular layer, while control tissues showed that the expression was distributed uniformly within the intact middle layer. Furthermore, there was no significant difference in localization, but the intensity decreased in blistered skin (Figure 4). IF analysis (Figures 5A–C), Western blotting, and PCR (Figure 5D) further confirmed these results. The expressions of K1, K5, and K10 were decreased in blistered skin compared with normal skin.

Phosphatidylinositol-3-kinase/protein kinase B expression was upregulated, and epidermal expression of tight junctions was decreased in blistered skin

Immunohistochemistry with antibodies against PI3K or AKT was conducted, and the expressions of PI3K and AKT increased significantly in blistered skin compared with normal skin (Figure 6). To further analyze the effects of blisters on the epidermis, the treated tissues were subjected to IF staining with antibodies against target TJ proteins, including claudin 1, claudin 2, and occludin. As a type of TJ protein, the expression of occludin was decreased significantly in blistered skin but normally distributed in normal skin. The expression of claudin 1 and 2 also decreased significantly in blistered skin compared with the control group (Figure 7).

Blistered skin exhibited downregulated occludin and claudin 1 and 2 protein expressions and increased phosphatidylinositol-3-kinase/protein kinase B pathway proteins

Occludin and claudins 1 and 2 are signaling molecules in the skin barrier. Western blot analysis revealed that the protein expressions of occludin and claudins 1 and 2 in the blister group were markedly decreased compared to those in the control group. Furthermore, Western blot analysis of PI3K, pPI3K, and AKT was performed and the expression of PI3K and AKT was found to have increased compared with that in the control group. These results further suggested that the blisters observed in the skin after tibial plateau fracture could contribute to increased fluid accumulation in human skin (Figures 8A–C).

Blistered skin exhibited downregulated occludin and claudins 1 and 2 mRNA expressions

To investigate the effect of the blisters on epidermal or dermal differentiation, the mRNA levels of occludin and claudins 1 and 2, which are proteins involved in the formation of the epidermal barrier, were evaluated using qPCR. The expressions of occludin and claudins 1 and 2 mRNA were found to be significantly decreased in blistered skin. The mRNA expression levels of PI3K, p-PI3K, and AKT were significantly increased in blistered skin (Figure 8D).

Discussion

Patients with severe tibial plateau fractures (Schatzker V and VI) were enrolled in this study due to the relatively severe fracture pattern and the fact that more blisters are observed in these patients than in patients with other tibial plateau fractures or fractures in other areas. Undoubtedly, blisters have always been a recognized entity observed on human skin, but blisters observed above tibial plateau fractures have continually been ignored in orthopedic studies. Fracture blisters are known to be associated with increased infection rates and wound breakdown, and the current research focused on the pathological characteristics of blistered skin has attempted to illustrate skin changes and determine the potential mechanism of fracture blister fluid formation. The expression of TJs was significantly decreased in blistered skin, and the paracellular pathway was opened, which contributed to the formation of blister fluid. This study opens a new door for understanding and explaining fracture blisters, which have been associated with reduced compartment pressure in the clinic.

Epithelia are sheets of cells that line body cavities and external surfaces in multicellular organisms. One key function of the epidermis is to act as a physical and chemical barrier that allows the selective transportation of solutes and water between compartments (Günzel and Yu, 2013). However, the definite mechanism of fracture blister fluid formation is still not clear, and many phenomena cannot be reasonably explained. First, it was found that manual intradermal injection of fluid under maximal pressure with a syringe did not result in blister formation (Stoughton, 1957). Furthermore, equal high pressures have also been observed in the corium in diseased states. Therefore, it seems very unlikely that the pressure itself can directly cause blister formation. Second, the blisters resulting from friction do not cause the direct separation of epidermal cells from the corium, which is actually secondary to the cell damage incurred by friction (Stoughton, 1957). Third, Bork (1978)reported that negative interstitial fluid pressure and the colloid osmotic pressure of the interstitial fluid were the main factors affecting blister fluid formation. However, the amount of fluid in the blister was potentially large, and the fast accumulation of blister fluid cannot be reasonably explained by only intracellular filtration pressure. Therefore, an understanding of the fluid transport mechanism in the skin is essential and beneficial to revealing the mechanism of fluid accumulation and decreased compartment pressure when blisters are observed in the skin above severe tibial plateau fractures.

Many factors can affect the permeability of the skin; for example, epidermal integrity can be disrupted by disulfide bond cleavage agents such as sodium lauryl sulfate and hydrogen bond breaking agents. It has also been reported that thermal injury can release enzymatic factors that cause the breakdown of intercellular bridges and result in epidermal cells separating from each other. Furthermore, the blood–brain barrier consists of TJs between endothelial cells that inhibit the transcellular or paracellular passage of molecules across it, and it was reported that circulating TJs were increased when the integrity of the blood–brain barrier was disrupted (Kniesel and Wolburg, 2000; Jiao et al., 2015). Similarly, epidermal cells are also attached to each other at their lateral membranes through a complex of intercellular junctions, such as TJs or zona occludens, and TJs are considered the major determinant of paracellular permeability (Stoughton, 1957; Ahmad et al., 2011). Researchers studying epithelial transport and TJs, which have always been considered to be impermeable structures, noted that they are actually variably permeable to ions and solutes (Van Itallie and Anderson, 2014). Consistent with the aforementioned research, it was found that the blistered skin in tibial plateau fractures had significantly decreased expression of TJ proteins such as claudins 1 and 2 and occludin. Along with the decreased expression of TJs, the AKT signaling pathway is considered to play an important regulatory role in the formation and maintenance of TJs. The results here illustrated that the expression of PI3K and AKT was increased in blistered skin compared with that in the control group, which indicates the potential role of PI3K in regulating the expression of TJs. Immunohistochemical images also showed that the staining intensity of cytokeratins 1, 5, and 10 decreased or even disappeared, reflecting that the epidermal integrity was disrupted in blistered skin.

10.3389/fbioe.2022.946261

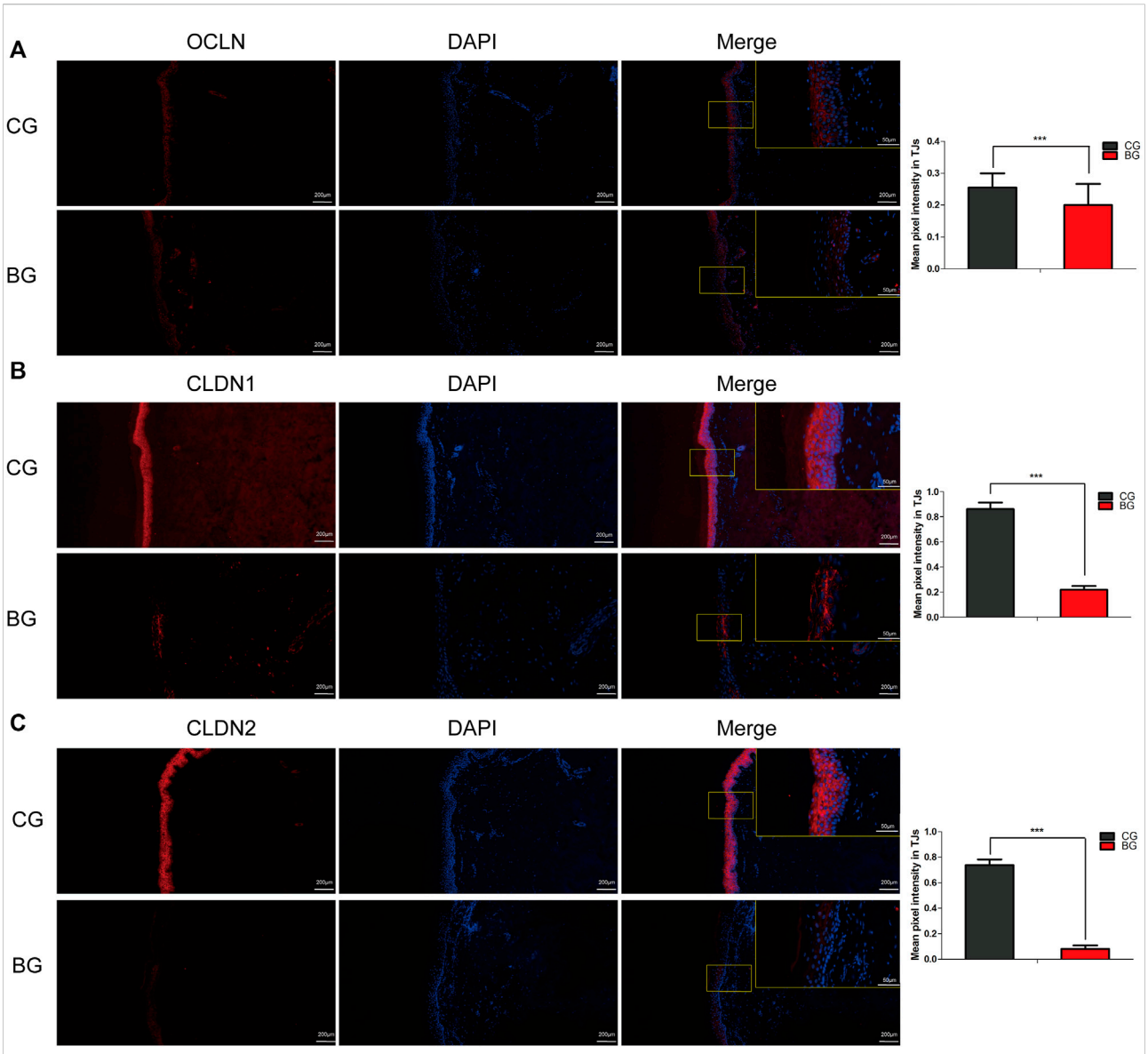

FIGURE 7
Immunofluorescence images of occludin, claudin 1, and claudin 2 in normal and blistered skin. The nuclei were stained with DAPI (blue), and red fluorescence indicates the lineage markers. The OCLN **(A)**, CLDN1 **(B)**, and CLDN2 **(C)** levels in each group were compared, and it was illustrated that the expression of these TJ markers decreased significantly in blister skin compared with normal skin. OCLN: occludin, CLDN1: claudin 1, CLDN 2: claudin 2. (Bars = 200 and 50 μm, *: $p < 0.05$, **: $p < 0.01$, and ***: $p < 0.001$).

It was also found that some residual epidermis of the stratum basale was retained with the decreased TJ expression. Therefore, after understanding the importance of TJs in the paracellular pathway of skin, it was concluded from our experimental results that decreased TJ expression in blistered skin was beneficial to the paracellular transportation of ions and solutes.

Due to the structural changes in blistered skin, fluid can migrate from the interstitial space into the blister space through the disrupted TJs. To achieve migration, physical forces that act on the interstitial fluid in the interstitial space must be present. What we hypothesized was that the high compartment pressure in a tibial plateau fracture, which is due to abnormal physical forces, might be conducted through the fascia tissue, muscles, and hypodermis to the interstitial space under the skin. Then, the fluid is pushed into the blisters, although transcellular or paracellular pathways adjusted after tight conjunction expressions were decreased during the process of fracture blister fluid formation. As the volume of fluid in the blister increases, the compartment pressure decreases. Furthermore, blood blisters are always observed in the clinic and can actually be identified as a marker of the disruption of TJs.

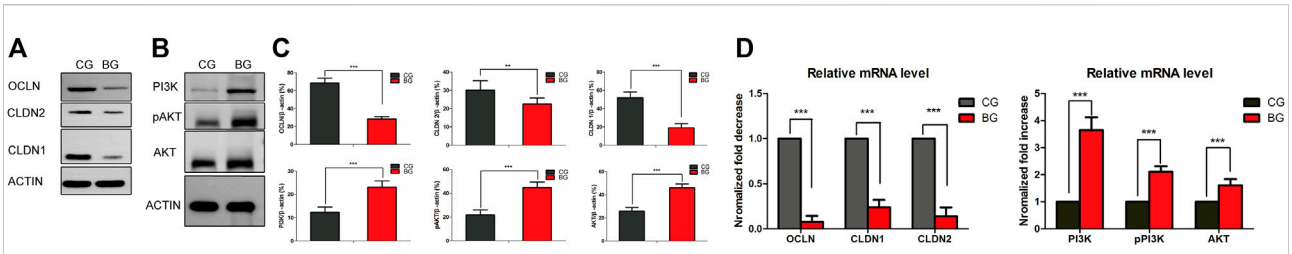

FIGURE 8
(A) Representative Western blots of the proteins OCLN, CLDN1, and CLDN2 in control and blistered human skin. **(B)** Representative Western blots of the proteins PI3K, AKT, and P-AKT in control and blistered human skin. **(C)** Expressions of the OCLN, CLDN1, and CLDN2 proteins were significantly decreased and those of PI3K, AKT, and pAKT were significantly increased in blistered skin compared with normal skin. OCLN: occludin, CLDN1: claudin 1, CLDN 2: claudin 2. (*: $p < 0.05$, **: $p < 0.01$, and ***: $p < 0.001$). **(D)** mRNA expression levels of occludin and claudins 1 and 2 were measured by qRT–PCR, and it was found that occludin, claudin 1, and claudin 2 expressions were decreased in blistered skin. In contrast, the mRNA expression levels of PI3K, p-PI3K, and AKT were significantly increased in blistered skin. The results are expressed as the mean ± SEM. ***: $p < 0.001$.

Electron-dense molecules such as hemoglobin are not permeable through the paracellular pathway under normal conditions. Studies have also shown that hemoglobin freely diffuses through the intercellular space but stops at the level of the TJ (Farquhar and Palade, 1963; Martinez-Palomo et al., 1971; Whittembury and Rawlins, 1971). Therefore, TJ disruption in blistered skin can be identified as an essential mechanism to accelerate fluid accumulation in blisters and indirectly decrease compartment pressure.

There are limitations to this research. One is that fluid migration was not monitored in real-time, and in our following research, tracer agents such as ruthenium red will be added to illustrate fluid transportation. However, experiments in humans are not easily conducted, so related animal experiments will be used to test the validity of our hypothesis. Second, related transcellular pathways were not explored here, and piezo or transient receptor potential vanilloids will be detected in our subsequent research in fascia and skin tissue samples. Crushing injury or vascular injury was also not considered in this study. To obtain a more comprehensive understanding of ACS, more patients and other injury mechanisms will be compared in our follow-up research.

Conclusion

In conclusion, the epidermal layer was disrupted and separated from the dermis with a portion of stratum basale residue, and the expression of TJ proteins such as claudins and occludin decreased significantly in the blistered skin, thus resulting in reduced barrier function. The changes in TJs after blister observation may be a potential channel for explaining blister fluid formation, which indirectly explains the decreased compartment pressure under blistered skin after severe tibial plateau fracture. The paracellular pathways regulated by TJs are regulated under physiological conditions and affected under pathological fractured states through the PI3K/AKT pathways.

Data availability statement

The original contributions presented in the study are included in the article/supplementary material; further inquiries can be directed to the corresponding authors.

Ethics statement

The studies involving human participants were reviewed and approved by NCT04529330 S2020-022-1. The patients/participants provided their written informed consent to participate in this study.

Author contributions

Conceptualization: YZ data curation: LJ formal analysis: WD investigation: XC methodology: JG project administration: JG resources: YZ software: ZL supervision: YZ validation: ZH visualization: ZH writing—original draft: JG writing—review and editing: JG.

Funding

The research was supported by the Science and Technology Project of the Hebei Education Department (SLRC2019046), the Government-funded Clinical Medicine Outstanding Talent Training Project (2019), the National Natural Science Foundation of China (82072523 and 82002281), the Natural Science Foundation of Hebei (H2020206193 and H2021206054), the Main Medical Scientific Research of Hebei (20210543), the China Postdoctoral Fund (2021 M701785), and the 14th Five-Year Clinical Medicine Innovation Research Team (2022). The funders had no role in study design, data

collection and analysis, decision to publish, or preparation of the manuscript.

Conflict of interest

The authors declare that the research was conducted in the absence of any commercial or financial relationships that could be construed as a potential conflict of interest.

Publisher's note

References

Ahmad, W., Shabbiri, K., Ijaz, B., Asad, S., Sarwar, M. T., Gull, S., et al. (2011). Claudin-1 required for HCV virus entry has high potential for phosphorylation and O-glycosylation. *Virol. J.* 8, 229. doi:10.1186/1743-422x-8-229

Bork, K. (1978). Physical forces in blister formation. The role of colloid osmotic pressure and of total osmolality in fluid migration into the rising blister. *J. Investig. Dermatol.* 71 (3), 209–212. doi:10.1111/1523-1747.ep12547271

Draelos, Z. D. (2012). New treatments for restoring impaired epidermal barrier permeability: Skin barrier repair creams. *Clin. dermatology* 30 (3), 345–348. doi:10.1016/j.clindermatol.2011.08.018

Farquhar, M. G., and Palade, G. E. (1963). Junctional complexes in various epithelia. *J. Cell. Biol.* 17 (2), 375–412. doi:10.1083/jcb.17.2.375

Frömter, E., and Diamond, J. (1972). Route of passive ion permeation in epithelia. *Nat. New Biol.* 235 (53), 9–13. doi:10.1038/newbio235009a0

Gamero-Estevez, E., Andonian, S., Jean-Claude, B., Gupta, I., and Ryan, A. K. (2019). Temporal effects of quercetin on tight junction barrier properties and claudin expression and localization in mdck ii cells. *Int. J. Mol. Sci.* 20, 4889. doi:10.3390/ijms20194889

Günzel, D., and Yu, A. S. (2013). Claudins and the modulation of tight junction permeability. *Physiol. Rev.* 93 (2), 525–569. doi:10.1152/physrev.00019.2012

Guo, J., Gao, Z., Wang, L., Feng, C., Hou, Z., Zhang, Y., et al. (2021). The blister occurring in severe tibial plateau fractures (Schatzker V-VI) decreases the risk of acute compartment syndrome. *Int. Orthop.* 45 (3), 743–749. doi:10.1007/s00264-020-04925-y

Guo, J., Yin, Y., Jin, L., Zhang, R., Hou, Z., Zhang, Y., et al. (2019). Acute compartment syndrome: Cause, diagnosis, and new viewpoint. *Med. Baltim.* 98 (27), e16260. doi:10.1097/md.0000000000016260

He, W.-Q., Wang, J., Sheng, J.-Y., Zha, J.-M., Graham, W. V., Turner, J. R., et al. (2020). Contributions of myosin light chain kinase to regulation of epithelial paracellular permeability and mucosal homeostasis. *Int. J. Mol. Sci.* 21, 993. doi:10.3390/ijms21030993

Jiao, X., He, P., Li, Y., Fan, Z., Si, M., Xie, Q., et al. (2015). The role of circulating tight junction proteins in evaluating blood brain barrier disruption following intracranial hemorrhage. *Dis. markers* 2015, 1–12. doi:10.1155/2015/860120

Jung, Y. O., Jeong, H., Cho, Y., Lee, E. O., Jang, H. W., Kim, J., et al. (2019). Lysates of a probiotic, lactobacillus rhamnosus, can improve skin barrier function in a reconstructed human epidermis model. *Int. J. Mol. Sci.* 20 (17), 4289. doi:10.3390/ijms20174289

Kniesel, U., and Wolburg, H. (2000). Tight junctions of the blood-brain barrier. *Cell. Mol. Neurobiol.* 20 (1), 57–76. doi:10.1023/a:1006995910836

Lobo de Sa, F. D., Butkevych, E., Nattramilarasu, P. K., Fromm, A., Mousavi, S., Moos, V., et al. (2019). Curcumin mitigates immune-induced epithelial barrier dysfunction by campylobacter jejuni. *Int. J. Mol. Sci.* 20, 4830. doi:10.3390/ijms20194830

Martinez-Palomo, A., Erlij, D., and Bracho, H. (1971). Localization of permeability barriers in the frog skin epithelium. *J. Cell. Biol.* 50 (2), 277–287. doi:10.1083/jcb.50.2.277

Stoughton, R. B. (1957). Mechanisms of blister formation. *Arch. Dermatol.* 76 (5), 584. doi:10.1001/archderm.1957.01550230050008

Strebel, S. J., Burbank, K. M., Tullar, J. M., Jenkins, M. D., and Caroom, C. (2020). A retrospective analysis of the aspiration of fracture blisters. *J. Clin. Orthop. trauma* 11 (Suppl. 1), S171–S173. doi:10.1016/j.jcot.2019.11.002

Uebbing, C. M., Walsh, M., Miller, J. B., Abraham, M., and Arnold, C. (2011). Fracture blisters. *West. J. Emerg. Med.* 12 (1), 131–133.

Van Itallie, C. M., and Anderson, J. M. (2014). Architecture of tight junctions and principles of molecular composition. *Seminars Cell. & Dev. Biol.* 36, 157–165. doi:10.1016/j.semcdb.2014.08.011

Whittembury, G., and Rawlins, F. A. (1971). Evidence of a paracellular pathway for ion flow in the kidney proximal tubule. Electromicroscopic demonstration of lanthanum precipitate in the tight junction. *Pflugers. Arch.* 330 (4), 302–309. doi:10.1007/bf00588582

frontiers | Frontiers in Bioengineering and Biotechnology

TYPE Review
PUBLISHED 22 August 2022
DOI 10.3389/fbioe.2022.978283

OPEN ACCESS

EDITED BY
Jingfeng Li,
Wuhan University, China

REVIEWED BY
Dongyang Qian,
Harvard Medical School, United States
Guohui Liu,
Huazhong University of Science and Technology, China

*CORRESPONDENCE
Hongmou Zhao,
zhaohongmou@xiyi.edu.cn

†These authors have contributed equally to this work

SPECIALTY SECTION
This article was submitted to Preclinical Cell and Gene Therapy, a section of the journal Frontiers in Bioengineering and Biotechnology

RECEIVED 25 June 2022
ACCEPTED 19 July 2022
PUBLISHED 22 August 2022

CITATION
Wen X, Wang J, Wang Q, Liu P and Zhao H (2022), Interaction between N6-methyladenosine and autophagy in the regulation of bone and tissue degeneration.
Front. Bioeng. Biotechnol. 10:978283.
doi: 10.3389/fbioe.2022.978283

Interaction between N6-methyladenosine and autophagy in the regulation of bone and tissue degeneration

Xiaodong Wen†, Junhu Wang†, Qiong Wang, Peilong Liu and Hongmou Zhao*

Department of Foot and Ankle Surgery, Honghui Hospital of Xi'an Jiaotong University, Xi'an, China

Bone and tissue degeneration are the most common skeletal disorders that seriously affect people's quality of life. N6-methyladenosine (m6A) is one of the most common RNA modifications in eukaryotic cells, affecting the alternative splicing, translation, stability and degradation of mRNA. Interestingly, increasing number of evidences have indicated that m6A modification could modulate the expression of autophagy-related (ATG) genes and promote autophagy in the cells. Autophagy is an important process regulating intracellular turnover and is evolutionarily conserved in eukaryotes. Abnormal autophagy results in a variety of diseases, including cardiomyopathy, degenerative disorders, and inflammation. Thus, the interaction between m6A modification and autophagy plays a prominent role in the onset and progression of bone and tissue degeneration. In this review, we summarize the current knowledge related to the effect of m6A modification on autophagy, and introduce the role of the crosstalk between m6A modification and autophagy in bone and tissue degeneration. An in-depth knowledge of the above crosstalk may help to improve our understanding of their effects on bone and tissue degeneration and provide novel insights for the future therapeutics.

KEYWORDS

degenerative, disease, M6A, autophagy, mRNA, osteoporosis

1 Introduction

Bone and tissue degeneration are common disorders with societal and economic impacts. The most common skeletal degeneration includes osteoporosis, arthritis, and lumbar muscle degeneration, and the common tissue disorders include intervertebral disc degeneration (IVDD) and disc herniation. The above degenerative disorders are characterized by dysfunctional bone- or tissue-derived stem or progenitor cells, and aberrant activation of signaling pathways such as the PTEN, WNT, SIRT1 pathways, and other related signaling pathways (Xiong et al., 2019a; Mi et al., 2020a; Zhang et al., 2023). Currently, researchers in the field of degeneration have focused on discovering the molecular mechanisms mediating the regeneration process and developing new

therapeutic strategies for improving the health of patients diagnosed with bone and tissue degeneration (Xiong et al., 2019b; Yu et al., 2020).

N6-methyladenosine (m6A) is one of the most prominent post-transcriptional modifications in eukaryotic mRNA (Mi et al., 2020b; Ren et al., 2022). m6A functionally regulates the eukaryotic transcriptome by influencing mRNA splicing, export, subcellular localization, translation, stability, and decay. Thus, aberrant m6A methylation modulates biological processes and promotes human diseases (Li et al., 2022a). Numerous studies have revealed that m6A methylation plays a crucial role in the regulation of the degeneration process and mediates the occurrence and progression of multiple degeneration-related disorders (Li et al., 2022b; Peng et al., 2022). Intriguingly, prior studies reported that epigenetic modifications including m6A methylation played a prominent role in autophagy regulation (Tang et al., 2022; Wilkinson et al., 2022). Moreover, m6A modification has been reported to directly regulate the expression of autophagy-related (ATG) genes and modulate the cellular autophagy level, and the effects of the m6A methylation on autophagy are dependent on the disease context (Han et al., 2021).

In this review, we aim to summarize the current findings related to the effect of m6A modification on autophagy, and introduce the crosstalk between m6A modification and autophagy with regards to bone and tissue degeneration. An in-depth knowledge of the m6A modification-autophagy axis may expand our understanding of their effects on bone and tissue degeneration and provide novel insights for developing novel therapeutic strategies in the future.

2 The current sight of m6A modifications

m6A modification is one of the most abundant modifications in eukaryotic mRNA and is regulated by both m6A methyltransferase and demethylase, which are specifically recognized and bound by the m6A recognition protein (Chen et al., 2022a). m6A modification is dynamically controlled by "writers", "erasers", and the "readers", which are the main methylation-related reading proteins (Table 1) (Shen et al., 2022a). m6A modification affects different stages of mRNA processing including its splicing, nuclear output, stability and translation, and plays a crucial role in gene expression (Zheng et al., 2022). In recent years, owing to the continuous development of methylated RNA immunoprecipitation technology (MeRIP), methylated RNA immunoprecipitation sequencing (MERIP-seq), liquid chromatography-tandem mass spectrometry (LC-MS/MS) and high-throughput sequencing, the methylation modification sites and distribution can be thoroughly identified and analyzed (Sun et al., 2022; Wang et al., 2022). Currently, m6A modifications have been reported to be involved in the modulation of a variety of chronic inflammatory conditions, pathological processes, and metabolism-related diseases (Grenov et al., 2022; Yang et al., 2022).

2.1 Enzymes involved in m6A modifications

m6A "Writers", the m6A methyltransferase complex, catalyzes the transfer of methyl groups from S-adenosyl methionine (SAM) to the nitrogen atom at the 6th position of adenine (Yu et al., 2021). m6A writers includes METTL3, METTL14, WTAP, KIAA1429 (VIRMA), RBM15, HAKAI, ZC3H13 (KIAA0853), and METTL16 (Qi et al., 2022). The METTL3-METTL14 methyltransferase complex has been well-documented for its regulatory role in m6A methylation (Liu et al., 2014; Wang et al., 2016). An excellent piece of previous work has suggested that METTL3 primarily functioned as the catalytic core, while METTL14 provided the RNA-binding platform, providing a prominent framework for the functional research of m6A methylation (Wang et al., 2016). Furthermore, another study revealed that METTL3 could interact with the homologous protein METTL14, and form a heterodimer complex, and that the METTL3/METTL14 complex co-catalyzed m6A modification of the target RNA (Liu et al., 2014). In addition to the METTL3-METTL14 methyltransferase complex, m6A-METTL-associated protein complex (MAPC) was also widely reported to be involved in the initiation of m6A modification. The MAPC is mainly formed by the interaction of the junction proteins including WTAP, KIAA1429, RBM15, ZC3H13 and HAKAI (Zhang et al., 2022). Although the RNA splice factor WTAP, has no methyltransferase activity, it acts as a connector protein to recruit the m6A-METTL complex to localize at the nuclear speckle, and thereby regulates the location of m6A modification (Paramasivam et al., 2021). Increasing number of studies have reported new m6A "writers", such as METTL5, METTL16, and ZCCHC4 (Oerum et al., 2021; Ruszkowska, 2021), suggesting that RNA methyltransferases may include the reported proteins as well as other components, which need to be identified.

m6A "erasers" are able to "elucidate" m6A modifications of the target RNA. Up to date, the fat mass and obesity associated protein (FTO) and ALKB homolog 5 (ALKBH5) are the main components of the m6A demethylases (Shen et al., 2022b). FTO-mediated m6A demethylation has been widely found in multiple biological processes (Li et al., 2017; Wang et al., 2021; Chen et al., 2022b). Li et al. (Li et al., 2017) demonstrated that FTO had a prominent oncogenic role in the development of acute myeloid leukemia (AML) in an m6A-dependent manner. Specifically, FTO promoted leukemic cell transformation and leukemogenesis, and suppressed all-trans-retinoic acid-mediated AML cell differentiation, through the reduction of

m6A levels in ASB2 and RARA mRNA transcripts (Li et al., 2017). In bone homeostasis, it was reported that FTO was able to markedly suppress the osteoblastic differentiation of bone marrow derived mesenchymal stem cells (BMSCs) through the demethylation of the m6A modification of runt related transcription factor 2 (Runx2) mRNA (Wang et al., 2021). Intriguingly, Chen et al. (Chen et al., 2022b) found that FTO enhanced the osteogenic differentiation of BMSCs by reducing the stability of PPARG mRNA in an YTHDF1-dependent manner. These seemingly contradictory findings suggest that the role of FTO in regulating bone formation requires further in-depth and accurate investigation. As the second class of m6A "erasers", ALKBH5 is a Fe^{2+} and α -ketoglutarate-dependent non-heme oxygenase, with a strong ability to demethylate m6A methylation of mRNA (Yu et al., 2022). Up-regulation of ALKBH5 was found to promote demethylate in osteosarcoma cells and suppress cell proliferation and migration, which suggested that ALKBH5 could serve as a potential therapeutic target for treating human osteosarcoma (Yang et al., 2022).

The m6A "readers" can selectively recognize the m6A methylation modifications in the target RNA, and participate in various of stages of RNA metabolism (Zhang and Su, 2022). "Readers" include proteins containing YTH domains (YTHDF1/2/3 and YTHDC1/2), heterogeneous ribonucleoproteins including heterogenous nuclear ribonucleoprotein (HNRNP) C (HNRNPC), G (HNRNPG), and A2B1 (HNRNPA2B1), and insulin-like growth factor 2 binding proteins (IGF2BPs), which are members of a protein family closely associated with several ageing diseases (Li et al., 2022c; Li et al., 2022d). Different "readers" have different cellular localizations and thus perform multiple biological functions (Li et al., 2022d). YTH domain family protein 1 (YTHDF1) initiates RNA translation by interacting with the translation initiation factors and ribosomes, whereas the YTH domain family protein 2 (YTHDF2) selectively binds to m6A modified transcripts and promotes their degradation (Li et al., 2022c). YTHDF1/2 and YTHDF3 play synergistic roles in promoting YTHDF1-mediated translation and suppress YTHDF2-mediated m6A modification (Li et al., 2022d). For example, it was reported that YTHDF2 induced an oncogenic and drug-desensitizing effects in a m6A modification-dependent manner, and could potentially serve as an immune modulating target for intrahepatic cholangiocarcinoma therapy (Huang et al., 2022).

2.2 Effect of m6A modifications on mRNA metabolism

mRNA transcription is the process that initiates protein synthesis, and the post-transcriptional modulation of mRNA is controlled by a wide variety of molecular mechanisms. Generally, m6A methylation has been demonstrated to regulate multiple stages of mRNA metabolism (Pan et al., 2021; Wu et al., 2021; Chen et al., 2022c). Chen et al. (Chen et al., 2022c) performed a comprehensive analysis of the relationship between METTL16-mediated m6A methylation and IVDD, and showed that the elevated levels of METTL16 impaired the balance between splicing, maturation, and degradation of MAT2A pre-mRNA and exacerbated IVDD. Furthermore, as the primary demethylase, ALKBH5 was found to inhibit the m6A modification of FOXO3 and enhance its stability (Wu et al., 2021). Here, the anti-tumor effects of ALKBH5 were investigated in-depth, which showed that downregulation of ALKBH5 was associated with poor prognosis in colorectal cancer patients, and revealed that targeting the FOXO3/miR-21/SPRY2 signaling axis could be of therapeutic value for colorectal cancer patients (Wu et al., 2021). Similarly, the critical role of m6A "readers" in mRNA regulation has been well-documented (Pan et al., 2021; Xu et al., 2022). The recent study from Xu et al. (Xu et al., 2022) demonstrated the relationship between YTHDF2 expression and the activation of mTOR/AKT signaling pathway, and showed that the up-regulation of YTHDF2 induced the expression of mTOR mRNA and exacerbated the development of lung squamous cell carcinoma.

2.3 Effect of m6A modifications on the maturation of non-coding RNAs

Non-coding RNAs include rRNA, tRNA, snRNA, snoRNA, miRNA, lncRNA, and circRNA. They have a variety of known functions, and at the same time, some of the non-coding RNAs have unknown functions. It was widely reported that m6A methylation is involved in mediating cell proliferation by the induction of miRNA maturation, and the translation and degradation of circRNA, and by altering the stability of lncRNAs (Lin et al., 2020a; Du et al., 2022; Liu and Jiang, 2022; Yan et al., 2022). METTL3-mediated m6A modification has been reported to promote the maturation of miR-146a-5p, which exacerbates the development of bladder cancer (Yan et al., 2022). Furthermore, METTL3 was previously demonstrated to enhance the binding ability of pri-miRNA-589–5p with DGCR8, promoting the malignant progression of hepatoma (Liu and Jiang, 2022). Similarly, a recent study indicated that deoxycholic acid could suppress tumor development by decreasing the maturation of miR-92b-3p in a m6A-dependent manner (Lin et al., 2020a). Moreover, m6A modification was also reported to regulate the translation and degradation of circRNA (Du et al., 2022). circ_0095868 has been identified as a new oncogenic non-coding RNA that was significantly over-expressed in hepatocellular carcinoma (Du et al., 2022). Mechanistically, the m6A "reader" IGF2BP1 was shown to bind to circ_0095868 and promote the stability of circ_0095868 (Du et al., 2022). The role of m6A modification in lncRNA metabolism has also been well-documented (Dai et al.,

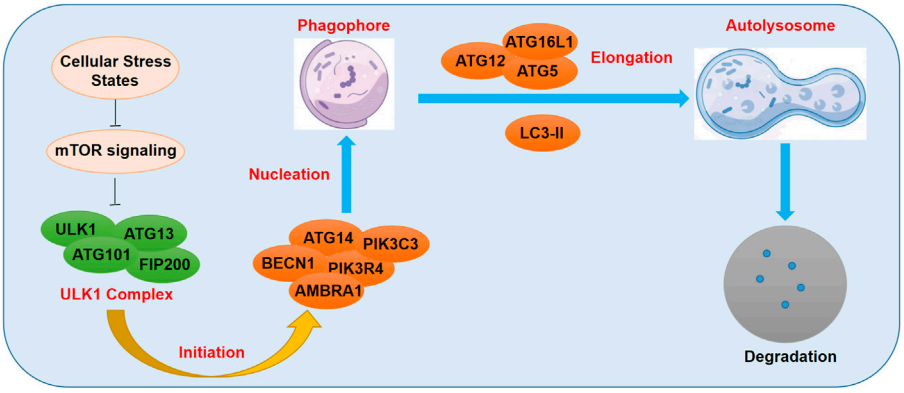

FIGURE 1
Schematic diagram of m6A methylation regulating autophagy.

2022). A recent study from Dai et al. (Dai et al., 2022) reported that METTL16 could target the lncRNA RAB11B-AS1, and impair its stability by elevating the level of m6A. All these findings indicate the strong role of m6A methylation in regulating non-coding RNAs metabolism and function.

3 Interaction between m6A and autophagy

3.1 Overview of autophagy

Autophagosome is a double-membrane-bound structure which is an important hallmark of the initiation of autophagy, having the ability to bind to the target cellular components (Affortit et al., 2022). Tthe autophagosomes deliver the detrimental cellular components to the lysosome for enzymolysis and degradation (Affortit et al., 2022). A wide range of ATG genes were previously demonstrated to be involved in this regulatory process (Zhang and Klionsky, 2022). Cellular stress states such as oxidative stress injury, hypoxia, and severe nutritional deficiency, were reported to suppress the activity of mTOR complex and activate the Unc-51 like kinase 1/2 (ULK1/2) signaling (Zhang and Klionsky, 2022). The activated ULK1/2 kinase could then induce the formation of FIP200-ATG13 complex, which further increased the level of phosphorylated ULK protein (Zhang and Klionsky, 2022). Subsequently, FIP200-ATG13 complex and the activated phosphorylated ULK proteins recruited more ATG proteins and promoted the formation of double-membrane autophagosomes (Affortit et al., 2022; Deretic and Lazarou, 2022; Zhang and Klionsky, 2022). LC3-II, one of the members of the LC3 family, has been well-documented to promote the formation of autolysosomes through the fusion of the autophagosomes to the lysosomes (Yao et al., 2022), which is a delicately-controlled dynamic process called the autophagy flux (Figure 1). Currently, emerging evidence has indicated that m6A methylation played a prominent role in the modulation of autophagy, and that the m6A-autophagy axis was dependent on the disease context.

3.2 Association between m6A and autophagy

m6A modification and the related factors regulate autophagy by modulating ATG expression and autophagy-related signaling pathways (Lin et al., 2020b; Li et al., 2020; Shen et al., 2022c). Li et al. (Li et al., 2020) found that the demethylase ALKBH5, suppressed the level of m6A modification of FIP200 mRNA and induced the expression of FIP200. The FIP200-mediated autophagy flux could subsequently reduce the apoptotic rate of nucleus pulposus cells (NPCs), and thereby ameliorate the development of IVDD (Li et al., 2020). Furthermore, Shen et al. (Shen et al., 2022c) reported that the down-regulation of m6A modification by FTO overexpression suppressed autophagy, which further alleviated liver fibrosis by inducing ferroptosis in hepatic stellate cells. Similarly, METTL3 has been shown to promote the methylation of FOXO3 and induce its binding to YTHDF1 to promote the translation of FOXO3 mRNA, which further inhibited the expression of ATG and suppressed autophagy (Lin et al., 2020b).

It is widely known that the dysregulation of autophagy caused diseases, many of which were closely associated with bone and tissue degeneration. Prior studies have revealed the marked impairment of autophagy in degenerative tissues (Zhong et al., 2022). Enhanced autophagy flux ameliorates oxidative stress, alleviates the progression of degenerative alterations, and enhances the cellular regenerative activity (Yao et al., 2018; Zheng et al., 2021). Increasing number of studies have indicated that m6A-mediated autophagy was involved in the

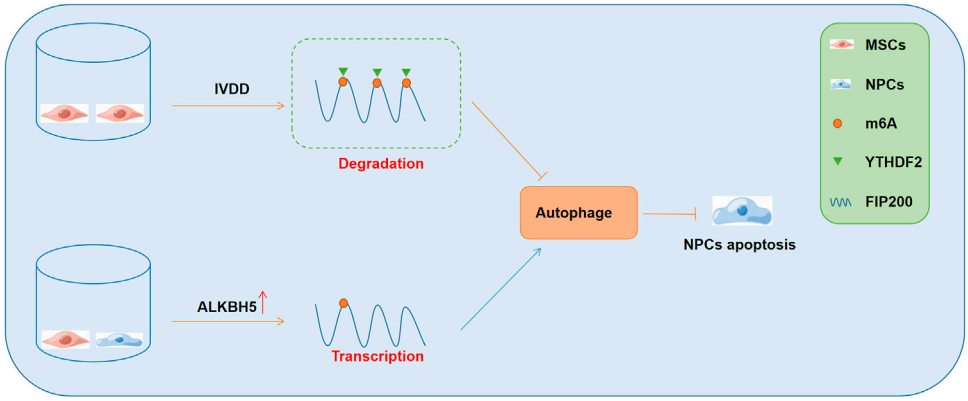

FIGURE 2
The role of m6A-autophagy axis in the regulation of IVDD development and the underlying mechanisms. NPCs, nucleus pulposus cells; IVDD, intervertebral disc degeneration; MSCs, mesenchymal stem cells.

regulation of IVDD and other degenerative diseases (Yao et al., 2018). Taken together, impaired autophagy is associated with the development of degenerative diseases, wherein the m6A autophagy axis plays a critical regulatory role in this process.

4 Role of m6A-autophagy axis in the regulation of degenerative diseases

Degenerative changes in NPCs are known to aggravate IVDD, which is the main cause of lower back pain (He et al., 2022). It has been shown that autophagy played a beneficial role in preventing the degeneration of NPCs and markedly ameliorated the progression of IVDD (Li et al., 2021). Similarly, senescence and dysregulation of MSCs are the most prominent reasons for the onset and progression of osteoporosis. Therefore, by enhancing autophagy, cellular senescence and osteogenic differentiation can be significantly rejuvenated.

A recent study showed that the co-culture of MSCs and NPCs elevated the expression of the demethylase ALKBH5, and inhibited m6A modification, which then enhanced the stability of FIP200 and subsequently promoted autophagy (Li et al., 2020). Furthermore, the enhanced autophagy was found to significantly promote the survival of NPCs and ameliorate the development of IVDD (Li et al., 2020). Mechanistically, in the cellular model of IVDD, m6A modification of FIP200 mRNA occurred, and the m6A "reader" YTHDF2 bound to the modified FIP200 transcripts and impaired their stability. However, in the co-culture model with MSCs and NPCs, MSCs significantly promoted the expression of AKLBH5 in the NPCs, which subsequently demethylated the FIP200 mRNAs and prevented their degradation. Consequently, the FIP200-mediated autophagy activity was promoted, which enhanced the survival of NPCs (Figure 2). In the cellular and animal models of osteoarthritis (OA), METTL3 expression was found to be suppressed (He et al., 2022). Furthermore, METTL3 was found to significantly inhibit inflammation-induced apoptosis and autophagy in chondrocytes and was beneficial for delaying the progression of OA (He et al., 2022). Mechanistically, the inhibition of METTL3 decreased the levels of m6A modified BCL-2 and impaired the YTHDF1-mediated mRNA transcription of BCL-2 (He et al., 2022). These findings indicated that METTL3 suppressed apoptosis and autophagy of chondrocytes under inflammatory conditions through the regulation of the m6A-autophagy axis.

5 Future perspectives

In summary, the above studies highlight that m6A modification is closely associated with the autophagy process. The up-regulation or suppression of autophagy by m6A methylation mainly depends on the level of m6A, the function of the downstream targets, and the changes in target RNA after methylation. Currently, a large number of studies have demonstrated that m6A modification could regulate the initiation and activation of autophagy by modulating the expression of ULK1, FIP200, and ATG5, ATG7, respectively. Although several researchers have focused on the molecular mechanisms involved, further in-depth studies are urgently needed to elucidate the interaction between m6A modification and autophagy under different pathological conditions.

Currently, the majority of studies have focused on the mediators of m6A. However, the direct regulatory mechanisms of m6A on its downstream targets are still unclear. For example, in hypoxia-induced cancer cells, YTHDF1 was found to enhance autophagy in hepatoma carcinoma cells by enhancing the translation of ATG2A and

TABLE 1 The common "Writers", "Erasers", and "Readers" of m6A methylation.

Category	Genes	Function
Writer	METTL3, METTL14, METTL16, WTAP, KIAA1492,RBM15, HAKAI	Catalyze RNA methylation *in vitro* and *in vivo*
Eraser	FTO, ALKBH5	• Mediate the demethylation of m6A •
Reader	YTHDF1, YTHDF2, YTHDF3	Recognize the information of RNA methylation modification and participate in the translation and degradation of downstream RNA

ATG14 (Li et al., 2021). Whether YTHDF1 could directly affect the expression of ATG2A and ATG14 in an m6A-independent manner and how the changes in m6A regulated ATG2A and ATG14, are topics that need further in-depth research. Additionally, the biggest challenge for revealing the interplay between m6A and autophagy in degenerative diseases is that there are often multiple functions of m6A in different diseases. m6A methylation may act as a "double-edged sword". For example, m6A not only inhibits the occurrence of IVDD by amelioration of apoptosis in NPCs (Li et al., 2020), but also aggravates apoptosis by inhibiting autophagy (Wang et al., 2020; Chen et al., 2021a; Chen et al., 2021b). The effect of m6A-autophagy axis in various degenerative diseases and the associated mechanisms need further investigation.

The interaction between m6A methylation and autophagy is a attractive topic in cellular biology research; in-depth understanding of the regulators of RNA modification expands the knowledge of the underlying molecular mechanisms. However, more in-depth explorations are required to develop novel therapeutic strategies based on the interaction between m6A methylation and autophagy.

Author contributions

XW and JW wrote the manuscript; QW and PL reviewed some papers and participated in the preparation of the manuscript; HZ provided the idea and supervised this study.

Funding

HZ, Key R & D plan of Shaanxi Province (No. 2021SF-025), Free exploration project of Xi'an Jiaotong University (No. xzy012022130); XW, Key R & D plan of Shaanxi Province (No. 2022SF-532)

Acknowledgments

The authors would like to thank all the reviewers who participated in the review and MJEditor (www.mjeditor.com) for its linguistic assistance during the preparation of this manuscript.

Conflict of interest

The authors declare that the research was conducted in the absence of any commercial or financial relationships that could be construed as a potential conflict of interest.

Publisher's note

All claims expressed in this article are solely those of the authors and do not necessarily represent those of their affiliated organizations, or those of the publisher, the editors and the reviewers. Any product that may be evaluated in this article, or claim that may be made by its manufacturer, is not guaranteed or endorsed by the publisher.

Supplementary material

The Supplementary Material for this article can be found online at: https://www.frontiersin.org/articles/10.3389/fbioe.2022.978283/full#supplementary-material

References

Affortit, C., Blanc, F., Nasr, J., Ceccato, J. C., Markossian, S., Guyot, R., et al. (2022). A disease-associated mutation in thyroid hormone receptor α1 causes hearing loss and sensory hair cell patterning defects in mice. *Sci. Signal.* 15, eabj4583. doi:10.1126/scisignal.abj4583

Chen, L., Zhang, M., Chen, P., Xiong, X. f., Liu, P. q., Wang, H. b., et al. (2022). The m6A demethylase FTO promotes the osteogenesis of mesenchymal stem cells by downregulating PPARG. *Acta Pharmacol. Sin.* 43, 1311–1323. doi:10.1038/s41401-021-00756-8

Chen, P., Shi, G., Liu, T., Li, B., Jiang, S. D., Zheng, X. F., et al. (2022). Oxidative stress aggravates apoptosis of nucleus pulposus cells through m6A modification of MAT2A pre-mRNA by METTL16. *Oxid. Med. Cell. Longev.* 2022, 1–15. doi:10.1155/2022/4036274

Chen, X., Wang, J., Tahir, M., Zhang, F., Ran, Y., Liu, Z., et al. (2021). Current insights into the implications of m6A RNA methylation and autophagy interaction in human diseases. *Cell Biosci.* 11, 147. doi:10.1186/s13578-021-00661-x

Chen, Y., Wang, J., Xu, D., Xiang, Z., Ding, J., Yang, X., et al. (2021). m^{6}A mRNA methylation regulates testosterone synthesis through modulating autophagy in Leydig cells. *Autophagy* 17, 457–475. doi:10.1080/15548627.2020.1720431

Chen, Y., Wu, Y., Zhu, L., Chen, C., Xu, S., Tang, D., et al. (2022). METTL3-Mediated N6-methyladenosine modification of Trim59 mRNA protects against sepsis-induced acute respiratory distress syndrome. *Front. Immunol.* 13, 897487. doi:10.3389/fimmu.2022.897487

Dai, Y., Liu, Y., Li, J., Chen, M. t., Huang, M., Wang, F., et al. (2022). METTL16 promotes hepatocellular carcinoma progression through downregulating RAB11B-AS1 in an m6A-dependent manner. *Cell. Mol. Biol. Lett.* 27, 41. doi:10.1186/s11658-022-00342-8

Deretic, V., and Lazarou, M. (2022). A guide to membrane atg8ylation and autophagy with reflections on immunity. *J. Cell Biol.*, e202203083. undefined. doi:10.1083/jcb.202203083

Du, A., Li, S., Zhou, Y., Disoma, C., Liao, Y., Zhang, Y., et al. (2022). M6A-mediated upregulation of circMDK promotes tumorigenesis and acts as a nanotherapeutic target in hepatocellular carcinoma. *Mol. Cancer* 21, 109. doi:10.1186/s12943-022-01575-z

Grenov, A., Hezroni, H., Lasman, L., Hanna, J. H., and Shulman, Z. (2022). YTHDF2 suppresses the plasmablast genetic program and promotes germinal center formation. *Cell Rep.* 39, 110778. doi:10.1016/j.celrep.2022.110778

Han, L., Lei, G., Chen, Z., Zhang, Y., Huang, C., and Chen, W. (2021). IGF2BP2 regulates MALAT1 by serving as an N6-methyladenosine reader to promote NSCLC proliferation. *Front. Mol. Biosci.* 8, 780089. doi:10.3389/fmolb.2021.780089

He, Y., Wang, W., Xu, X., Yang, B., Yu, X., Wu, Y., et al. (2022). Mettl3 inhibits the apoptosis and autophagy of chondrocytes in inflammation through mediating Bcl2 stability via Ythdf1-mediated m6A modification. *Bone* 154, 116182. doi:10.1016/j.bone.2021.116182

Huang, C., Zhu, Y., Xu, Q., Chen, S., Huang, Y., Zhao, G., et al. (2022). YTHDF2 promotes intrahepatic cholangiocarcinoma progression and desensitises cisplatin treatment by increasing CDKN1B mRNA degradation. *Clin. Transl. Med.* 12, e848. doi:10.1002/ctm2.848

Li, G., Luo, R., Zhang, W., He, S., Wang, B., Liang, H., et al. (2022). m6A hypomethylation of DNMT3B regulated by ALKBH5 promotes intervertebral disc degeneration via E4F1 deficiency. *Clin. Transl. Med.* 12, e765. doi:10.1002/ctm2.765

Li, G., Ma, L., He, S., Luo, R., Wang, B., Zhang, W., et al. (2022). WTAP-mediated m6A modification of lncRNA NORAD promotes intervertebral disc degeneration. *Nat. Commun.* 13, 1469. doi:10.1038/s41467-022-28990-6

Li, G., Song, Y., Liao, Z., Wang, K., Luo, R., Lu, S., et al. (2020). Bone-derived mesenchymal stem cells alleviate compression-induced apoptosis of nucleus pulposus cells by N6 methyladenosine of autophagy. *Cell Death Dis.* 11, 103. doi:10.1038/s41419-020-2284-8

Li, H., Zhong, Y., Cao, G., Shi, H., Liu, Y., Li, L., et al. (2022). METTL3 promotes cell cycle progression via m^{6}A/YTHDF1-dependent regulation of *CDC25B* translation. *Int. J. Biol. Sci.* 18, 3223–3236. doi:10.7150/ijbs.70335

Li, Q., Ni, Y., Zhang, L., Jiang, R., Xu, J., Yang, H., et al. (2021). HIF-1α-induced expression of m6A reader YTHDF1 drives hypoxia-induced autophagy and malignancy of hepatocellular carcinoma by promoting ATG2A and ATG14 translation. *Signal Transduct. Target. Ther.* 6, 76. doi:10.1038/s41392-020-00453-8

Li, S., Zhang, L., and Zou, G., (2022). Infralimbic YTHDF1 is necessary for the beneficial effects of acute mild exercise on auditory fear extinction retention. *Cereb. Cortex*. undefined: undefined.

Li, Z., Weng, H., Su, R., Weng, X., Zuo, Z., Li, C., et al. (2017). FTO plays an oncogenic role in acute myeloid leukemia as a N 6 -methyladenosine RNA demethylase. *Cancer Cell* 31, 127–141. doi:10.1016/j.ccell.2016.11.017

Lin, R., Zhan, M., Yang, L., Wang, H., Shen, H., Huang, S., et al. (2020). Deoxycholic acid modulates the progression of gallbladder cancer through N6-methyladenosine-dependent microRNA maturation. *Oncogene* 39, 4983–5000. doi:10.1038/s41388-020-1349-6

Lin, Z., Niu, Y., Wan, A., Chen, D., Liang, H., Chen, X., et al. (2020). RNA m ^{6} A methylation regulates sorafenib resistance in liver cancer through FOXO 3-mediated autophagy. *EMBO J.* 39, e103181. doi:10.15252/embj.2019103181

Liu, J., and Jiang, K. (2022). METTL3-mediated maturation of miR-589-5p promotes the malignant development of liver cancer. *J. Cell. Mol. Med.* 26, 2505–2519. doi:10.1111/jcmm.16845

Liu, J., Yue, Y., Han, D., Wang, X., Fu, Y., Zhang, L., et al. (2014). A METTL3-METTL14 complex mediates mammalian nuclear RNA N6-adenosine methylation. *Nat. Chem. Biol.* 10, 93–95. doi:10.1038/nchembio.1432

Mi, B., Xiong, Y., Yan, C., Chen, L., Xue, H., Panayi, A. C., et al. (2020). Methyltransferase-like 3-mediated N6-methyladenosine modification of miR-7212-5p drives osteoblast differentiation and fracture healing. *J. Cell. Mol. Med.* 24, 6385–6396. doi:10.1111/jcmm.15284

Mi, B., Yan, C., Xue, H., Chen, L., Panayi, A. C., Hu, L., et al. (2020). Inhibition of circulating miR-194-5p reverses osteoporosis through wnt5a/β-catenin-dependent induction of osteogenic differentiation. *Mol. Ther. - Nucleic Acids* 21, 814–823. doi:10.1016/j.omtn.2020.07.023

Oerum, S., Meynier, V., Catala, M., and Tisne, C. (2021). A comprehensive review of m6A/m6Am RNA methyltransferase structures. *Nucleic Acids Res.* 49, 7239–7255. doi:10.1093/nar/gkab378

Pan, H., Pan, Z., Guo, F., Meng, F., Zu, L., Fan, Y., et al. (2021). MicroRNA-1915-3p inhibits cell migration and invasion by targeting SET in non-small-cell lung cancer. *BMC Cancer* 21, 1218. doi:10.1186/s12885-021-08961-8

Paramasivam, A., George, R., and Priyadharsini, J. V. (2021). Genomic and transcriptomic alterations in m6A regulatory genes are associated with tumorigenesis and poor prognosis in head and neck squamous cell carcinoma. *Am. J. Cancer Res.* 11, 3688–3697.

Peng, J., Zhan, Y., and Zong, Y. (2022). METTL3-mediated LINC00657 promotes osteogenic differentiation of mesenchymal stem cells via miR-144-3p/BMPR1B axis. *Cell Tissue Res.* 388, 301–312. doi:10.1007/s00441-022-03588-y

Qi, S., Mota, J., and Chan, S., (2022). NRNA binding to human METTL3-METTL14 restricts -deoxyadenosine methylation of DNA *in vitro*. *Elife* 11. undefined.

Ren, J., Li, Y., Wuermanbieke, S., Hu, S., and Huang, G. (2022). N6-methyladenosine (m6A) methyltransferase METTL3-mediated LINC00680 accelerates osteoarthritis through m6A/SIRT1 manner. *Cell Death Discov.* 8, 240. doi:10.1038/s41420-022-00890-0

Ruszkowska, A. (2021). METTL16, methyltransferase-like protein 16: Current insights into structure and function. *Int. J. Mol. Sci.* 22, 2176. undefined. doi:10.3390/ijms22042176

Shen, D., Wang, B., Gao, Y., Zhao, L., Bi, Y., Zhang, J., et al. (2022). Detailed resume of RNA m6A demethylases. *Acta Pharm. Sin. B* 12, 2193–2205. doi:10.1016/j.apsb.2022.01.003

Shen, M., Guo, M., Li, Y., Wang, Y., Qiu, Y., Shao, J., et al. (2022). m6A methylation is required for dihydroartemisinin to alleviate liver fibrosis by inducing ferroptosis in hepatic stellate cells. *Free Radic. Biol. Med.* 182, 246–259. doi:10.1016/j.freeradbiomed.2022.02.028

Shen, W., Zhu, M., Wang, Q., Zhou, X., Wang, J., Wang, T., et al. (2022). DARS-AS1 recruits METTL3/METTL14 to bind and enhance DARS mRNA m^{6}A modification and translation for cytoprotective autophagy in cervical cancer. *RNA Biol.* 19, 751–763. doi:10.1080/15476286.2022.2079889

Sun, S., Liu, Y., Zhou, M., Wen, J., Xue, L., Han, S., et al. (2022). PA2G4 promotes the metastasis of hepatocellular carcinoma by stabilizing FYN mRNA in a YTHDF2-dependent manner. *Cell Biosci.* 12, 55. doi:10.1186/s13578-022-00788-5

Tang, F., Chen, L., Gao, H., Xiao, D., and Li, X. (2022). m6A: An emerging role in programmed cell death. *Front. Cell Dev. Biol.* 10, 817112. doi:10.3389/fcell.2022.817112

Wang, J., Fu, Q., Yang, J., Liu, J. L., Hou, S. M., Huang, X., et al. (2021). RNA N6-methyladenosine demethylase FTO promotes osteoporosis through demethylating Runx2 mRNA and inhibiting osteogenic differentiation. *Aging (Albany NY)* 13, 21134–21141. doi:10.18632/aging.203377

Wang, X., Feng, J., Xue, Y., Guan, Z., Zhang, D., Liu, Z., et al. (2016). Structural basis of N(6)-adenosine methylation by the METTL3-METTL14 complex. *Nature* 534, 575–578. doi:10.1038/nature18298

Wang, X., Wu, R., Liu, Y., Zhao, Y., Bi, Z., Yao, Y., et al. (2020). m^{6}A mRNA methylation controls autophagy and adipogenesis by targeting *Atg5* and *Atg7*. *Autophagy* 16, 1221–1235. doi:10.1080/15548627.2019.1659617

Wang, Z., Pan, J., Hu, J., Zhang, J. Q., Huang, L., Huang, Y., et al. (2022). SRSF3-mediated regulation of N6-methyladenosine modification-related lncRNA ANRIL splicing promotes resistance of pancreatic cancer to gemcitabine. *Cell Rep.* 39, 110813. doi:10.1016/j.celrep.2022.110813

Wilkinson, E., Cui, Y., and He, Y. (2022). Roles of RNA modifications in diverse cellular functions. *Front. Cell Dev. Biol.* 10, 828683. doi:10.3389/fcell.2022.828683

Wu, X., Dai, M., Li, J., Cai, J., Zuo, Z., Ni, S., et al. (2021). m(6 A demethylase ALKBH5 inhibits cell proliferation and the metastasis of colorectal cancer by

regulating the FOXO3/miR-21/SPRY2 axis. *Am. J. Transl. Res.* 13, 11209–11222.

Xiong, Y., Cao, F., Hu, L., Yan, C., Chen, L., Panayi, A. C., et al. (2019). miRNA-26a-5p accelerates healing via downregulation of PTEN in fracture patients with traumatic brain injury. *Mol. Ther. - Nucleic Acids* 17, 223–234. doi:10.1016/j.omtn.2019.06.001

Xiong, Y., Mi, B., Liu, M., Xue, H., Wu, Q. p., and Liu, G. h. (2019). Bioinformatics analysis and identification of genes and molecular pathways involved in synovial inflammation in rheumatoid arthritis. *Med. Sci. Monit.* 25, 2246–2256. doi:10.12659/msm.915451

Xu, P., Hu, K., Zhang, P., Sun, Z. G., and Zhang, N. (2022). Hypoxia-mediated YTHDF2 overexpression promotes lung squamous cell carcinoma progression by activation of the mTOR/AKT axis. *Cancer Cell Int.* 22, 13. doi:10.1186/s12935-021-02368-y

Yan, R., Dai, W., Wu, R., Huang, H., and Shu, M. (2022). Therapeutic targeting m6A-guided miR-146a-5p signaling contributes to the melittin-induced selective suppression of bladder cancer. *Cancer Lett.* 534, 215615. doi:10.1016/j.canlet.2022.215615

Yang, Z., Cai, Z., Yang, C., Luo, Z., and Bao, X. (2022). ALKBH5 regulates STAT3 activity to affect the proliferation and tumorigenicity of osteosarcoma via an m6A-YTHDF2-dependent manner. *EBioMedicine* 80, 104019. doi:10.1016/j.ebiom.2022.104019

Yao, J., Qiu, Y., Frontera, E., Jia, L., Khan, N. W., Klionsky, D. J., et al. (2018). Inhibiting autophagy reduces retinal degeneration caused by protein misfolding. *Autophagy* 14, 1226–1238. doi:10.1080/15548627.2018.1463121

Yao, Y., Zhu, J., Qin, S., Zhou, Z., Zeng, Q., Long, R., et al. (2022). Resveratrol induces autophagy impeding BAFF-stimulated B-cell proliferation and survival by inhibiting the Akt/mTOR pathway. *Biochem. Pharmacol.* 202, 115139. doi:10.1016/j.bcp.2022.115139

Yu, D., Horton, J. R., Yang, J., Hajian, T., Vedadi, M., Sagum, C., et al. (2021). Human MettL3-MettL14 RNA adenine methyltransferase complex is active on double-stranded DNA containing lesions. *Nucleic Acids Res.* 49, 11629–11642. doi:10.1093/nar/gkab460

Yu, T., Wang, Z., You, X., Zhou, H., He, W., Li, B., et al. (2020). Resveratrol promotes osteogenesis and alleviates osteoporosis by inhibiting p53. *Aging (Albany NY)* 12, 10359–10369. doi:10.18632/aging.103262

Yu, T., Yao, L., Yin, H., Teng, Y., Hong, M., and Wu, Q. (2022). ALKBH5 promotes multiple myeloma tumorigenicity through inducing m^6A-demethylation of SAV1 mRNA and myeloma stem cell phenotype. *Int. J. Biol. Sci.* 18, 2235–2248. doi:10.7150/ijbs.64943

Zhang, L., and Su, X. (2022). Bioactive peptide inhibits acute myeloid leukemia cell proliferation by downregulating ALKBH5-mediated m6A demethylation of EIF4EBP1 and MLST8 mRNA. *Cell. Oncol.* 45, 355–365. doi:10.1007/s13402-022-00666-9

Zhang, N., Ding, C., Zuo, Y., Peng, Y., and Zuo, L. (2022). N6-methyladenosine and neurological diseases. *Mol. Neurobiol.* 59, 1925–1937. doi:10.1007/s12035-022-02739-0

Zhang, W., Zhou, X., Hou, W., Chen, E., Ye, C., Chen, M., et al. (2023). Reversing the imbalance in bone homeostasis via sustained release of SIRT-1 agonist to promote bone healing under osteoporotic condition. *Bioact. Mat.* 19, 429–443. doi:10.1016/j.bioactmat.2022.04.017

Zhang, Z., and Klionsky, D. J. (2022). CCT2, a newly identified aggrephagy receptor in mammals, specifically mediates the autophagic clearance of solid protein aggregates. *Autophagy* undefined, 1483–1485. doi:10.1080/15548627.2022.2083305

Zheng, Q., Shen, H., Tong, Z., Cheng, L., Xu, Y., Feng, Z., et al. (2021). A thermosensitive, reactive oxygen species-responsive, MR409-encapsulated hydrogel ameliorates disc degeneration in rats by inhibiting the secretory autophagy pathway. *Theranostics* 11, 147–163. doi:10.7150/thno.47723

Zheng, Y., Li, Y., Ran, X., Wang, D., Zheng, X., Zhang, M., et al. (2022). Mettl14 mediates the inflammatory response of macrophages in atherosclerosis through the NF-κB/IL-6 signaling pathway. *Cell. Mol. Life Sci.* 79, 311. doi:10.1007/s00018-022-04331-0

Zhong, H., Yang, C., Gao, Y., Cao, P., Tian, Y., Shen, X., et al. (2022). PERK signaling activation restores nucleus pulposus degeneration by activating autophagy under hypoxia environment. *Osteoarthr. Cartil.* 30, 341–353. doi:10.1016/j.joca.2021.11.005

frontiers | Frontiers in Bioengineering and Biotechnology

TYPE Review
PUBLISHED 10 October 2022
DOI 10.3389/fbioe.2022.1023877

OPEN ACCESS

EDITED BY
Yuan Xiong,
Huazhong University of Science and Technology, China

REVIEWED BY
Qizhao Huang,
Southern Medical University, China
Qicong Shen,
Naval Medical Universtity, China

*CORRESPONDENCE
Ming Yan,
yanming_spine@163.com
Zebing Hu,
zebinghu@fmmu.edu.cn
Bo Gao,
gaobofmmu@hotmail.com

†These authors have contributed equally to this work

SPECIALTY SECTION
This article was submitted to Preclinical Cell and Gene Therapy, a section of the journal Frontiers in Bioengineering and Biotechnology

RECEIVED 20 August 2022
ACCEPTED 27 September 2022
PUBLISHED 10 October 2022

CITATION
Wei B, Zhao Y, Li W, Zhang S, Yan M, Hu Z and Gao B (2022), Innovative immune mechanisms and antioxidative therapies of intervertebral disc degeneration.
Front. Bioeng. Biotechnol. 10:1023877.
doi: 10.3389/fbioe.2022.1023877

Innovative immune mechanisms and antioxidative therapies of intervertebral disc degeneration

Bingqian Wei[1,2†], Yingjing Zhao[3†], Weihang Li[1], Shilei Zhang[1], Ming Yan[1*], Zebing Hu[4*] and Bo Gao[1*]

[1]Institute of Orthopedic Surgery, Xijing Hospital, Air Force Medical University, Xi'an, China, [2]Basic Medical College, Air Force Medical University, Xi'an, China, [3]Department of Critical Care Medicine, Nanjing First Hospital, Nanjing Medical University, Nanjing, China, [4]The Key Laboratory of Aerospace Medicine, Ministry of Education, Air Force Medical University, Xi'an, China

Intervertebral disc degeneration (IDD) is the basic pathological process of many degenerative diseases of the spine, characterized by series of symptoms, among which low back pain (LBP) is the most common symptom that patients suffer a lot, which not only makes patients and individual families bear a huge pain and psychological burden, but also consumes a lot of medical resources. IDD is usually thought to be relevant with various factors such as genetic predisposition, trauma and aging, and IDD progression is tightly relevant with structural and functional alterations. IDD processes are caused by series of pathological processes, including oxidative stress, matrix decomposition, inflammatory reaction, apoptosis, abnormal proliferation, cell senescence, autophagy as well as sepsis process, among which the oxidative stress and inflammatory response are considered as key link in IDD. The production and clearance of ROS are tightly connected with oxidative stress, which would further simulate various signaling pathways. The phenotype of disc cells could change from matrix anabolism-to matrix catabolism- and proinflammatory-phenotype during IDD. Recent decades, with the relevant reports about oxidative stress and inflammatory response in IDD increasing gradually, the mechanisms researches have attracted much more attention. Consequently, this study focused on the indispensable roles of the oxidative stress and inflammatory response (especially macrophages and cytokines) to illustrate the origin, development, and deterioration of IDD, aiming to provide novel insights in the molecular mechanisms as well as significant clinical values for IDD.

KEYWORDS

intervertebral disc degeneration(IDD), inflammatory response, antioxidative therapies, macrophages, cytokines

1 Introduction

1.1 Background

Intervertebral disc degeneration (IDD) is the basic pathological process of many degenerative diseases of the spine, which is clinically manifested as spinal stenosis, vertebral segment instability, lumbar and leg pain, cervical spondylosis, intervertebral disc herniation etc., and the patient's nerve roots and spinal cord are compressed to produce a series of complications, among which low back pain (LBP) is the most common symptom that patients suffer a lot, which not only makes patients and individual families bear a huge pain and psychological burden, but also consumes a lot of medical resources (Li et al., 2021a). Existed studies believed that biomechanical property is the main factor to keep the spinal flexibility as well as mechanical stability (Lam et al., 2011), among them pilots are the main victims that usually suffer from serious damage to the cervical and lumbar vertebrae (Albermann et al., 2020). But increasing researches have suggested that in addition to biomechanical factors, the autoimmune system also behaves an essential role in the degeneration process of IDD, including oxidative stress, exosomes, inflammatory cytokines, etc. (Peng, 2008; Johnson et al., 2015; Li et al., 2021a; Xiang et al., 2022). Therefore, this study combined and focused on the researches about the roles of oxidative stress, cytokines mediums and inflammatory reaction on IDD in recent decades, aiming to provide novel insights in the molecular mechanisms, as well as guidance and references for the potential therapeutic strategies for IDD.

1.2 Structures of intervertebral disc

Intervertebral disc (IVD) is primarily comprised of three parts, including nucleus pulposus (NP), annulus fibrous ring (AF) and cartilage endplate (CEP). NP is a highly watery, jelly-shaped tissue in the middle part, with a dense network of collagen fibers located inside the NP, each layer of collagen fibers covered with a mucopolysacly protein complex and chondroitin sulfate, so that the nucleus of the medullary can bind to water, acting as a fulcrum in adjacent vertebral activity, like a ball, moving forward and backward with the flexion and extension of the spine (Le Maitre et al., 2007). AF is surrounded by almost concentric rings of fibers, containing three layers: outer, medium and inner, the outer layer is composed of collagen fiber bands, and the inner layer is composed of fiber cartilage bands, which are tightly attached to the CEP to keep the stability of the spine. The CEP contained fibrochondrite, located between the body of the vertebrae above and lower, which could withstand pressure and prevent the vertebrae from being overloaded by pressure (Kadow et al., 2015). Under physiological state, due to the special location of the NP that is surrounded by CEP and fibrous rings, the NP located in a closed space and is isolated from the immune systematic reactions, which is served as the largest immune privilege organ within body (Sun et al., 2020a).

1.3 Oxidative stress

Redox homeostasis is essential for the maintenance of physiological process in many cellular activities, the dysregulation of redox homeostasis would influence human health and is directly related to pathological conditions (Akanji et al., 2021). Within this process, oxidative stress is regarded as the imbalance situation between two different states, including the generation of active metabolites and free radicals [also known as reactive oxygen species (ROS) or oxidants] and the removal of the above substances by antioxidants. This imbalance has serious damage not only to biomolecules and cells, but also to the entire organism (Ďuračková, 2010). Increasing evidences have illustrated the pivotal roles of oxidative stress in the pathogenesis of various diseases including degenerative skeletal diseases (Kimball et al., 2021; Kulkarni et al., 2021; Zhao et al., 2021).

ROS is the product of normal cellular metabolism, which is mostly produced by mitochondrial respiratory chains (Poyton et al., 2009), which can respond to changes of environmental conditions inside/outside the cell and react accordingly to signaling pathway modulation. In endogenous metabolic reactions, ROS is mostly the normal product of molecular oxygen biological reduction, such as superoxide anions (O_2–), hydroxyl radicals (OH•), hydrogen peroxide (H_2O_2), and organic peroxides (Fridovich, 1978). However, the excessive accumulation of ROS by continuous environmental stress or other pathological processes *in vivo*, could induce and promote oxidative stress, which may cause damage to biological macromolecules like nucleic acids, carbohydrates proteins and lipids, and finally destroyed the cell structure and functions of body (Kumar et al., 2008; Fang et al., 2009; Venza et al., 2015).

Existed studies have reported the complex antioxidative system with different functions participated to protect the body from excess oxidants damage, among which the antioxidants behaved essential roles, such as glutathione peroxidase (GPx), superoxide dismutase (SOD), catalase and glutathione reductase (enzymatic antioxidants), and also vitamin C/D and glutathione (GSH) (non-enzymatic antioxidants) (Sies, 1991). The theoretical foundation have also provided guidelines in the treatment IDD (Feng et al., 2017).

1.4 Autoimmune theory

In 1977, Gertzbein proposed the hypothesis of autoimmune theory in IDD through a large number of

animal experiments and clinical studies, he found that degenerative disk overexpressed Toll-like receptors Toll-2 and Toll-4, which could be stimulated by the products of extracellular matrix and enhance the inflammatory and immune response; and the evidence for autoimmune mechanism in IDD came from the existence of cellular reaction through both lymphocyte transformation test and leukocyte-migration inhibition test (Gertzbein, 1977; Gertzbein et al., 1977). Bobechko and Hirshl reported the responses of regional lymph nodes of rabbits with ears implanted by autologous disc material (Bobechko and Hirsch, 1965). In the physiological state, the NP tissue is isolated from the body's immune monitor due to the encapsulation of the AF ring and the CEP, and has no direct contact with the peripheral circulation. When the IVD is damaged or injured, the NP tissue breaks through the encirclement of the AF ring and the posterior longitudinal ligament. While during repair process, the neovascular vessel grows into the NP tissue so that the NP tissue is in close contact with the immune system (Binch et al., 2014; Li et al., 2022). Glycoproteins and β proteins are served as antigens in the stroma of the NP, and the body may produce immune response under the continuous stimulation of these antigens, which is also involved the IVD of other segments, further causing degeneration of the IVD (Gertzbein, 1977).

2 Oxidative stress and antioxidative therapies in IDD

2.1 Interactions between oxidative stress/inflammation and IDD

As previously mentioned, there remained imbalance states between ROS production and clearance in degenerative discs. There were a great deal of evidences that ROS was widely participated in metabolic modulation, signaling transduction, cell death, cell aging, phenotypic transformation of IVD cells, which jointly to regulate the activity and functions of disc and further accelerate the development of IDD (Feng et al., 2017). Oxidative stress reactions caused by excessive ROS could further stimulate a variety of aberrant signaling pathways in IVD cells, like MAPK and NF-κB pathways, and ultimately strengthening both local and systemic oxidative stress (Li et al., 2021b; Chen et al., 2022; Zhu et al., 2022). The phenotype of IVD cells changed from matrix anabolism phenotype to matrix catabolism and pro-inflammatory phenotype, suggesting significant matrix loss and increased inflammation in IVD circumstances. In addition, IVD cells also secreted chemokines that enhanced inflammation by recruiting immune cells into the disc, which further secrete more cytokines and chemokines in turn, thus worsening the activity and functions of IVD cells, finally leading a vicious circle (Risbud and Shapiro, 2014; Li et al., 2022).

2.2 Antioxidative therapies in IDD

Glutathione (GSH) is a natural peptide and it's the primary antioxidant in living cells. Yang et al. (2014a) suggested that GSH could effectively prevent the harmful effects of H2O2 or IL-1β in NP, thereby inhibiting ROS production, apoptosis as well as matrix decomposition in human NP cells. N-Acetylcysteine (NAC) served as the progenitor of GSH, have been studied to prevent the progression of IDD by lowering ROS levels and weakening MAPK signaling pathway mediated by ROS or TNF-α in AF cells (Suzuki et al., 2015). At the same time, premature aging of IVD cells has also been improved: treatment with NAC could reverse the NP cell apoptosis and ECM degradation; within needle-induced disc degeneration in rat model, oral NAC inhibited oxidative stress, stromal catabolism, and inflammation. Additionally, commonly served as a supplement, NAC had few toxic side effects reports, which could be used as a great option for IVD degeneration treatment (Seol et al., 2021; Bai et al., 2022).

Resveratrol (RSV) was a polyphenol product which mainly existed in vegetation. Research by Li et al. reported the effective anabolic effects of RSV about IVD homeostasis on bovine: RSV could inhibit MMP-13 expression and promote proteoglycan synthesis in NP cells, which could also reverse the catabolism roles of IL-1 and bFGF which were responsible for oxidative stress, proliferation and apoptosis. They also elucidated the responses of multiple downstream cascade molecules after RSV activation, which made the roles of RSV better understand, such as anti-inflammatory, antioxidant and antiproliferative effects, etc. (Li et al., 2008). Among them, RSV could protect NP cells from degradation by elevating cell survival and functions, which may be related to the suppression of JAK/STAT3 phosphorylation and the decrease of IL-6 products (Wu et al., 2021). Previous studies have reported that epigallocatechin 3-gallate (EGCG), a polyphenol product existed in thea viridis, could inhibit the inflammation response of diagnostic cells *in vivo* or *in vitro*, which also displayed analgesic activity for disc-relevant radiculopathy in animals (Krupkova et al., 2014). Studies by Krupkova et al. have shown that EGCG activated PI3K/AKT signaling pathway, which was an important pro-activation mechanism under deadly oxidative stress (Krupkova et al., 2016). Combined with these biological effects and functions of EGCG mentioned above, we believed that EGCG could be further used to develop new therapies for oxidative stress in degenerative disc disease.

Pyrroloquinoline (PQQ) was a redox cofactor of bacterial dehydrogenase, which had the potential to eliminate ROS production and reduce apoptotic process. The results of Yang et al. showed that PQQ enabled NP cells to exhibit high cell viability, which inhibited excessive generation of ROS in rat NP cells induced by H_2O_2, and thereby protecting NP cells from apoptosis. It also antagonized downregulation of type II collagen and agrican in H_2O_2-induced NP cells. Therefore, PQQ could be

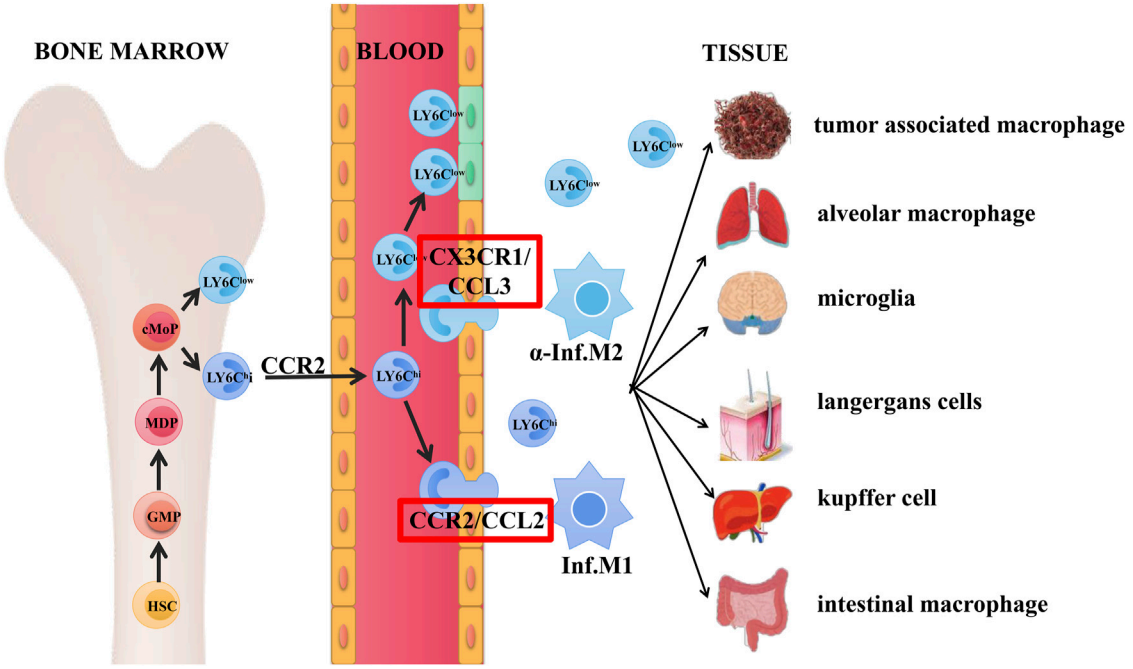

FIGURE 1
Origin and differentiation of macrophages. Hematopoietic stem cell (HSC)–derived GMPs promoted the generation of MDPs and subsequently enhanced cMoPs production, which was the direct progenitors of LY6C^{hi} and LY6C^{low} monocytes. LY6C^{hi} monocytes circulating in the blood relied on the CCR2-dependent extravasation.

regarded as potential lead compound in the prevention of IDD (Yang et al., 2015).

3 The roles of macrophages in the development of IDD

3.1 Origin and differentiation of macrophages

Mouse LY6C^{hi}/LY6C^{low} cells are the same as human CD14^{+}/CD14^{low}CD16^{+} monocyte/macrophage sub populations, respectively (Sun et al., 2020b). Present hematopoietic project pointed out that hematopoietic stem cell (HSC)–derived GMPs promoted the generation of MDPs and MDPs further enhanced cMoPs production, which was the direct progenitor of LY6C^{hi} and LY6C^{low} macrophages, and LY6C^{hi} macrophages circulating in blood mostly relied on the CCR2-dependent extravasation (Ginhoux and Jung, 2014; Guilliams et al., 2018).

Within the homeostatic state, LY6C^{hi} and LY6C^{low} macrophage sub populations in the circulation generated developmental continuum with different functions: Macrophage-like LY6C^{low} cells in the blood monitored the endothelial surface and enrolled neutrophils as needed to manipulate the reconstruction process; they were recruited together and then differentiated into different states like M2Mϕ, thereby secreting anti-inflammatory cytokines to promote tissue repair. By contrast, LY6C^{hi} monocytes served as "canonical monocytes", were clustered into inflammatory region and could be regarded as the progenitors of peripheral mononuclear phagocytes to behave roles. They would differentiate into mature inflammatory M1Mϕ, contributing to tissue degradation and T cell activation (Shi and Pamer, 2011; Yang et al., 2014b; Ginhoux and Jung, 2014; Varol et al., 2015). LY6C^{hi} macrophage could transform into diversity of cells under certain circumstances, like langerhans cells, microglia cells, kupffer cells, alveolar macrophages, and intestinal macrophage in different tissues. Besides, macrophages could also transform into tumor-associated macrophages with tumor development and metastasis functions (Gentek et al., 2014; Varol et al., 2015), the detailed developmental process of these subtypes and possible signaling pathways were shown in Figure 1.

As mentioned above, in the steady state, macrophage-like LY6C^{low} cells acted as patrol and monitored the intravascular dynamics, while LY6C^{hi} macrophages acted as "canonical monocytes" and were clustered into inflammation region. Ly6C^{low} macrophages were recruited together by interactive roles of CX3CR1/CCL3 pair through LAF/ICAM1 signaling pathway and thus transformed into M2Mϕ state, secreting

anti-inflammatory cytokines and finally enhanced the tissue restore (Cros et al., 2010). In the aspect of vascular inflammation, $LY6C^{hi}$ monocytes were activated and infiltrated into tissue by interaction roles of CCR2/CCL2(MPC-1) through VLA-1/VCAM1 transduction, which were then transformed into inflammatory M1Mϕ state, finally contributing to tissue deterioration and T cell stimulation (Yang et al., 2014b).

3.2 Different roles of M1 and M2 in IDD

Basically, phenotype with high levels of IL-12, IL-23, and low levels of IL-10 were mainly existed in M1 cells, which were effector molecules like nitrogen intermediates, ROS, and inflammatory mediators. As inducers and effector cells, M1 macrophages participated in the polarization Th1 response, and regulated the tolerance of parasites and neoplasms. On the contrary, M2 macrophages mainly possessed low levels of IL-12, IL-23, and high levels of IL-10 phenotypes, and their generated inflammatory cytokines chiefly depended on different signaling pathways. Generally, M2 cells were involved in the polarization Th2 response, parasite clearance, inflammation inhibition, tissue remodeling promotion, angiogenesis, tumor progression, and immunomodulation.

At present, the researches of macrophages in degenerative disc were mainly focused on M1, M2a, and M2c, the cell markers were defined as $CCR7^+$, $CD206^+$, and $CD163^+$, respectively. Studies have shown that $CCR7^+$, $CD163^+$, and $CD206^+$ cells were existed in human IVD. $CCR7^+$, and $CD163^+$ cells increased with the degree of IVD deterioration; M1 and M2c macrophage phenotypes were highly expressed in the IVD region with irregular and defective structures (Nakazawa et al., 2018). $CCR7^+$ M1 phenotype was known to secrete pro-inflammatory cytokines like TNF-α and IL-1β; and $CD163^+$ M2c phenotype produced high levels of MMP required for ECM remodeling; while $CD206^+$ M2a phenotype with anti-inflammatory functions was often connected with the last stages of wound healing, tissue restore, ECM decomposition as well as fibrosis (Ni et al., 2019; Li et al., 2021c). Thus, the accumulation in M1-and M2c-like cells (not M2a) kept pro-inflammatory and remodeling state in IDD without transitioning to wound healing. In addition, all three macrophage markers in epes increased significantly with the degree of deterioration, while only $CCR7^+$ in NP increased significantly, and macrophage markers did not exist in the AF region (Nakazawa et al., 2018). Therefore, the trend between the positive rate percentage and degradation grade of macrophage markers did not always match the changes in each region across IVD. Compared to normal CEP cells as well as the irregular morphology and organization of these cells, the degradation trends of $CCR7^+$, $CD163^+$, and $CD206^+$ macrophages in CEP gave evidence for the hypothesis that exogenous macrophages infiltrated through the CEP, especially through cell migration from the CEP to NP region, which has already been well described (Jimbo et al., 2005; Jia et al., 2020).

CHI3L1, namely chitinase 3-like 1 protein, was a secretory glycoprotein which promoted tumor infiltration and migration in various neoplasms by elevating the expression levels of matrix metalloproteinase (MMPs) family genes (Studer et al., 2011; Fang and Jiang, 2016; Jin et al., 2019). Research also reported that the expression of CHI3L1was highly increased in M2a compared to other types of macrophages (Wang et al., 2019). The roles between M2a cells and CHI3L1 in IDD was demonstrated by Li et al. through rat IDD models: M2a cells generated CHI3L1 protein and acted on the underlying receptor IL-13R, mediating ECM degradation in NP cells through ERK and JNK-specific pathways rather than p38 pathways. In this process, the recombinant CHI3L1 significantly enhanced the expression of MMP3 and MMP9, and inhibited agglomerated sugar and collagen II expression in NP cells. Besides, the roles of CHI3L1 in degeneration of IDD was behaved upon concentration- and time-dependent manner (Li et al., 2021d).

3.3 Potential treatment of IDD targeting macrophages

Wang et al. (2020a) have shown that macrophages could activate T cells through the JAK-STAT signaling pathway, causing a cascade of inflammatory responses. More than 50 cytokines, including IFN-γ, IL-2, IL-6, IL-12, and IL-23, which were dependent on the JAK-STAT pathway, and drugs that inhibited the JAK protein could simultaneously prevent the activity of these cytokines. Therefore, drugs destroying communication networks induced by cytokines may be an efficient way to treat these diseases including IDD.

There remained four FDA-approved JAK inhibitors currently: Ruxolitinib, Tofacitinib, Baracitinib and Upadacitinib. Other JAK inhibitors were in different preclinical and clinical stages, which were mainly used to treat multiple autoimmune and autoinflammatory diseases (Panés et al., 2017; Ma et al., 2019). A preclinical *in-vivo* testing of Tofacitinib in bovine IDD model by Li et al. have reported the potential roles of anti-inflammatory drug Tofacitinib in ameliorating IDD, by downregulating IL-1β, IL-6, IL-8, MMP1, MMP3 in NP tissue, and MMP3, COX2 (cyclooxygenase-2), NGF (nerve growth factor) in AF tissue, thereby neutralizing pro-inflammatory and catabolic circumstance in IDD model (Li et al., 2020). Besides, served as a potent pan-JAK inhibitor, Tofacitinib could inhibit M1 macrophages polarization by suppressing the activation of STAT1, which have shown prospects in the treatment of corneal allograft rejection (Yu et al., 2022). A case report by Yi et al.

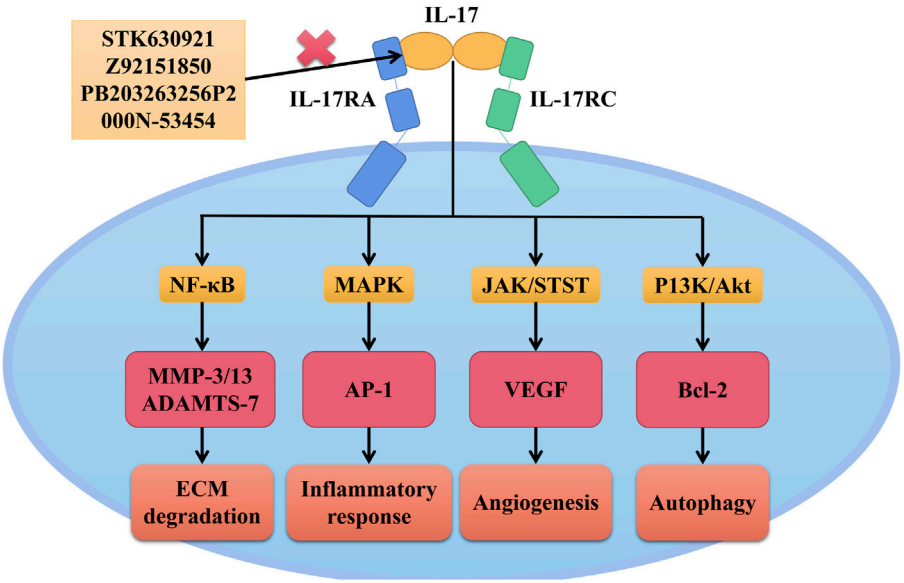

FIGURE 2
Interactive roles of IL-17 in IDD. After IL-17 binding to its receptors, IL-17 could increase the levels of MMP-3, MMP-13 and ADAMTS-7 by motivating the nuclear translocation of NF-κB, thus promoting ECM degradation; IL-17 stimulated the MAPK/AP-1 transduction to modulate the generation of pro-inflammatory substances. IL-17 could induce angiogenesis by upregulating the JAK/STAT/VEGF signal axis, and prevented NP cell from autophagy by promoting the PI3K/AKT/Bcl-2 signaling cascade. STK630921, Z92151850, PB203263256, and P2000N-53454 were small molecular drugs blocking the interaction roles between IL-17 and IL-17RA.

suggested that Baracitinib was an option in the maintenance therapy of macrophage activation syndrome, which was potentially beneficial to prevent the recurrence (Yi et al., 2022). However, the relevant researches of these JAK inhibitors on IDD remained insufficient. Considering the close connections between these JAK inhibitors and macrophages, as well as the macrophage roles in IDD, the relationships between JAK inhibitors and IDD were subtle. Based on the promising prospects of ameliorating NP cells from degradation through JAK inhibition by recent study, we believed JAK inhibitors would also be a kind of potential compounds in the treatment of IDD targeting macrophages (Wu et al., 2021). More researches about the detailed mechanisms of these JAK inhibitors in the treatment of IDD still need further exploration.

4 The relationships between cytokines and IDD

4.1 IL-17

In recent years, accumulating evidences suggested that IL-17, also known as IL-17A, behaved pivotal roles in the development of IDD, which was produced by T helper cell 17 (Th17), a sub population of CD4 T cells (Liu et al., 2019). Unlike the classic Th1 and Th2 lineages, IL-17 was absent in human normal AF cells and lowly expressed in normal NP cells, while especially increased in human degenerative NP cells. More importantly, the expression levels of IL-17 in IVD increased with the IDD degree, displaying that IL-17 may be an effective indicator reflecting severity of IDD (Tan et al., 2022).

Studies have suggested that IL-17 could increase the levels of MMP-3, MMP-13, and ADAMTS-7 by motivating the nuclear translocation of NF-κB, thus promoting ECM degradation (Tan et al., 2022); IL-17 also stimulated the MAPK/AP-1 transduction to modulate the generation of pro-inflammatory substances (Li et al., 2016); Besides, IL-17 could induce angiogenesis by upregulating the JAK/STAT/VEGF signal axis, and also prevented NP cells from autophagy by promoting the PI3K/AKT/Bcl-2 signaling cascade (Hu et al., 2017). These findings implied the essential roles of IL-17 in the development of IDD. STK630921, Z92151850, PB203263256, and P2000N-53454 were small molecular drugs blocking the interaction roles between IL-17 and IL-17RA (Suyama et al., 2018; Tan et al., 2022). The application of these inhibitors has been shown to inhibit ECM decomposition and pro-inflammatory substances production in IL-17-induced rat NP cells under hypoxic conditions, among which STK630921 displayed the most effective results (Tan et al., 2022). Consequently, IL-17 was a potential biomarker reflecting the severity of IDD degree, and inhibitors which blocked IL-17 and IL-17RA could be served as an important direction for future

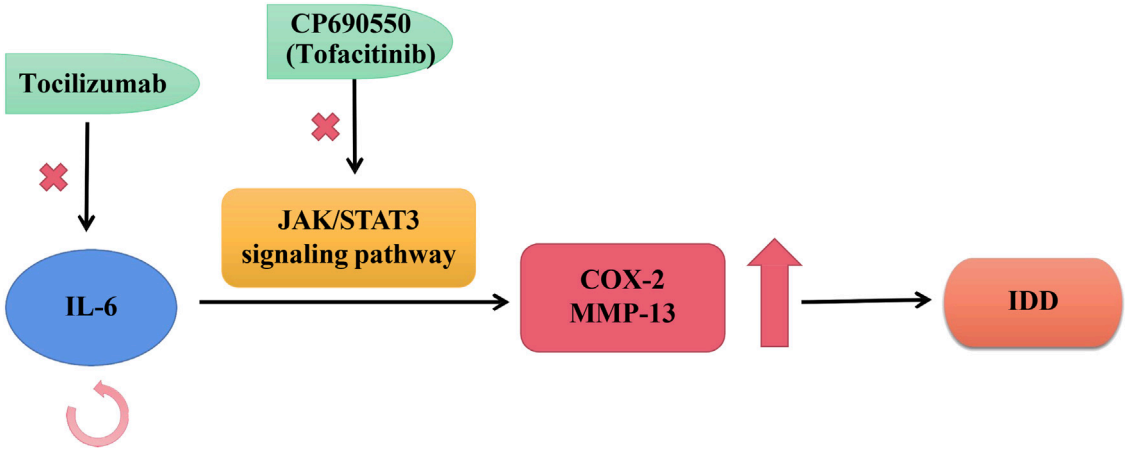

FIGURE 3
Roles of IL-6 in IVD. IL-6 self-stimulated expression and enhances the expression of mediators like COX-2 and MMP-13, thus exacerbating IDD progression through the JAK/STAT3 transduction. Tocilizumab was a kind of humanized monoclonal antibody against human IL-6 receptors; CP690550 was an oral JAK antagonist, also called tofacitinib, was being developed to treat auto-immune diseases like RA.

clinical drug discovery. The detailed mechanism roles of the current IL-17 inhibitors were illustrated in Figure 2.

4.2 IL-6

Suzuki et al. reported a high expression situation of IL-6 during degenerative IVD in rats and humans, which self-amplified its own expression and promoted the expression levels of mediators like COX-2 and MMP-13, thereby exacerbating IVD degeneration through the JAK/STAT3 signaling pathway (Suzuki et al., 2017). CP690550, also called Tofacitinib, was an oral JAK antagonist, which was currently being developed as the effective approach for RA (rheumatoid arthritis) and other auto-immune diseases (Ohtori et al., 2012). CP690550 also significantly inhibited IL-6-mediated gene expression to ameliorate IDD by pharmacological inhibition of JAK3 activity (Ohtori et al., 2012; Suzuki et al., 2017). These findings strongly demonstrated a causal relationship between the IL-6/JAK/STAT3 cascade reactions and the development of IDD. Therefore, this intracellular pathway could provide evidence for targeted treatment of preventing IDD. There is evidence that epidural Tocilizumab was effective in relieving low back pain for patients with IDD (Ohtori et al., 2012), as shown in Figure 3.

Moreover, recent clinical data suggested that IL-6 could also be a reasonable and efficient target in bone degenerative disease in addition to IDD. The humanized monoclonal antibody Tocilizumab against human IL-6 receptors has been widely applied in the treatment of RA, indicating the essential roles of target therapy based on IL-6 in skeletal destructions (Smolen et al., 2008).

4.3 IL-β

Numerous studies have found that IL-1β was involved in the development of IDD through different ways. IL-1β behaved roles in creating pro-inflammatory/degenerative IVD conditions; When exposure to IL-1β, the production of mononuclear cytochemical aspiration proteins-1, IL-6, IL-8, and prostaglandin E2 increased significantly (Yuan et al., 2018). Additionally, exposure to IL-1β stimulated the production of IL-17 in degenerative IVD cells, which has been elaborated above (Gruber et al., 2013). IL-1β could also improve its own generation by promoting the activation of NLRP3 inflammasomes, while the NLRP3 inflammation and NF-κB activation could be blocked by IKK-β selective inhibitor Bay11-7082 (Zhang et al., 2017; Chen et al., 2020). Consequently, BAY11-7082 may also be a potential aspect of IDD clinical drug therapy research, the detailed mechanisms need further exploration.

In terms of oxidative stress, Liu et al. demonstrated that IL-1β could significantly increase ROS and catabolic activity within mouse vertebral bone marrow stromal cells (vBMSCs), this process could be effectively prevented by fullerol (Liu et al., 2013). Therefore, considering the connections about IL-1β and fullerol in IDD and ROS respectively, fullerol may be served as a valid biological therapy to treat IDD, further experimental studies need to focus on fullerol to validate these effects.

4.4 TNF-α

Existed researches have demonstrated that TNF-α could promote the accumulation of IL-6, IL-8 and IL-17 in AF cells, stimulating the secretion of inflammatory substances such as NO

and PGE2, and aggravated the inflammatory response, the same as IL-1β (Huang et al., 2020; Qi et al., 2020). Furthermore, Liu et al. have found that the TNF-α stimulated IVD cells could expression enhance the expression levels of CCL3, CCL20, CXCL2, and CXCL5 genes, which were associated with the ECM decomposition, damage, inflammatory reactions, and the regulation of apoptosis (Gabr et al., 2011). Besides, TNF-α could improve the levels of intercellular adhesion molecules (ICAM-1) in human IVD cells, which was one of the most important pairs of adhesion molecules (Wang et al., 2020b). Thus, more relationships between TNF-α, ICAM-1 and IDD were worth studying.

5 Summary and outlook

The pathogenesis of IDD is complex, involving multiple cellular activities and multiple regulatory pathways. In this review, we discussed the pivotal roles of oxidative stress and inflammatory response in IDD and potential therapies with oral drugs. There remained imbalance between ROS production and clearance in degenerative discs, oxidative stress reactions caused by excessive ROS could further stimulate a variety of signaling pathways and ultimately strengthen both local and systemic oxidative stress. Besides, natural antioxidants such as GSH, RSV and PQQ all provided promising prospects in the treatment of IDD, which were used to develop novel therapies in IDD.

Additionally, macrophages and cytokines also played important roles in inflammatory response through various signaling pathways, providing a great number of targets to treat IDD including JAK inhibitors, IKK-β selective inhibitor and humanized monoclonal antibody against human IL-6 andIL-17 receptors, etc. However, the drug treatment of IDD based on the targets mentioned above remained little studied, thus there is still a long way to go to comprehensively explore the potential values of these drugs in the treatment of IDD.

Author contributions

This study was completed with teamwork. Each author had made corresponding contribution to the study. Conceived the idea: BW, YZ, and BG. Wrote the main manuscript: BW, YZ and WL. Prepared figures: BW, YZ, and WL. Redressed the manuscript: BW, WL, SZ, and BG. Reviewed the manuscript: MY, ZH, and BG.

Funding

This study was supported by grants from the National Natural Science Foundation of China (Nos. 82172475 and 81902240).

Conflict of interest

The authors declare that the research was conducted in the absence of any commercial or financial relationships that could be construed as a potential conflict of interest.

Publisher's note

References

Akanji, M. A., Rotimi, D. E., Elebiyo, T. C., Awakan, O. J., and Adeyemi, O. S. (2021). Redox homeostasis and prospects for therapeutic targeting in neurodegenerative disorders. *Oxid. Med. Cell. Longev.* 2021, 1–14. doi:10.1155/2021/9971885

Albermann, M., Lehmann, M., Eiche, C., Schmidt, J., and Prottengeier, J. (2020). Low back pain in commercial airline pilots. *Aerosp. Med. Hum. Perform.* 91 (12), 940–947. doi:10.3357/amhp.5656.2020

Bai, X., Lian, Y., Hu, C., Yang, S., Pei, B., Yao, M., et al. (2022). Cyanidin-3-glucoside protects against high glucose-induced injury in human nucleus pulposus cells by regulating the Nrf2/HO-1 signaling. *J. Appl. Toxicol.* 42 (7), 1137–1145. doi:10.1002/jat.4281

Binch, A. L., Cole, A. A., Breakwell, L. M., Michael, A. L., Chiverton, N., Cross, A. K., et al. (2014). Expression and regulation of neurotrophic and angiogenic factors during human intervertebral disc degeneration. *Arthritis Res. Ther.* 16 (5), 416. doi:10.1186/s13075-014-0416-1

Bobechko, W. P., and Hirsch, C. (1965). Auto-immune response to nucleus pulposus in the rabbit. *J. Bone Jt. Surg. Br. volume* 47, 574–580. doi:10.1302/0301-620x.47b3.574

Chen, F., Jiang, G., Liu, H., Li, Z., Pei, Y., Wang, H., et al. (2020). Melatonin alleviates intervertebral disc degeneration by disrupting the IL-1β/NF-κB-NLRP3 inflammasome positive feedback loop. *Bone Res.* 8, 10. doi:10.1038/s41413-020-0087-2

Chen, T., Li, P., Qiu, J., Hu, W., Li, S., Shi, H., et al. (2022). Aloin regulates matrix metabolism and apoptosis in human nucleus pulposus cells via the TAK1/NF-B/NLRP3 signaling pathway. *Stem Cells Int.* 2022, 5865011–5865012. doi:10.1155/2022/5865011

Cros, J., Cagnard, N., Woollard, K., Patey, N., Zhang, S-Y., Senechal, B., et al. (2010). Human CD14dim monocytes patrol and sense nucleic acids and viruses via TLR7 and TLR8 receptors. *Immunity* 33 (3), 375–386. doi:10.1016/j.immuni.2010.08.012

Ďuračková, Z. (2010). Some current insights into oxidative stress. *Physiol. Res.* 59 (4), 459–469. doi:10.33549/physiolres.931844

Fang, F., and Jiang, D. (2016). IL-1β/HMGB1 signalling promotes the inflammatory cytokines release via TLR signalling in human intervertebral disc cells. *Biosci. Rep.* 36 (5), e00379. doi:10.1042/bsr20160118

Fang, J., Seki, T., and Maeda, H. (2009). Therapeutic strategies by modulating oxygen stress in cancer and inflammation. *Adv. Drug Deliv. Rev.* 61 (4), 290–302. doi:10.1016/j.addr.2009.02.005

Feng, C., Yang, M., Lan, M., Chang, L., Yang, Z., Huang, B., et al. (2017). Ros: Crucial intermediators in the pathogenesis of intervertebral disc degeneration. *Oxidative Med. Cell. Longev.* 2017, 1–12. doi:10.1155/2017/5601593

Fridovich, I. (1978). The biology of oxygen radicals. *Science* 201 (4359), 875–880. doi:10.1126/science.210504

Gabr, M. A., Jing, L., Helbling, A. R., Sinclair, S. M., Allen, K. D., Shamji, M. F., et al. (2011). Interleukin-17 synergizes with IFNγ or TNFα to promote inflammatory mediator release and intercellular adhesion molecule-1 (ICAM-1) expression in human intervertebral disc cells. *J. Orthop. Res.* 29 (1), 1–7. doi:10.1002/jor.21206

Gentek, R., Molawi, K., and Sieweke, M. H. (2014). Tissue macrophage identity and self-renewal. *Immunol. Rev.* 262 (1), 56–73. doi:10.1111/imr.12224

Gertzbein, S. D. (1977). Degenerative disk disease of the lumbar spine: Immunological implications. *Clin. Orthop. Relat. Res.* 129, 68–71. doi:10.1097/00003086-197711000-00007

Gertzbein, S. D., Tait, J. H., and Devlin, S. R. (1977). The stimulation of lymphocytes by nucleus pulposus in patients with degenerative disk disease of the lumbar spine. *Clin. Orthop. Relat. Res.* 123, 149–154. doi:10.1097/00003086-197703000-00058

Ginhoux, F., and Jung, S. (2014). Monocytes and macrophages: Developmental pathways and tissue homeostasis. *Nat. Rev. Immunol.* 14 (6), 392–404. doi:10.1038/nri3671

Gruber, H. E., Hoelscher, G. L., Ingram, J. A., Norton, H. J., and Hanley, E. N., Jr (2013). Increased IL-17 expression in degenerated human discs and increased production in cultured annulus cells exposed to IL-1ß and TNF-α. *Biotech. Histochem.* 88 (6), 302–310. doi:10.3109/10520295.2013.783235

Guilliams, M., Mildner, A., and Yona, S. (2018). Developmental and functional heterogeneity of monocytes. *Immunity* 49 (4), 595–613. doi:10.1016/j.immuni.2018.10.005

Hu, B., Wang, J., Wu, X., Chen, Y., Yuan, W., and Chen, H. (2017). Interleukin-17 upregulates vascular endothelial growth factor by activating the JAK/STAT pathway in nucleus pulposus cells. *Jt. Bone Spine* 84 (3), 327–334. doi:10.1016/j.jbspin.2016.05.014

Huang, J-F., Zheng, X-Q., Lin, J-L., Zhang, K., Tian, H-J., Zhou, W-X., et al. (2020). Sinapic acid inhibits IL-1β-induced apoptosis and catabolism in nucleus pulposus cells and ameliorates intervertebral disk degeneration. *J. Inflamm. Res.* 13, 883–895. doi:10.2147/jir.s278556

Jia, J., Nie, L., and Liu, Y. (2020). Butyrate alleviates inflammatory response and NF-κB activation in human degenerated intervertebral disc tissues. *Int. Immunopharmacol.* 78, 106004. doi:10.1016/j.intimp.2019.106004

Jimbo, K., Park, J. S., Yokosuka, K., Sato, K., and Nagata, K. (2005). Positive feedback loop of interleukin-1β upregulating production of inflammatory mediators in human intervertebral disc cells *in vitro*. *J. Neurosurg. Spine* 2 (5), 589–595. doi:10.3171/spi.2005.2.5.0589

Jin, H., Wang, Q., Wu, J., Han, X., Qian, T., Zhang, Z., et al. (2019). Baicalein inhibits the IL-1β-induced inflammatory response in nucleus pulposus cells and attenuates disc degeneration *in vivo*. *Inflammation* 42 (3), 1032–1044. doi:10.1007/s10753-019-00965-8

Johnson, Z. I., Schoepflin, Z. R., Choi, H., Shapiro, I. M., and Risbud, M. V. (2015). Disc in flames: Roles of TNF-α and IL-1β in intervertebral disc degeneration. *Eur. Cell. Mat.* 30, 104–117. doi:10.22203/ecm.v030a08

Kadow, T., Sowa, G., Vo, N., and Kang, J. D. (2015). Molecular basis of intervertebral disc degeneration and herniations: What are the important translational questions? *Clin. Orthop. Relat. Res.* 473 (6), 1903–1912. doi:10.1007/s11999-014-3774-8

Kimball, J. S., Johnson, J. P., and Carlson, D. A. (2021). Oxidative stress and osteoporosis. *J. Bone Jt. Surg.* 103 (15), 1451–1461. doi:10.2106/jbjs.20.00989

Krupkova, O., Handa, J., Hlavna, M., Klasen, J., Ospelt, C., Ferguson, S. J., et al. (2016). The natural polyphenol epigallocatechin gallate protects intervertebral disc cells from oxidative stress. *Oxid. Med. Cell. Longev.* 2016, 1–17. doi:10.1155/2016/7031397

Krupkova, O., Sekiguchi, M., Klasen, J., Hausmann, O., Konno, S., Ferguson, S. J., et al. (2014). Epigallocatechin 3-gallate suppresses interleukin-1β-induced inflammatory responses in intervertebral disc cells *in vitro* and reduces radiculopathic pain in rats. *Eur. Cell. Mat.* 28, 372–386. doi:10.22203/ecm.v028a26

Kulkarni, P., Martson, A., Vidya, R., Chitnavis, S., and Harsulkar, A. (2021). Pathophysiological landscape of osteoarthritis. *Adv. Clin. Chem.* 100, 37–90. doi:10.1016/bs.acc.2020.04.002

Kumar, B., Koul, S., Khandrika, L., Meacham, R. B., and Koul, H. K. (2008). Oxidative stress is inherent in prostate cancer cells and is required for aggressive phenotype. *Cancer Res.* 68 (6), 1777–1785. doi:10.1158/0008-5472.can-07-5259

Lam, S. K. L., Chan, S. C. W., Leung, V. Y. L., Lu, W. W., Cheung, K. M. C., and Luk, K. D. K. (2011). The role of cryopreservation in the biomechanical properties of the intervertebral disc. *Eur. Cell. Mat.* 22, 393–402. doi:10.22203/ecm.v022a29

Le Maitre, C. L., Pockert, A., Buttle, D. J., Freemont, A. J., and Hoyland, J. A. (2007). Matrix synthesis and degradation in human intervertebral disc degeneration. *Biochem. Soc. Trans.* 35 (4), 652–655. doi:10.1042/bst0350652

Li, F., Sun, X., Zheng, B., Sun, K., Zhu, J., Ji, C., et al. (2021). Arginase II promotes intervertebral disc degeneration through exacerbating senescence and apoptosis caused by oxidative stress and inflammation via the NF-κB pathway. *Front. Cell Dev. Biol.* 9, 737809. doi:10.3389/fcell.2021.737809

Li, J. K., Nie, L., Zhao, Y. P., Zhang, Y. Q., Wang, X., Wang, S. S., et al. (2016). IL-17 mediates inflammatory reactions via p38/c-Fos and JNK/c-Jun activation in an AP-1-dependent manner in human nucleus pulposus cells. *J. Transl. Med.* 14, 77. doi:10.1186/s12967-016-0833-9

Li, L., Wei, K., Ding, Y., Ahati, P., Xu, H., Fang, H., et al. (2021). M2a macrophage-secreted CHI3L1 promotes extracellular matrix metabolic imbalances via activation of IL-13rα2/MAPK pathway in rat intervertebral disc degeneration. *Front. Immunol.* 12, 666361. doi:10.3389/fimmu.2021.666361

Li, W., Ding, Z., Wang, D., Li, C., Pan, Y., Zhao, Y., et al. (2021). Ten-gene signature reveals the significance of clinical prognosis and immuno-correlation of osteosarcoma and study on novel skeleton inhibitors regarding MMP9. *Cancer Cell Int.* 21 (1), 377. doi:10.1186/s12935-021-02041-4

Li, W., Zhang, S., Wang, D., Zhang, H., Shi, Q., Zhang, Y., et al. (2021). Exosomes immunity strategy: A novel approach for ameliorating intervertebral disc degeneration. *Front. Cell Dev. Biol.* 9, 822149. doi:10.3389/fcell.2021.822149

Li, W., Zhang, S., Zhao, Y., Wang, D., Shi, Q., Ding, Z., et al. (2022). Revealing the key MSCs niches and pathogenic genes in influencing CEP homeostasis: A conjoint analysis of single-cell and wgcna. *Front. Immunol.* 13, 933721. doi:10.3389/fimmu.2022.933721

Li, X., Phillips, F. M., An, H. S., Ellman, M., Thonar, E. J., Wu, W., et al. (2008). The action of resveratrol, a phytoestrogen found in grapes, on the intervertebral disc. *Spine (Phila Pa 1976)* 33 (24), 2586–2595. doi:10.1097/brs.0b013e3181883883

Li, Z., Gehlen, Y., Heizmann, F., Grad, S., Alini, M., Richards, R. G., et al. (2020). Preclinical *ex-vivo* testing of anti-inflammatory drugs in a bovine intervertebral degenerative disc model. *Front. Bioeng. Biotechnol.* 8, 583. doi:10.3389/fbioe.2020.00583

Liu, Q., Jin, L., Shen, F. H., Balian, G., and Li, X. J. (2013). Fullerol nanoparticles suppress inflammatory response and adipogenesis of vertebral bone marrow stromal cells-a potential novel treatment for intervertebral disc degeneration. *Spine J.* 13 (11), 1571–1580. doi:10.1016/j.spinee.2013.04.004

Liu, Y., Qu, Y., Liu, L., Zhao, H., Ma, H., Si, M., et al. (2019). PPAR-γ agonist pioglitazone protects against IL-17 induced intervertebral disc inflammation and degeneration via suppression of NF-κB signaling pathway. *Int. Immunopharmacol.* 72, 138–147. doi:10.1016/j.intimp.2019.04.012

Ma, C., Jairath, V., and Vande Casteele, N. (2019). Pharmacology, efficacy and safety of JAK inhibitors in Crohn's disease. *Best. Pract. Res. Clin. Gastroenterol.* 38-39, 101606. doi:10.1016/j.bpg.2019.03.002

Nakazawa, K. R., Walter, B. A., Laudier, D. M., Krishnamoorthy, D., Mosley, G. E., Spiller, K. L., et al. (2018). Accumulation and localization of macrophage phenotypes with human intervertebral disc degeneration. *Spine J.* 18 (2), 343–356. doi:10.1016/j.spinee.2017.09.018

Ni, L., Zheng, Y., Gong, T., Xiu, C., Li, K., Saijilafu, et al. (2019). Proinflammatory macrophages promote degenerative phenotypes in rat nucleus pulpous cells partly through ERK and JNK signaling. *J. Cell. Physiol.* 234 (5), 5362–5371. doi:10.1002/jcp.27507

Ohtori, S., Miyagi, M., Eguchi, Y., Inoue, G., Orita, S., Ochiai, N., et al. (2012). Efficacy of epidural administration of anti-interleukin-6 receptor antibody onto spinal nerve for treatment of sciatica. *Eur. Spine J.* 21 (10), 2079–2084. doi:10.1007/s00586-012-2183-5

Panés, J., Sandborn, W. J., Schreiber, S., Sands, B. E., Vermeire, S., D'Haens, G., et al. (2017). Tofacitinib for induction and maintenance therapy of crohn's disease: Results of two phase IIb randomised placebo-controlled trials. *Gut* 66 (6), 1049–1059. doi:10.1136/gutjnl-2016-312735

Peng, B. (2008). Issues concerning the biological repair of intervertebral disc degeneration. *Nat. Clin. Pract. Rheumatol.* 4 (5), 226–227. doi:10.1038/ncprheum0771

Poyton, R. O., Ball, K. A., and Castello, P. R. (2009). Mitochondrial generation of free radicals and hypoxic signaling. *Trends Endocrinol. Metabolism* 20 (7), 332–340. doi:10.1016/j.tem.2009.04.001

Qi, W., Ren, D., Wang, P., Song, Z., Wu, H., Yao, S., et al. (2020). Upregulation of Sirt1 by tyrosol suppresses apoptosis and inflammation and modulates extracellular matrix remodeling in interleukin-1β-stimulated human nucleus pulposus cells through activation of PI3K/Akt pathway. *Int. Immunopharmacol.* 88, 106904. doi:10.1016/j.intimp.2020.106904

Risbud, M. V., and Shapiro, I. M. (2014). Role of cytokines in intervertebral disc degeneration: Pain and disc content. *Nat. Rev. Rheumatol.* 10 (1), 44–56. doi:10.1038/nrrheum.2013.160

Seol, D., Coleman, M. C., Martin, J. A., Song, I., Jaidev, L. R., Salem, A. K., et al. (2021). Targeting oxidative stress with amobarbital to prevent intervertebral disc degeneration: Part I. *In vitro* and *ex vivo* studies. *Spine J.* 21 (6), 1021–1030. doi:10.1016/j.spinee.2021.02.008

Shi, C., and Pamer, E. G. (2011). Monocyte recruitment during infection and inflammation. *Nat. Rev. Immunol.* 11 (11), 762–774. doi:10.1038/nri3070

Sies, H. (1991). Oxidative stress: From basic research to clinical application. *Am. J. Med.* 91 (3), 31s–38s. doi:10.1016/0002-9343(91)90281-2

Smolen, J. S., Beaulieu, A., Rubbert-Roth, A., Ramos-Remus, C., Rovensky, J., Alecock, E., et al. (2008). Effect of interleukin-6 receptor inhibition with tocilizumab in patients with rheumatoid arthritis (OPTION study): A double-blind, placebo-controlled, randomised trial. *Lancet* 371 (9617), 987–997. doi:10.1016/s0140-6736(08)60453-5

Studer, R. K., Vo, N., Sowa, G., Ondeck, C., and Kang, J. (2011). Human nucleus pulposus cells react to IL-6: Independent actions and amplification of response to IL-1 and TNF-α. *Spine (Phila Pa 1976)* 36 (8), 593–599. doi:10.1097/brs.0b013e3181da38d5

Sun, D., Zhang, M., Sun, P., Liu, G., Strickland, A. B., Chen, Y., et al. (2020). VCAM1/VLA4 interaction mediates Ly6Clow monocyte recruitment to the brain in a TNFR signaling dependent manner during fungal infection. *PLoS Pathog.* 16 (2), e1008361. doi:10.1371/journal.ppat.1008361

Sun, Z., Liu, B., and Luo, Z-J. (2020). The immune privilege of the intervertebral disc: Implications for intervertebral disc degeneration treatment. *Int. J. Med. Sci.* 17 (5), 685–692. doi:10.7150/ijms.42238

Suyama, K., Sakai, D., Hirayama, N., Nakamura, Y., Matsushita, E., Terayama, H., et al. (2018). Effects of interleukin-17A in nucleus pulposus cells and its small-molecule inhibitors for intervertebral disc disease. *J. Cell. Mol. Med.* 22 (11), 5539–5551. doi:10.1111/jcmm.13828

Suzuki, S., Fujita, N., Fujii, T., Watanabe, K., Yagi, M., Tsuji, T., et al. (2017). Potential involvement of the IL-6/JAK/STAT3 pathway in the pathogenesis of intervertebral disc degeneration. *Spine (Phila Pa 1976)* 42 (14), E817–e824. doi:10.1097/brs.0000000000001982

Suzuki, S., Fujita, N., Hosogane, N., Watanabe, K., Ishii, K., Toyama, Y., et al. (2015). Excessive reactive oxygen species are therapeutic targets for intervertebral disc degeneration. *Arthritis Res. Ther.* 17, 316. doi:10.1186/s13075-015-0834-8

Tan, J. H., Li, Z. P., Liu, L. L., Liu, H., and Xue, J. B. (2022). IL-17 in intervertebral disc degeneration: Mechanistic insights and therapeutic implications. *Cell Biol. Int.* 46 (4), 535–547. doi:10.1002/cbin.11767

Varol, C., Mildner, A., and Jung, S. (2015). Macrophages: Development and tissue specialization. *Annu. Rev. Immunol.* 33, 643–675. doi:10.1146/annurev-immunol-032414-112220

Venza, M., Visalli, M., Beninati, C., De Gaetano, G. V., Teti, D., and Venza, I. (2015). Cellular mechanisms of oxidative stress and action in melanoma. *Oxid. Med. Cell. Longev.* 2015, 1–11. doi:10.1155/2015/481782

Wang, A., Singh, K., Ibrahim, W., King, B., and Damsky, W. (2020). The promise of JAK inhibitors for treatment of sarcoidosis and other inflammatory disorders with macrophage activation: A review of the literature. *Yale J. Biol. Med.* 93 (1), 187–195.

Wang, K., Chen, T., Ying, X., Zhang, Z., Shao, Z., Lin, J., et al. (2019). Ligustilide alleviated IL-1β induced apoptosis and extracellular matrix degradation of nucleus pulposus cells and attenuates intervertebral disc degeneration *in vivo*. *Int. Immunopharmacol.* 69, 398–407. doi:10.1016/j.intimp.2019.01.004

Wang, Y., Che, M., Xin, J., Zheng, Z., Li, J., and Zhang, S. (2020). The role of IL-1β and TNF-α in intervertebral disc degeneration. *Biomed. Pharmacother.* 131, 110660. doi:10.1016/j.biopha.2020.110660

Wu, C., Ge, J., Yang, M., Yan, Q., Wang, Y., Yu, H., et al. (2021). Resveratrol protects human nucleus pulposus cells from degeneration by blocking IL-6/JAK/STAT3 pathway. *Eur. J. Med. Res.* 26 (1), 81. doi:10.1186/s40001-021-00555-1

Xiang, Q., Zhao, Y., Lin, J., Jiang, S., and Li, W. (2022). The Nrf2 antioxidant defense system in intervertebral disc degeneration: Molecular insights. *Exp. Mol. Med.* 54 (8), 1067–1075. doi:10.1038/s12276-022-00829-6

Yang, D., Wang, D., Shimer, A., Shen, F. H., Li, X., and Yang, X. (2014). Glutathione protects human nucleus pulposus cells from cell apoptosis and inhibition of matrix synthesis. *Connect. Tissue Res.* 55 (2), 132–139. doi:10.3109/03008207.2013.876421

Yang, J., Zhang, L., Yu, C., Yang, X. F., and Wang, H. (2014). Monocyte and macrophage differentiation: Circulation inflammatory monocyte as biomarker for inflammatory diseases. *Biomark. Res.* 2 (1), 1. doi:10.1186/2050-7771-2-1

Yang, L., Rong, Z., Zeng, M., Cao, Y., Gong, X., Lin, L., et al. (2015). Pyrroloquinoline quinone protects nucleus pulposus cells from hydrogen peroxide-induced apoptosis by inhibiting the mitochondria-mediated pathway. *Eur. Spine J.* 24 (8), 1702–1710. doi:10.1007/s00586-014-3630-2

Yi, G., Huang, Z., Huang, Z., Wang, Y., Deng, W., Zheng, S., et al. (2022). Case report: Baricitinib as an alternative in the maintenance therapy for macrophage activation syndrome secondary to nodular panniculitis. *Front. Immunol.* 13, 914265. doi:10.3389/fimmu.2022.914265

Yu, J., Li, P., Li, Z., Li, Y., Luo, J., Su, W., et al. (2022). Topical administration of 0.3% tofacitinib suppresses M1 macrophage polarization and allograft corneal rejection by blocking STAT1 activation in the rat cornea. *Transl. Vis. Sci. Technol.* 11 (3), 34. doi:10.1167/tvst.11.3.34

Yuan, Y., Chen, Y., Zhou, Z., Jiao, Y., Li, C., Zheng, Y., et al. (2018). Association between chronic inflammation and latent infection of propionibacterium acnes in non-pyogenic degenerated intervertebral discs: A pilot study. *Eur. Spine J.* 27 (10), 2506–2517. doi:10.1007/s00586-017-5363-5

Zhang, A., Wang, K., Ding, L., Bao, X., Wang, X., Qiu, X., et al. (2017). Bay11-7082 attenuates neuropathic pain via inhibition of nuclear factor-kappa B and nucleotide-binding domain-like receptor protein 3 inflammasome activation in dorsal root ganglions in a rat model of lumbar disc herniation. *J. Pain Res.* 10, 375–382. doi:10.2147/jpr.s119820

Zhao, M-J., Yuan, S., Zi, H., Gu, J-M., Fang, C., and Zeng, X-T. (2021). Oxidative stress links aging-associated cardiovascular diseases and prostatic diseases. *Oxid. Med. Cell. Longev.* 2021, 1–12. doi:10.1155/2021/5896136

Zhu, F., Duan, W., Zhong, C., Ji, B., and Liu, X. (2022). The protective effects of dezocine on interleukin-1β-induced inflammation, oxidative stress and apoptosis of human nucleus pulposus cells and the possible mechanisms. *Bioengineered* 13 (1), 1399–1410. doi:10.1080/21655979.2021.2017700

frontiers | Frontiers in Bioengineering and Biotechnology

TYPE Systematic Review
PUBLISHED 16 December 2022
DOI 10.3389/fbioe.2022.980548

OPEN ACCESS

EDITED BY
Jingfeng Li,
Zhongnan Hospital, Wuhan University, China

REVIEWED BY
Yuchang Wang,
Huazhong University of Science and Technology, China
Guoyuan Yang,
Shanghai Jiao Tong University, China

*CORRESPONDENCE
Yun Luo,
ly20040423@126.com
Xiaobo Sun,
sun_xiaobo163@163.com

SPECIALTY SECTION
This article was submitted to Preclinical Cell and Gene Therapy, a section of the journal Frontiers in Bioengineering and Biotechnology

RECEIVED 28 June 2022
ACCEPTED 06 December 2022
PUBLISHED 16 December 2022

CITATION
Jin M, Zhang S, Wang M, Li Q, Ren J, Luo Y and Sun X (2022), Exosomes in pathogenesis, diagnosis, and therapy of ischemic stroke.
Front. Bioeng. Biotechnol. 10:980548.
doi: 10.3389/fbioe.2022.980548

Exosomes in pathogenesis, diagnosis, and therapy of ischemic stroke

Meiqi Jin[1,2,3,4], Shuxia Zhang[1,2,3,4], Mengchen Wang[1,2,3,4], Qiaoyu Li[1,2,3,4], Jiahui Ren[1,2,3], Yun Luo[1,2,3,4]* and Xiaobo Sun[1,2,3,4]*

[1]Institute of Medicinal Plant Development, Peking Union Medical College and Chinese Academy of Medical Science, Beijing, China, [2]Beijing Key Laboratory of Innovative Drug Discovery of Traditional Chinese Medicine (Natural Medicine) and Translational Medicine, Beijing, China, [3]Key Laboratory of Bioactive Substances and Resource Utilization of Chinese Herbal Medicine, Ministry of Education, Beijing, China, [4]NMPA Key Laboratory for Research and Evaluation of Pharmacovigilance, Beijing, China

Ischemic stroke is one of the major contributors to death and disability worldwide. Thus, there is an urgent need to develop early brain tissue perfusion therapies following acute stroke and to enhance functional recovery in stroke survivors. The morbidity, therapy, and recovery processes are highly orchestrated interactions involving the brain with other tissues. Exosomes are natural and ideal mediators of intercellular information transfer and recognized as biomarkers for disease diagnosis and prognosis. Changes in exosome contents express throughout the physiological process. Accumulating evidence demonstrates the use of exosomes in exploring unknown cellular and molecular mechanisms of intercellular communication and organ homeostasis and indicates their potential role in ischemic stroke. Inspired by the unique properties of exosomes, this review focuses on the communication, diagnosis, and therapeutic role of various derived exosomes, and their development and challenges for the treatment of cerebral ischemic stroke.

KEYWORDS

exosomes, ischemic stroke, blood vessels, neuron, inflammation, the blood-brain barrier (BBB), engineered exosomes

1 Introduction

Exosomes were first discovered in sheep reticulocytes in 1983 (Zhang et al., 2020a). Johnstone et al. tracked transferrin receptors during the maturation of reticulocytes and found that the formation of exosomes is the mechanism for the loss of transferrin receptors in mature red blood cells (Johnstone et al., 1987). The International Society for Extracellular Vesicles uses the generic term extracellular vesicle (EV) to refer to particles that are naturally released from cells, enclosed in a lipid bilayer, and cannot replicate. Exosomes are considered subtypes of EVs. Some studies have compared EVs recovered using medium-speed centrifugation (referred to as large oncosomes, ectosomes,

microvesicles, cell debris, or large or medium EVs) with those recovered using 100,000 × *g* ultracentrifugation (referred to as exosomes in the first four studies or small EVs in the last two); some of these studies used different density gradients for separation (Théry et al., 2018). Both prokaryotic and eukaryotic cells can release exosomes in either normal or pathological states. When secreted into the extracellular space, exosomes play a critical role in cell–cell communication by delivering bioactive substances between source and recipient cells. They also have targeting abilities and inherit specific characteristics. Thus, exosomes are of particular interest in biology because their formation involves a distinct extracellular regulatory process (Kalluri and LeBleu 2020). Under the conditions of specific physiological and pathological processes, some cell-derived exosomes undergo biological variations that include changes in the expression of proteins and nucleic acids. These are used to investigate mechanisms of biodegradation and biosynthesis, pathogenic injury, organ remodeling, and tissue repair (Sharma et al., 2019; Cheng et al., 2020). Although purification and identification of exosomes remain challenging, exciting discoveries concerning their molecular mechanisms in the field of stroke have emerged and their potential in diagnostic and therapeutic functions has been demonstrated (Yang et al., 2018a; Shin et al., 2020; Zhang et al., 2021a).

Extensive advances in the epidemiology, etiology, mechanism, and prognosis of stroke have been made; however, safe and effective treatments have not been developed for most patients. Disability and death are a huge burden on patients and their families worldwide (Zhang et al., 2020b). Cerebral stroke is an acute cerebrovascular disease that includes ischemic and hemorrhagic stroke. Ischemic stroke is the main type of cerebral stroke wherein blood cannot flow to the brain, resulting in the blockage of blood vessels, leading to brain tissue injury (Liang et al., 2016; Hong et al., 2019). When thrombogenesis blocks blood flow in the brain, the energy supply is disrupted, causing damage to the blood vessels and neuronal death. Blood–brain barrier (BBB) breakdown occurs in the first few hours after ischemic stroke and influences the permeability, induces secondary neuron inflammation, and accelerates the process of ischemic tissue damage (Liebner et al., 2018; Tuo et al., 2022). Meanwhile, an inflammatory reaction induced by gliocyte activation could also potentiate damage to the integrity of the BBB (Walsh et al., 2021). Primary cerebral ischemic treatment is to restore blood flow as soon as possible after the onset of symptoms. Alteplase is a recombinant tissue plasminogen activator (rt-PA) and only approved to treat cerebral ischemia stroke by the United States Food and Drug Administration. However, its therapeutic potential is limited by the hemolytic risk and short treatment window (4.5 h), with only a few patients benefitting from its use (Ishiguro et al., 2012; Bruch et al., 2019; Anfray et al., 2021). Therefore, finding a new therapeutic strategy against ischemic stroke is crucial.

Numerous studies have explained the mechanisms of ischemic stroke and ischemia/reperfusion (I/R) and offered several strategies for the use of exosomes for their diagnosis and treatment (Fei et al., 2021; Sun et al., 2021; Zhu et al., 2021). This review briefly describes exosomal biogenesis, collection methods, and communication. It investigates the role of exosomes in the diagnosis, neuroprotection, angiogenesis, anti-inflammation, and the BBB in ischemic stroke and focuses on the development of engineered exosomes. It reveals the mode of communication in various parts of the body in the ischemic stroke environment and the use of exosomes in repair or protective mechanisms. This review also reveals the challenges faced in these studies and provides new strategies for future research and therapeutic schemes for clinical treatment.

2 Exosomal composition and communication

2.1 Exosomal biogenesis and composition

Associating an EV with a particular biogenesis pathway remains extraordinarily difficult unless the EV is captured during release using live imaging techniques. Furthermore, using fluorescent exosome labeling and animal imaging technologies, the acting positions of exosomes can be dynamically tracked with the aim of providing technical support for increased accuracy in gene therapy. However, most studies suggest that exosomes are generated through a process involving the double invagination of the plasma membrane and formation of intracellular multivesicular bodies (MVBs) containing intraluminal vesicles (ILVs) (Théry et al., 2018). Exosomes are initially formed by endocytosis. The cell membrane is internalized to generate endosomes. Thereafter, many vesicles are formed within the endosome by internalizing a portion of the endosomal membrane. Finally, MVBs fuse with the cell membrane, releasing the intraluminal endoplasmic vesicles into the extracellular space to form exosomes (Gruenberg and van der Goot 2006). During this biogenesis process, exosomes carry multiple bioactive components, including proteins, nucleic acids, and lipids, and play a role in the biological functions especially in cellular communication. (Théry et al., 2002) (Figure 1). The heterogeneity of exosomes not only mirrors their size, content, and cellular origin but also reflects a regulated sorting mechanism. Ongoing technological and experimental advances are likely to yield valuable information regarding their heterogeneity and biological function(s), as well as enhance our ability to harness their therapeutic and diagnostic potential. Developing more standardized purification and analytical procedures to study

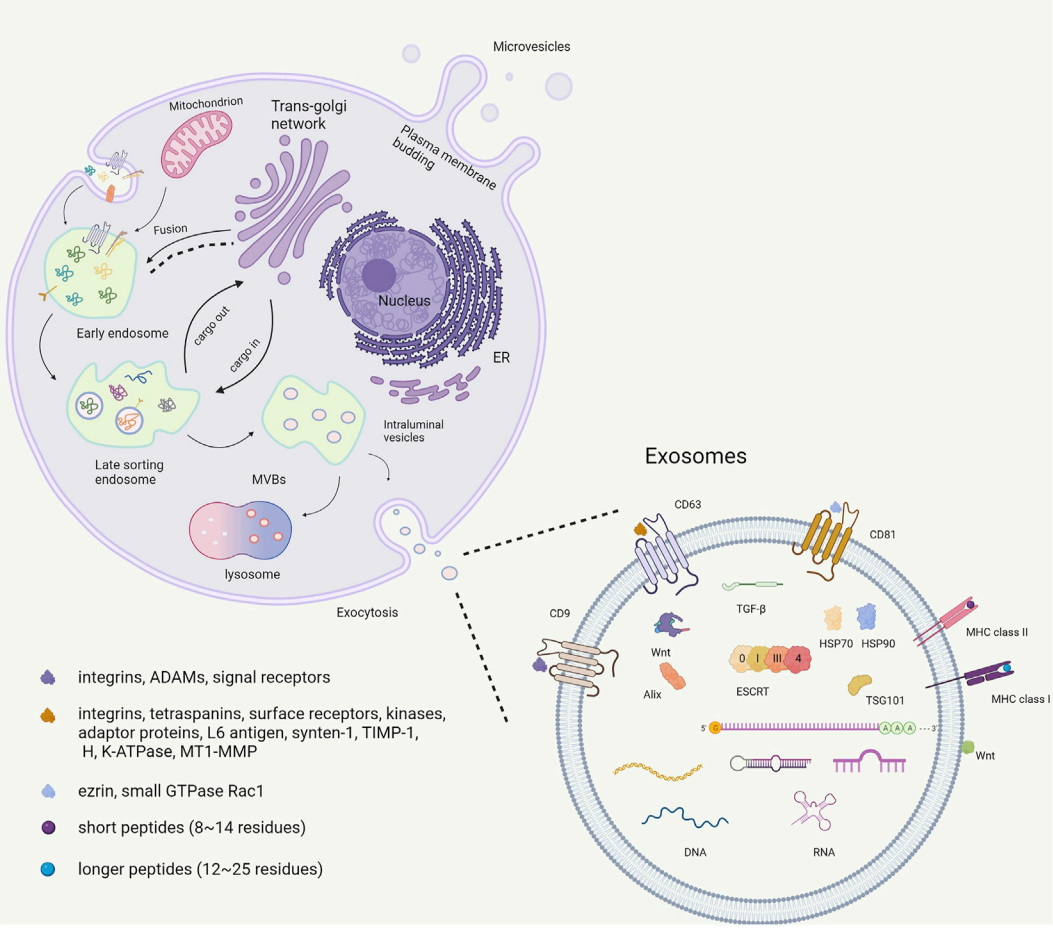

FIGURE 1
The biogenesis and contains of exosome.

exosomes will potentially lead to the uncovering of their functional heterogeneity (Kalluri and LeBleu 2020).

The exosome membrane is a phospholipid bilayer structure with a lipid composition, and it contains are similar to the plasmalemma component of the source cell. (Jeppesen et al., 2019). Exosomal proteins include membrane and intramembrane proteins. Membrane proteins are found in almost all exosomes, such as several tetraspanins (CD9, CD63, and CD81) and major histocompatibility complex class II (MHC II). Tetraspanins play important roles in normal (e.g., cell adhesion, motility, activation, and proliferation) and pathological conditions (e.g., metastasis and viral infection) (Yu et al., 2017). By contrast with many other cell surface proteins, CD9 does not have an obvious receptor function; it may participate in the organization of surface multiprotein complexes through association with other transmembrane molecules, including integrins, ADAMs, and signal receptors, thereby mediating various cellular and physiological functions (Liu et al., 2019a). CD63 interacts with many different proteins either directly or indirectly. Its interaction partners include integrins (α4β1, α3β1, α6β1, LFA-1, and β2), other tetraspanins (CD81, CD82, CD9, CD151), cell surface receptors (MHCII, CD3, FcεRI, and CXCR4), kinases (phosphatidylinositol 4-kinase and the Src family tyrosine kinases Lyn and Hck), adaptor proteins (AP-2, AP-3, and AP-4), and other proteins, including L6 antigen, syntenin-1, TIMP-1, H, K-ATPase, and MT1-MMP (Pols and Klumperman 2009). CD81 has an important function in the immune system. Proteins such as ezrin and the small GTPase Rac1 have been suggested to interact with the C-terminal domain of CD81, providing a potential link between tetraspanins and the cytoskeleton (Sala-Valdés et al., 2006). CD9, CD63, and CD81 are considered exosome markers. Exosomes are known to display two main types of MHC molecules: MHC I and II. MHC I is recognized by $CD8^+$ T-cell and MHC II is recognized by $CD4^+$ T-cell. MHC molecules can bind both self and non-self peptides. MHC I bind short (roughly 8–14 residues) peptides derived from intracellular proteins, such as phosphorylated peptides. MHC II molecules are

primarily expressed in antigen-presenting cells, and bind longer peptides (roughly 12–25 residues) (Racle et al., 2019). Thus, interactions of MHC in exosomes with immune cells can provide novel immunotherapy strategies for ischemic stroke. Moreover, peripheral surface proteins include Wnt and are rich in extracellular matrix (ECM) proteins, which play a role in adhesion and signaling (Zhang et al., 2015; Lerner et al., 2020). Another class of extracellular factors outside the membrane includes transforming growth factor (TGF-β). In addition to external characterization, there is inclusion characterization, and exosomes contain unique proteins, including heat shock proteins (HSP70, HSP90), ESCRT complexes composed of ESCRT-0, ESCRT-1, ESCRT-2, ESCRT-3, and a class of exosomal scaffolding protein Alix (Pegtel and Gould 2019).

Exosomal nucleic acids contain DNA, mRNA, and non-coding RNA. An increasing number of researchers noted the function of mRNA and non-coding RNA in exosomes. The mRNA component carried by exosomes has been shown to enter the plasma membrane and can be translated into proteins (Valadi et al., 2007). Particularly, specific microRNAs (miRNAs), approximately 18–25 nucleotides long, are categorized as small non-coding RNA. They can control the expression of specific genes by binding to complementary sequences in the 3′ untranslated regions (UTRs) of target mRNA transcripts to inhibit or activate mRNA translation and transcription (Sun et al., 2018a; Isaac et al., 2021). miRNAs play a vital information transfer role in intercellular communication by transferring large amounts of biological cargo encapsulated in recipient cells to regulate posttranscriptional gene expression. miRNAs are also involved in the development of neurodegenerative diseases (Kojima et al., 2018), neuropsychiatric disorders (Xu et al., 2012), and tumors (Zhao et al., 2020).

2.2 Intercellular communication

Previously, exosomes were considered cellular debris. However, emerging research results in multiple fields have shown that it is a critical player in mediating intercellular communication (Lande et al., 2020). The biological process of exosomes include initiation, endocytosis, polycystic formation, and fusion with the plasma membrane; this process is precise at every step. mRNA, miRNAs, and other cargo in exosomes can be released by source cells to deliver messages to neighboring cells and distant cells, thereby regulating the function of recipient cells. Exosomes allow for the intercellular transport of proteins and RNA and are also capable of antigen presentation (Chen et al., 2019). They make contact with target cells in three ways: firstly, exosomal membrane proteins bind to recipient cell membrane proteins, activating intracellular signaling pathways in recipient cells. Secondly, exosomal membrane proteins are undetected on the source cell membrane. This indicates that, in an extracellular matrix, the sheared fragments produced by proteases cleave exosomal membrane proteins and could act as ligands to combine with receptors on the membrane and activate intracellular signaling pathways. Thirdly, the exosomal membrane and that of the recipient cell fuse directly, leading to the release of proteins, mRNA, and miRNA in their cargo (Zagrean et al., 2018). Thus, exosomes enable communication between neighboring cells and between source and distant cells through humoral circulation without direct contact (Koide et al., 2022). In several studies, the exosome-mediated transfer of miRNAs has explained the neurovascular unit (NVU) interaction in brain remodeling and cerebral ischemic protection.

3 Extraction and identification of exosomes

3.1 Method of exosome extraction

Exosomes that occur naturally or that are engineered require sensitive extraction and analysis techniques for subsequent research on ischemic stroke. Currently, the gold standard technique for isolation and purification of exosomes from biological fluids or cell supernatants is ultracentrifugation or a combination with ultrafiltration membranes (density gradient centrifugation) (Yan et al., 2019). Density gradient centrifugation has been performed on exosomes in a sample enriched with sucrose in a density range of 1.13–1.19 g/ml by ultracentrifugation (Wang et al., 2014). Immunomagnetic extraction is another innovative method of enrichment and extraction of exosomes. This method uses exosomal membranes to express specific proteins, which are separated and enriched based on the specific binding of antigens and antibodies and the magnetic properties of magnetic beads (Clayton et al., 2001). Therefore, the exosomes extracted using the immunomagnetic method are of high purity. This method is not limited by instruments and reagents and is suitable for use with urine, blood, cell medium, and other sample types (Cai et al., 2018). However, specificity is both an advantage and a disadvantage because exosomes secreted by different cells differ in the type of membrane protein expression as well. Specific antibody-modified immunomagnetic beads are not universally applicable when extracting exosomes from different cell sources. In experiments, several methods are often combined to save time and improve purity.

3.2 Physical characterization

Conventional optical microscopes with magnification limits close to the size of exosomes (a diameter of 30–100 nm) are important; however, they are not adequate for observation. The

TABLE 1 Summary of various exosomes in ischemic stroke.

Derived	Pre-treatment	Cargo	Change	Outcome	References
BMECs	OGD/R	-	-	Protect PC12 cells against OGD/R injury	Zeng et al. (2020)
BMECs	OGD	microRNA-134	Downregulated	Suppressed OLs apoptosis	Xiao et al. (2019)
MECs	MCAO mice	miR-542-3p	Downregulated	Prevented ischemia-induced glial cell inflammatory response	Cai et al. (2021)
	OGD	TLR4	Upregulated		
ASCs	OGD/RP	miR-22-3p	Upregulated	Alleviate brain ischemic injury	Zhang et al. (2021b)
Primary stem cell	OGD/R EA treated	miR-146b	Upregulated	Promotes the differentiation of endogenous neural stem cells improve neurological injury after ischemic stroke	Zhang et al. (2020b)
DPSCs	-	-	-	Alleviated neurological impairment	Li et al. (2020c)
iPSC-NPCs	-	-	-	Promoting the survival and growth of neurons	Li et al. (2021a)
USC	MCAO rats	miR-26a	-	Promoted both proliferation and neuronal differentiation of NSCs after OGD/R	Ling et al. (2020)
NSC	OGD	-	-	Neuroprotection against experimental stroke	Sun et al. (2019)
BV2	Treated with IL-4	miR-137	Upregulated	Attenuated neuronal apoptosis decreased infarct volume	Zhang et al. (2021c)
Astrocyte	OGD	-	-	Suppress autophagy	Pei et al. (2019)
				Ameliorate neuronal damage	
Astrocyte	OGD	miR-17-5p	Upregulated	Improved neurobehaviors	Du et al. (2021)
				Reduced neuronal apoptosis	
Astrocyte	OGD/R	miR-34c	Upregulated	Reduces neurological damage	Wu et al. (2020)
HUVECs	OGD	miR-1290	Upregulated	Protects neurons by attenuating apoptosis	Yue et al. (2019)
HUVECs	H/R	miR-21-3P	Downregulated	Inhibited neurons apoptosis	Jiang et al. (2018a)
Serum	Young rats	CD46	High expression	Attenuated synaptic dysfunction and improve post-stroke functional recovery	Zhang et al. (2021d)
ECEs	Ischemic rats	Proteins and miRNA	Altering miRNAs and target protein profiles	Promotes axonal growth of cortical neurons	Zhang et al. (2020c)
ADSCs	MCAO rat	miR-181-5p	Upregulated	Promote the angiogenesis of BMECs after OGD	Yang et al. (2018a)
BMSCs	-	miRNA-29-3p	-	Promoting angiogenesis	Hou et al. (2020)
				Suppressing neuronal apoptosis	
BMSCs	CXCR4 transfect	-	-	Promote the proliferation and tube formation for angiogenesis	Li et al. (2020d)
				Protecting brain endothelial	
MSCs	-	miR-126	Overexpressing	Enhance the survival and angiogenic function of H/R-injured EC	Pan et al. (2019)
MSCs	-	miR-132-3p	Overexpressing	Reducing cerebral vascular ROS production, BBB injury, and brain injury	Pan et al. (2020)
Microglial	OGD	miR-424-5p	Upregulated	Cell damage	Xie et al. (2020)
				Permeability of BMEC	

(Continued on following page)

TABLE 1 (*Continued*) Summary of various exosomes in ischemic stroke.

Derived	Pre-treatment	Cargo	Change	Outcome	References
BV2	IL-4	miR-26a	Upregulated	Promoted the tube formation	Tian et al. (2019)
ADSCs	-	miR-30d-5p	Overexpressing	Suppression of autophagy	Jiang et al. (2018b)
				Reduced the OGD-innduce inflammatory response	
ADSCs	Hypoxic pre-treated	circ-Rps5	Upregulated	Improved cognitive function by reducing neuronal damage	Yang et al. (2022a)
SCs	-	-	-	Ameliorate brain injury cause by cerebral I/R	Zhang et al. (2021e)
BMSCs	Hypoxia preconditioning	-	-	Alleviating OGD/R-induced injury	Yu et al. (2021)
				Promoting the anti-inflammatory polarization of microglia	
BMECs	-	-	-	I/R injury-induced M1-polarized microglia could be shifted toward M2 phenotype	Liu et al. (2021)
BMSCs	Hypoxic pre-treated	-	-	Neuroprotective effects against NLRP3 inflammasom-mediated pyroptosis	Kang et al. (2021)
hUCMSCs		miR-26b-5p	-	Repress M1 polarization of microglia by targeting CH25H to inactivate the TLR pathway	Li et al. (2020a)
hWJ-MSC	-	-	-	Reduced microglia-mediated neuroinflammation	Thomi et al. (2019)
Plasma	melatonin-treated	-	The miRNA profiles changed	Decreased the infarct volume	Wang et al. (2020)
				Reduces the secretion of inflammatory cytokines	
				Alleviate inflammation	
Microglial	GW4869 treated	-	-	Reversed ischemia-induced microglial activation, inflammatory response	Gao et al. (2020)
Cortical neurons	OGD	miR-181c-3p	Downregulated	Decreased astrocyte expression of CXCL1 and inflammatory factors	Song et al., 2019a
BV2	Treated with IL-4	miR-124	Knockdown	Attenuated ischemic brain	Song et al., 2019b
				Promoted neuronal survival	
bEnd.3	OGD	Protein and miRNA	Changes of exosomal miRNA and surface protein profiles	Provide new therapeutic targets for BBB protection in ischemic stroke	Yang et al. (2021b)
Macrophage	-	-	-	Cross the BBB	Yuan et al. (2017)
				Deliver BDNF to the brain	
Neuron	-	miR-132	-	Maintain brain vascular integrity	Xu et al. (2017)
ECFCs	-	-	-	Increased TJ protein expression	Gao et al. (2018)
				Contribute to BBB integrity	
MSCs	-	-	-	Improve BBB integrity	Williams et al. (2020)
NSCs	-	-	-	Protect the integrity of the blood–brain barrier	Webb et al. (2018)

physical characterization of exosomes, including morphology, size, and distribution, is often measured by more precise microscopic techniques (Raposo and Stoorvogel 2013; Hong et al., 2019). Scanning electron microscopy (SEM), transmission electron microscopy (TEM), and atomic force microscopy (AFM) are reliable and widely used techniques. They are different in the manner in which they analyze exosomes. TEM allows for observation of the internal

structure. SEM primarily allows observation of the morphology and has a stereoscopic sense; however, it is limited to the surface structure of exosomes (Pascucci et al., 2014; Tegegn et al., 2016). The advantage of AFM is that the samples are intact, and the requirements for sample analysis can be readily met compared with those of SEM and TEM, as exosomes can be directly analyzed in atmospheric and liquid environments. Dynamic light scattering can calculate the drug encapsulation rate of exosomes and test their stability in different environments before and after encapsulation. Furthermore, nanoparticle tracking analysis (NTA) allows simultaneous analysis of particle size and concentration of exosomes, and when the concentration is too low, NTA can satisfactorily perform the detection. Compared with other techniques, NTA guarantees the original state of the exosomes and has faster detection.

The most commonly used method for determining exosome purity is the quantification of the total protein amount and total particle number. and lipid amounts and the total number of particles. Thus, ratios of proteins: particles, lipids: particles or lipids: protein should be reported along with global quantification estimation estimates as a measure of purity and thus reliability of the quantity measure (Théry et al., 2018).

4 Pathogenesis and potential therapeutic role of exosomes in ischemic stroke

Ischemic stroke is caused by reduced cerebral blood flow and insufficient supply of oxygen to the brain tissue due to vascular embolism. The longer the condition persists, the more serious the brain damage. However, while treatments reopen the occluded cerebral vessels, the pathological damage to the ischemic tissues, blood vessels, and the nervous system is often further aggravated or even irreversible, and the clinical symptoms worsen, causing cerebral I/R injury. Exosomes are also part of this physiological process, allowing critical intercellular communication. Numerous researchers found that exosomes could cross the BBB and communicate using proteins, mRNA, or miRNA in the NVU to maintain the homeostasis of the central nervous system (CNS) (Forró et al., 2021). Furthermore, various derived exosomes repair injured tissues and exhibit anti-apoptotic, anti-inflammatory, and protection on nerves and vasculature. Table 1 summarizes the relevant studies on various derived exosomes in ischemic stroke.

4.1 Neuroprotection and nerve regeneration

A stroke is among the leading causes of death, and post-stroke neurological disorders are the leading cause of disability worldwide (Liang et al., 2017). Following the onset of ischemic stroke, nerve injury worsens with prolonged ischemia. Moreover, the effect of cerebral I/R injury on neurological damage and brain dysfunction is severe. Stem cells have multiple differentiation potentials and differentiation and developmental plasticity. In previous studies, conditioned medium derived from various stem cells was shown to be effective in treating I/R injury (Mathew et al., 2019; Li et al., 2020a; Lee et al., 2021; Tian et al., 2021). Studies have indicated that bone marrow mesenchymal stem cell (BMSC)-derived exosomes could increase neuron viability in oxygen-glucose deprivation/reperfusion (OGD/R) by reducing NLRP3 inflammatory vesicle-mediated scorch death *via* the promotion of AMPK-dependent autophagic flux (Zeng et al., 2020). In a study, the level of miRNA-134 from BMSC-derived exosomes decreased while brain microvascular endothelial cells (BMECs) were disposed of with OGD. Thereafter, the OGD-disposed oligodendroglia cells (OLs) were treated with BMECs. The results showed that miR-134 inhibitors exacerbated the changes in the expression of the procaspase-8- and caspase-8-cleaved product proteins, which was caused by ODG (Xiao et al., 2019). Mesenchymal stem cells (MSCs) can directly affect the function of brain parenchymal cells *via* MSC-exos (Cai et al., 2021); and Zhang et al. showed that when adipose-derived MSC (ASC)-exos and neurons were co-cultured, miR-22–3p in ASC-exos increased, thus increasing neuron viability *in vitro* and alleviating nerve injury (Zhang et al., 2021a). In addition, tail vein injections of several types of stem cell-free derived exosomes for treatment of middle cerebral artery occlusion (MCAO)/R in mice could promote neural function recovery (Sun et al., 2019; Zhang et al., 2020c; Ling et al., 2020; Li et al., 2021a; Li et al., 2021b; Zhang et al., 2021b). Moreover, the level of astrocyte-derived exosomes, including miR-3c and miR-17–5p, could be used to target TLR7 and BINP2, further decreasing neuronal damage, reducing apoptosis and oxidation, increasing neuronal activity, and improving neurobehaviors (Pei et al., 2019; Wu et al., 2020; Du et al., 2021). Endothelial cell-derived exosomes, such as those from human umbilical vein endothelial cells (HUVECs) and brain-derived endothelial cells (bEnd.3), could influence I/R injury. The miRNA expression of hypoxia/reoxygenation (H/R)-treated HUVECs changes considerably, in that 249 and 104 miRNAs were downregulated and upregulated, respectively. Further studies suggested that miR-12–3p *via* HUVEC-exos could protect neurons against H/R apoptosis (Jiang et al., 2018a). Through the proteomics analysis of exosomes, a study found that pro-inflammatory mediators (C1q, C3a, and C3b) in serum exosomes increase whereas the exosomal levels of CD46, a C3b/C4b-inactivating factor, decrease with age. The microglial expression of C3a, C3b, and the C3a receptor (C3aR) increased after treatment with aged rat-derived exosomes. By replacing aging exosomes with young exosomes, it was possible to reverse the decline of synaptic and neurological functions and deliver therapeutic benefits after stroke (Zhang et al., 2021c). Non-ischemic and ischemic cerebral endothelial cell-derived exosomes facilitate axonal

growth by altering miRNAs and their target protein profiles in recipient neurons (Zhang et al., 2020a).

4.2 Vascular protection and angiogenesis

It was initially thought that stem cells could accumulate in damaged tissues and replace damaged cells by self-renewal and directed differentiation. Recent studies showed that the tissue repair and regenerative functions performed by stem cells are mediated by their paracrine effects at stem cells that are less differentiated and unstable at the site of injury (Rong et al., 2019). There is evidence that the paracrine role of stem cells may be an important mechanism for their function in angiogenesis. Cerebral I/R could change the metabolism and function of endothelial cells (ECs), which could trigger EC damage, which may lead to cell death, and multiple signaling pathways. Therefore, the repair of damaged ECs and the promotion of angiogenesis in the damaged area are of vital importance in cerebral ischemia-induced vascular injury. Adipose-derived stem cells (ADSCs) promote cerebral blood vessel remodeling. Similarly, ADSC-derived exosomes could act on the miRNA-181b/TRPM7 axis to improve injury of ECs subjected to OGD/R and ameliorate mobility and angiogenesis of BMECs; therefore, miR-181–5p contributes to angiogenesis (Yang et al., 2018b). MSCs are different from other stem cells in that they are primarily found in connective tissue and interstitial organs. In addition, structural and functional alterations in the brain microvasculature might be major barriers to adequate reperfusion of cerebral ischemia (Cipolla 2021; Yang et al., 2022a). Hou et al. found that miRNA-29–3p in BMSC-exos was downregulated after BMSCs were subjected to OGD. Additionally, PTEN was upregulated and angiogenesis decreased in MCAO rats (Hou et al., 2020). Li et al. transfected BMSCs with lentivirus encoded by CXCR4. Thereafter, BMSC-exos^{CXCR4} was injected into the ipsilateral lateral ventricle of MCAO model rat brain. The results indicated that BMSC-exo ^{CXCR4} could attenuate the activation of the Wnt-3a/β-catenin pathway, achieve anti-apoptosis, and promote the proliferation and tube formation of microvascular ECs (Li et al., 2020a). Moreover, miR-126 is an important regulator of EC functions and angiogenesis. MSC-exo upregulate the level of VEGF, EGF, PDGF, and bFGF in H/R-injured ECs *via* delivery of miR-126, activate PI3K/Akt/eNOS pathway, and promote angiogenesis (Pan et al., 2019). Similarly, MSC-exo $^{miR-132-3p}$ has been shown to act on the PI3K signaling pathway, have anti-apoptotic effects, and improve the function of oxidative stress-affected ECs (Pan et al., 2020). Except for the H/R-injured condition, polarized BV2 microglial cells also show pro-angiogenesis effects (Xie et al., 2020). Tian et al. demonstrated the polarization of microglia using LPS and interleukin 4 (IL-4). The transfer of polarized BV2 cells was performed by intravenous injection into MCAO mice. Thereafter, the expression of BV2-exo miRNA under different conditions was compared using miRNA microarray technology. The study found that miRNA-26a contains more IL-4-polarized BV2 cell-derived exosomes. Moreover, IL-4-polarized BV2 cells promoted tube formation of ECs by secreting exosomes and had a therapeutic effect on stroke (Tian et al., 2019).

4.3 Inflammation reaction

I/R of the CNS could elicit an inflammatory response that stimulates the innate immune system to activate a series of inflammatory cascades (Sun et al., 2020). The immune cells that initially respond are microglia. They are normally quiescent, and when they are activated by damage, they become immune effector cells of the CNS (Choi et al., 2009; Dixon et al., 2021). In fact, microglia are activated to M1 phenotypes, typically releasing pro-inflammatory mediators and exacerbating brain injury. Switching the polarization of microglia from the pro-inflammatory M1 phenotype to the anti-inflammatory M2 phenotype is a promising therapeutic strategy for ischemic stroke (Yang et al., 2011; Zheng et al., 2019). Neutrophils exacerbate oxidative stress and BBB damage and participate in the pathological responses to injury and inflammation (Kolaczkowska and Kubes 2013). Hence, mitigating the immune-mediated inflammatory response is a crucial goal for ischemic stroke treatment. In acute ischemic stroke, the expression of inflammation factors increases and that of miR-30days-5p decreases in animal and patient models. Jiang et al. demonstrated that miR-30days-5p enhances ADSC-exos, inhibiting autophagy-mediated microglia polarization, thereby preventing cerebral injury (Jiang et al., 2018b). In contrast to previous studies, circular RNAs (circRNAs) in exosomes also mediate biological mechanisms *via* gene regulation. miR-124–3p and SIRT7 are circ-Rps5 downstream targets, while hypoxia pretreatment with ADSC-exo$^{circ-Rps5}$ could shift microglia from an M1 to M2 phenotype in the hippocampus, decreasing MCAO-induced inflammatory factor (IL-6, IL-1β, and TNF-α) expression (Yang et al., 2022b). Likewise, stem cells (Zhang et al., 2021c), BMSCs (Kang et al., 2021; Liu et al., 2021; Yu et al., 2021), human umbilical cord MSC-derived exosomes (Li et al., 2020b), human Wharton's jelly MSCs (Thomi et al., 2019), and the plasma-derived exosomes (Wang et al., 2020) can ameliorate cerebral I/R injury attributed to the modulation of microglia polarization. Additionally, glutaminase 1 (GLS1), a mitochondrial enzyme, causes chronic neuroinflammation, learning deficits, and synaptic dysfunctions in transgenic animal models. Gao et al. observed that GLS1-mediated exosome release might play a key role in the formation of a neuroinflammatory microenvironment (Gao et al., 2020). Besides microglia, inflammation factors released by astrocytes also have a profound impact on the inflammatory response in

cerebral ischemia. Song et al. investigated whether the *CXCL1* gene was upregulated in ischemia brain injury and if it promoted an inflammatory response in MCAO rats. Subsequent studies found that exosomes derived from cortical neurons that underwent OGD decrease the expression of *CXCL1* and inflammatory factors in astrocytes, following delivery of miR-181c-3p *via* exosomes (Song et al., 2019a). Alternatively, M2 microglia-derived exosomes attenuate ischemic brain injury and promote neuronal survival *via* exosomal miR-124 and its downstream target, USP14 (Song et al., 2019b). Proximity barcoding assay experiments showed that the numbers of bEnd.3-derived exosomes carrying various proteins (bFGF, CD146, EPHA2, ABCB5, and ITGB2) increase markedly during ischemia. Such proteins are related to angiogenesis, cell proliferation, and cell inflammation (Yang et al., 2021a).

4.4 Crossing and maintaining the BBB

As part of the NVU, the BBB is a dynamic regulatory boundary that controls and limits the exchange of molecules, ions, and cells between blood and the CNS (Yang et al., 2019). The BBB has a massive impact on maintaining the homeostatic microenvironment of the CNS and normal neuronal function. Following an ischemic stroke, the structural integrity of the BBB is affected, leading to a substantial increase in the paracellular permeability in the cerebral microvasculature, a noteworthy pathological characteristic of ischemic stroke (Jiang Y. et al., 2018). Furthermore, an impaired BBB aggravates cerebral injury progression and increases hemorrhage risk, which leads to poor patient outcomes and limits the use of tPA for treatment (Liu and Chopp 2016). Yuan et al. first demonstrated that exosomes do not necessarily have to be modified to penetrate the BBB in mammals (Yuan et al., 2017). Notably, native macrophage-derived exosomes interact with BMECs and regulate intercellular adhesion molecule-1 (ICAM-1), whose expression plays a key role in BBB support (Bendorius et al., 2018).

Neurons can regulate brain vascular integrity. A study conducted by Xu et al. showed that miR-132 functions as an intercellular signal, mediating neural regulation of brain vascular integrity, and indicated that neuronal exosomes are a novel communication mechanism for the brain (Xu et al., 2017). Moreover, a marker of BBB disruption is disruption of the tight junction (TJ) protein complex. Hypoxia pretreatment with endothelial colony-forming cell (ECFC)-derived exosomes increase TJ protein expression and target the PTEN/AKT signaling pathway; thus, the study showed that exosomes derived from ECFCs contribute to BBB integrity (Gao et al., 2018). Naturally, MSC- and neural stem cell derived exosomes may be neuroprotective, decreasing the severity of brain injury in addition to maintaining the BBB integrity (Webb et al., 2018; Williams et al., 2020). Vascular protection and revascularization in ischemic stroke diseases are different from other disease conditions, and the treatment of cerebral ischemia is usually concerned with increasing collateral circulation and maintaining CNS homeostasis rather than the peripheral (Monteforte et al., 2017). Simultaneously, several studies have demonstrated the unique advantage of vascular endothelium-derived exosomes in a variety of diseases and in crossing the BBB up to the CNS, thus focusing on cerebral ischemia.

5 Diagnosis of ischemic stroke

Based on the European Stroke Organization's guidelines on intravenous thrombolysis for acute ischemic stroke, the use of rt-PA is conditional at onset depending on medical history and other parameters. Moreover, the type of the drug, tenecteplase-tPA or rt-PA, and the dose to be administered is determined according to differing degrees of onset. The main diagnostic tool for cerebral stroke is advanced imaging, which is utilized to determine whether the conditions for mechanical embolization are satisfied. If an acute stroke is to be treated with intravenous thrombolysis based on the current guidelines, a rapid, sensitive, and accurate diagnostic tool is required for such a short therapeutic window. Meanwhile, the profile of exosomes in blood, urine, and other media have considerable differences amongst patients with a particular disease and healthy individuals and can be easily analyzed for assessing disease risk (Yang et al., 2022c). Based on the above pathogenesis research, not all miRNAs with differential expression can be used as diagnostic biomarkers; however, those that are should be specific and stable.

Exosomes are secreted by all types of cells and are present in biological fluids, making their sampling appealing for tracking disease progression in liquid biopsies. Therefore, exosomes have diagnostic abilities as potential biomarkers, making distinct stages of ischemic stroke easier to diagnose based on differences in the levels of miRNA. The level of miR-134 in plasma exosomes in patients with acute ischemic stroke is higher than in normal controls, and infarct volume is positively associated with a worse prognosis in patients with stroke (Zhou et al., 2018). miRNA expression changes throughout the various phases of the stroke, including during the time of early symptoms, symptom appearance, and prognosis. During pathogenesis [comprising the hyperacute phase IS (HIS, <6 h), acute ischemic stroke (one to three and 4–7 days), subacute phase IS (SIS, 8–14 days), and recovery phase (RIS, >14 days)] of cerebral ischemia, the expression of miRNA in plasma varies in clinical investigations, i.e., the expression of mi-R-30a-5p, miR-422a, miR-21–5p, and miR-1256-2-3p were found to be different in the four phases (Chen et al., 2015; Kerr et al., 2018; Wang et al., 2018). Similarly, compared with the control group, the expression of miR-223 in serum exosomes of patients with acute ischemic stroke was notably upregulated. Moreover,

exosomal miR-223 expression is higher in stroke patients with poor outcomes than in those with favorable outcomes (Chen et al., 2017), showing positive correlation with NIH Stroke Scale/Score. Moreover, transient ischemic attack and permanent cerebral ischemia are different. Three hours after permanent cerebral ischemia, a rapid reduction in the level of serum exosomal miR-126 occurs, and it returns to normal after 24 h (Chen et al., 2015). In addition, patients with large artery atherosclerosis show the lowest serum exosome miR-152–3p levels compared with those with small vessel occlusion, cardiac embolism, and stroke of undetermined etiology. Moreover, the level of miR-152–3p in serum exosomes is lower in acute ischemic stroke than in the chronic phase (Song et al., 2020).

Furthermore, atherosclerosis can promote thrombosis and is strongly associated with acute cerebrovascular morbidity; its progression involves exosomes delivering bioactive messages. miR-21, miR-29, miR-126, miR-133, miR-146, and miR-155 in EC-derived exosomes may act as functional biomarkers to diagnose and predict the outcomes of atherosclerosis (Hulsmans and Holvoet 2013; Cervio et al., 2015; Lu et al., 2019). Moreover, growth arrest and DNA damage-inducible protein-34 (GADD34) has opposing effects on different stimulus-induced cell apoptotic events in many diseases affecting the nervous system. There is an increase in GADD34 levels in plasma exosomes of cerebral ischemic rats, indicating that exosome GADD34 could be used as a diagnostic biomarker and therapeutic target in ischemic strokes (Yang et al., 2021b). Therefore, based on the combination of these specific miRNAs and proteins within the group, it could be recognized as potential biomarkers of exosomes to diagnose ischemic stroke.

6 Development of engineered exosomes

Natural exosomes express transmembrane proteins and membrane-anchored proteins that allow them to be biocompatible. Exosomes as natural vehicles can achieve the objectives of nucleic acid delivery and drug targeting across physiological barriers and have advantages of lower immunogenicity and toxicity and favorable pharmacokinetics (Song Y. et al., 2019; Li Y. J. et al., 2021). However, the short half-life ($t_{1/2}$) and weak targeting ability of exosomes limit their clinical application; engineered exosomes are capable of breaking through these limitations (Han et al., 2019). By engineering exosomes, we can impart additional functionality to the exosomes with the aim of enabling *in vivo* imaging and tracking, which facilitates the understanding of their fate *in vivo*, including the uptake mechanisms and biodistribution. Exosome engineering can significantly promote the application of exosomes for therapy and targeted drug delivery in various brain pathologies. We plan to focus on the availability of engineered exosomes as delivery nanotechnologies and in *in vivo* imaging and tracking next. Table 2 summarizes the relevant studies on engineered exosomes in the brain.

6.1 Delivery nanotechnologies

Exosomal delivery nanotechnologies are attractive because of their ability to improve the solubility and targeting specificity of natural compounds. Guo et al. enhanced the stability and solubility of quercetin by preparing quercetin-loaded exosomes. A monoclonal antibody GAP43 (a neuron-specific protein) continued to be modified on the surface of drug-loaded exosomes to alleviate neuronal damage by targeting ischemic penumbra (Guo et al., 2021). Briefly, curcumin (cur), an anti-inflammatory and neuroprotective molecule, could load macrophage (Ex-cur) and embryonic stem cell-derived exosomes (MESC-exo^{cur}). They could downregulate ROS accumulation, alleviate BBB damage in lesions, reduce the expression of inflammation and the excitatory amino acid receptor, and improve neurovascular restoration (Kalani et al., 2016; He et al., 2020). Macrophage-derived exosomes containing Edaravone (Exo + Edv) could improve bioavailability, prolong $t_{1/2}$, and have neuroprotective effects on permanent MCAO rats (Li et al., 2020b). The investigation showed that tar-exo-enkephalin (exosomes, combined with transferrin and enkephalin, were packaged into the vesicle) was capable of crossing the BBB and inhibited neuron apoptosis caused by glutamate by decreasing p53 and caspase-3 levels. This result was verified in transient MCAO rats (Liu et al., 2019b).

In addition to molecular drug delivery, nucleic acid and peptide delivery can be achieved. Pigment epithelium-derived factor (PEDF) was overexpressed in ADSCs, and PEDF-modified ADSC-derived exosomes were obtained. These ameliorated neuron OGD-induced apoptosis and I/R injury by activating autophagy (Huang et al., 2018). Yang et al. found that rabies virus glycoprotein (RVG)-modified exosomes could promote cortical neurogenesis to attenuate ischemic injury by delivering miR-124 to the infarct (Yang et al., 2017). Similarly, Yang et al. first found that nerve growth factor-Exo^{RVG} reduced ischemic injury by reducing inflammation and cell death (Yang et al., 2020). MSC-exos were conjugated to c (RGDyK) peptides and loaded with cholesterol-modified miR-210 to target the ischemic brain. Considerable improvement in angiogenesis and survival was observed in MCAO/R mice using near-infrared fluorescence imaging (Zhang et al., 2019). The receptor for advanced glycation end-products (RAGE)-binding-peptide linked to exosomes (RBP-Exo) was used for nose-to-brain delivery of anti-miRNA oligonucleotide. Moreover, compared with unmodified exosomes, RBP-Exo could downregulate RAGE more efficiently to deliver AMO181a, and reduced damage to the ischemic brain (Kim et al., 2021).

TABLE 2 Summary of engineered exosomes in ischemic stroke.

Derived	Engineered method	Outcome	References
Whole blood of SD rats	Que loaded and mAb GAP43 conjugated	Targeting and therapeutic drug delivery system	Guo et al. (2021)
Macrophage	Curcumin loaded	Accumulated Ex-cur in ischemic regions to reduce ROS accumulation	He et al. (2020)
MESC	Curcumin loaded	Neurovascular restoration following I/R injury	Kalani et al. (2016)
Macrophage	Edaravone Loaded	Improved the biovailability of Edv and prolonged	Li et al. (2020b)
Mesenchymal cells	Transferrin combined and enkephalin packaged	Promote neurological recovery after stroke	Liu et al. (2019b)
ADSC	PEDF overexpressed	Activating autophagy and suppressing neuronal apoptosis	Huang et al. (2018)
BM-MSC	Modified exosomes with RVG fused to exosomal protein Lamp2b	Utilized therapeutically for the targeted delivery of gene drugs to the brain	Yang et al. (2017)
HEK293	RVG peptide on the surface and loaded NGF	Neuron targeting and NGF was delivered in to ischemic cortex	Yang et al. (2020)
MSC	c (RGDyK) peptide was conjugated and cholesterol-modified miR-210 loaded	Targets the lesion region of the ischemic brain to angiogenesis	Zhang et al. (2019)
HEK293T	Linked to RAGE-binding-piptide	Nose-to-brain delivery of AMO181a-chol and exerted neuroprotective effects	Kim et al. (2021)
	Loaded with cholesterol-modified AMO181a		
Brain endothelial cells	Rhodamine 123-loaded exosomes	the ability of exosomes to deliver drugs across the BBB	Yang et al. (2015)
MSC	MSC-exo combined with AuNPs as labeling agents	developed a method for longitudinal and quantitative *in vivo* neuroimaging of exosomes	Perets et al. (2019)
MSC	Glucose-coated gold nanoparticle (GNP) labeling and computed tomography imaging	The technique can serve as a powerful diagnostic tool for various brain disorders	Betzer et al. (2017)
HEK293	Using a slight modification of the adenovirus-free transient transfection methods	The use of exo-AAVs as an efficient gene delivery tool	Orefice et al. (2019)
Raw264.7	Loaded superparamagnetic iron oxide nanoparticles (SPIONs) and curcumin (Cur) into exosomes	Carry nanomaterials and chemical agents for simultaneous diagnosis and treatment of glioma	Zhang et al. (2019)

6.2 *In vivo* imaging and tracking

Translating exosome therapies to clinical settings is challenging and assessing treatment outcomes can only be achieved by evaluating symptom improvement, which typically takes weeks to months after treatment. Imaging of engineered exosomes allows real-time assessment of the exosomes' fate and reveals information regarding the function, viability, and circulation of the exosomes *in vivo*. In a study, rhodamine 123-loaded exosomes were injected into zebrafish embryos, and the fluorescence of rhodamine 123 was examined in the brain tissue. The results confirmed the ability of exosomes to deliver drugs across the BBB, highlighting their potential for the treatment of brain diseases (Yang et al., 2015). Gold nanoparticles (AuNPs) are widely used in various bioanalytical and biomedical detection techniques. Perets et al. developed a method for longitudinal and quantitative *in vivo* neuroimaging of exosomes based on the superior visualization abilities of classical X-ray computed tomography (CT), combined with AuNPs as labeling agents. This technique has been proven to track the migration and homing patterns of intranasally-administered exosomes derived from MSC-exos in different brain pathologies (Perets et al., 2019). Furthermore, a previous study has established a method for non-invasive *in vivo* neuroimaging and tracking of exosomes based on glucose-coated AuNP (GNP) labeling and CT imaging. Using a mouse model of focal brain ischemia, the authors could track intranasally-administered GNP-labeled exosomes in a non-invasive manner (Betzer et al., 2017). This strategy could also be used to assess and compare the spread of exosome-enveloped adeno-associated virus (exo-AAVs) or unassociated AAVs (std-AAVs) in the brain through *in vivo* optical imaging techniques, such as probe-based confocal laser endomicroscopy (pCLE) and *ex vivo* fluorescence microscopy. The results suggest that the strategy

TABLE 3 The application of exosomes and EVs in stroke clinical trials.

ClinicalTrials.gov identifier	Official tittle	Study type	First posted	Estimated/ Actual study start date	Condition or disease	Intervention/ Treatement
NCT05326724	The Role of Acupuncture-induced Exosome in Treating Post-stroke Dementia	Interventional (clinical trial)	13 April 2022	1 August 2022	Exosome Post-stroke Dementia Acupuncture	Device: Acupuncture
NCT03384433	Allogenic Mesenchymal Stem Cell Derived Exosome in Patients with Acute Ischemic Stroke	Interventional (clinical trial)	27 December 2017	17 April 2019	Cerebrovascular disorders	Biological: exosome
NCT05370105	Extracellular Vesicles as Stroke Biomarkers (EXO4STROKE)	Observational	11 May 2022	25 June 2018	Stroke Rehabilitation	Other: blood withdrawal
NCT05524506	PROgnostic Value of MicroParticles and Markers of Hemostasis in TIA and Ischemic Stroke (PROMPTS)	Observational	1 September 2022	June 2007	Brain Ischemia Cerebral Ischemia Extracellular Vesicles Hemostasis Prognosis	-

enables tracking of exo-AAV spread and that exo-AAVs allow for widespread, long-term gene expression in the CNS, supporting the use of exo-AAVs as an efficient gene delivery tool. Moreover, a new type of engineered exosomes has been designed (Orefice et al., 2019). In this strategy, superparamagnetic iron oxide nanoparticles and Cur were loaded into exosomes and the exosomal membrane was conjugated with neuropilin-1-targeted peptides (RGERPPR peptide) using click chemistry to obtain exosomes that possess imaging and therapeutic functions, thus providing a potential approach for improving the diagnosis and treatment effects (Jia et al., 2018). Engineering can be made to achieve an efficient, targeted, or controlled release. However, precise exertion of a slow and controlled release after modification remains a great challenge. This strategy should also be compatible with cell culture conditions and must not affect the exosome itself.

7 Perspectives and conclusion

A key limitation for the precise characterization of EVs is the technical difficulty in isolating and characterizing pure populations of specific subtypes, as the methods currently at our disposal lead to systematic co-isolation of EVs of distinct subcellular origins. Thus, although many research articles use the term "exosome" to refer to EV preparations that have been separated from larger EVs *via* physical and biological processes (western blotting, NTA, TEM, *etc.*), it is likely that they are instead referring to a mixture of small EVs possessing both an exosomal and a non-exosomal properties. Hence, unless their MVB origin has been clearly established, using the more generic term "small EVs" is preferable.

Most research on ischemic stroke treatment and pre-development of new drugs have focused on neuron and EC development or have studied each part separately, ignoring the holistic nature of brain organization and the interactions between the parts. The NVU includes ECs, pericytes, neurons, glial cells, and ECM; this highlights the connection between the vasculature, the nerves, and the surrounding environment (Cai et al., 2017). As a prominent intercellular communication messenger, exosomes transmit biological information within the NVU and allow communication between the brain and distant tissues through the circulation of body fluids (He et al., 2021). This may explain why most neuroprotective agents were effective in preclinical studies but failed in clinical trials (Paul and Candelario-Jalil 2021). Additionally, tissue interactions in a variety of diseases, such as other neurodegenerative diseases (Guo et al., 2020), cancer (Chen et al., 2021), atherosclerosis (Zhu et al., 2019), and diabetes (Sun et al., 2018b), can be elucidated by exosomes.

miRNAs in exosomes are thought to have a substantial therapeutic impact. miRNAs are key regulatory substances carried by exosomes and have specific characteristics compared to free miRNAs. Their characteristics determine homeostasis during the treatment of ischemic stroke (Rappa et al., 2019). Moreover, the risk of microvascular occlusion is reduced in exosome therapy compared with cell therapy (Nikfarjam et al., 2020; Moghadasi et al., 2021). It has been

shown that cell therapy and the use of exosomes are almost consistent. Exosomes are more stable as they show resistance to degradation and can act as a nanocarrier to deliver miRNAs and siRNAs to the CNS (Kim et al., 2019; Chen et al., 2020).

This review summarizes an abundant amount of research reporting that miRNAs in exosomes are involved in a wide range of paracrine and endocrine biological activities and fulfill important functions in different types of target cells in ischemic stroke. However, this point of view remains controversial. In general, studies examining this particular function have typically been conducted with a large excess of exosomes; these studies could not ascertain the feasibility of utilizing endogenous exosomes as functional miRNA transfer vehicles in native physiological settings (Chevillet et al., 2014). One study revealed that the number of miRNA molecules carried by the EVs is too small to make a biologically significant difference in recipient cells (Toh et al., 2018). This could be explained by one of two possibilities: either the miRNA levels in the EVs are insufficient to regulate their target mRNAs in recipient cells upon EV-mediated delivery, or the RNA-containing EVs themselves are not functional in recipient cells. Thus, it is critical to determine the effects of both the miRNA and protein on biochemical potency to reach the therapeutic dose required to elicit a relevant biochemical effect.

The protein range is rather limited when initially analyzing the protein composition of exosomes. Exosome preparations do not contain any proteins originating from the nucleus, mitochondria, endoplasmic reticulum, or Golgi apparatus. Instead, almost all identified exosomal proteins are found in the cytosol, plasma membrane, and membranes of endocytic compartments. The exosomes are formed of plasma membrane fragments as they lack abundant cell surface proteins (Théry et al., 2001; Théry et al., 2002). With the development of exosome proteomics and databases such as ExoCarta, EVpedia, and Vesiclepedia, a wealth of exosome proteins could be elucidated including different species, tissue, and uncertain cellular sources. Moreover, a previous study suggested that proteomes of MSC-derived exosomes are involved in many key biological processes that are important in cellular communication and structure; inflammation; exosome biogenesis and development; tissue repair and regeneration; and metabolism (Lai et al., 2012). Based on these studies, it can be deduced that exosome proteins have the potential to modulate many biological processes involved in disease pathogenesis and tissue repair and regeneration.

Both natural and engineered exosomes have certain targeting capabilities with the advantages of low immunogenicity (Yu et al., 2014), high membrane structure stability, low drug dose, sensitivity, and reduced drug toxicity (Yu et al., 2019; Liang et al., 2021) compared with non-biological carriers. Drug-mediated or -induced exosomes in ischemic stroke therapy are also noteworthy (Zang et al., 2020; Zhai et al., 2021); however, their targeting ability still requires improvement. Ensuring that exosomes are not disturbed by exogenous substances is also a challenge.

In most studies, only one miRNA with considerable differences in exosomes was explored. There are differences in exosome-derived miRNAs, with no uniform criteria for diagnosis and treatment of diseases. Therefore, the selected biomarker should be specific and well-established, and the exosome preparation technique should be easily repeatable. Numerous studies have analyzed miRNA sequencing in various derived exosomes after ischemic stroke or OGD/R pretreatment and found that miRNAs are differentially expressed under disease conditions (Zhang et al., 2020b; Yang et al., 2021a). Nevertheless, whether each miRNA or several mRNAs synergistically play a more effective role is yet to be elucidated. Furthermore, except for the process of diagnosis and treatment, there are several limitations that need to be overcome prior to clinical therapeutic application, and this includes a better understanding of the mechanism by which exosome therapy may lead to enhanced recovery.

Exosome manufacturing is scalable and more amenable to process optimization as the producer cells can be clonally selected and derived. Clinical focus on exosomes as natural carriers could enable nucleic acid delivery, targeted drug delivery, and non-invasive diagnosis. Therefore, it is critical to ensure standardized and reproducible production of exosomes for clinical translation. Addressing process development and scaling up exosome production would be easier if a regulatory-accepted definition of what an exosome is could be settled on. Regarding the matter, the International Society for Extracellular Vesicles provided information on upstream cell culture and downstream processing that will potentially advance exosomes toward routine manufacture. For cell culture fluid-derived exosomes, the number of cell passages, inoculation density, culture volume, and whether stimulation or other treatments have occurred, should be recorded, and details regarding medium composition and preparation, including components, such as glucose, antibiotics, growth factors, and other supplements affecting the production and composition of exosomes, should be provided in the methods. In particular, components containing exosomes, such as the serum, and cell culture history (conversion of media and adaptation steps) should also be included. For exosomes obtained from sources such as plasma, serum, and other derivatives of biological fluids, in addition to the need to control for initial volume, detailed information is required, including donor age, physiological sex, time of collection (circadian rhythm variation), diet, body mass index, specific infectious and non-infectious diseases, medications, and other factors that may affect exosome secretion (Thery et al., 2018). There are also significant downstream processing challenges to manufacturing exosomes. Different methods of preparation and purification might affect the reproducibility of obtaining exosomes (Colao et al., 2018). Although the ultracentrifugation method is the gold

standard for exosome extraction, exosome purity still requires improvement. While tools such as immunomagnetic and transmission surface plasmon resonance may not fit the requirements of a large-scale purification platform, they are potentially label-free methods that may aid isolation of exosomes that can be subsequently characterized (Lobb et al., 2015; Colao et al., 2018; Whitford and Guterstam 2019).

In this review, we have included studies that investigated the application of exosomes and EVs clinically in stroke cases; however, to our knowledge, only a few studies were found (search date: 1 November 2022; Table 3). This may be due to problems with clinical sample collection and difficulty in controlling the time of onset of ischemic stroke.

Data Availability statement

The original contributions presented in the study are included in the article/Supplementary Material, further inquiries can be directed to the corresponding authors.

Author contributions

MJ drafted the manuscript. SZ and MW revised the manuscript. QL and JR designed the outline of the article. YL and XS supervised the whole project and reviewed the manuscript. All authors provided ideas and approved the final version of the manuscript.

Funding

This work was supported by the CAMS Innovation Fund for Medical Sciences (CIFMS) (No. 2021-I2M-1-031) and the National Natural Science Foundation of China (No. 81891012, U20A20405).

Conflict of interest

The authors declare that the research was conducted in the absence of any commercial or financial relationships that could be construed as a potential conflict of interest.

Publisher's note

All claims expressed in this article are solely those of the authors and do not necessarily represent those of their affiliated organizations, or those of the publisher, the editors and the reviewers. Any product that may be evaluated in this article, or claim that may be made by its manufacturer, is not guaranteed or endorsed by the publisher.

References

Anfray, A., Brodin, C., Drieu, A., Potzeha, F., Dalarun, B., Agin, V., et al. (2021). Single- and two- chain tissue type plasminogen activator treatments differentially influence cerebral recovery after stroke. *Exp. Neurol.* 338, 113606. doi:10.1016/j.expneurol.2021.113606

Bendorius, M., Po, C., Muller, S., and Jeltsch-David, H. (2018). From systemic inflammation to neuroinflammation: The case of neurolupus. *Int. J. Mol. Sci.* 19, E3588. doi:10.3390/ijms19113588

Betzer, O., Perets, N., Angel, A., Motiei, M., Sadan, T., Yadid, G., et al. (2017). *In vivo* neuroimaging of exosomes using gold nanoparticles. *ACS Nano* 11, 10883–10893. doi:10.1021/acsnano.7b04495

Bruch, G. E., Fernandes, L. F., Bassi, B. L. T., Alves, M. T. R., Pereira, I. O., Frézard, F., et al. (2019). Liposomes for drug delivery in stroke. *Brain Res. Bull.* 152, 246–256. doi:10.1016/j.brainresbull.2019.07.015

Cai, G., Cai, G., Zhou, H., Zhuang, Z., Liu, K., Pei, S., et al. (2021). Mesenchymal stem cell-derived exosome miR-542-3p suppresses inflammation and prevents cerebral infarction. *Stem Cell. Res. Ther.* 12, 2. doi:10.1186/s13287-020-02030-w

Cai, S., Luo, B., Jiang, P., Zhou, X., Lan, F., Yi, Q., et al. (2018). Immuno-modified superparamagnetic nanoparticles via host-guest interactions for high-purity capture and mild release of exosomes. *Nanoscale* 10, 14280–14289. doi:10.1039/c8nr02871k

Cai, W., Zhang, K., Li, P., Zhu, L., Xu, J., Yang, B., et al. (2017). Dysfunction of the neurovascular unit in ischemic stroke and neurodegenerative diseases: An aging effect. *Ageing Res. Rev.* 34, 77–87. doi:10.1016/j.arr.2016.09.006

Cervio, E., Barile, L., Moccetti, T., and Vassalli, G. (2015). Exosomes for intramyocardial intercellular communication. *Stem Cells Int.* 2015 (482171), 1–10. doi:10.1155/2015/482171

Chen, B. Y., Sung, C. W., Chen, C., Cheng, C. M., Lin, D. P., Huang, C. T., et al. (2019). Advances in exosomes technology. *Clin. Chim. Acta* 493, 14–19. doi:10.1016/j.cca.2019.02.021

Chen, F., Du, Y., Esposito, E., Liu, Y., Guo, S., Wang, X., et al. (2015). Effects of focal cerebral ischemia on exosomal versus serum miR126. *Transl. Stroke Res.* 6, 478–484. doi:10.1007/s12975-015-0429-3

Chen, J., Zhang, K., Zhi, Y., Wu, Y., Chen, B., Bai, J., et al. (2021). Tumor-derived exosomal miR-19b-3p facilitates M2 macrophage polarization and exosomal LINC00273 secretion to promote lung adenocarcinoma metastasis via Hippo pathway. *Clin. Transl. Med.* 11, e478. doi:10.1002/ctm2.478

Chen, S. Y., Lin, M. C., Tsai, J. S., He, P. L., Luo, W. T., Chiu, I. M., et al. (2020). Exosomal 2', 3'-CNP from mesenchymal stem cells promotes hippocampus CA1 neurogenesis/neuritogenesis and contributes to rescue of cognition/learning deficiencies of damaged brain. *Stem Cells Transl. Med.* 9, 499–517. doi:10.1002/sctm.19-0174

Chen, Y., Song, Y., Huang, J., Qu, M., Zhang, Y., Geng, J., et al. (2017). Increased circulating exosomal miRNA-223 is associated with acute ischemic stroke. *Front. Neurol.* 8, 57. doi:10.3389/fneur.2017.00057

Cheng, J., Meng, J., Zhu, L., and Peng, Y. (2020). Exosomal noncoding RNAs in glioma: Biological functions and potential clinical applications. *Mol. Cancer* 19, 66. doi:10.1186/s12943-020-01189-3

Chevillet, J. R., Kang, Q., Ruf, I. K., Briggs, H. A., Vojtech, L. N., Hughes, S. M., et al. (2014). Quantitative and stoichiometric analysis of the microRNA content of exosomes. *Proc. Natl. Acad. Sci. U. S. A.* 111, 14888–14893. doi:10.1073/pnas.1408301111

Choi, S. H., Aid, S., and Bosetti, F. (2009). The distinct roles of cyclooxygenase-1 and -2 in neuroinflammation: Implications for translational research. *Trends Pharmacol. Sci.* 30, 174–181. doi:10.1016/j.tips.2009.01.002

Cipolla, M. J. (2021). Thomas willis lecture: Targeting brain arterioles for acute stroke treatment. *Stroke* 52, 2465–2477. doi:10.1161/strokeaha.121.034620

Clayton, A., Court, J., Navabi, H., Adams, M., Mason, M. D., Hobot, J. A., et al. (2001). Analysis of antigen presenting cell derived exosomes, based on immuno-magnetic isolation and flow cytometry. *J. Immunol. Methods* 247, 163–174. doi:10.1016/s0022-1759(00)00321-5

Colao, I. L., Corteling, R., Bracewell, D., and Wall, I. (2018). Manufacturing exosomes: A promising therapeutic platform. *Trends Mol. Med.* 24, 242–256. doi:10.1016/j.molmed.2018.01.006

Dixon, M. A., Greferath, U., Fletcher, E. L., and Jobling, A. I. (2021). The contribution of microglia to the development and maturation of the visual system. *Front. Cell. Neurosci.* 15, 659843. doi:10.3389/fncel.2021.659843

Du, L., Jiang, Y., and Sun, Y. (2021). Astrocyte-derived exosomes carry microRNA-17-5p to protect neonatal rats from hypoxic-ischemic brain damage via inhibiting BNIP-2 expression. *Neurotoxicology* 83, 28–39. doi:10.1016/j.neuro.2020.12.006

Fei, Y., Zhao, B., Zhu, J., Fang, W., and Li, Y. (2021). XQ-1H promotes cerebral angiogenesis via activating PI3K/Akt/GSK3β/β-catenin/VEGF signal in mice exposed to cerebral ischemic injury. *Life Sci.* 272, 119234. doi:10.1016/j.lfs.2021.119234

Forró, T., Bajkó, Z., Bălașa, A., and Bălașa, R. (2021). Dysfunction of the neurovascular unit in ischemic stroke: Highlights on microRNAs and exosomes as potential biomarkers and therapy. *Int. J. Mol. Sci.* 22, 5621. doi:10.3390/ijms22115621

Gao, G., Li, C., Zhu, J., Wang, Y., Huang, Y., Zhao, S., et al. (2020). Glutaminase 1 regulates neuroinflammation after cerebral ischemia through enhancing microglial activation and pro-inflammatory exosome release. *Front. Immunol.* 11, 161. doi:10.3389/fimmu.2020.00161

Gao, W., Li, F., Liu, L., Xu, X., Zhang, B., Wu, Y., et al. (2018). Endothelial colony-forming cell-derived exosomes restore blood-brain barrier continuity in mice subjected to traumatic brain injury. *Exp. Neurol.* 307, 99–108. doi:10.1016/j.expneurol.2018.06.001

Gruenberg, J., and van der Goot, F. G. (2006). Mechanisms of pathogen entry through the endosomal compartments. *Nat. Rev. Mol. Cell. Biol.* 7, 495–504. doi:10.1038/nrm1959

Guo, L., Huang, Z., Huang, L., Liang, J., Wang, P., Zhao, L., et al. (2021). Surface-modified engineered exosomes attenuated cerebral ischemia/reperfusion injury by targeting the delivery of quercetin towards impaired neurons. *J. Nanobiotechnology* 19, 141. doi:10.1186/s12951-021-00879-4

Guo, M., Wang, J., Zhao, Y., Feng, Y., Han, S., Dong, Q., et al. (2020). Microglial exosomes facilitate α-synuclein transmission in Parkinson's disease. *Brain* 143, 1476–1497. doi:10.1093/brain/awaa090

Han, C., Zhou, J., Liu, B., Liang, C., Pan, X., Zhang, Y., et al. (2019). Delivery of miR-675 by stem cell-derived exosomes encapsulated in silk fibroin hydrogel prevents aging-induced vascular dysfunction in mouse hindlimb. *Mater. Sci. Eng. C* 99, 322–332. doi:10.1016/j.msec.2019.01.122

He, R., Jiang, Y., Shi, Y., Liang, J., and Zhao, L. (2020). Curcumin-laden exosomes target ischemic brain tissue and alleviate cerebral ischemia-reperfusion injury by inhibiting ROS-mediated mitochondrial apoptosis. *Mater. Sci. Eng. C* 117, 111314. doi:10.1016/j.msec.2020.111314

He, X., Kuang, G., Wu, Y., and Ou, C. (2021). Emerging roles of exosomal miRNAs in diabetes mellitus. *Clin. Transl. Med.* 11, e468. doi:10.1002/ctm2.468

Hong, S. B., Yang, H., Manaenko, A., Lu, J., Mei, Q., and Hu, Q. (2019). Potential of exosomes for the treatment of stroke. *Cell. Transpl.* 28, 662–670. doi:10.1177/0963689718816990

Hou, K., Li, G., Zhao, J., Xu, B., Zhang, Y., Yu, J., et al. (2020). RETRACTED ARTICLE:Bone mesenchymal stemcell-derived exosomal microRNA-29b-3p prevents hypoxic-ischemic injury in rat brain byactivating the PTEN-mediated Akt signaling pathway. *J. Neuroinflammation* 17, 46. doi:10.1186/s12974-020-1725-8

Huang, X., Ding, J., Li, Y., Liu, W., Ji, J., Wang, H., et al. (2018). Exosomes derived from PEDF modified adipose-derived mesenchymal stem cells ameliorate cerebral ischemia-reperfusion injury by regulation of autophagy and apoptosis. *Exp. Cell. Res.* 371, 269–277. doi:10.1016/j.yexcr.2018.08.021

Hulsmans, M., and Holvoet, P. (2013). MicroRNA-containing microvesicles regulating inflammation in association with atherosclerotic disease. *Cardiovasc. Res.* 100, 7–18. doi:10.1093/cvr/cvt161

Isaac, R., Reis, F. C. G., Ying, W., and Olefsky, J. M. (2021). Exosomes as mediators of intercellular crosstalk in metabolism. *Cell. Metab.* 33, 1744–1762. doi:10.1016/j.cmet.2021.08.006

Ishiguro, M., Kawasaki, K., Suzuki, Y., Ishizuka, F., Mishiro, K., Egashira, Y., et al. (2012). A Rho kinase (ROCK) inhibitor, fasudil, prevents matrix metalloproteinase-9-related hemorrhagic transformation in mice treated with tissue plasminogen activator. *Neuroscience* 220, 302–312. doi:10.1016/j.neuroscience.2012.06.015

Jeppesen, D. K., Fenix, A. M., Franklin, J. L., Higginbotham, J. N., Zhang, Q., Zimmerman, L. J., et al. (2019). Reassessment of exosome composition. *Cell.* 177, 428–445.e18. doi:10.1016/j.cell.2019.02.029

Jia, G., Han, Y., An, Y., Ding, Y., He, C., Wang, X., et al. (2018). NRP-1 targeted and cargo-loaded exosomes facilitate simultaneous imaging and therapy of glioma *in vitro* and *in vivo*. *Biomaterials* 178, 302–316. doi:10.1016/j.biomaterials.2018.06.029

Jiang, M., Wang, H., Jin, M., Yang, X., Ji, H., Jiang, Y., et al. (2018a). Exosomes from MiR-30d-5p-ADSCs reverse acute ischemic stroke-induced, autophagy-mediated brain injury by promoting M2 microglial/macrophage polarization. *Cell. Physiol. biochem.* 47, 864–878. doi:10.1159/000490078

Jiang, X., Andjelkovic, A. V., Zhu, L., Yang, T., Bennett, M. V. L., Chen, J., et al. (2018b). Blood-brain barrier dysfunction and recovery after ischemic stroke. *Prog. Neurobiol.* 163-164, 144–171. doi:10.1016/j.pneurobio.2017.10.001

Jiang, Y., Xie, H., Tu, W., Fang, H., Ji, C., Yan, T., et al. (2018c). Exosomes secreted by HUVECs attenuate hypoxia/reoxygenation-induced apoptosis in neural cells by suppressing miR-21-3p. *Am. J. Transl. Res.* 10, 3529–3541.

Johnstone, R. M., Adam, M., Hammond, J. R., Orr, L., and Turbide, C. (1987). Vesicle formation during reticulocyte maturation. Association of plasma membrane activities with released vesicles (exosomes). *J. Biol. Chem.* 262, 9412–9420. doi:10.1016/s0021-9258(18)48095-7

Kalluri, R., and LeBleu, V. S. (2020). The biology, function, and biomedical applications of exosomes. *Science* 367, eaau6977. doi:10.1126/science.aau6977

Kalani, A., Chaturvedi, P., Kamat, P. K., Maldonado, C., Bauer, P., Joshua, I. G., et al. (2016). Curcumin-loaded embryonic stem cell exosomes restored neurovascular unit following ischemia-reperfusion injury. *Int. J. Biochem. Cell. Biol.* 79, 360–369. doi:10.1016/j.biocel.2016.09.002

Kang, X., Jiang, L., Chen, X., Wang, X., Gu, S., Wang, J., et al. (2021). Exosomes derived from hypoxic bone marrow mesenchymal stem cells rescue OGD-induced injury in neural cells by suppressing NLRP3 inflammasome-mediated pyroptosis. *Exp. Cell. Res.* 405, 112635. doi:10.1016/j.yexcr.2021.112635

Kerr, N., García-Contreras, M., Abbassi, S., Mejias, N. H., Desousa, B. R., Ricordi, C., et al. (2018). Inflammasome proteins in serum and serum-derived extracellular vesicles as biomarkers of stroke. *Front. Mol. Neurosci.* 11, 309. doi:10.3389/fnmol.2018.00309

Kim, M., Kim, G., Hwang, D. W., and Lee, M. (2019). Delivery of high mobility group box-1 siRNA using brain-targeting exosomes for ischemic stroke therapy. *J. Biomed. Nanotechnol.* 15, 2401–2412. doi:10.1166/jbn.2019.2866

Kim, M., Lee, Y., and Lee, M. (2021). Hypoxia-specific anti-RAGE exosomes for nose-to-brain delivery of anti-miR-181a oligonucleotide in an ischemic stroke model. *Nanoscale* 13, 14166–14178. doi:10.1039/d0nr07516g

Koide, R., Hirane, N., Kambe, D., Yokoi, Y., Otaki, M., and Nishimura, S. I. (2022). Antiadhesive nanosome elicits role of glycocalyx of tumor cell-derived exosomes in the organotropic cancer metastasis. *Biomaterials* 280, 121314. doi:10.1016/j.biomaterials.2021.121314

Kojima, R., Bojar, D., Rizzi, G., Hamri, G. C., El-Baba, M. D., Saxena, P., et al. (2018). Designer exosomes produced by implanted cells intracerebrally deliver therapeutic cargo for Parkinson's disease treatment. *Nat. Commun.* 9, 1305. doi:10.1038/s41467-018-03733-8

Kolaczkowska, E., and Kubes, P. (2013). Neutrophil recruitment and function in health and inflammation. *Nat. Rev. Immunol.* 13, 159–175. doi:10.1038/nri3399

Lai, R. C., Tan, S. S., Teh, B. J., Sze, S. K., Arslan, F., de Kleijn, D. P., et al. (2012). Proteolytic potential of the MSC exosome proteome: Implications for an exosome-mediated delivery of therapeutic proteasome. *Int. J. Proteomics* 2012, 1–14. doi:10.1155/2012/971907

Lande, K., Gupta, J., Ranjan, R., Kiran, M., Torres Solis, L. F., Solís Herrera, A., et al. (2020). Exosomes: Insights from retinoblastoma and other eye cancers. *Int. J. Mol. Sci.* 21, E7055. doi:10.3390/ijms21197055

Lee, T. L., Lai, T. C., Lin, S. R., Lin, S. W., Chen, Y. C., Pu, C. M., et al. (2021). Conditioned medium from adipose-derived stem cells attenuates ischemia/reperfusion-induced cardiac injury through the microRNA-221/222/PUMA/ETS-1 pathway. *Theranostics* 11, 3131–3149. doi:10.7150/thno.52677

Lerner, N., Schreiber-Avissar, S., and Beit-Yannai, E. (2020). Extracellular vesicle-mediated crosstalk between NPCE cells and TM cells result in modulation of Wnt signalling pathway and ECM remodelling. *J. Cell. Mol. Med.* 24, 4646–4658. doi:10.1111/jcmm.15129

Li, F., Zhao, L., Shi, Y., and Liang, J. (2020a). Edaravone-loaded macrophage-derived exosomes enhance neuroprotection in the rat permanent middle cerebral artery occlusion model of stroke. *Mol. Pharm.* 17, 3192–3201. doi:10.1021/acs.molpharmaceut.0c00245

Li, G., Xiao, L., Qin, H., Zhuang, Q., Zhang, W., Liu, L., et al. (2020b). Exosomes-carried microRNA-26b-5p regulates microglia M1 polarization after cerebral ischemia/reperfusion. *Cell. Cycle* 19, 1022–1035. doi:10.1080/15384101.2020.1743912

Li, S., Luo, L., He, Y., Li, R., Xiang, Y., Xing, Z., et al. (2021a). Dental pulp stem cell-derived exosomes alleviate cerebral ischaemia-reperfusion injury through suppressing inflammatory response. *Cell. Prolif.* 54, e13093. doi:10.1111/cpr.13093

Li, W. Y., Zhu, Q. B., Jin, L. Y., Yang, Y., Xu, X. Y., and Hu, X. Y. (2021b). Exosomes derived from human induced pluripotent stem cell-derived neural progenitor cells protect neuronal function under ischemic conditions. *Neural Regen. Res.* 16, 2064–2070. doi:10.4103/1673-5374.308665

Li, X., Liao, J., Su, X., Li, W., Bi, Z., Wang, J., et al. (2020c). Human urine-derived stem cells protect against renal ischemia/reperfusion injury in a rat model via exosomal miR-146a-5p which targets IRAK1. *Theranostics* 10, 9561–9578. doi:10.7150/thno.42153

Li, X., Zhang, Y., Wang, Y., Zhao, D., Sun, C., Zhou, S., et al. (2020d). Exosomes derived from CXCR4-overexpressing BMSC promoted activation of microvascular endothelial cells in cerebral ischemia/reperfusion injury. *Neural Plast.* 2020, 1–13. doi:10.1155/2020/8814239

Li, Y. J., Wu, J. Y., Liu, J., Xu, W., Qiu, X., Huang, S., et al. (2021c). Artificial exosomes for translational nanomedicine. *J. Nanobiotechnology* 19, 242. doi:10.1186/s12951-021-00986-2

Liang, C. C., Shaw, S. W., Huang, Y. H., Lin, Y. H., and Lee, T. H. (2017). Bladder transplantation of amniotic fluid stem cell may ameliorate bladder dysfunction after focal cerebral ischemia in rat. *Stem Cells Transl. Med.* 6, 1227–1236. doi:10.1002/sctm.16-0212

Liang, Y., Duan, L., Lu, J., and Xia, J. (2021). Engineering exosomes for targeted drug delivery. *Theranostics* 11, 3183–3195. doi:10.7150/thno.52570

Liang, Z., Wu, G., Fan, C., Xu, J., Jiang, S., Yan, X., et al. (2016). The emerging role of signal transducer and activator of transcription 3 in cerebral ischemic and hemorrhagic stroke. *Prog. Neurobiol.* 137, 1–16. doi:10.1016/j.pneurobio.2015.11.001

Liebner, S., Dijkhuizen, R. M., Reiss, Y., Plate, K. H., Agalliu, D., and Constantin, G. (2018). Functional morphology of the blood-brain barrier in health and disease. *Acta Neuropathol.* 135, 311–336. doi:10.1007/s00401-018-1815-1

Ling, X., Zhang, G., Xia, Y., Zhu, Q., Zhang, J., Li, Q., et al. (2020). Exosomes from human urine-derived stem cells enhanced neurogenesis via miR-26a/HDAC6 axis after ischaemic stroke. *J. Cell. Mol. Med.* 24, 640–654. doi:10.1111/jcmm.14774

Liu, J., Zhu, G., Jia, N., Wang, W., Wang, Y., Yin, M., et al. (2019a). CD9 regulates keratinocyte migration by negatively modulating the sheddase activity of ADAM17. *Int. J. Biol. Sci.* 15, 493–506. doi:10.7150/ijbs.29404

Liu, X., Zhang, M., Liu, H., Zhu, R., He, H., Zhou, Y., et al. (2021). Bone marrow mesenchymal stem cell-derived exosomes attenuate cerebral ischemia-reperfusion injury-induced neuroinflammation and pyroptosis by modulating microglia M1/M2 phenotypes. *Exp. Neurol.* 341, 113700. doi:10.1016/j.expneurol.2021.113700

Liu, Y., Fu, N., Su, J., Wang, X., and Li, X. (2019b). Rapid enkephalin delivery using exosomes to promote neurons recovery in ischemic stroke by inhibiting neuronal p53/caspase-3. *Biomed. Res. Int.* 2019, 1–11. doi:10.1155/2019/4273290

Liu, Z., and Chopp, M. (2016). Astrocytes, therapeutic targets for neuroprotection and neurorestoration in ischemic stroke. *Prog. Neurobiol.* 144, 103–120. doi:10.1016/j.pneurobio.2015.09.008

Lobb, R. J., Becker, M., Wen, S. W., Wong, C. S., Wiegmans, A. P., Leimgruber, A., et al. (2015). Optimized exosome isolation protocol for cell culture supernatant and human plasma. *J. Extracell. Vesicles* 4, 27031. doi:10.3402/jev.v4.27031

Lu, M., Yuan, S., Li, S., Li, L., Liu, M., and Wan, S. (2019). The exosome-derived biomarker in atherosclerosis and its clinical application. *J. Cardiovasc. Transl. Res.* 12, 68–74. doi:10.1007/s12265-018-9796-y

Mathew, B., Ravindran, S., Liu, X., Torres, L., Chennakesavalu, M., Huang, C. C., et al. (2019). Mesenchymal stem cell-derived extracellular vesicles and retinal ischemia-reperfusion. *Biomaterials* 197, 146–160. doi:10.1016/j.biomaterials.2019.01.016

Moghadasi, S., Elveny, M., Rahman, H. S., Suksatan, W., Jalil, A. T., Abdelbasset, W. K., et al. (2021). A paradigm shift in cell-free approach: The emerging role of MSCs-derived exosomes in regenerative medicine. *J. Transl. Med.* 19, 302. doi:10.1186/s12967-021-02980-6

Monteforte, A., Lam, B., Sherman, M. B., Henderson, K., Sligar, A. D., Spencer, A., et al. (2017). <sup/>Glioblastoma exosomes for therapeutic angiogenesis in peripheral ischemia. *Tissue Eng. Part A* 23, 1251–1261. doi:10.1089/ten.tea.2016.0508

Nikfarjam, S., Rezaie, J., Zolbanin, N. M., and Jafari, R. (2020). Mesenchymal stem cell derived-exosomes: A modern approach in translational medicine. *J. Transl. Med.* 18, 449. doi:10.1186/s12967-020-02622-3

Orefice, N. S., Souchet, B., Braudeau, J., Alves, S., Piguet, F., Collaud, F., et al. (2019). Real-time monitoring of exosome enveloped-AAV spreading by endomicroscopy approach: A new tool for gene delivery in the brain. *Mol. Ther. - Methods & Clin. Dev.* 14, 237–251. doi:10.1016/j.omtm.2019.06.005

Pan, Q., Kuang, X., Cai, S., Wang, X., Du, D., Wang, J., et al. (2020). miR-132-3p priming enhances the effects of mesenchymal stromal cell-derived exosomes on ameliorating brain ischemic injury. *Stem Cell. Res. Ther.* 11, 260. doi:10.1186/s13287-020-01761-0

Pan, Q., Wang, Y., Lan, Q., Wu, W., Li, Z., Ma, X., et al. (2019). Exosomes derived from mesenchymal stem cells ameliorate hypoxia/reoxygenation-injured ECs via transferring MicroRNA-126. *Stem Cells Int.* 2019, 1–13. doi:10.1155/2019/2831756

Pascucci, L., Coccè, V., Bonomi, A., Ami, D., Ceccarelli, P., Ciusani, E., et al. (2014). Paclitaxel is incorporated by mesenchymal stromal cells and released in exosomes that inhibit *in vitro* tumor growth: A new approach for drug delivery. *J. Control. Release* 192, 262–270. doi:10.1016/j.jconrel.2014.07.042

Paul, S., and Candelario-Jalil, E. (2021). Emerging neuroprotective strategies for the treatment of ischemic stroke: An overview of clinical and preclinical studies. *Exp. Neurol.* 335, 113518. doi:10.1016/j.expneurol.2020.113518

Pegtel, D. M., and Gould, S. J. (2019). Exosomes. *Annu. Rev. Biochem.* 88, 487–514. doi:10.1146/annurev-biochem-013118-111902

Pei, X., Li, Y., Zhu, L., and Zhou, Z. (2019). Astrocyte-derived exosomes suppress autophagy and ameliorate neuronal damage in experimental ischemic stroke. *Exp. Cell. Res.* 382, 111474. doi:10.1016/j.yexcr.2019.06.019

Perets, N., Betzer, O., Shapira, R., Brenstein, S., Angel, A., Sadan, T., et al. (2019). Golden exosomes selectively target brain pathologies in neurodegenerative and neurodevelopmental disorders. *Nano Lett.* 19, 3422–3431. doi:10.1021/acs.nanolett.8b04148

Pols, M. S., and Klumperman, J. (2009). Trafficking and function of the tetraspanin CD63. *Exp. Cell. Res.* 315, 1584–1592. doi:10.1016/j.yexcr.2008.09.020

Racle, J., Michaux, J., Rockinger, G. A., Arnaud, M., Bobisse, S., Chong, C., et al. (2019). Robust prediction of HLA class II epitopes by deep motif deconvolution of immunopeptidomes. *Nat. Biotechnol.* 37, 1283–1286. doi:10.1038/s41587-019-0289-6

Raposo, G., and Stoorvogel, W. (2013). Extracellular vesicles: Exosomes, microvesicles, and friends. *J. Cell. Biol.* 200, 373–383. doi:10.1083/jcb.201211138

Rappa, G., Puglisi, C., Santos, M. F., Forte, S., Memeo, L., and Lorico, A. (2019). Extracellular vesicles from thyroid carcinoma: The new frontier of liquid biopsy. *Int. J. Mol. Sci.* 20, E1114. doi:10.3390/ijms20051114

Rong, Y., Liu, W., Wang, J., Fan, J., Luo, Y., Li, L., et al. (2019). Neural stem cell-derived small extracellular vesicles attenuate apoptosis and neuroinflammation after traumatic spinal cord injury by activating autophagy. *Cell. Death Dis.* 10, 340. doi:10.1038/s41419-019-1571-8

Sala-Valdés, M., Ursa, A., Charrin, S., Rubinstein, E., Hemler, M. E., Sánchez-Madrid, F., et al. (2006). EWI-2 and EWI-F link the tetraspanin web to the actin cytoskeleton through their direct association with ezrin-radixin-moesin proteins. *J. Biol. Chem.* 281, 19665–19675. doi:10.1074/jbc.m602116200

Sharma, P., Mesci, P., Carromeu, C., McClatchy, D. R., Schiapparelli, L., Yates, J. R., et al. (2019). Exosomes regulate neurogenesis and circuit assembly. *Proc. Natl. Acad. Sci. U. S. A.* 116, 16086–16094. doi:10.1073/pnas.1902513116

Shin, H., Oh, S., Hong, S., Kang, M., Kang, D., Ji, Y. G., et al. (2020). Early-stage lung cancer diagnosis by deep learning-based spectroscopic analysis of circulating exosomes. *ACS Nano* 14, 5435–5444. doi:10.1021/acsnano.9b09119

Song, H., Li, X., Zhao, Z., Qian, J., Wang, Y., Cui, J., et al. (2019a). Reversal of osteoporotic activity by endothelial cell-secreted bone targeting and biocompatible exosomes. *Nano Lett.* 19, 3040–3048. doi:10.1021/acs.nanolett.9b00287

Song, H., Zhang, X., Chen, R., Miao, J., Wang, L., Cui, L., et al. (2019b). Cortical neuron-derived exosomal MicroRNA-181c-3p inhibits neuroinflammation by downregulating CXCL1 in astrocytes of a rat model with ischemic brain injury. *Neuroimmunomodulation* 26, 217–233. doi:10.1159/000502694

Song, P., Sun, H., Chen, H., Wang, Y., and Zhang, Q. (2020). Decreased serum exosomal miR-152-3p contributes to the progression of acute ischemic stroke. *Clin. Lab.* 66. doi:10.7754/clin.lab.2020.200106

Song, Y., Li, Z., He, T., Qu, M., Jiang, L., Li, W., et al. (2019c). M2 microglia-derived exosomes protect the mouse brain from ischemia-reperfusion injury via exosomal miR-124. *Theranostics* 9, 2910–2923. doi:10.7150/thno.30879

Sun, R., Peng, M., Xu, P., Huang, F., Xie, Y., Li, J., et al. (2020). Low-density lipoprotein receptor (LDLR) regulates NLRP3-mediated neuronal pyroptosis following cerebral ischemia/reperfusion injury. *J. Neuroinflammation* 17, 330. doi:10.1186/s12974-020-01988-x

Sun, X., Jung, J. H., Arvola, O., Santoso, M. R., Giffard, R. G., Yang, P. C., et al. (2019). Stem cell-derived exosomes protect astrocyte cultures from *in vitro* ischemia and decrease injury as post-stroke intravenous therapy. *Front. Cell. Neurosci.* 13, 394. doi:10.3389/fncel.2019.00394

Sun, Y., Shi, H., Yin, S., Ji, C., Zhang, X., Zhang, B., et al. (2018a). Human mesenchymal stem cell derived exosomes alleviate type 2 diabetes mellitus by reversing peripheral insulin resistance and relieving β-cell destruction. *ACS Nano* 12, 7613–7628. doi:10.1021/acsnano.7b07643

Sun, Y. W., Zhang, L. Y., Gong, S. J., Hu, Y. Y., Zhang, J. G., Xian, X. H., et al. (2021). The p38 MAPK/NF-κB pathway mediates GLT-1 up-regulation during cerebral ischemic preconditioning-induced brain ischemic tolerance in rats. *Brain Res. Bull.* 175, 224–233. doi:10.1016/j.brainresbull.2021.07.029

Sun, Z., Shi, K., Yang, S., Liu, J., Zhou, Q., Wang, G., et al. (2018b). Effect of exosomal miRNA on cancer biology and clinical applications. *Mol. Cancer* 17, 147. doi:10.1186/s12943-018-0897-7

Tegegn, T. Z., De Paoli, S. H., Orecna, M., Elhelu, O. K., Woodle, S. A., Tarandovskiy, I. D., et al. (2016). Characterization of procoagulant extracellular vesicles and platelet membrane disintegration in DMSO-cryopreserved platelets. *J. Extracell. Vesicles* 5, 30422. doi:10.3402/jev.v5.30422

Théry, C., Boussac, M., Véron, P., Ricciardi-Castagnoli, P., Raposo, G., Garin, J., et al. (2001). Proteomic analysis of dendritic cell-derived exosomes: A secreted subcellular compartment distinct from apoptotic vesicles. *J. Immunol.* 166, 7309–7318. doi:10.4049/jimmunol.166.12.7309

Théry, C., Witwer, K. W., Aikawa, E., Alcaraz, M. J., Anderson, J. D., Andriantsitohaina, R., et al. (2018). Minimal information for studies of extracellular vesicles 2018 (MISEV2018): A position statement of the international society for extracellular vesicles and update of the MISEV2014 guidelines. *J. Extracell. Vesicles* 7, 1461450. doi:10.1080/20013078.2018.1461450

Théry, C., Zitvogel, L., and Amigorena, S. (2002). Exosomes: Composition, biogenesis and function. *Nat. Rev. Immunol.* 2, 569–579. doi:10.1038/nri855

Thomi, G., Surbek, D., Haesler, V., Joerger-Messerli, M., and Schoeberlein, A. (2019). Exosomes derived from umbilical cord mesenchymal stem cells reduce microglia-mediated neuroinflammation in perinatal brain injury. *Stem Cell. Res. Ther.* 10, 105. doi:10.1186/s13287-019-1207-z

Tian, T., Cao, L., He, C., Ye, Q., Liang, R., You, W., et al. (2021). Targeted delivery of neural progenitor cell-derived extracellular vesicles for anti-inflammation after cerebral ischemia. *Theranostics* 11, 6507–6521. doi:10.7150/thno.56367

Tian, Y., Zhu, P., Liu, S., Jin, Z., Li, D., Zhao, H., et al. (2019). IL-4-polarized BV2 microglia cells promote angiogenesis by secreting exosomes. *Adv. Clin. Exp. Med.* 28, 421–430. doi:10.17219/acem/91826

Toh, W. S., Lai, R. C., Zhang, B., and Lim, S. K. (2018). MSC exosome works through a protein-based mechanism of action. *Biochem. Soc. Trans.* 46, 843–853. doi:10.1042/bst20180079

Tuo, Q. Z., Zhang, S. T., and Lei, P. (2022). Mechanisms of neuronal cell death in ischemic stroke and their therapeutic implications. *Med. Res. Rev.* 42, 259–305. doi:10.1002/med.21817

Valadi, H., Ekström, K., Bossios, A., Sjöstrand, M., Lee, J. J., and Lötvall, J. O. (2007). Exosome-mediated transfer of mRNAs and microRNAs is a novel mechanism of genetic exchange between cells. *Nat. Cell. Biol.* 9, 654–659. doi:10.1038/ncb1596

Walsh, J., Tozer, D. J., Sari, H., Hong, Y. T., Drazyk, A., Williams, G., et al. (2021). Microglial activation and blood-brain barrier permeability in cerebral small vessel disease. *Brain* 144, 1361–1371. doi:10.1093/brain/awab003

Wang, K., Ru, J., Zhang, H., Chen, J., Lin, X., Lin, Z., et al. (2020). Melatonin enhances the therapeutic effect of plasma exosomes against cerebral ischemia-induced pyroptosis through the TLR4/NF-κB pathway. *Front. Neurosci.* 14, 848. doi:10.3389/fnins.2020.00848

Wang, W., Li, D. B., Li, R. Y., Zhou, X., Yu, D. J., Lan, X. Y., et al. (2018). Diagnosis of hyperacute and acute ischaemic stroke: The potential utility of exosomal MicroRNA-21-5p and MicroRNA-30a-5p. *Cerebrovasc. Dis.* 45, 204–212. doi:10.1159/000488365

Wang, Y., Wang, G., Wang, Z., Zhang, H., Zhang, L., and Cheng, Z. (2014). Chicken biliary exosomes enhance CD4(+)T proliferation and inhibit ALV-J replication in liver. *Biochem. Cell. Biol.* 92, 145–151. doi:10.1139/bcb-2013-0096

Webb, R. L., Kaiser, E. E., Jurgielewicz, B. J., Spellicy, S., Scoville, S. L., Thompson, T. A., et al. (2018). Human neural stem cell extracellular vesicles improve recovery in a porcine model of ischemic stroke. *Stroke* 49, 1248–1256. doi:10.1161/strokeaha.117.020353

Whitford, W., and Guterstam, P. (2019). Exosome manufacturing status. *Future Med. Chem.* 11, 1225–1236. doi:10.4155/fmc-2018-0417

Williams, A. M., Bhatti, U. F., Brown, J. F., Biesterveld, B. E., Kathawate, R. G., Graham, N. J., et al. (2020). Early single-dose treatment with exosomes provides neuroprotection and improves blood-brain barrier integrity in swine model of traumatic brain injury and hemorrhagic shock. *J. Trauma Acute Care Surg.* 88, 207–218. doi:10.1097/ta.0000000000002563

Wu, W., Liu, J., Yang, C., Xu, Z., Huang, J., and Lin, J. (2020). Astrocyte-derived exosome-transported microRNA-34c is neuroprotective against cerebral ischemia/reperfusion injury via TLR7 and the NF-κB/MAPK pathways. *Brain Res. Bull.* 163, 84–94. doi:10.1016/j.brainresbull.2020.07.013

Xiao, Y., Geng, F., Wang, G., Li, X., Zhu, J., and Zhu, W. (2019). Bone marrow-derived mesenchymal stem cells-derived exosomes prevent oligodendrocyte apoptosis through exosomal miR-134 by targeting caspase-8. *J. Cell. Biochem.* 120, 2109–2118. doi:10.1002/jcb.27519

Xie, L., Zhao, H., Wang, Y., and Chen, Z. (2020). Exosomal shuttled miR-424-5p from ischemic preconditioned microglia mediates cerebral endothelial cell injury through negatively regulation of FGF2/STAT3 pathway. *Exp. Neurol.* 333, 113411. doi:10.1016/j.expneurol.2020.113411

Xu, B., Hsu, P. K., Karayiorgou, M., and Gogos, J. A. (2012). MicroRNA dysregulation in neuropsychiatric disorders and cognitive dysfunction. *Neurobiol. Dis.* 46, 291–301. doi:10.1016/j.nbd.2012.02.016

Xu, B., Zhang, Y., Du, X. F., Li, J., Zi, H. X., Bu, J. W., et al. (2017). Neurons secrete miR-132-containing exosomes to regulate brain vascular integrity. *Cell. Res.* 27, 882–897. doi:10.1038/cr.2017.62

Yan, Z., Dutta, S., Liu, Z., Yu, X., Mesgarzadeh, N., Ji, F., et al. (2019). A label-free platform for identification of exosomes from different sources. *ACS Sens.* 4, 488–497. doi:10.1021/acssensors.8b01564

Yang, Y., Jalal, F. Y., Thompson, J. F., Walker, E. J., Candelario-Jalil, E., Li, L., et al. (2011). Tissue inhibitor of metalloproteinases-3 mediates the death of immature oligodendrocytes via TNF-α/TACE in focal cerebral ischemia in mice. *J. Neuroinflammation* 8, 108. doi:10.1186/1742-2094-8-108

Yang, T., Martin, P., Fogarty, B., Brown, A., Schurman, K., Phipps, R., et al. (2015). Exosome delivered anticancer drugs across the blood-brain barrier for brain cancer therapy in *Danio rerio*. *Pharm. Res.* 32, 2003–2014. doi:10.1007/s11095-014-1593-y

Yang, J., Zhang, X., Chen, X., Wang, L., and Yang, G. (2017). Exosome mediated delivery of miR-124 promotes neurogenesis after ischemia. *Mol. Ther. - Nucleic Acids* 7, 278–287. doi:10.1016/j.omtn.2017.04.010

Yang, Y., Cai, Y., Zhang, Y., Liu, J., and Xu, Z. (2018a). Exosomes secreted by adipose-derived stem cells contribute to angiogenesis of brain microvascular endothelial cells following oxygen-glucose deprivation *in vitro* through MicroRNA-181b/TRPM7 Axis. *J. Mol. Neurosci.* 65, 74–83. doi:10.1007/s12031-018-1071-9

Yang, Y., Kannisto, E., Yu, G., Reid, M. E., Patnaik, S. K., and Wu, Y. (2018b). An immuno-biochip selectively captures tumor-derived exosomes and detects exosomal RNAs for cancer diagnosis. *ACS Appl. Mat. Interfaces* 10, 43375–43386. doi:10.1021/acsami.8b13971

Yang, C., Hawkins, K. E., Doré, S., and Candelario-Jalil, E. (2019). Neuroinflammatory mechanisms of blood-brain barrier damage in ischemic stroke. *Am. J. Physiology-Cell Physiology* 316, C135–C153. doi:10.1152/ajpcell.00136.2018

Yang, J., Wu, S., Hou, L., Zhu, D., Yin, S., Yang, G., et al. (2020). Therapeutic effects of simultaneous delivery of nerve growth factor mRNA and protein via exosomes on cerebral ischemia. *Mol. Ther. - Nucleic Acids* 21, 512–522. doi:10.1016/j.omtn.2020.06.013

Yang, D., Li, Z., Gao, G., Li, X., Liao, Z., Wang, Y., et al. (2021a). Combined analysis of surface protein profile and microRNA expression profile of exosomes derived from brain microvascular endothelial cells in early cerebral ischemia. *ACS Omega* 6, 22410–22421. doi:10.1021/acsomega.1c03248

Yang, T., He, R., Li, G., Liang, J., Zhao, L., Zhao, X., et al. (2021b). Growth arrest and DNA damage-inducible protein 34 (GADD34) contributes to cerebral ischemic injury and can be detected in plasma exosomes. *Neurosci. Lett.* 758, 136004. doi:10.1016/j.neulet.2021.136004

Yang, H., Tu, Z., Yang, D., Hu, M., Zhou, L., Li, Q., et al. (2022a). Exosomes from hypoxic pre-treated ADSCs attenuate acute ischemic stroke-induced brain injury via delivery of circ-Rps5 and promote M2 microglia/macrophage polarization. *Neurosci. Lett.* 769, 136389. doi:10.1016/j.neulet.2021.136389

Yang, J., Shin, T. S., Kim, J. S., Jee, Y. K., and Kim, Y. K. (2022b). A new horizon of precision medicine: Combination of the microbiome and extracellular vesicles. *Exp. Mol. Med.* 54, 466–482. doi:10.1038/s12276-022-00748-6

Yang, Z., Huang, C., Wen, X., Liu, W., Huang, X., Li, Y., et al. (2022c). Circular RNA circ-FoxO3 attenuates blood-brain barrier damage by inducing autophagy during ischemia/reperfusion. *Mol. Ther.* 30, 1275–1287. doi:10.1016/j.ymthe.2021.11.004

Yu, B., Zhang, X., and Li, X. (2014). Exosomes derived from mesenchymal stem cells. *Int. J. Mol. Sci.* 15, 4142–4157. doi:10.3390/ijms15034142

Yu, H., Xu, Z., Qu, G., Wang, H., Lin, L., Li, X., et al. (2021). Hypoxic preconditioning enhances the efficacy of mesenchymal stem cells-derived conditioned medium in switching microglia toward anti-inflammatory polarization in ischemia/reperfusion. *Cell. Mol. Neurobiol.* 41, 505–524. doi:10.1007/s10571-020-00868-5

Yu, J., Lee, C. Y., Changou, C. A., Cedano-Prieto, D. M., Takada, Y. K., and Takada, Y. (2017). The CD9, CD81, and CD151 EC2 domains bind to the classical RGD-binding site of integrin αvβ3. *Biochem. J.* 474, 589–596. doi:10.1042/bcj20160998

Yu, M., Gai, C., Li, Z., Ding, D., Zheng, J., Zhang, W., et al. (2019). Targeted exosome-encapsulated erastin induced ferroptosis in triple negative breast cancer cells. *Cancer Sci.* 110, 3173–3182. doi:10.1111/cas.14181

Yuan, D., Zhao, Y., Banks, W. A., Bullock, K. M., Haney, M., Batrakova, E., et al. (2017). Macrophage exosomes as natural nanocarriers for protein delivery to inflamed brain. *Biomaterials* 142, 1–12. doi:10.1016/j.biomaterials.2017.07.011

Yue, K. Y., Zhang, P. R., Zheng, M. H., Cao, X. L., Cao, Y., Zhang, Y. Z., et al. (2019). Neurons can upregulate Cav-1 to increase intake of endothelial cells-derived extracellular vesicles that attenuate apoptosis *via* miR-1290. *Cell Death Dis.* 10 (12), 869. doi:10.1038/s41419-019-2100-5

Zagrean, A. M., Hermann, D. M., Opris, I., Zagrean, L., and Popa-Wagner, A. (2018). Multicellular crosstalk between exosomes and the neurovascular unit after cerebral ischemia. Therapeutic implications. *Front. Neurosci.* 12, 811. doi:10.3389/fnins.2018.00811

Zang, J., Wu, Y., Su, X., Zhang, T., Tang, X., Ma, D., et al. (2020). Inhibition of PDE1-B by vinpocetine regulates microglial exosomes and polarization through enhancing autophagic flux for neuroprotection against ischemic stroke. *Front. Cell. Dev. Biol.* 8, 616590. doi:10.3389/fcell.2020.616590

Zeng, Q., Zhou, Y., Liang, D., He, H., Liu, X., Zhu, R., et al. (2020). Exosomes secreted from bone marrow mesenchymal stem cells attenuate oxygen-glucose deprivation/reoxygenation-induced pyroptosis in PC12 cells by promoting AMPK-dependent autophagic flux. *Front. Cell. Neurosci.* 14, 182. doi:10.3389/fncel.2020.00182

Zhai, K., Duan, H., Wang, W., Zhao, S., Khan, G. J., Wang, M., et al. (2021). Ginsenoside Rg1 ameliorates blood-brain barrier disruption and traumatic brain injury via attenuating macrophages derived exosomes miR-21 release. *Acta Pharm. Sin. B* 11, 3493–3507. doi:10.1016/j.apsb.2021.03.032

Zhang, J., Li, S., Li, L., Li, M., Guo, C., Yao, J., et al. (2015). Exosome and exosomal microRNA: Trafficking, sorting, and function. *Genomics Proteomics Bioinforma.* 13, 17–24. doi:10.1016/j.gpb.2015.02.001

Zhang, H., Wu, J., Wu, J., Fan, Q., Zhou, J., Wu, J., et al. (2019). Exosome-mediated targeted delivery of miR-210 for angiogenic therapy after cerebral ischemia in mice. *J. Nanobiotechnology* 17, 29. doi:10.1186/s12951-019-0461-7

Zhang, G., Zhu, Z., Wang, H., Yu, Y., Chen, W., Waqas, A., et al. (2020a). Exosomes derived from human neural stem cells stimulated by interferon gamma improve therapeutic ability in ischemic stroke model. *J. Adv. Res.* 24, 435–445. doi:10.1016/j.jare.2020.05.017

Zhang, S., Jin, T., Wang, L., Liu, W., Zhang, Y., Zheng, Y., et al. (2020b). Electroacupuncture promotes the differentiation of endogenous neural stem cells via exosomal microRNA 146b after ischemic stroke. *Front. Cell. Neurosci.* 14, 223. doi:10.3389/fncel.2020.00223

Zhang, Y., Qin, Y., Chopp, M., Li, C., Kemper, A., Liu, X., et al. (2020c). Ischemic cerebral endothelial cell-derived exosomes promote axonal growth. *Stroke* 51, 3701–3712. doi:10.1161/strokeaha.120.031728

Zhang, D., Cai, G., Liu, K., Zhuang, Z., Jia, K., Pei, S., et al. (2021a). Microglia exosomal miRNA-137 attenuates ischemic brain injury through targeting Notch1. *Aging (Albany NY)* 13, 4079–4095. doi:10.18632/aging.202373

Zhang, H., Lin, S., McElroy, C. L., Wang, B., Jin, D., Uteshev, V. V., et al. (2021b). Circulating pro-inflammatory exosomes worsen stroke outcomes in aging. *Circ. Res.* 129, e121–e140. doi:10.1161/circresaha.121.318897

Zhang, Q., Loghry, H. J., Qian, J., Kimber, M. J., Dong, L., and Lu, M. (2021c). Towards nanovesicle-based disease diagnostics: A rapid single-step exosome assay within one hour through *in situ* immunomagnetic extraction and nanophotonic label-free detection. *Lab. Chip* 21, 3541–3549. doi:10.1039/d1lc00446h

Zhang, Y., Liu, J., Su, M., Wang, X., and Xie, C. (2021d). Exosomal microRNA-22-3p alleviates cerebral ischemic injury by modulating KDM6B/BMP2/BMF axis. *Stem Cell. Res. Ther.* 12, 111. doi:10.1186/s13287-020-02091-x

Zhang, Y., Yu, J., Liu, J., Liu, H., and Li, J. (2021e). Effects of stem cell-derived exosomes on neuronal apoptosis and inflammatory cytokines in rats with cerebral ischemia-reperfusion injury via PI3K/AKT pathway-mediated mitochondrial apoptosis. *Immunopharmacol. Immunotoxicol.* 43, 731–740. doi:10.1080/08923973.2021.1976794

Zhao, S., Mi, Y., Guan, B., Zheng, B., Wei, P., Gu, Y., et al. (2020). Tumor-derived exosomal miR-934 induces macrophage M2 polarization to promote liver metastasis of colorectal cancer. *J. Hematol. Oncol.* 13, 156. doi:10.1186/s13045-020-00991-2

Zheng, Y., He, R., Wang, P., Shi, Y., Zhao, L., and Liang, J. (2019). Exosomes from LPS-stimulated macrophages induce neuroprotection and functional improvement after ischemic stroke by modulating microglial polarization. *Biomater. Sci.* 7, 2037–2049. doi:10.1039/c8bm01449c

Zhou, J., Chen, L., Chen, B., Huang, S., Zeng, C., Wu, H., et al. (2018). Increased serum exosomal miR-134 expression in the acute ischemic stroke patients. *BMC Neurol.* 18, 198. doi:10.1186/s12883-018-1196-z

Zhu, J., Liu, B., Wang, Z., Wang, D., Ni, H., Zhang, L., et al. (2019). Exosomes from nicotine-stimulated macrophages accelerate atherosclerosis through miR-21-3p/PTEN-mediated VSMC migration and proliferation. *Theranostics* 9, 6901–6919. doi:10.7150/thno.37357

Zhu, T., Xie, W. J., Wang, L., Jin, X. B., Meng, X. B., Sun, G. B., et al. (2021). Notoginsenoside R1 activates the NAMPT-NAD+-SIRT1 cascade to promote postischemic angiogenesis by modulating Notch signaling. *Biomed. Pharmacother.* 140, 111693. doi:10.1016/j.biopha.2021.111693

frontiers | Frontiers in Bioengineering and Biotechnology

TYPE Review
PUBLISHED 16 January 2023
DOI 10.3389/fbioe.2022.1094968

OPEN ACCESS

EDITED BY
Jingfeng Li,
Zhongnan Hospital, Wuhan University, China

REVIEWED BY
Krishna Ramajayam,
Unchained labs LLC, United States
Stewart Smith,
The University of Edinburgh, United Kingdom
Shenghui Lan,
Shanghai Eighth People's Hospital, China

*CORRESPONDENCE
Veronika Malyško-Ptašinskė,
veronika.malysko-ptasinske@vilniustech.lt
Vitalij Novickij,
vitalij.novickij@vilniustech.lt

SPECIALTY SECTION
This article was submitted to Preclinical Cell and Gene Therapy, a section of the journal Frontiers in Bioengineering and Biotechnology

RECEIVED 10 November 2022
ACCEPTED 28 December 2022
PUBLISHED 16 January 2023

CITATION
Malyško-Ptašinskė V, Staigvila G and Novickij V (2023), Invasive and non-invasive electrodes for successful drug and gene delivery in electroporation-based treatments.
Front. Bioeng. Biotechnol. 10:1094968.
doi: 10.3389/fbioe.2022.1094968

Invasive and non-invasive electrodes for successful drug and gene delivery in electroporation-based treatments

Veronika Malyško-Ptašinskė[1]*, Gediminas Staigvila[1] and Vitalij Novickij[1,2]*

[1]Faculty of Electronics, Vilnius Gediminas Technical University, Vilnius, Lithuania, [2]Department of Immunology, State Research Institute Centre of Innovative Medicine, Vilnius, Lithuania

Electroporation is an effective physical method for irreversible or reversible permeabilization of plasma membranes of biological cells and is typically used for tissue ablation or targeted drug/DNA delivery into living cells. In the context of cancer treatment, full recovery from an electroporation-based procedure is frequently dependent on the spatial distribution/homogeneity of the electric field in the tissue; therefore, the structure of electrodes/applicators plays an important role. This review focuses on the analysis of electrodes and *in silico* models used for electroporation in cancer treatment and gene therapy. We have reviewed various invasive and non-invasive electrodes; analyzed the spatial electric field distribution using finite element method analysis; evaluated parametric compatibility, and the pros and cons of application; and summarized options for improvement. Additionally, this review highlights the importance of tissue bioimpedance for accurate treatment planning using numerical modeling and the effects of pulse frequency on tissue conductivity and relative permittivity values.

KEYWORDS

electrodes, electroporation, spatial electric field distribution, tumors, electrical tissue properties

1 Introduction

Electroporation is a phenomenon in which the cell plasma membrane is permeabilized by the application of short, high-intensity electric field pulses. The increased permeabilization of the cell membrane is related to the formation of transient aqueous pores, creating pathways for drugs or DNA molecules to enter the cell (Freeman et al., 1994; Du et al., 2018; Bö et al., 2020). However, in order to create these pores, the transmembrane potential of the cell must exceed the electroporation threshold (Kinosita and Tsong, 1977). Thus, depending on the PEF parameters (pulse duration, strength, repetition frequency, etc.), different cell responses to the treatment could be triggered (Szlasa et al., 2021; Vižintin et al., 2021). In the case of reversible electroporation (RE), after a specific resealing time, membrane integrity is restored and the cell survives. RE can be used in electrochemotherapy (ECT), which is a combination of chemotherapy and electroporation, resulting in a highly effective method for cancer treatment. Additionally, electroporation can be used for controlled electro-transfer of DNA, known as gene electro-transfer (GET) or electro-transfection. However, if the intensity of the PEF is further increased, it may lead to irreversible electroporation (IRE) and consequently cell death, resulting in tissue ablation (Sersa et al., 2008a; Korohoda et al., 2013; Calvet and Mir, 2016; Cemazar and Sersa, 2019). Therefore, depending on the purpose, the desired outcome can be

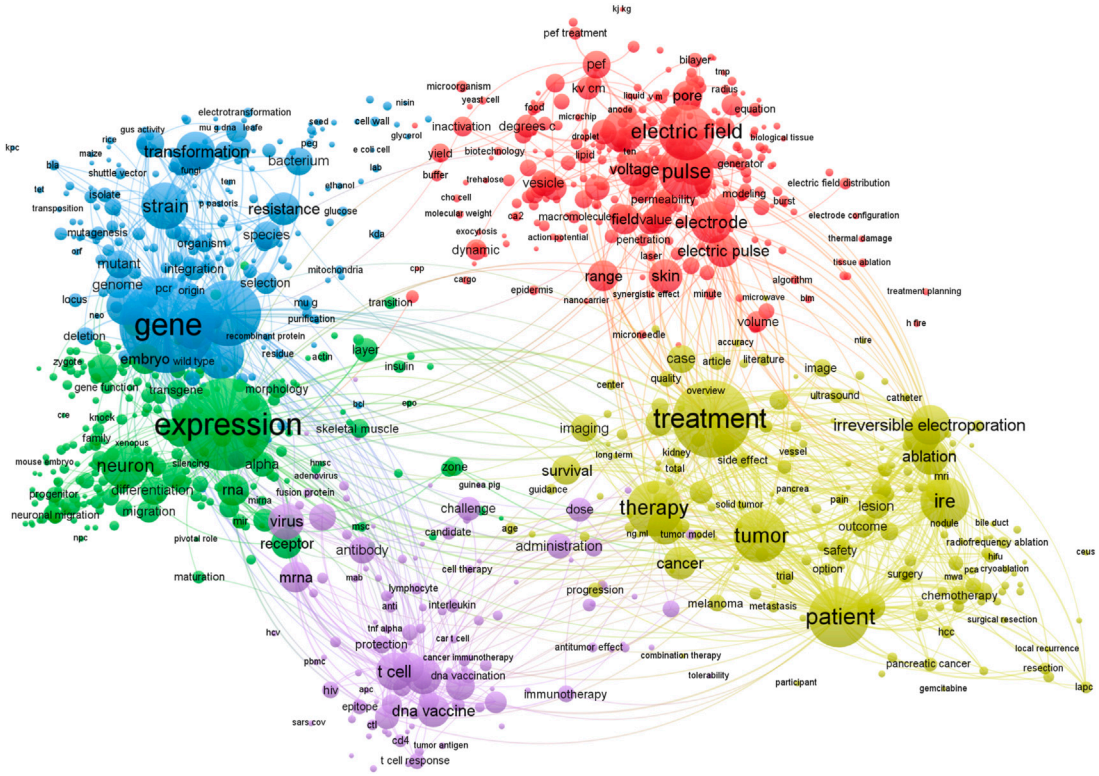

FIGURE 1
Most common keywords used in electroporation studies. Visualized using VOSviewer software, version 1.6.18 (Leiden University) (VOSviewer - Visualizing scientific landscapes, 2022). A filter of at least 30 minimum occurrences of the keywords has been used. Bigger circle size indicates higher rate of occurrence of a specific keyword.

achieved and successfully controlled by modulating the PEF parameters. In clinical settings, in order to predict the effect of electroporation on various tissues and ensure precise electrode positioning, a wide spectrum of techniques is employed (Neal II et al., 2012), including magnetic resonance imaging (Figini et al., 2017; Boc et al., 2018); however, numerical modeling is the most popular method for treatment planning (Kranjc et al., 2017; Asadi et al., 2019). Numerical models can serve as an aid for accurate prediction of electroporation outcome and better pretreatment planning by simulation of the spatial electric field distribution (Miklavčič et al., 1998; Pavšelj and Miklavčič, 2008).

As a result, electroporation-based technologies and applications are an interdisciplinary field involving research in electronics and electrical engineering, biophysics, biomedicine, microbiology, and food technology. Based on Clarivate Analytics Web of Science, there are 17,179 papers featuring the keyword “electroporation” (Access date: 2022–03-01). A visual map of the most common keywords in electroporation papers is shown in Figure 1.

It can be seen that the applied aspects of electroporation dominate the field, although there is an inevitable interconnectivity with the electric field, electrodes, voltage, and pulse characterization in order to ensure repeatability of the research and protocols (arrangement of red circles).

Generally, electrical pulses are delivered using a high-power generator (electroporator) and electrodes (applicator), where the electrodes transfer the energy of the pulse to the biological tissue. As a result, various models and prototypes of electrodes for electroporation-based treatments are constantly being proposed (Dermol-Černe et al., 2020). Each electrode configuration is unique and frequently limited to a specific target tissue or designated area of application. In this work, we provide an overview of various electrode structures and describe the pros and cons, suitable protocols, and applications. To support better understanding and enable adequate comparison, we also performed the simulation of spatial electric field distribution using the finite element method (FEM). The modeling and comparative analysis of various electrode types are presented in Section 2 of the review. Also, the summary of pulse parameters and protocols used with different electrode types is presented in Section 3.

Nevertheless, the accuracy of any model is determined by the extent of the approximations included. For better pretreatment planning through numerical modeling, inclusion of the peculiarities of the treated object structure is critical. The composition of biological tissues is heterogeneous; i.e., it consists of various layers and structures with specific electrical properties and, thus, different responses to PEF. In order to analyze the outcome of electrical pulsing on tissues, its composition and dielectric properties (specific conductivity and relative permittivity) have to be considered. Therefore, this review also summarizes the frequency-dependent dielectric properties of various healthy and cancerous tissues.

2 Mammalian tissue electroporation

By *in vivo* and clinical electroporation procedures, various types of tumors can be treated (Li, 2008), which may be grouped simply as

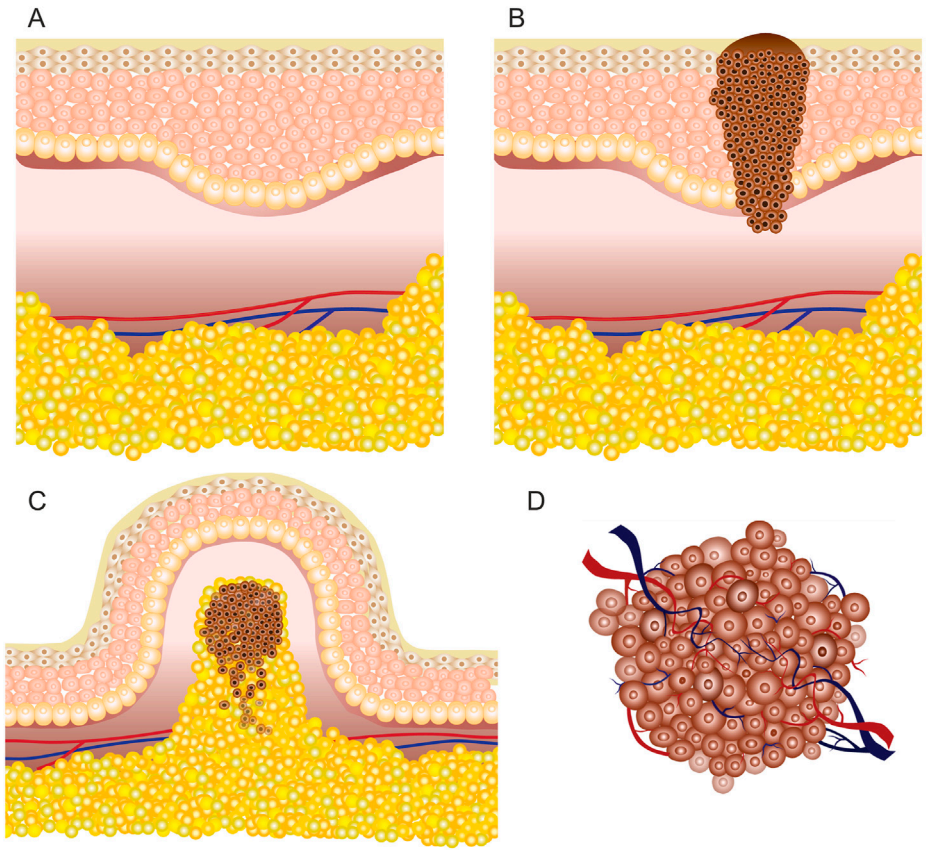

FIGURE 2
Skin illustration: **(A)** healthy tissue; **(B)** cutaneous tumor (melanoma); **(C)** superficial or exophytic tumor; **(D)** deep-seated tumor.

cutaneous (located on the skin) or subcutaneous (located under the skin in the subcutaneous tissues) lesions (Figure 2). According to available research, GET, ECT, and IRE are applicable for both deep-seated targets such as tumors/lesions located in muscles and superficial targets located directly on the skin or under the skin (Matthiessen et al., 2012; Heller and Heller, 2015). Consequently, each approach requires specific applicators and their precise positioning, taking into account the location of the target tissue (Zupanic et al., 2012).

According to the European Standard Operating Procedures of Electrochemotherapy (ESOPE) for subcutaneous tumors, pulsed electric field must be generated in deeper tissues; hence, invasive electrodes are required. In contrast, non-invasive electrodes are frequently used for cutaneous targets and have limited applicability for deep-seated tumors (Cvetkoska et al., 2020). Electroporation-based treatment success depends on the coverage of the tumor tissue by sufficiently high local electric field, requiring good contact area between the tissue and the electrodes (Čorović et al., 2008; Sachdev et al., 2022). Simulation of the electric field distribution is usually performed using the FEM analysis (Pintar et al., 2018). However, for accurate prediction, the electrical parameters of the tissue should be known and the heterogeneity should be taken into account, especially for treatment of superficial tumors (Figure 2C) due to high heterogeneity of the skin.

The skin has several functions, including protection of internal organs from environmental influence (Monteiro-riviere and Riviere, 1999; Hayes et al., 2022). A thorough understanding of the skin structure and its electrical properties is crucial to make subcutaneous tumors permeable. Basically, the skin consists of the stratum corneum, epidermis, dermis, hypodermis, fat (subcutaneous adipose tissue), and muscle tissue under the hypodermis (Huclova et al., 2012; Ventrelli et al., 2015). The outer layer (stratum corneum) is mostly composed of dead skin cells and is the thinnest; however, it has the highest resistivity. As a result, the skin is considered a barrier for successful electroporation applications when non-invasive electrodes are employed. The epidermis and dermis are located beneath the stratum corneum and have much lower resistance; therefore, there is a considerable voltage drop across the stratum corneum (Alkilani et al., 2015; Lu et al., 2018). However, once the stratum corneum is permeabilized by the formation of local transport regions (Gelker et al., 2018), deeper layers of the skin can be affected.

However, for deep-seated tumors (Figure 2D) such as tumors of the liver or pancreas, either invasive electrodes are used percutaneously or the treatment is performed during an open surgery (Granata et al., 2021); therefore, the skin has little to no effect on the electroporation procedure. Nevertheless, in most cases with deep-seated tumors, the tumors are intact with healthy organs (Edhemovic et al., 2014) or the tumors are encapsulated into the organs (Ghossein, 2010) and surrounded by large blood vessels (Djokic et al., 2018a). The complexity of such tumor composition influences the inhomogeneity of the target tissue, which may result in non-uniform treatment. As a consequence, the electrical properties of

such tumors and tissues in vicinity may vary and, therefore, must be taken into account.

Tissue electrical properties can be described by the concept of bioimpedance, which is a frequency-dependent parameter specific to tissue composition, including water content (Chumlea and Guo, 1994). Biological tissue is considered neither a good conductor nor an insulator but rather something in between that allows the flow of a certain amount of current. This is due to the influence of aqueous, for instance the muscle, and non-aqueous components, such as bone or fat structures. In the low- and high-frequency range, the current density vectors vary, and the bioimpedance decreases in the high-frequency range, enabling a more homogeneous treatment (Raja et al., 2006). Therefore, the conductivity and relative permittivity changes in the tissue and their dependence on the applied pulse frequency should always be taken into account (Miklavčič et al., 2006; Zhang and He, 2010).

Thus, the tissue electrical properties are characterized by its specific conductivity σ and relative permittivity ε_r. It is known that the increase in electric conductivity is related to the formation of local transport regions after the application of electric pulses (Pliquett et al., 1998). Hence, conductivity is the ability of aqueous solutions to transfer electric charge. Simultaneously, the ability of a material to be polarized is characterized by relative permittivity. Consequently, these properties are vital for numerical modeling of the tissue. According to previous studies, the value of conductivity may exhibit a significant increase with the increase in pulse repetition frequency when pulses are applied in bursts with repetition frequency above 100 kHz (de Santis et al., 2015; Weinert and Ramos, 2021), while an opposite dependence is observed for relative permittivity (Valdastri et al., 2004; Peyman et al., 2005). A summary of various tissue conductivities and relative permittivities for different frequency ranges is presented in Supplementary Table S1.

In order to reduce the complexity of numerical models and simplify the calculations, conductivity and relative permittivity may be considered as constant values for low or high PEF frequency ranges, while it should be understood that both parameters are dependent on the applied burst frequency.

Additionally, each electroporation procedure (IRE or RE) requires different pulse parameters and a specific field strength (Čorović et al., 2012; Forjanic et al., 2019). IRE is associated with tissue ablation; therefore, a higher PEF intensity is required. On the contrary, RE or gene therapy focuses on transient permeabilization of cells; therefore, the required electric field strength is much lower. Depending on the tissue heterogeneity and electrical parameters, electroporation thresholds may vary. Nevertheless, numerical modeling could serve as a basis for treatment planning and selection of appropriate pulse parameters.

3 Electrodes

In this study, comparison of different electrode types was performed using FEM modeling in COMSOL Multiphysics, version 5.5 (COMSOL, Los Angeles, CA, United States). In order to simplify the calculations, each tumor was modeled as a three-dimensional homogeneous mass of tissue with conductivity 1.5 S/m and a relative permittivity of 80. Positive and zero potentials were set to corresponding electrode pairs depending on the electrode configuration. The electric potential value for each electrode configuration varied depending on the previously published protocols and is, therefore, reported along with the simulations. Outer boundaries of the geometry were treated as electrically insulated. Stationary analysis was performed to estimate the spatial distribution of the electric field.

3.1 Invasive electrodes

Invasive electrodes require electrode penetration into a tissue. The electrode is usually needle-shaped, with a sharp tip. Therefore, most invasive electrodes deliver the electric pulses through typically stainless-steel needles of different length. Currently, fixed-position as well as adjustable position (electrodes, IGEA Medical; Electrodes for *in vivo* electroporation, 2021a) or needle composition (Adjustable Electrodes, 2022) electrode pairs or arrays are commercially available. Fixed-position electrodes are further categorized into two-needle electrodes (Isobe et al., 2004; Chen et al., 2015; Langus et al., 2016; Zager et al., 2016; Yao et al., 2017) and longitudinal or hexagonal electrode arrays. Basically, in this category, the electric field distribution is dependent on the number of needles (Adeyanju et al., 2012), length of the needles, gap spacing, and diameter of the needle tip (Davalos et al., 2005). The electric field distribution of the two-needle electrode configuration, including variation of gap size and length, is shown in Figures 3A–C.

Free position electrodes are advantageous when the tumor or tissue composition is not predetermined. Usually, this type of electrode is combined with an adjustable handle to fix the position after insertion into the target. Nevertheless, the needles are very thin; therefore, the distance between electrodes in deeper tissues may vary, which means the effects of non-parallelism should be considered since it affects the spatial electric field distribution (Figures 3G–I).

As can be seen in the aforementioned figures, the visible gap size in each case is the same—5 mm; therefore, the top view does not change (Figures 3G–I). However, non-parallelism may occur in deeper tissues, especially when using longer needles. Typically, this occurs due to skin surface curvature and composition (Wei et al., 2017; Kopcewicz et al., 2020). Therefore, non-parallelism leads to electric field inhomogeneity and non-uniform treatment, as potentially healthy tissue is affected and target tissues (white dashed lines representing the tumor) remain unaffected or treated insufficiently. It is clear from Figure 3 that using two-needle electrode configurations may involve inhomogeneity of the PEF distribution. This limitation can be minimized using an array of adjustable needles as shown in Figure 4.

Needle arrays or repositioning of needles can be used to ensure more homogeneous deep-seated tumor electroporation. Placement of needle electrodes of variable geometry is adjusted to the individual size and shape of the tumor. To obtain an above-threshold electric field and cover the entire tumor volume, multiple needles are placed at the tumor margins and/or within the tumor. At the same time, the number of needles should be limited to reduce treatment invasiveness and complexity. The electrical pulses are, therefore, subsequently delivered between predetermined needle pairs. Such an electroporation procedure requires very precise pretreatment planning and PEF parameter evaluation (Miklavcic et al., 2010; Pavliha et al., 2012a; Blazevski et al., 2020). However, it enables efficient treatment of tumors with multiple nodules (Figure 4B). Nevertheless, non-parallelism is still a problem and is usually solved by x-ray imaging during the operation after electrode

10.3389/fbioe.2022.1094968

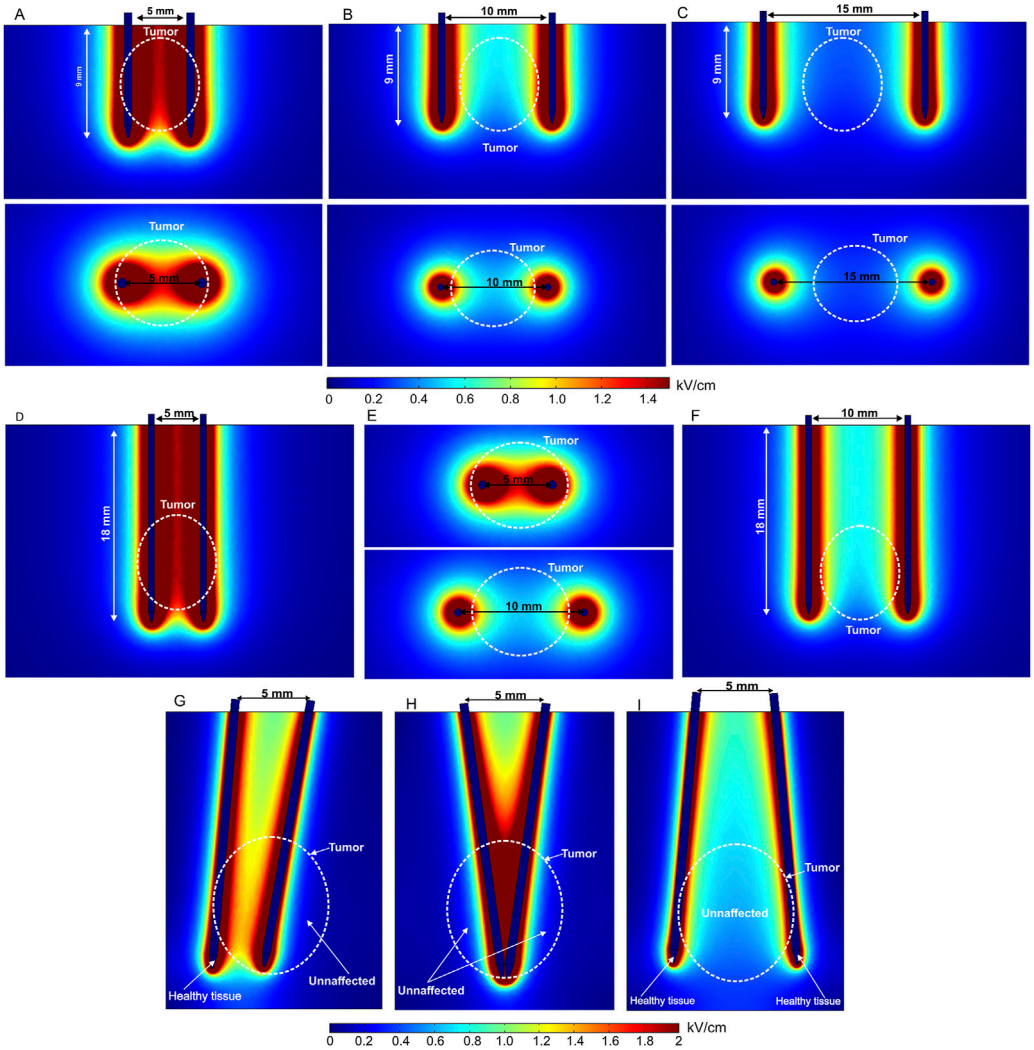

FIGURE 3
Spatial electric field distribution of two-needle fixed-position electrodes **(A–F)** and non-parallelism issue with adjustable electrodes **(G–I)** with different lengths and gap size, using 500 V terminal voltage: **(A)** 5 mm gap between electrodes; **(B)** 10 mm gap between electrodes; **(C)** 15 mm gap between electrodes; **(D)** 20 mm length electrodes with 5 mm gap; **(E)** 20 mm length electrodes with 5 mm and 10 mm gap, top view; **(F)** 20 mm length electrodes with 10 mm gap, side view; **(G)** electrodes are rotated by 10° and 5°; **(H)** both electrodes are rotated by 8° and −8°; **(I)** both electrodes are rotated by −10° and 10°.

positioning and fixation (Moreta-Martínez et al., 2022). If non-parallelism is detected, adjustment of the treatment parameters and/or repositioning of the electrodes can be performed.

When the target tissue or tumor is subcutaneous, the electroporation procedure requires access to deep-seated cancer lesions without making a large incision in the skin. Such treatment is performed using an open laparoscopy approach or trans-oral and trans-anal endoscopy through a catheter (Lee et al., 2019; Li et al., 2021). Therefore, the requirements for the electrodes become more complex: electrodes have to be placed strictly parallel in order to ensure homogeneous PEF; the procedure must be performed on a relatively small probe area; and at the same time, the operating area has to cover the whole tumor volume.

An electrode prototype considering the aforementioned features was presented by Izzo et al. (2020). The study shows the evaluation of the effectiveness and suitability of deployable and expandable 4-needle or 5-needle electrode configurations for IRE *via* laparoscopy and open surgery in the liver of a pig. The electrodes were also tested with trans-anal and trans-oral endoscopic approaches using different electrode configurations. All procedures were performed under ultrasound guidance. The authors state that the electrodes and their mechanical functionality are suitable for the listed procedures, and the electrodes are compatible with the 5-mm laparoscopic trocar and other surgical instruments. Laparoscopic and endoscopic approaches to deep-seated tumors could potentially minimize the risk of bleeding and infection. The FEM model of such an electrode array is presented in Figures 5A, B. Colored needle parts represent the non-conductive adjustable 2-, 3-, or 4-cm-length electrodes, positioned at 0°, 10°, 20°, and 30° angles. The deployable electrodes connected to high and ground potentials are shown in red and blue, respectively, with a fixed length of 2 cm.

The expected spatial electric field distribution at different insertion angles of the electrodes (0° 10°, 20°, and 30°) is shown in Figures 5C–J. The computations were performed with 2-cm needle extension.

10.3389/fbioe.2022.1094968

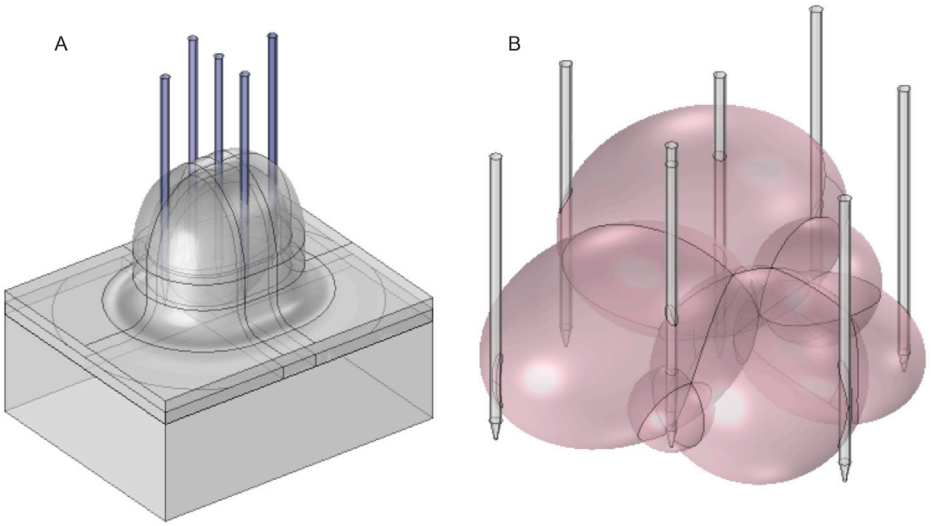

FIGURE 4
Array of adjustable needle electrodes for **(A)** corneous tumors and **(B)** deep-seated tumors.

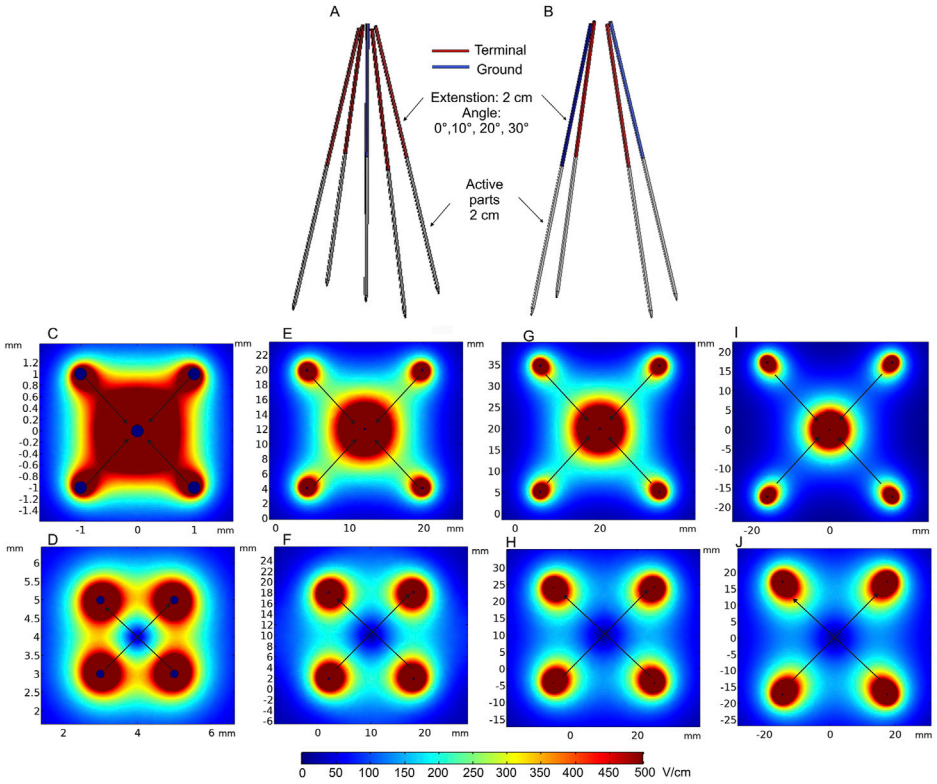

FIGURE 5
Deployable expandable electrodes: **(A)** 5-needle electrode structure; **(B)** 4-needle electrode structure with 2 cm extension; **(C)** spatial electric field distribution of the 5-needle electrode when positioned at 0° angle; **(D)** spatial electric field distribution of the 4-needle electrode when positioned at 0° angle; **(E)** spatial electric field distribution of the 5-needle electrode when positioned at 10° angle; **(F)** spatial electric field distribution of the 4-needle electrode when positioned at 10° angle; **(G)** spatial electric field distribution of the 5-needle electrode when positioned at 20° angle; **(H)** spatial electric field distribution of the 4-needle electrode when positioned at 20° angle; **(I)** spatial electric field distribution of the 5-needle electrode when positioned at 30° angle; **(J)** spatial electric field distribution of the 4-needle electrode when positioned at 30° angle. **Simulation performed includes single diagonal and semi-diagonal terminal voltages (0°—120 V, 10°—1100 V, and 20° and 30°—1700 V).*

10.3389/fbioe.2022.1094968

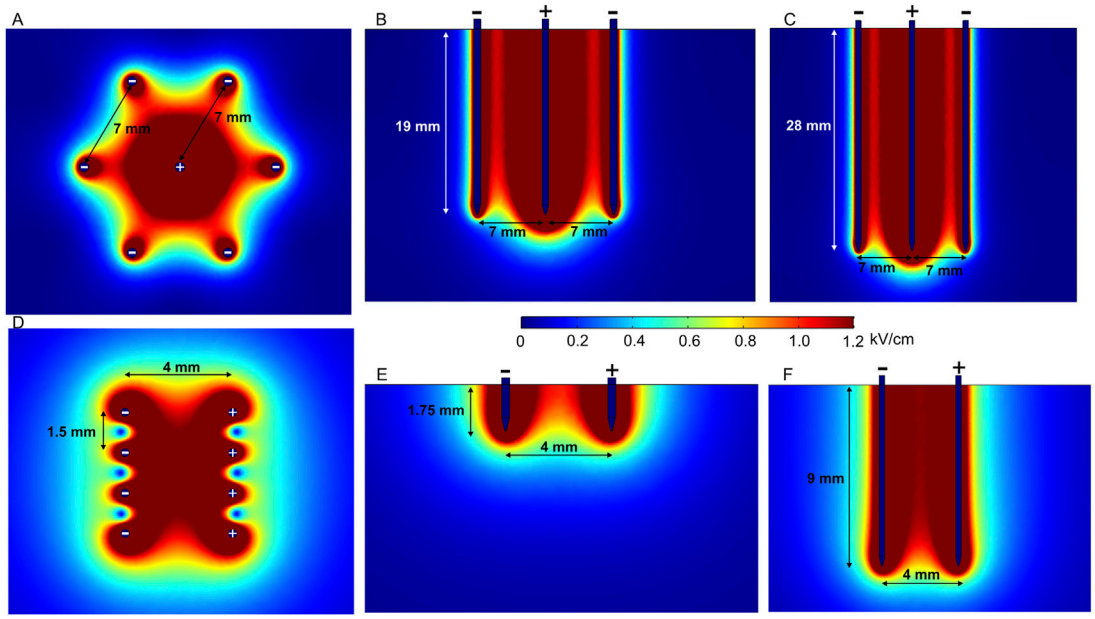

FIGURE 6
Spatial electric field distribution generated by hexagonal and intradermal needle-type electrode arrays with 1500 V and 600 V terminal voltages, respectively, taking into account different depths of penetration. **(A)** Hexagonal electrodes, top view; **(B)** hexagonal 20-mm-length electrodes, side view; **(C)** hexagonal 30-mm-length electrodes, side view; **(D)** intradermal electrodes, top view; **(E)** intradermal 2-mm-length electrodes, side view; **(F)** intradermal 10-mm-length electrodes, side view.

Diagonal and semi-diagonal black arrows represent the pairs of electrodes where the voltage is applied. It can be seen that by changing the active electrode pairs, the volume of the electroporated tissue can be controlled. If required, the whole volume could be ablated and/or reversibly electroporated due to overlapping of the high-intensity PEF regions. The capability to increase the length of each needle independently also allows for controlling the depth of the electroporated volume. Essentially, these electrodes are a specific case of the applicators presented in Figure 4, but when non-parallelism is intentional. The problems of precise needle positioning are still applicable.

At the same time, fixed-position electrodes are advantageous for minimizing non-parallelism during needle insertion. Electric field distribution analysis of a hexagonal array of four-needle pair fixed electrodes is represented in Figures 6A–F. In the first case (Figures 6D–F), the applied voltage is 600 V, which induces a relatively homogeneous electric field between the positive and negative electrode pairs of 2- and 10-mm needle lengths.

Such electrodes are commercially available and used for intradermal (ID) electroporation, featuring 2- and 10-mm electrode lengths (Needle Array Electrodes for BTX AgilePulse *In Vivo*, 2021; Fixed Electrodes, 2022b). Intradermal electrodes are used when the penetration of outer skin layers, i.e., the stratum corneum, dermis, and epidermis, is sufficient. The spatial electric field distribution generated by an ID electrode with two rows of four needles is presented in Figures 6D–F. There is a notable difference in spatial electric field distribution in the tissue; 10-mm needles inserted at approximately 7 mm depth provide a uniform electric field; on the contrary, 2-mm electrodes feature a less homogeneous electric field distribution in the effective volume of effect. Nevertheless, when the limitations are taken into account, electrodes can be successfully utilized in practice (Roos et al., 2006; 2009; Lladser et al., 2010).

In the case of hexagonal electrodes (Figures 6A–C), the electric field is located around the positively charged electrode; therefore, the electric field is highest in the central part of the target tissue, while potentially healthy tissue on the edges remains intact. These electrodes are suitable for bigger tumors in the ECT context (Pichi et al., 2018), and different similar configurations can be used for gene therapy (Gilbert et al., 1997).

To summarize, fixed-position electrodes are likely to produce a more uniform electric field due to better control of tissue penetration—the chances of non-parallelism of electrodes are minimized. However, fixed-position electrodes are suitable only for tumors of predetermined size and, therefore, are less flexible for cancer treatment, especially when the tumor size is significantly smaller or bigger than the gap between the fixed electrodes. ID electrodes are appropriate for gene therapy; however, the penetration depth should be considered to ensure sufficient homogeneity of the electric field.

One of the solutions to minimize the challenges of electrode positioning is the use of single-needle electrode configuration (Neal et al., 2010; Garcia et al., 2014). Such an electrode type consists of an electrode body, cathode, insulator, and anode on the sharp tip of the needle, where each part has a predetermined length and width (Figure 7A). Figure 7B shows the spatial electric field distribution. It can be seen that the design solves the problem of non-parallelism; however, as a trade-off, the electric field distribution is relatively non-homogeneous. Moreover, the diameter of this electrode is relatively large; therefore, it is applicable mainly for bigger tumors.

The new prototype of invasive electrodes, called curved electrodes, was proposed by Ritter et al. (2018). Curved electrodes are minimally invasive electrodes consisting of a penetrating central

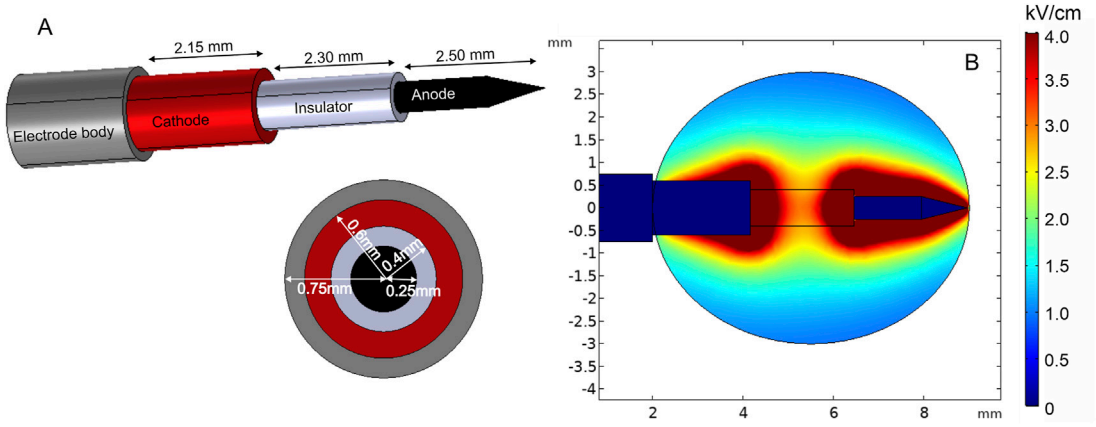

FIGURE 7
Single-needle electrode model: **(A)** electrode structure; **(B)** spatial electric field distribution with 1300 V terminal voltage.

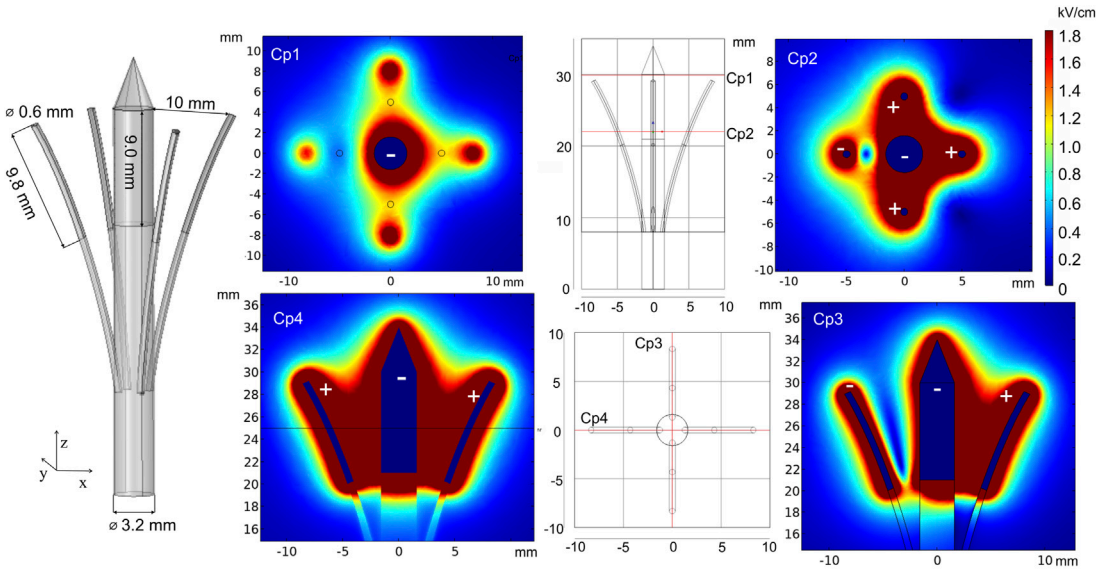

FIGURE 8
Curved electrodes using 1500 V terminal voltage. *Cp represents cut planes for electric field distribution analysis.

needle and four thin hollow expandable electrodes for pulse application and injection of chemotherapeutic agents. For simulation, the electrode terminal voltage was set to 1500 V. Furthermore, electric field distribution analysis was performed and is presented in Figure 8. Cut plane Cp1 shows the field strength on the surface when the penetration depth is shallow. As it can be seen, the highest electric field is around the central needle and at the positively charged satellite electrode tips. As a consequence, other areas will be treated with a lower PEF. However, penetration into deeper tissue layers results in a more homogeneous treatment (Cp2), which is also supported by the side view simulation (Cp3 and Cp4). Changing the number of active electrodes allows for controlling of the treatment volume. Moreover, the position of satellite needles can be adjusted with the movable part, which introduces additional flexibility.

To conclude, needle electrodes are advantageous for deep-seated tumors and intramuscular or intradermal GET targets. Both fixed-position and independent needle arrays show acceptable performance and are applied in clinical treatment. Fixed-position electrodes are easier to apply, but they are mostly suitable for specific size targets, i.e., the target should be of similar size as the gap distance. Otherwise, the healthy tissue will receive unnecessary pulsing. On the contrary, if the target exceeds the space between the electrodes, the treatment will result in partial response due to only a fraction of the tumor being affected. To overcome this problem, manual needle repositioning or more accurate multiple needle application along with a brachytherapy grid (van den Bos et al., 2016) may be considered. In addition, such fixing equipment and non-conductive ring nuts or “stoppers” help minimize non-parallelism after needle penetration. When the tumor is deep-seated, the requirements for treatment and electroporation

10.3389/fbioe.2022.1094968

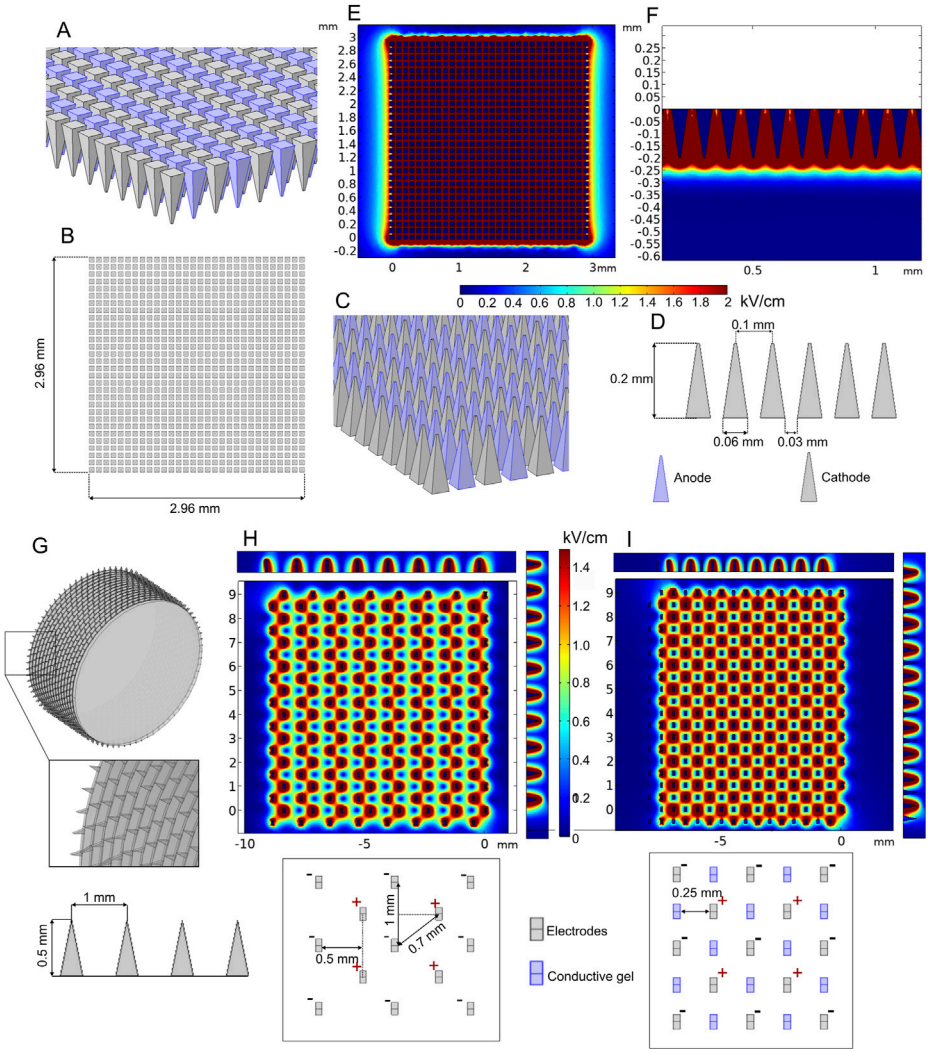

FIGURE 9
Microneedle array **(A–F)** and multi-needle roller **(G–I)** electrodes when 100 V voltage is applied: **(A–D)** microneedle array model; **(E)** spatial electric field distribution, top view; **(F)** spatial electric field distribution, side view; **(G)** multi-needle roller model; **(H)** spatial electric field distribution without conductive gel; **(I)** spatial electric field distribution with conductive gel channels.

electrodes are even more intricate; thus, tumor boundaries cannot be seen with the naked eye. Real-time imaging, such as ultrasound (van den Bos et al., 2016; Hsiao and Huang, 2017) or fluoroscopy (Pavliha et al., 2012b) guidance, is a solution. The combination of invasive electrodes with an imaging procedure gives the possibility for more accurate target boundary assessment, minimizing the possibility of multiple pulsing on the same area of the tissue since the field strength for each electrode pair is predetermined. Real-time imaging is also advantageous when tumors can be reached through the skin without incision (Lee et al., 2007).

3.2 Minimally invasive electrodes

Various minimally invasive (Choi et al., 2010; Yan et al., 2010; Xia et al., 2021) and non-invasive (Heller et al., 2010; Guo et al., 2011) microneedle array electrodes are mainly designed for transdermal drug delivery. The aim of microneedles is to affect the outer skin layers or muscle and ensure distribution of sufficient electric field for reversible electroporation, which is usually employed for electroporation-based gene delivery (also called gene vaccination). An example of such an array of electrodes is presented in Figures 9A–F.

The model consists of 900 (30 per row and 30 per column) 0.2-mm-length microneedles placed at 0.1 mm distance between needle tips. Terminal and ground potential electrodes are distributed in each row as shown in Figures 9A, C, and field analysis was performed using 100 V terminal voltage. The results are summarized in Figures 9E, F.

It can be seen that the depth of high-intensity electric field penetration is limited; however, it is still sufficient for transdermal gene delivery. The most significant disadvantage of most gene therapy electrodes is the relatively small operating area. In order to increase the effective area of the minimally invasive electrodes, roller type electrodes can be used as proposed by Yang et al. (2021). In Figure 9G, the model of such an electrode structure is shown, and the expected electric field distribution is presented in Figure 9H.

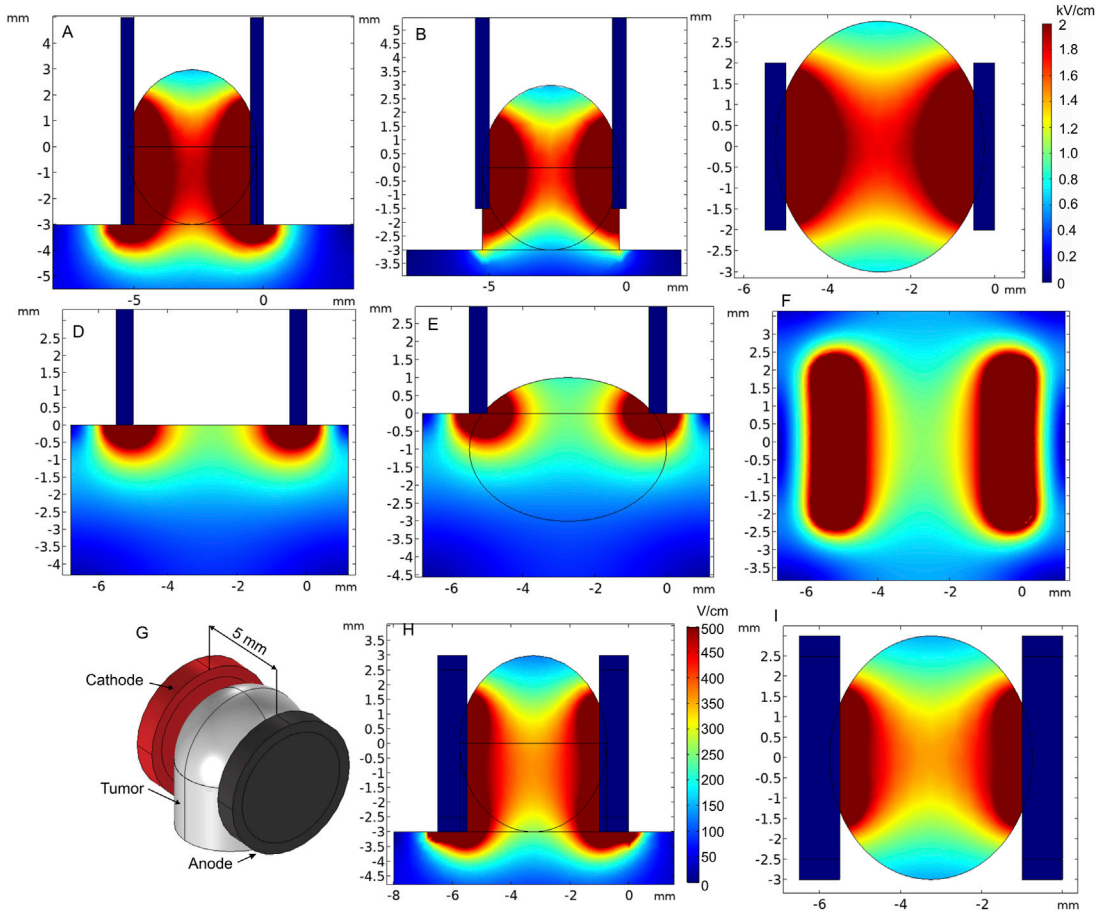

FIGURE 10
Spatial electric field distribution of plate and round tweezer electrodes using 1000 V and 200 V terminal voltages, respectively. **(A)** Electroporation of a superficial tumor, when plates embrace the tumor sufficiently, side view; **(B)** electroporation of a superficial tumor, when plates embrace the tumor insufficiently, side view; **(C)** electroporation of the superficial tumor, top view; **(D)** electroporation of the skin, side view; **(E)** electroporation of melanoma or a small superficial tumor; **(F)** electroporation of the skin or melanoma, top view; **(G)** round tweezer electrode simulation model; **(H)** spatial electric field distribution, side view; **(I)** spatial electric field distribution, top view.

The FEM analysis results indicated that the highest value of electric field strength is located around the microneedle tips; however, it decreases drastically in the gap between the negatively and positively charged needle pairs (Figure 9H). A similar electrode type was analyzed by Huang et al. (2018). In order to improve the non-homogeneity, it was proposed to combine the structure with conductive gel microchannels, which are formed by applying gel on the skin and rolling the needles on the skin ten times before the pulsing. As an approximation, our simulation of this treatment covers the electric field distribution with one layer of microchannels filled with conductive gel (Figure 9I). The results indicated that the conductive gel channels can improve electric field homogeneity.

3.3 Non-invasive electrodes

As previously mentioned, non-invasive electrodes interact through the skin interface. Non-invasive electrodes are less suitable for deep subcutaneous tumors; however, they may be advantageous on exophytic tumors or melanoma, which appears on the skin surface. Several configurations of such electrodes are presented in the following.

Plate electrodes are most commonly used as a non-invasive electrode type (Al-Sakere et al., 2007; Sedlar et al., 2012; Novickij et al., 2021). The configuration consists of two rectangular stainless steel plates with fixed gap size [or adjustable with clippers (Caliper Electrodes for Electroporation Applications, 2022; Wang et al., 2008)] placed in parallel representing the anode and cathode (Fixed Electrodes, 2022a). Figures 10D-F show the application of plate electrodes for electroporation of skin (Figure 10D) and small skin lump (Figure 10E).

Tweezer-type electrodes are also a sub-population of parallel plate electrodes that are comfortable to be used when the gap between electrodes need to be adjustable. An example of round tweezer electrodes with adjustable 1–20 mm gap size is shown in Figures 10G–I (Tweezertrodes Electrodes for *In Vivo* and In Utero Electroporation Applications, 2022). For prediction of electric field distribution, we used a specific case with 5-mm-diameter and 4.5-mm-gap electrodes covering a tissue lump. As expected, due to limited contact area, the electric field was not homogeneous. Proper and maximum contact of the electrode surface with the tissue should be

10.3389/fbioe.2022.1094968

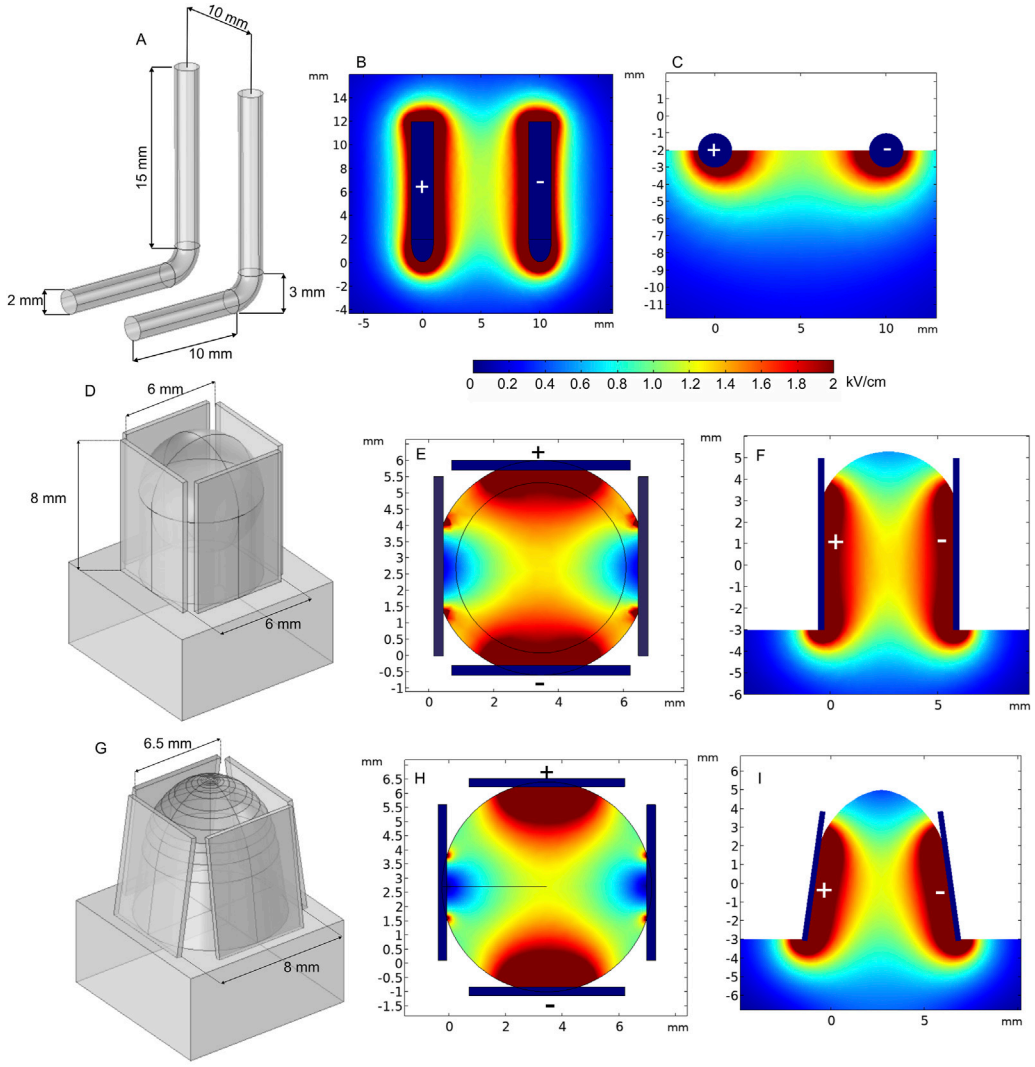

FIGURE 11
L-shaped **(A–B)** and 4-plate electrodes with **(D–F)** and without expansion **(G–I)** when 1300 V terminal voltage is used. **(A)** L-shaped electrode structure; **(B)** spatial electric field distribution, top view; **(C)** spatial electric field distribution, side view; **(D)** 4–plate electrode structure without plate expansion; **(E)** spatial electric field distribution without plate expansion, top view; **(F)** spatial electric field distribution without plate expansion, side view; **(G)** 4-plate electrode structure with plate expansion; **(H)** spatial electric field distribution with plate expansion by 8°, top view; **(I)** spatial electric field distribution without plate expansion by 8°, side view.

ensured for the electrodes to be applicable in cancer treatment. Nevertheless, the requirements for electric field homogeneity during gene therapy are lower; thus, this type of tweezer electrodes is sometimes favorable due to the ease of use and compactness (Maiorano and Mallamaci, 2009; Shi et al., 2010; Zhang et al., 2022). Tweezer electrodes are available in a variety of tip shapes and sizes (Tweezertrodes Electrodes for *In Vivo* and In Utero Electroporation Applications, 2022).

In the case of superficial tumors, good contact between the electrodes and the tissue is essential, as it may dramatically affect the electric field distribution (Figures 10A, B). Also, forming a lump can be sometimes advantageous. Nevertheless, it can be clearly seen that the top and bottom of the tumor are covered by a significantly lower electric field, especially when the tumor is embraced insufficiently (Figure 10B). If not taken into account during the treatment planning step, it may result in re-occurrence of the tumor.

L-shaped electrodes are another commonly used applicator for electroporation-based treatments. This type of electrodes is mostly used for large cutaneous margins and is designed for the treatment of skin tumors of all sizes. An example of such a commercially available electrode arrangement is shown in Figure 11A (Accessories ElectroVet, 2021). For the simulation, the electrodes were placed on the tissue boundary and pushed into the skin; furthermore, 1300 V voltage was applied. Figures 11B, C show that the electric field of the L-shaped electrodes is inhomogeneous, i.e., the highest dose of PEF is expected at the skin surface, while deeper tissue layers are affected by a significantly lower electric field.

Similar L-shaped electrode configurations have been employed for *in vivo* electroporation for both gene therapy and electrochemotherapy by Mazères et al. (2008). In their study, electrodes were repositioned by 90° after each pulse train to

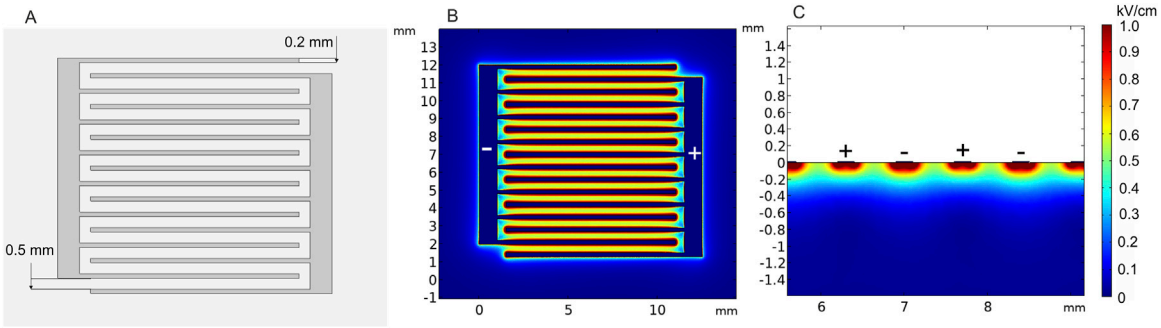

FIGURE 12
Micromachined pliable electroporation patch (ep-Patch) with rectanglular parallel gold electrodes, using 50 V terminal voltage. **(A)** Electrode structure; **(B)** spatial electric field distribution, top view; **(C)** spatial electric field distribution, side view.

compensate electric field inhomogeneity. The results showed 93% of complete response on treated animals, and the electrodes were efficient on tumors of up to 5 cm diameter. Gene therapy was also successful when performed using 4-mm-gap electrodes. However, ablation of the skin was observed.

Another option of non-invasive electrodes is the 4-plate electrode (4PE), where pulses are delivered by two parallel electrode pairs instead of rotating two plates by 90°. The 4PE was developed by Heller et al. initially for gene electro-transfer procedures (Heller et al., 2007). The electrodes operate as follows: metal plates are placed on the target to "grab" the desirable skin fold, and the non-conductive ring-shaped nut is tightened to establish a constant gap size. Two different gap sizes were analyzed—6 mm, without plate expansion, and 8 mm, with 8° expansion (Figures 11D,G, respectively). As can be seen from Figures 11E, F, the spatial electric field distribution of the 4PE is similar to that of two-plate electrodes. However, since the pulsing is performed between 90° shifted electrode pairs, during the second pulse train, the non-homogeneity of the treated volume can be better compensated.

According to the spatial electric field distribution presented in Figure 11F, the value of the electric field decreases at the top and the bottom of the electroporated tissue. The problem is even more apparent when the plates are expanded (Figure 11I). However, when the target tissue is larger in size, such expansion may be advantageous, which ensures a wider contact area by squeezing the tissue between all the plates.

Another type of superficial electrode currently being developed is the pliable electroporation patch with thin flexible electrodes. Currently, such electrodes are successfully employed for gene delivery. Flexible electrodes adapt to the skin surface and, therefore, ensure good contact. Figure 12 illustrates the micromachined pliable electroporation patch (ep-Patch), which consists of rectangular parallel gold electrodes presented by Wei et al. (2015). We analyzed a model with 0.2 mm width and 0.5 mm spacing between the electrodes (Figure 12A). The electric field distribution was evaluated with 50 V terminal voltage (Figures 12B, C). It can be seen that the electrodes ensure acceptable transdermal electric field distribution, while the flexibility to adapt to the skin surface is advantageous for practical applications.

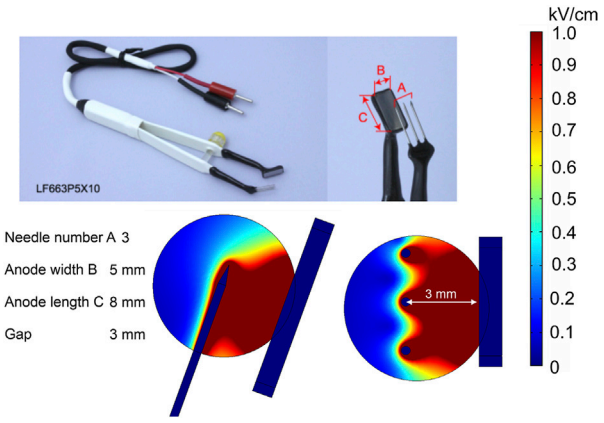

FIGURE 13
Plate-and-fork-type electrodes using 500 V terminal voltage. **(A)** Commercially available electrodes; **(B)** electrode structure; **(C)** spatial electric field distribution, side view; **(D)** spatial electric field distribution, top view.

As previously pointed out, electroporation success strongly depends on the electric field distribution in the tissue (Miklavcic et al., 2006). In order to guarantee effective treatment, homogeneous PEF must be spread through the whole target; otherwise, only partial treatment of the target will be achieved. This problem is especially apparent for non-invasive electrodes in ECT, resulting in tumor re-occurrence (Shankayi and Firoozabadi, 2012). Therefore, either alternative electrode configurations should be considered or a repositioning strategy developed during the treatment planning step.

Simulation results showed that non-invasive applicators are not capable of reaching subcutaneous or deeper tissues with sufficient PEF value. A higher pulse amplitude could be considered, but it would trigger IRE of the tumor in close proximity with the electrode terminals, which is not always desired. Increasing the amount of conductive gel between the electrodes and tissue fold improves the PEF distribution (Ivorra et al., 2008); however, the parts of the tumor without direct contact with the electrodes are likely to be affected by the insufficient electric field (Novickij et al., 2021). Additionally, too

much conductive gel, especially in the top part of the tumor, can short-circuit the generator.

3.4 Partly invasive electrodes

Plate-and-fork-type electrodes are commercially available electrodes (Electrodes for *in vivo* electroporation, 2021b) that are effective for gene therapy (Maruyama et al., 2001).

The analyzed model consists of a pair of tweezers, one with a stainless steel fork consisting of 3-mm needles and the other with a 5 × 8-mm plate, and a spherical tumor (Figure 13). The fork with needles is inserted into the tissue, and simultaneously, the rectangular plate embraces the target. This electrode also contains a fixing part to keep the gap size stable between the fork and the plate while applying the pulses. Clearly, this is a convenient way for tight and accurate grasp of the target tissue; however, it does not solve the field homogeneity problem; thus, the application is limited to gene therapy.

4 Applications *in vivo* and in clinical trials

A variety of electrode prototypes and electrode geometries are commercially available; however, electrode structure is only one component of electroporation success. Optimal pulsing parameters need to be selected and adjusted according to the electrode structure and tissue properties to enhance treatment efficacy. In order to produce the aforementioned threshold PEF value, adequate pulse amplitude must be applied. Furthermore, modifications of other pulsing properties, i.e., duration, pulse shape, number of pulses, and repetition frequency, are considered and adapted to the electroporation protocol. The interest in pulsing parameter optimization is growing, following the possibility to manipulate the treatment outcome at the same time minimizing the side effects such as muscle contractions (Arena et al., 2011a), thermal damage (Mi et al., 2017), or pain sensation (Cvetkoska et al., 2022). Therefore, determination of appropriate pulsing protocol properties is an essential step in electroporation-based procedures. Currently, a wide range of PEF protocols have been introduced and applied in practice. We have summarized the pulsing protocols and applications of previously reported electrodes in Supplementary Table S2.

The presented limitations and advantages of each electrode structure can significantly determine the electroporation-based clinical treatments. For instance, skin cancer (melanoma, squamous or basal carcinoma, etc.) patients are typically cured via plate or needle array (parallel row or hexagonal) electrodes combined with the ECT procedure, which includes chemotherapeutic agents and ESOPE established electric pulses (Miklavčič et al., 2014). In order to overcome the presented non-homogeneity of the electric field, especially at the central part of the tissue, the electrodes are repositioned or slightly shifted sideward, and simultaneously, subsequent doses of PEF are applied (Campana et al., 2014). The strategy indeed has a positive influence on improving the electric field and, thus, diminishing the growth dynamics of cancerous cells, although it cannot guarantee a minimal ablation area. The necrotic skin areas that were in contact with the electrodes were reported to heal within a month (Quaglino et al., 2008) in most cases, followed by mild to severe pain (Kunte et al., 2017). The mentioned factors may cause discomfort for patients. Nonetheless, ECT may offer an effective treatment for cancerous skin lesions: basal cell carcinoma, 100% complete response within 15–56 months (Kis et al., 2019); melanoma metastases, 89% complete response within 24 months (Ricotti et al., 2014) and 60% complete response within 6 months (Matthiessen et al., 2011); and malignant melanoma, 53.5% (Ferioli et al., 2022). Partial or negative tumor response may potentially be associated with inappropriate drug concentration, non-uniform PEF distribution, and other factors, including immune response to the treatment (Sersa et al., 2008b; Cadossi et al., 2014).

ECT has also proved to be an efficient method in the treatment of deep-seated tumors. The procedure is usually performed with fixed or variable length, composition, and number of needle electrodes, which are injected with ultrasound guidance percutaneously or with open surgery (Gerlini et al., 2013; Djokic et al., 2020). However, ultrasound real-time monitoring alone may sometimes not be accurate enough for precise targeting of the target tissue (Eisele et al., 2014). Recently, laparoscopic approaches with ultrasound support for ECT have been introduced to facilitate electrode guidance for tissue penetration (Stillström et al., 2017; Izzo et al., 2020). Such procedures are advantageous in terms of lesser complications, faster procedure, and smoother patient recovery. The appropriate needle positioning strategy for each specific procedure is performed individually using computed tomography and/or magnetic resonance images prior to treatment (Djokic et al., 2018b). The placement, number of needles, and exposure activation plan are then selected in the most efficient manner using various techniques or software. One such technique was introduced by Marčan et al. The developed web-based electric field distribution visualization tool can be successfully adopted for accurate and time-efficient pre-treatment planning (Groselj et al., 2015; Marčan et al., 2015). Nevertheless, the complete response of deep-seated targets in different locations is still considerably lower than that of skin treatments: 55.5% in <1 month (Coletti et al., 2017), 63% within 20.2 months (Edhemovic et al., 2020), and 50% within 2 months (Matthiessen et al., 2018)), although, in most cases, chemotherapy or radiotherapy is performed before ECT.

IRE is another commonly used electroporation-based tumor ablation method (Aycock and Davalos, 2019). IRE procedures are traditionally performed using relatively long (10 μs–20 ms) monophasic pulses with 1 Hz pulse repetition frequency (Jiang et al., 2015). However, studies confirm that such electric pulsing protocols distinguish many negative factors, i.e., muscle contractions and thermal damage. In recent years, the novel modality of bipolar high-frequency pulses for non-thermal IRE treatment, termed H-FIRE, was proposed (Arena et al., 2011b). The H-FIRE procedure with adjustable position needle electrodes has been recently employed for prostate cancer. The results showed good tumor response to treatment and reduced muscle contractions during the procedure (Dong et al., 2018).

Gene electro-transfer procedures focus on the delivery of DNA encoding therapeutic transgenes mainly for cancer-related therapies or infectious disease vaccines (Heller and Heller, 2015), which addresses the activation of immune response to the treatment (Cervia and Yuan, 2018). Currently, these methods are under investigation in *in vitro* or animal models (Milevoj et al., 2019; Brezar et al., 2020). So far, the procedure was employed only in several clinical treatments, including melanoma (NCT00323206) with interleukin-12 plasmid (Daud et al., 2008), malignant

tumors with AMEP plasmid (NCT01664273) (terminated), metastatic melanoma with AMEP plasmid (NCT01045915) (Spanggaard et al., 2013), and cutaneous basal cell carcinoma located in the head and neck region with phIL12 plasmid (NCT05077033) (Groselj et al., 2022). Depending on the target tissue, invasive (needles or needle arrays), minimally invasive (microneedle array or microneedle roller), or non-invasive (plate, patch, etc.) electrodes are selected to achieve maximum GET efficiency. Interestingly, it was found that moderate tissue preheating before pulse exposure could potentially enhance gene expression while reducing the PEF strength. The minimally invasive electrode array (MEA) with optical fibers for heat production was introduced by the Heller group (Edelblute et al., 2021). The purposed technique was applied on the skin; however, gene expression was also present in deeper layers, including the muscle (Bulysheva et al., 2019). DNA vaccines are another promising field of GET application; however, they still require improvement before clinical applications (Gothelf and Gehl, 2012; Cao et al., 2022).

5 Conclusion

Electroporation effectiveness varies depending on PEF spatial distribution in the tissue. Therefore, research and development of optimal pulsing protocols and applicators for electrochemotherapy (ECT), gene therapy (GT), or irreversible electroporation (IRE) is constantly performed. Currently, there are many types of electrodes (invasive, non-invasive, or minimally invasive); however, all of them have a niche for application and a universal structure is yet to be proposed. The current state-of-the-art is to compensate the problems of tissue heterogeneity and field inhomogeneity with real-time imaging during the procedure. Additionally, treatment planning steps may include FEM simulation of spatial electric field distribution and possible thermal effects.

Author contributions

VM-P and VN prepared and validated the manuscript. VM-P and GS performed the FEM analysis. VN supervised the research. All authors contributed to the article and approved the submitted version.

Acknowledgments

The authors acknowledge the contributions of specific colleagues, institutions, or agencies that aided the efforts of the authors.

Conflict of interest

The authors declare that the research was conducted in the absence of any commercial or financial relationships that could be construed as a potential conflict of interest.

Publisher's note

Supplementary material

The Supplementary Material for this article can be found online at: https://www.frontiersin.org/articles/10.3389/fbioe.2022.1094968/full#supplementary-material

References

Accessories ElectroVet (2021). *LEROY biotech*. Available at: https://www.leroybiotech.com/electrovet-ez/accessories/ (Accessed November 12, 2021).

Adeyanju, O. O., Al-Angari, H. M., and Sahakian, A. v. (2012). The optimization of needle electrode number and placement for irreversible electroporation of hepatocellular carcinoma. *Radiol. Oncol.* 46, 126–135. doi:10.2478/v10019-012-0026-y

Adjustable Electrodes (2022). *EPSA series | IGEA medical*. Available at: https://www.igeamedical.com/en/electrochemotherapy/products/electrodes/adjustable-epsa-series (Accessed December 18, 2022).

Ahad, M. A., Narayanaswami, P., Kasselman, L. J., and Rutkove, S. B. (2010). The effect of subacute denervation on the electrical anisotropy of skeletal muscle: Implications for clinical diagnostic testing. *Clin. Neurophysiol.* 121, 882–886. doi:10.1016/j.clinph.2010.01.017

Al-Sakere, B., André, F., Bernat, C., Connault, E., Opolon, P., Davalos, R. v., et al. (2007). Tumor ablation with irreversible electroporation. *PLoS One* 2, e1135–e1138. doi:10.1371/journal.pone.0001135

Alkilani, A. Z., McCrudden, M. T. C., and Donnelly, R. F. (2015). Transdermal drug delivery: Innovative pharmaceutical developments based on disruption of the barrier properties of the stratum corneum. *Pharmaceutics* 7, 438–470. doi:10.3390/pharmaceutics7040438

Arab, H., Chioukh, L., Dashti Ardakani, M., Dufour, S., and Tatu, S. O. (2020). Early-stage detection of melanoma skin cancer using contactless millimeter-wave sensors. *IEEE Sens. J.* 20, 7310–7317. doi:10.1109/JSEN.2020.2969414

Arena, C. B., Sano, M. B., Rossmeisl, J. H., Caldwell, J. L., Garcia, P. A., Rylander, M. N., et al. (2011a). High-frequency irreversible electroporation (H-FIRE) for non-thermal ablation without muscle contraction. *Biomed. Eng. Online* 10, 102. doi:10.1186/1475-925X-10-102

Arena, C. B., Sano, M. B., Rossmeisl, J. H., Caldwell, J. L., Garcia, P. A., Rylander, M. N., et al. (2011b). High-frequency irreversible electroporation (H-FIRE) for non-thermal ablation without muscle contraction. *Biomed. Eng. Online* 10, 102. doi:10.1186/1475-925X-10-102

Asadi, M., Beik, J., Hashemian, R., Laurent, S., Farashahi, A., Mobini, M., et al. (2019). MRI-based numerical modeling strategy for simulation and treatment planning of nanoparticle-assisted photothermal therapy. *Phys. Medica* 66, 124–132. doi:10.1016/j.ejmp.2019.10.002

Aycock, K. N., and Davalos, R. v. (2019). Irreversible electroporation: Background, theory, and review of recent developments in clinical oncology. *Bioelectricity* 1, 214–234. doi:10.1089/bioe.2019.0029

Birgersson, U., Birgersson, E., Åberg, P., Nicander, I., and Ollmar, S. (2011). Non-invasive bioimpedance of intact skin: Mathematical modeling and experiments. *Physiol. Meas.* 32, 1–18. doi:10.1088/0967-3334/32/1/001

Blazevski, A., Scheltema, M. J., Amin, A., Thompson, J. E., Lawrentschuk, N., and Stricker, P. D. (2020). Irreversible electroporation (IRE): A narrative review of the development of IRE from the laboratory to a prostate cancer treatment. *BJU Int.* 125, 369–378. doi:10.1111/bju.14951

Bö, R. A., de Groot, B. L., Kakorin, S., Neumann, E., and Grubmü, H. (2020). *Kinetics, statistics, and energetics of lipid membrane electroporation studied by molecular dynamics simulations*. doi:10.1529/biophysj.108.129437

Boc, N., Edhemovic, I., Kos, B., Music, M. M., Brecelj, E., Trotovsek, B., et al. (2018). Ultrasonographic changes in the liver tumors as indicators of adequate tumor coverage with electric field for effective electrochemotherapy. *Radiol. Oncol.* 52, 383–391. doi:10.2478/raon-2018-0041

Brezar, S. K., Mrak, V., Bosnjak, M., Savarin, M., Sersa, G., and Cemazar, M. (2020). Intratumoral gene electrotransfer of plasmid DNA encoding shRNA against melanoma cell adhesion molecule radiosensitizes tumors by antivascular effects and activation of an immune response. *Vaccines (Basel)* 8, 135. doi:10.3390/vaccines8010135

Bulysheva, A., Hornef, J., Edelblute, C., Jiang, C., Schoenbach, K., Lundberg, C., et al. (2019). Coalesced thermal and electrotransfer mediated delivery of plasmid DNA to the skin. *Bioelectrochemistry* 125, 127–133. doi:10.1016/j.bioelechem.2018.10.004

Cadossi, R., Ronchetti, M., and Cadossi, M. (2014). Locally enhanced chemotherapy by electroporation: Clinical experiences and perspective of use of electrochemotherapy. *Future Oncol.* 10, 877–890. doi:10.2217/fon.13.235

Caliper Electrodes for Electroporation Applications (2022). *Caliper electrodes*. Available at: https://www.btxonline.com/caliper-electrodes.html (Accessed August 8, 2022).

Calvet, C. Y., and Mir, L. M. (2016). The promising alliance of anti-cancer electrochemotherapy with immunotherapy. *Cancer Metastasis Rev.* 35, 165–177. doi:10.1007/s10555-016-9615-3

Campana, L. G., Testori, A., Mozzillo, N., and Rossi, C. R. (2014). Treatment of metastatic melanoma with electrochemotherapy. *J. Surg. Oncol.* 109, 301–307. doi:10.1002/jso.23512

Cao, Y., Hayashi, C. T. H., Zavala, F., Tripathi, A. K., Simonyan, H., Young, C. N., et al. (2022). Effective functional immunogenicity of a DNA vaccine combination delivered via *in vivo* electroporation targeting malaria infection and transmission. *Vaccines (Basel)* 10 (7), 1–18. doi:10.3390/vaccines10071134

Cemazar, M., and Sersa, G. (2019). Recent advances in electrochemotherapy. *Bioelectricity* 1, 204–213. doi:10.1089/bioe.2019.0028

Cervia, L. D., and Yuan, F. (2018). Current progress in electrotransfection as a nonviral method for gene delivery. *Mol. Pharm.* 15, 3617–3624. doi:10.1021/acs.molpharmaceut.8b00207

Chen, X., Ren, Z., Zhu, T., Zhang, X., Peng, Z., Xie, H., et al. (2015). Electric ablation with irreversible electroporation (IRE) in vital hepatic structures and follow-up investigation. *Sci. Rep.* 5, 16233–16239. doi:10.1038/srep16233

Cheng, Y., and Fu, M. (2018). Dielectric properties for non-invasive detection of normal, benign, and malignant breast tissues using microwave theories. *Thorac. Cancer* 9, 459–465. doi:10.1111/1759-7714.12605

Choi, S. O., Kim, Y. C., Park, J. H., Hutcheson, J., Gill, H. S., Yoon, Y. K., et al. (2010). An electrically active microneedle array for electroporation. *Biomed. Microdevices* 12, 263–273. doi:10.1007/s10544-009-9381-x

Chumlea, W. C., and Guo, S. S. (1994). Bioelectrical impedance and body composition: Present status and future directions. *Nutr. Rev.* 52, 123–131. doi:10.1111/j.1753-4887.1994.tb01404.x

Coletti, L., Battaglia, V., de Simone, P., Turturici, L., Bartolozzi, C., and Filipponi, F. (2017). Safety and feasibility of electrochemotherapy in patients with unresectable colorectal liver metastases: A pilot study. *Int. J. Surg.* 44, 26–32. doi:10.1016/j.ijsu.2017.06.033

Čorović, S., al Sakere, B., Haddad, V., Miklavčič, D., and Mir, L. M. (2008). Importance of contact surface between electrodes and treated tissue in electrochemotherapy. *Technol. Cancer Res. Treat.* 7, 393–399. doi:10.1177/153303460800700507

Čorović, S., Mir, L. M., and Miklavčič, D. (2012). *In vivo* muscle electroporation threshold determination: Realistic numerical models and *in vivo* experiments. *J. Membr. Biol.* 245, 509–520. doi:10.1007/s00232-012-9432-8

Cvetkoska, A., Maček-Lebar, A., Trdina, P., Miklavčič, D., and Reberšek, M. (2022). Muscle contractions and pain sensation accompanying high-frequency electroporation pulses. *Sci. Rep.* 12, 1–15. doi:10.1038/s41598-022-12112-9

Cvetkoska, A., Piro, E., Reberšek, M., Magjarević, R., and Miklavčič, D. (2020). Towards standardization of electroporation devices and protocols. *IEEE Instrum. Meas. Mag.* 23, 74–81. doi:10.1109/MIM.2020.9062692

Daud, A. I., DeConti, R. C., Andrews, S., Urbas, P., Riker, A. I., Sondak, V. K., et al. (2008). Phase I trial of interleukin-12 plasmid electroporation in patients with metastatic melanoma. *J. Clin. Oncol.* 26, 5896–5903. doi:10.1200/JCO.2007.15.6794

Davalos, R. v., Mir, L. M., and Rubinsky, B. (2005). Tissue ablation with irreversible electroporation. *Ann. Biomed. Eng.* 33, 223–231. doi:10.1007/s10439-005-8981-8

de Santis, V., Chen, X. L., Laakso, I., and Hirata, A. (2015). An equivalent skin conductivity model for low-frequency magnetic field dosimetry. *Biomed. Phys. Eng. Express* 1, 015201. doi:10.1088/2057-1976/1/1/015201

Dermol-Černe, J., Pirc, E., and Miklavčič, D. (2020). "Mechanistic view of skin electroporation–models and dosimetry for successful applications: An expert review," in *Expert opinion on drug delivery* (Taylor and Francis Ltd.) Vol. 17 (5), 689–704. doi:10.1080/17425247.2020.1745772

Djokic, M., Cemazar, M., Popovic, P., Kos, B., Dezman, R., Bosnjak, M., et al. (2018a). Electrochemotherapy as treatment option for hepatocellular carcinoma, a prospective pilot study. *Eur. J. Surg. Oncol.* 44, 651–657. doi:10.1016/j.ejso.2018.01.090

Djokic, M., Cemazar, M., Popovic, P., Kos, B., Dezman, R., Bosnjak, M., et al. (2018b). Electrochemotherapy as treatment option for hepatocellular carcinoma, a prospective pilot study. *Eur. J. Surg. Oncol.* 44, 651–657. doi:10.1016/j.ejso.2018.01.090

Djokic, M., Dezman, R., Cemazar, M., Stabuc, M., Petric, M., Smid, L. M., et al. (2020). Percutaneous image guided electrochemotherapy of hepatocellular carcinoma: Technological advancement. *Radiol. Oncol.* 54, 347–352. doi:10.2478/raon-2020-0038

Dong, S., Wang, H., Zhao, Y., Sun, Y., and Yao, C. (2018). First human trial of high-frequency irreversible electroporation therapy for prostate cancer. *Technol. Cancer Res. Treat.* 17, 153303381878969–9. doi:10.1177/1533033818789692

Du, X., Wang, J., Zhou, Q., Zhang, L., Wang, S., Zhang, Z., et al. (2018). Advanced physical techniques for gene delivery based on membrane perforation. *Drug Deliv.* 25, 1516–1525. doi:10.1080/10717544.2018.1480674

Edelblute, C., Mangiamele, C., and Heller, R. (2021). Moderate heat-assisted gene electrotransfer as a potential delivery approach for protein replacement therapy through the skin. *Pharmaceutics* 13, 1908. doi:10.3390/pharmaceutics13111908

Edhemovic, I., Brecelj, E., Cemazar, M., Boc, N., Trotovsek, B., Djokic, M., et al. (2020). Intraoperative electrochemotherapy of colorectal liver metastases: A prospective phase II study. *Eur. J. Surg. Oncol.* 46, 1628–1633. doi:10.1016/j.ejso.2020.04.037

Edhemovic, I., Brecelj, E., Gasljevic, G., Marolt Music, M., Gorjup, V., Mali, B., et al. (2014). Intraoperative electrochemotherapy of colorectal liver metastases. *J. Surg. Oncol.* 110, 320–327. doi:10.1002/jso.23625

Eisele, R., Chopra, S., Glanemann, M., and Gebauer, B. (2014). Risk of local failure after ultrasound guided irreversible electroporation of malignant liver tumors. *Interv. Med. Appl. Sci.* 6, 147–153. doi:10.1556/IMAS.6.2014.4.2

Electrodes for *in vivo* electroporation (2021a). *Bex CO., ltd*. Available at: https://www.bexnet.co.jp/english/product/device/*in-vivo*/2.html (Accessed November 12, 2021a).

Electrodes for *in vivo* electroporation (2022b). *Bex CO., ltd*. Available at: https://www.bexnet.co.jp/english/product/device/*in-vivo*/2.html (Accessed July 20, 2022b).

Electrodes | 2022 *IGEA medical* Available at: https://www.igeamedical.com/en/electrochemotherapy/products/electrodes (Accessed March 1, 2022).

Ferioli, M., Lancellotta, V., Perrone, A. M., Arcelli, A., Galuppi, A., Strigari, L., et al. (2022). Electrochemotherapy of skin metastases from malignant melanoma: A PRISMA-compliant systematic review. *Clin. Exp. Metastasis* 39, 743–755. doi:10.1007/s10585-022-10180-9

Figini, M., Wang, X., Lyu, T., Su, Z., Procissi, D., Yaghmai, V., et al. (2017). Preclinical and clinical evaluation of the liver tumor irreversible electroporation by magnetic resonance imaging. *Am. J. Transl. Res.* 9, 580–590.

Fixed Electrodes (2022a). *EPS series | IGEA medical*. Available at: https://www.igeamedical.com/en/electrochemotherapy/products/electrodes/fixed-eps-series (Accessed July 7, 2022a).

Fixed Electrodes (2022b). *EPS series | IGEA medical*. Available at: https://www.igeamedical.com/en/electrochemotherapy/products/electrodes/fixed-eps-series (Accessed July 25, 2022b).

Forjanic, T., Markelc, B., Marcan, M., Bellard, E., Couillaud, F., Golzio, M., et al. (2019). Electroporation-Induced stress response and its effect on gene electrotransfer efficacy: *In vivo* imaging and numerical modeling. *IEEE Trans. Biomed. Eng.* 66, 2671–2683. doi:10.1109/TBME.2019.2894659

Freeman, S. A., Wang, M. A., and Weavert, J. C. (1994). Theory of electroporation of planar bilayer membranes: Predictions of the aqueous area, change in capacitance, and pore-pore separation. *Biophys. J.* 67, 42–56. doi:10.1016/s0006-3495(94)80453-9

Gabriel, C., Peyman, A., and Grant, E. H. (2009). Electrical conductivity of tissue at frequencies below 1 MHz. *Phys. Med. Biol.* 54, 4863–4878. doi:10.1088/0031-9155/54/16/002

Gabriel, S., Lau, R. W., and Gabriel, C. (1996). The dielectric properties of biological tissues: III. Parametric models for the dielectric spectrum of tissues. *Phys. Med. Biol.* 41, 2271–2293. doi:10.1088/0031-9155/41/11/003

Garcia, P. A., Davalos, R. v., and Miklavcic, D. (2014). A numerical investigation of the electric and thermal cell kill distributions in electroporation-based therapies in tissue. *PLoS One* 9, e103083. doi:10.1371/journal.pone.0103083

Gelker, M., Müller-Goymann, C. C., and Viöl, W. (2018). Permeabilization of human stratum corneum and full-thickness skin samples by a direct dielectric barrier discharge. *Clin. Plasma Med.* 9, 34–40. doi:10.1016/j.cpme.2018.02.001

Gerlini, G., Sestini, S., di Gennaro, P., Urso, C., Pimpinelli, N., and Borgognoni, L. (2013). Dendritic cells recruitment in melanoma metastasis treated by electrochemotherapy. *Clin. Exp. Metastasis* 30, 37–45. doi:10.1007/s10585-012-9505-1

Ghossein, R. (2010). Encapsulated malignant follicular cell-derived thyroid tumors. *Endocr. Pathol.* 21, 212–218. doi:10.1007/s12022-010-9141-8

Gilbert, R. A., Jaroszeski, M. J., and Heller, R. (1997). Novel electrode designs for electrochemotherapy. *Biochim. Biophys. Acta Gen. Subj.* 1334, 9–14. doi:10.1016/S0304-4165(96)00119-5

Glickman, Y. A., Filo, O., David, M., Yayon, A., Topaz, M., Zamir, B., et al. (2003). Electrical impedance scanning: A new approach to skin cancer diagnosis. *Skin Res. Technol.* 9, 262–268. doi:10.1034/j.1600-0846.2003.00022.x

Gothelf, A., and Gehl, J. (2012). What you always needed to know about electroporation based DNA vaccines. *Hum. Vaccin Immunother.* 8, 1694–1702. doi:10.4161/hv.22062

Granata, V., Fusco, R., D'alessio, V., Giannini, A., Venanzio Setola, S., Belli, A., et al. (2021). Electroporation-based treatments in minimally invasive percutaneous, laparoscopy and endoscopy procedures for treatment of deep-seated tumors. *Eur. Rev. Med. Pharmacol. Sci.* 25, 3536–3545. doi:10.26355/eurrev_202105_25836

Groselj, A., Bosnjak, M., Jesenko, T., Cemazar, M., Markelc, B., Strojan, P., et al. (2022). Treatment of skin tumors with intratumoral interleukin 12 gene electrotransfer in the head and neck region: A first-in-human clinical trial protocol. *Radiol. Oncol.* 56, 398–408. doi:10.2478/raon-2022-0021

Groselj, A., Kos, B., Cemazar, M., Urbancic, J., Kragelj, G., Bosnjak, M., et al. (2015). Coupling treatment planning with navigation system: A new technological approach in treatment of head and neck tumors by electrochemotherapy. *Biomed. Eng. Online* 14, S2–S14. doi:10.1186/1475-925X-14-S3-S2

Gun, L., Ning, D., and Liang, Z. (2017). Effective permittivity of biological tissue: Comparison of theoretical model and experiment. *Math. Probl. Eng.* 2017, 1–7. doi:10.1155/2017/7249672

Guo, S., Donate, A., Basu, G., Lundberg, C., Heller, L., and Heller, R. (2011). Electro-gene transfer to skin using a noninvasive multielectrode array. *J. Control. Release* 151, 256–262. doi:10.1016/j.jconrel.2011.01.014

Haemmerich, D., Schutt, D. J., Wright, A. W., Webster, J. G., and Mahvi, D. M. (2009). Electrical conductivity measurement of excised human metastatic liver tumours before and after thermal ablation. *Physiol. Meas.* 30, 459–466. doi:10.1088/0967-3334/30/5/003

Hayes, A. W., Thomas, J. A., and Gardner, D. E. (2022). *Series editors T oxicology of the*.

Heller, L. C., Jaroszeski, M. J., Coppola, D., Mccray, A. N., Hickey, J., and Heller, R. (2007). Optimization of cutaneous electrically mediated plasmid DNA delivery using novel electrode. *Gene Ther.* 14, 275–280. doi:10.1038/sj.gt.3302867

Heller, R., Cruz, Y., Heller, L. C., Gilbert, R. A., and Jaroszeski, M. J. (2010). Electrically mediated delivery of plasmid DNA to the skin, using a multielectrode array. *Hum. Gene Ther.* 21, 357–362. doi:10.1089/hum.2009.065

Heller, R., and Heller, L. C. (2015). *Gene electrotransfer clinical trials*. Elsevier. doi:10.1016/bs.adgen.2014.10.006

Hershkovich, H. S., Urman, N., Yesharim, O., Naveh, A., and Bomzon, Z. (2019). The dielectric properties of skin and their influence on the delivery of tumor treating fields to the torso: A study combining *in vivo* measurements with numerical simulations. *Phys. Med. Biol.* 64, 185014. doi:10.1088/1361-6560/ab33c6

Hsiao, C. Y., and Huang, K. W. (2017). Irreversible electroporation: A novel ultrasound-guided modality for non-thermal tumor ablation. *J. Med. Ultrasound* 25, 195–200. doi:10.1016/j.jmu.2017.08.003

Huang, D., Zhao, D., Wang, X., Li, C., Yang, T., Du, L., et al. (2018). Efficient delivery of nucleic acid molecules into skin by combined use of microneedle roller and flexible interdigitated electroporation array. *Theranostics* 8, 2361–2376. doi:10.7150/thno.23438

Huclova, S., Erni, D., and Fröhlich, J. (2012). Modelling and validation of dielectric properties of human skin in the MHz region focusing on skin layer morphology and material composition. *J. Phys. D. Appl. Phys.* 45, 025301. doi:10.1088/0022-3727/45/2/025301

Isobe, K., Shimizu, T., Nikaido, T., and Takaoka, K. (2004). Low-voltage electrochemotherapy with low-dose methotrexate enhances survival in mice with osteosarcoma. *Clin. Orthop. Relat. Res.* 426, 226–231. doi:10.1097/01.blo.0000138962.42433.db

Ivorra, A., Al-Sakere, B., Rubinsky, B., and Mir, L. M. (2009). *In vivo* electrical conductivity measurements during and after tumor electroporation: Conductivity changes reflect the treatment outcome. *Phys. Med. Biol.* 54, 5949–5963. doi:10.1088/0031-9155/54/19/019

Ivorra, A., Al-Sakere, B., Rubinsky, B., and Mir, L. M. (2008). Use of conductive gels for electric field homogenization increases the antitumor efficacy of electroporation therapies. *Phys. Med. Biol.* 53, 6605–6618. doi:10.1088/0031-9155/53/22/020

Izzo, F., Ionna, F., Granata, V., Albino, V., Patrone, R., Longo, F., et al. (2020). New deployable expandable electrodes in the electroporation treatment in a pig model: A feasibility and usability preliminary study. *Cancers (Basel)* 12, 515. doi:10.3390/cancers12020515

Jiang, C., Davalos, R. v., and Bischof, J. C. (2015). A review of basic to clinical studies of irreversible electroporation therapy. *IEEE Trans. Biomed. Eng.* 62, 4–20. doi:10.1109/TBME.2014.2367543

Kinosita, K., and Tsong, Y. (1977). Voltage-Induced pore formation and hemolysis of human erythrocytes. *Biochim. Biophys. Acta* 471, 227–242. doi:10.1016/0005-2736(77)90252-8

Kis, E. G., Baltás, E., Ócsai, H., Vass, A., Németh, I. B., Varga, E., et al. (2019). Electrochemotherapy in the treatment of locally advanced or recurrent eyelid-periocular basal cell carcinomas. *Sci. Rep.* 9, 4285–4287. doi:10.1038/s41598-019-41026-2

Kopcewicz, M., Walendzik, K., Bukowska, J., Kur-Piotrowska, A., Machcinska, S., Gimble, J. M., et al. (2020). Cutaneous wound healing in aged, high fat diet-induced obese female or male C57BL/6 mice. *Aging* 12, 7066–7111. doi:10.18632/aging.103064

Korohoda, W., Grys, M., and Madeja, Z. (2013). Reversible and irreversible electroporation of cell suspensions flowing through a localized DC electric field. *Cell. Mol. Biol. Lett.* 18, 102–119. doi:10.2478/s11658-012-0042-3

Kranjc, M., Kranjc, S., Bajd, F., Serša, G., Serša, I., and Miklavčič, D. (2017). Predicting irreversible electroporation-induced tissue damage by means of magnetic resonance electrical impedance tomography. *Sci. Rep.* 7, 1–10. doi:10.1038/s41598-017-10846-5

Kunte, C., Letulé, V., Gehl, J., Dahlstroem, K., Curatolo, P., Rotunno, R., et al. (2017). Electrochemotherapy in the treatment of metastatic malignant melanoma: A prospective cohort study by InspECT. *Br. J. Dermatology* 176, 1475–1485. doi:10.1111/bjd.15340

Langus, J., Kranjc, M., Kos, B., Šuštar, T., and Miklavčič, D. (2016). Dynamic finite-element model for efficient modelling of electric currents in electroporated tissue. *Sci. Rep.* 6, 26409. doi:10.1038/srep26409

Laufer, S., Ivorra, A., Reuter, V. E., Rubinsky, B., and Solomon, S. B. (2010). Electrical impedance characterization of normal and cancerous human hepatic tissue. *Physiol. Meas.* 31, 995–1009. doi:10.1088/0967-3334/31/7/009

Lee, E. W., Loh, C. T., and Kee, S. T. (2007). Imaging guided percutaneous irreversible electroporation: Ultrasound and immunohistological correlation. *Technol. Cancer Res. Treat.* 6, 287–293. doi:10.1177/153303460700600404

Lee, J. M., Choi, H. S., Chun, H. J., Kim, E. S., Keum, B., Seo, Y. S., et al. (2019). EUS-guided irreversible electroporation using endoscopic needle-electrode in porcine pancreas. *Surg. Endosc.* 33, 658–662. doi:10.1007/s00464-018-6425-4

Li, Q., Gao, X., Zhang, Y., Han, X., Li, Z., Zhang, Y., et al. (2021). Magnetic anchoring and guidance-assisted endoscopic irreversible electroporation for gastric mucosal ablation: A preclinical study in canine model. *Surg. Endosc.* 35, 5665–5674. doi:10.1007/s00464-020-08245-5

Li, S. (2008). *Electroporation protocols*.

Lladser, A., Ljungberg, K., Tufvesson, H., Tazzari, M., Roos, A. K., Quest, A. F. G., et al. (2010). Intradermal DNA electroporation induces survivin-specific CTLs, suppresses angiogenesis and confers protection against mouse melanoma. *Cancer Immunol. Immunother.* 59, 81–92. doi:10.1007/s00262-009-0725-4

Low-Frequency-Conductivity (2022). *Low frequency (conductivity) » IT'IS foundation*. Available at: https://itis.swiss/virtual-population/tissue-properties/database/low-frequency-conductivity/ (Accessed February 25, 2022).

Lu, F., Wang, C., Zhao, R., Du, L., Fang, Z., Guo, X., et al. (2018). Review of stratum corneum impedance measurement in non-invasive penetration application. *Biosens. (Basel)* 8, 31. doi:10.3390/bios8020031

Maiorano, N. A., and Mallamaci, A. (2009). *Neural Development Promotion of embryonic cortico-cerebral neuronogenesis by*. miR-124. doi:10.1186/1749-8104-4-40

Marčan, M., Pavliha, D., Kos, B., Forjanič, T., and Miklavčič, D. (2015). Web-based tool for visualization of electric field distribution in deep-seated body structures and planning of electroporation-based treatments. *Biomed. Eng. Online* 14, S4. doi:10.1186/1475-925X-14-S3-S4

Maruyama, H., Ataka, K., Higuchi, N., Sakamoto, F., Gejyo, F., and Miyazaki, J. (2001). Skin-targeted gene transfer using *in vivo* electroporation. *Gene Ther.* 8, 1808–1812. –1812Available at: doi:10.1038/sj.gt.3301604 www.nature.com/gt (Accessed November 12, 2021).

Matthiessen, L. W., Chalmers, R. L., Sainsbury, D. C. G., Veeramani, S., Kessell, G., Humphreys, A. C., et al. (2011). Management of cutaneous metastases using electrochemotherapy. *Acta Oncol. Madr.* 50, 621–629. doi:10.3109/0284186X.2011.573626

Matthiessen, L. W., Johannesen, H. H., Hendel, H. W., Moss, T., Kamby, C., and Gehl, J. (2012). Electrochemotherapy for large cutaneous recurrence of breast cancer: A phase II clinical trial. *Acta Oncol. Madr.* 51, 713–721. doi:10.3109/0284186X.2012.685524

Matthiessen, L. W., Keshtgar, M., Curatolo, P., Kunte, C., Grischke, E. M., Odili, J., et al. (2018). Electrochemotherapy for breast cancer—results from the INSPECT database. *Clin. Breast Cancer* 18, e909–e917. doi:10.1016/j.clbc.2018.03.007

Mazères, S., Sel, D., Golzio, M., Pucihar, G., Tamzali, Y., Miklavcic, D., et al. (2008). *Non invasive contact electrodes for* in vivo *localized cutaneous electropulsation and associated drug and nucleic acid delivery*. doi:10.1016/j.jconrel.2008.11.003

Mi, Y., Rui, S., Li, C., Yao, C., Xu, J., Bian, C., et al. (2017). Multi-parametric study of temperature and thermal damage of tumor exposed to high-frequency nanosecond-pulsed electric fields based on finite element simulation. *Med. Biol. Eng. Comput.* 55, 1109–1122. doi:10.1007/s11517-016-1589-3

Miklavčič, D., Beravs, K., Šemrov, D., Čemažar, M., Demšar, F., and Serša, G. (1998). The importance of electric field distribution for effective *in vivo* electroporation of tissues. *Biophys. J.* 74, 2152–2158. doi:10.1016/S0006-3495(98)77924-X

Miklavcic, D., Corovic, S., Pucihar, G., and Pavselj, N. (2006). Importance of tumour coverage by sufficiently high local electric field for effective electrochemotherapy. *Eur. J. Cancer* 4, 45–51. *Supplement* 4. doi:10.1016/j.ejcsup.2006.08.006

Miklavčič, D., Mali, B., Kos, B., Heller, R., and Serša, G. (2014). Electrochemotherapy: From the drawing board into medical practice. *Biomed. Eng. Online* 13, 29–20. doi:10.1186/1475-925X-13-29

Miklavčič, D., Pavšelj, N., and Hart, F. X. (2006). *Electric Properties of Tissues*. Wiley Encyclopedia of Biomedical Engineering, 1–12. doi:10.1002/9780471740360.ebs0403

Miklavcic, D., Snoj, M., Zupanic, A., Kos, B., Cemazar, M., Kropivnik, M., et al. (2010). Towards treatment planning and treatment of deep-seated solid tumors by electrochemotherapy. Available at: http://www.biomedical-engineering-online.com/content/9/1/10 (Accessed September 16, 2022).

Milevoj, N., Tratar, U. L., Nemec, A., Brožič, A., Žnidar, K., Serša, G., et al. (2019). A combination of electrochemotherapy, gene electrotransfer of plasmid encoding canine IL-12 and cytoreductive surgery in the treatment of canine oral malignant melanoma. *Res. Vet. Sci.* 122, 40–49. doi:10.1016/j.rvsc.2018.11.001

Monteiro-riviere, N. A., and Riviere, J. I. M. E. (1999). *C h a p t e r* 18.

Moreta-Martínez, R., Rubio-Pérez, I., García-Sevilla, M., García-Elcano, L., and Pascau, J. (2022). Evaluation of optical tracking and augmented reality for needle navigation in sacral nerve stimulation. *Comput. Methods Programs Biomed.* 224, 106991. doi:10.1016/j.cmpb.2022.106991

Nagy, J. A., DiDonato, C. J., Rutkove, S. B., and Sanchez, B. (2019). Permittivity of *ex vivo* healthy and diseased murine skeletal muscle from 10 kHz to 1 MHz. *Sci. Data* 6, 37. doi:10.1038/s41597-019-0045-2

Neal, R. E., II, Cheung, W., Kavnoudias, H., and Thomson, K. R. (2012). Spectrum of imaging and characteristics for liver tumors treated with irreversible electroporation. *J. Biomed. Sci. Eng.* 05, 813–818. doi:10.4236/jbise.2012.512a102

Neal, R. E., Millar, J. L., Kavnoudias, H., Royce, P., Rosenfeldt, F., Pham, A., et al. (2014). *In vivo* characterization and numerical simulation of prostate properties for non-thermal irreversible electroporation ablation. *Prostate* 74, 458–468. doi:10.1002/pros.22760

Neal, R. E., Singh, R., Hatcher, H. C., Kock, N. D., Torti, S. v., and Davalos, R. v. (2010). Treatment of breast cancer through the application of irreversible electroporation using a novel minimally invasive single needle electrode. *Breast Cancer Res. Treat.* 123, 295–301. doi:10.1007/s10549-010-0803-5

Needle Array Electrodes for BTX AgilePulse *In Vivo* (2021). *Needle array electrodes for BTX AgilePulse* in vivo. Available at: https://www.btxonline.com/needle-array-electrodes-for-agilepulse-in-vivo.html (Accessed November 12, 2021).

Novickij, V., Baleviciute, A., Malysko, V., Zelvys, A., Radzeviciute, E., Kos, B., et al. (2021). Effects of time delay between unipolar pulses in high frequency nano-electrochemotherapy. *IEEE Trans. Biomed. Eng.* 69, 1726–1732. doi:10.1109/TBME.2021.3129176

Novickij, V., Malyško, V., Želvys, A., Balevičiūte, A., Zinkevičiene, A., Novickij, J., et al. (2020). Electrochemotherapy using doxorubicin and nanosecond electric field pulses: A pilot *in vivo* study. *Molecules* 25, 4601. doi:10.3390/molecules25204601

O'Brien, T. J., Passeri, M., Lorenzo, M. F., Sulzer, J. K., Lyman, W. B., Swet, J. H., et al. (2019). Experimental high-frequency irreversible electroporation using a single-needle delivery approach for nonthermal pancreatic ablation *in vivo*. *J. Vasc. Interventional Radiology* 30, 854–862.e7. e7. doi:10.1016/j.jvir.2019.01.032

Partridge, B. R., O'Brien, T. J., Lorenzo, M. F., Coutermarsh-Ott, S. L., Barry, S. L., Stadler, K., et al. (2020). High-frequency irreversible electroporation for treatment of primary liver cancer: A proof-of-principle study in canine hepatocellular carcinoma. *J. Vasc. Interventional Radiology* 31, 482–491.e4. e4. doi:10.1016/j.jvir.2019.10.015

Pavliha, D., Kos, B., Županič, A., Marčan, M., Serša, G., and Miklavčič, D. (2012a). Patient-specific treatment planning of electrochemotherapy: Procedure design and possible pitfalls. *Bioelectrochemistry* 87, 265–273. doi:10.1016/j.bioelechem.2012.01.007

Pavliha, D., Kos, B., Županič, A., Marčan, M., Serša, G., and Miklavčič, D. (2012b). Patient-specific treatment planning of electrochemotherapy: Procedure design and possible pitfalls. *Bioelectrochemistry* 87, 265–273. doi:10.1016/j.bioelechem.2012.01.007

Pavšelj, N., and Miklavčič, D. (2008). Numerical modeling in electroporation-based biomedical applications. *Radiol. Oncol.* 42, 159–168. doi:10.2478/v10019-008-0008-2

Peyman, A., Holden, S., and Gabriel, C. (2005). Mobile telecommunications and health research programme: Dielectric properties of tissues at microwave frequencies. *Mob. Telecommun. Health Res. Programme*. Available at: http://www.mthr.org.uk/research_projects/documents/Rum3FinalReport.pdf.

Pichi, B., Pellini, R., de Virgilio, A., and Spriano, G. (2018). Electrochemotherapy: A well-accepted palliative treatment by patients with head and neck tumours. *Acta Otorhinolaryngol. Ital.* 38, 181–187. doi:10.14639/0392-100X-1262

Pintar, M., Langus, J., Edhemović, I., Brecelj, E., Kranjc, M., Sersa, G., et al. (2018). Time-dependent finite element analysis of *in vivo* electrochemotherapy treatment. *Technol. Cancer Res. Treat.* 17, 153303381879051–153303381879059. doi:10.1177/1533033818790510

Pliquett, U. F., Vanbever, R., Preat, V., and Weaver, J. C. (1998). Local transport regions (LTRs) in human stratum corneum due to long and short `high voltage' pulses. *Bioelectrochemistry Bioenergetics* 47, 151–161. doi:10.1016/S0302-4598(98)00180-9

Quaglino, P., Mortera, C., Osella-Abate, S., Barberis, M., Illengo, M., Rissone, M., et al. (2008). Electrochemotherapy with intravenous bleomycin in the local treatment of skin melanoma metastases. *Ann. Surg. Oncol.* 15, 2215–2222. doi:10.1245/s10434-008-9976-0

Raja, M. K., Raymer, G. H., Moran, G. R., Marsh, G., and Thompson, R. T. (2006). Changes in tissue water content measured with multiple-frequency bioimpedance and metabolism measured with31P-MRS during progressive forearm exercise. *J. Appl. Physiol.* 101, 1070–1075. doi:10.1152/japplphysiol.01322.2005

Ricotti, F., Giuliodori, K., Cataldi, I., Campanati, A., Ganzetti, G., Ricotti, G., et al. (2014). Electrochemotherapy: An effective local treatment of cutaneous and subcutaneous melanoma metastases. *Dermatol Ther.* 27, 148–152. doi:10.1111/dth.12098

Ritter, A., Bruners, P., Isfort, P., Barabasch, A., Pfeffer, J., Schmitz, J., et al. (2018). Electroporation of the liver: More than 2 concurrently active, curved electrodes allow new concepts for irreversible electroporation and electrochemotherapy. *Technol. Cancer Res. Treat.* 17, 153303381880999–8. doi:10.1177/1533033818809994

Roos, A. K., Eriksson, F., Walters, D. C., Pisa, P., and King, A. D. (2009). Optimization of skin electroporation in mice to increase tolerability of DNA vaccine delivery to patients. *Mol. Ther.* 17, 1637–1642. doi:10.1038/mt.2009.120

Roos, A. K., Moreno, S., Leder, C., Pavlenko, M., King, A., and Pisa, P. (2006). Enhancement of cellular immune response to a prostate cancer DNA vaccine by intradermal electroporation. *Mol. Ther.* 13, 320–327. doi:10.1016/j.ymthe.2005.08.005

Sachdev, S., Potočnik, T., Rems, L., and Miklavčič, D. (2022). Revisiting the role of pulsed electric fields in overcoming the barriers to *in vivo* gene electrotransfer. *Bioelectrochemistry* 144, 107994. doi:10.1016/j.bioelechem.2021.107994

Santamaría, L., Alonso, L., Ingelmo, I., Pozuelo, J. M., and Rodriguez, R. (2007). The human prostate. *Adv. Anat. Embryol. Cell. Biol.* 194, 2–11. doi:10.1007/978-3-540-69816-6_2

Sedlar, A., Dolinsek, T., Markelc, B., Prosen, L., Kranjc, S., Bosnjak, M., et al. (2012). Potentiation of electrochemotherapy by intramuscular IL-12 gene electrotransfer in murine sarcoma and carcinoma with different immunogenicity. *Radiol. Oncol.* 46, 302–311. doi:10.2478/v10019-012-0044-9

Sersa, G., Miklavcic, D., Cemazar, M., Rudolf, Z., Pucihar, G., and Snoj, M. (2008a). Electrochemotherapy in treatment of tumours. *Eur. J. Surg. Oncol.* 34, 232–240. doi:10.1016/j.ejso.2007.05.016

Sersa, G., Miklavcic, D., Cemazar, M., Rudolf, Z., Pucihar, G., and Snoj, M. (2008b). Electrochemotherapy in treatment of tumours. *Eur. J. Surg. Oncol.* 34, 232–240. doi:10.1016/j.ejso.2007.05.016

Shankayi, Z., and Firoozabadi, S. M. (2012). Antitumor efficiency of electrochemotherapy by high and low frequencies and repetitive therapy in the treatment of invasive ductal carcinoma in balb/c mice. *Cell. J.* 14, 110–115.

Shi, W., Shi, T., Chen, Z., Lin, J., Jia, X., Wang, J., et al. (2010). Generation of <italic>sp3111</italic> transgenic RNAi mice via permanent integration of small hairpin RNAs in repopulating spermatogonial cells <italic>*in vivo*</italic>. *Acta Biochim. Biophys. Sin. (Shanghai)* 42, 116–121. doi:10.1093/abbs/gmp110

Spanggaard, I., Snoj, M., Cavalcanti, A., Bouquet, C., Sersa, G., Robert, C., et al. (2013). Gene electrotransfer of plasmid antiangiogenic metargidin peptide (AMEP) in disseminated melanoma: Safety and efficacy results of a phase i first-in-man study. *Hum. Gene Ther. Clin. Dev.* 24, 99–107. doi:10.1089/humc.2012.240

Stillström, D., Nilsson, H., Jesse, M., Peterhans, M., Jonas, E., and Freedman, J. (2017). A new technique for minimally invasive irreversible electroporation of tumors in the head and body of the pancreas. *Surg. Endosc.* 31, 1982–1985. doi:10.1007/s00464-016-5173-6

Szlasa, W., Kiełbik, A., Szewczyk, A., Novickij, V., Tarek, M., Łapińska, Z., et al. (2021). Atorvastatin modulates the efficacy of electroporation and calcium electrochemotherapy. *Int. J. Mol. Sci.* 22, 11245. doi:10.3390/IJMS222011245

Tellado, M., Michinski, S., Impellizeri, J., Marshall, G., Signori, E., and Maglietti, F. (2022). Electrochemotherapy using thin-needle electrode improves recovery in feline nasal planum squamous cell carcinoma - a translational model. *Cancer Drug Resist.* 5, 595–611. doi:10.20517/cdr.2022.24

Tremble, L. F., O'Brien, M. A., Soden, D. M., and Forde, P. F. (2019). Electrochemotherapy with cisplatin increases survival and induces immunogenic responses in murine models of lung cancer and colorectal cancer. *Cancer Lett.* 442, 475–482. doi:10.1016/j.canlet.2018.11.015

Tsai, B., Xue, H., Birgersson, E., Ollmar, S., and Birgersson, U. (2019). Dielectrical properties of living epidermis and dermis in the frequency range from 1 kHz to 1 MHz. *J. Electr. Bioimpedance* 10, 14–23. doi:10.2478/joeb-2019-0003

Tweezertrodes Electrodes for *In Vivo* and In Utero Electroporation Applications (2022). *Tweezertrodes electrodes*. Available at: https://www.btxonline.com/tweezertrodes-electrodes.html (Accessed July 15, 2022).

Valdastri, P., Menciassi, A., Arena, A., Caccamo, C., and Dario, P. (2004). An implantable telemetry platform system for *in vivo* monitoring of physiological parameters. *IEEE Trans. Inf. Technol. Biomed.* 8, 271–278. doi:10.1109/TITB.2004.834389

van den Bos, W., de Bruin, D. M., Jurhill, R. R., Savci-Heijink, C. D., Muller, B. G., Varkarakis, I. M., et al. (2016). The correlation between the electrode configuration and histopathology of irreversible electroporation ablations in prostate cancer patients. *World J. Urol.* 34, 657–664. doi:10.1007/s00345-015-1661-x

Ventrelli, L., Marsilio Strambini, L., and Barillaro, G. (2015). Microneedles for transdermal biosensing: Current picture and future direction. *Adv. Healthc. Mater* 4, 2606–2640. doi:10.1002/adhm.201500450

Vižintin, A., Marković, S., Ščančar, J., and Miklavčič, D. (2021). Electroporation with nanosecond pulses and bleomycin or cisplatin results in efficient cell kill and low metal release from electrodes. *Bioelectrochemistry* 140, 107798. doi:10.1016/j.bioelechem.2021.107798

VOSviewer - Visualizing scientific landscapes (2020). Available at: https://www.vosviewer.com/ (Accessed Febrauary 21, 2022).

Wake, K., Sasaki, K., and Watanabe, S. (2016). Conductivities of epidermis, dermis, and subcutaneous tissue at intermediate frequencies. *Phys. Med. Biol.* 61, 4376–4389. doi:10.1088/0031-9155/61/12/4376

Wang, J. R., Sun, B. Y., Wang, H. X., Pang, S., Xu, X., and Sun, Q. (2014). Experimental study of dielectric properties of human lung tissue *in vitro*. *J. Med. Biol. Eng.* 34, 598–604. doi:10.5405/jmbe.1774

Wang, S., Zhang, C., Zhang, L., Li, J., Huang, Z., and Lu, S. (2008). The relative immunogenicity of DNA vaccines delivered by the intramuscular needle injection, electroporation and gene gun methods. *Vaccine* 26, 2100–2110. doi:10.1016/j.vaccine.2008.02.033

Wei, J. C. J., Edwards, G. A., Martin, D. J., Huang, H., Crichton, M. L., and Kendall, M. A. F. (2017). Allometric scaling of skin thickness, elasticity, viscoelasticity to mass for micro-

medical device translation: From mice, rats, rabbits, pigs to humans. *Sci. Rep.* 7, 15885–17. doi:10.1038/s41598-017-15830-7

Wei, Z., Huang, Y., Zhao, D., Hu, Z., Li, Z., and Liang, Z. (2015). A pliable electroporation patch (ep-Patch) for efficient delivery of nucleic acid molecules into animal tissues with irregular surface shapes. *Sci. Rep.* 5, 7618–9. doi:10.1038/srep07618

Weinert, R. L., and Ramos, A. (2021). Electroporation threshold, conductivity and memory effect in rat liver. *Biomed. Signal Process Control* 64, 102275. doi:10.1016/j.bspc.2020.102275

Xia, D., Jin, R., Byagathvalli, G., Yu, H., Ye, L., Lu, C. Y., et al. (2021). An ultra-low-cost electroporator with microneedle electrodes (ePatch) for SARS-CoV-2 vaccination. *Proc. Natl. Acad. Sci. U. S. A.* 118, e2110817118. doi:10.1073/pnas.2110817118

Yamamoto, T., and Yamamoto, Y. (1976). Dielectric constant and resistivity of epidermal stratum corneum. *Med. Biol. Eng.* 14, 494–500. doi:10.1007/BF02478045

Yamazaki, N., Watanabe, H., Lu, X., Isobe, Y., Kobayashi, Y., Miyashita, T., et al. (2013). The relation between temperature distribution for lung RFA and electromagnetic wave frequency dependence of electrical conductivity with changing a lung's internal air volumes. *Proc. Annu. Int. Conf. IEEE Eng. Med. Biol. Soc. EMBS* 2013, 386–391. –391. doi:10.1109/EMBC.2013.6609518

Yan, K., Todo, H., and Sugibayashi, K. (2010). Transdermal drug delivery by in-skin electroporation using a microneedle array. *Int. J. Pharm.* 397, 77–83. doi:10.1016/j.ijpharm.2010.06.052

Yang, T., Huang, D., Li, C., Zhao, D., Li, J., Zhang, M., et al. (2021). Rolling microneedle electrode array (RoMEA) empowered nucleic acid delivery and cancer immunotherapy. *Nano Today* 36, 101017. doi:10.1016/j.nantod.2020.101017

Yao, C., Dong, S., Zhao, Y., Lv, Y., Liu, H., Gong, L., et al. (2017). Bipolar microsecond pulses and insulated needle electrodes for reducing muscle contractions during irreversible electroporation. *IEEE Trans. Biomed. Eng.* 64, 2924–2937. doi:10.1109/TBME.2017.2690624

Zager, Y., Kain, D., Landa, N., Leor, J., and Maor, E. (2016). Optimization of irreversible electroporation protocols for *in-vivo* myocardial decellularization. *PLoS One* 11, e0165475–15. doi:10.1371/journal.pone.0165475

Zhang, L., Getz, S. A., and Bordey, A. (2022). Dual *in utero* electroporation in mice to manipulate two specific neuronal populations in the developing cortex. *Front. Bioeng. Biotechnol.* 9, 814638–9. doi:10.3389/fbioe.2021.814638

Zhang, X., and He, B. (2010). Imaging electric properties of human brain tissues by B1 mapping: A simulation study. *J. Phys. Conf. Ser.* 224, 012077–481. doi:10.1088/1742-6596/224/1/012077

Zupanic, A., Kos, B., and Miklavcic, D. (2012). Treatment planning of electroporation-based medical interventions: Electrochemotherapy, gene electrotransfer and irreversible electroporation. *Phys. Med. Biol.* 57, 5425–5440. doi:10.1088/0031-9155/57/17/5425

frontiers | Frontiers in Bioengineering and Biotechnology

TYPE Original Research
PUBLISHED 10 February 2023
DOI 10.3389/fbioe.2023.1073238

OPEN ACCESS

EDITED BY
Yuan Xiong,
Huazhong University of Science and Technology, China

REVIEWED BY
Glyn Palmer,
University of Florida, United States
Yiqiang Hu,
Huazhong University of Science and Technology, China

*CORRESPONDENCE
Bin Li,
binleechn@126.com
Xigao Cheng,
ndefy12160@ncu.edu.cn

SPECIALTY SECTION
This article was submitted to Preclinical Cell and Gene Therapy, a section of the journal Frontiers in Bioengineering and Biotechnology

RECEIVED 18 October 2022
ACCEPTED 03 February 2023
PUBLISHED 10 February 2023

CITATION
Chen Q, Yang Q, Pan C, Ding R, Wu T, Cao J, Wu H, Zhao X, Li B and Cheng X (2023), Quiescence preconditioned nucleus pulposus stem cells alleviate intervertebral disc degeneration by enhancing cell survival *via* adaptive metabolism pattern in rats.
Front. Bioeng. Biotechnol. 11:1073238.
doi: 10.3389/fbioe.2023.1073238

Quiescence preconditioned nucleus pulposus stem cells alleviate intervertebral disc degeneration by enhancing cell survival *via* adaptive metabolism pattern in rats

Qi Chen[1,2,3,4], Qu Yang[2], Chongzhi Pan[1,2,3], Rui Ding[1,2,4], Tianlong Wu[1,2,3], Jian Cao[1,3], Hui Wu[1,3], Xiaokun Zhao[1,4], Bin Li[1,2,3]* and Xigao Cheng[1,2,3,4]*

[1]Department of Orthopedics, The Second Affiliated Hospital of Nanchang University, Nanchang, Jiangxi, China, [2]Second Clinical Medical College, Nanchang University, Nanchang, Jiangxi, China, [3]Institute of Orthopedics of Jiangxi Province, Nanchang, Jiangxi, China, [4]Institute of Minimally Invasive Orthopedics, Nanchang University, Nanchang, Jiangxi, China

Quiescence is a cellular state of reversible growth arrest required to maintain homeostasis and self-renewal. Entering quiescence allows the cells to remain in the non-dividing stage for an extended period of time and enact mechanisms to protect themselves from damage. Due to the extreme nutrient-deficient microenvironment in the intervertebral disc (IVD), the therapeutic effect of cell transplantation is limited. In this study, nucleus pulposus stem cells (NPSCs) were preconditioned into quiescence through serum starvation *in vitro* and transplanted to repair intervertebral disc degeneration (IDD). *In vitro*, we investigated apoptosis and survival of quiescent NPSCs in a glucose-free medium without fetal bovine serum. Non-preconditioned proliferating NPSCs served as controls. *In vivo*, the cells were transplanted into a rat model of IDD induced by acupuncture, and the intervertebral disc height, histological changes, and extracellular matrix synthesis were observed. Finally, to elucidate the mechanisms underlying the quiescent state of NPSCs, the metabolic patterns of the cells were investigated through metabolomics. The results revealed that quiescent NPSCs decreased apoptosis and increased cell survival when compared to proliferating NPSCs both *in vitro* and *in vivo*, as well as maintained the disc height and histological structure significantly better than that by proliferating NPSCs. Furthermore, quiescent NPSCs have generally downregulated metabolism and reduced energy requirements in response to a switch to a nutrient-deficient environment. These findings support that quiescence preconditioning maintains the proliferation and biological function potential of NPSCs, increases cell survival under the extreme environment of IVD, and further alleviates IDD *via* adaptive metabolic patterns.

KEYWORDS

intervertebral disc degeneration, nucleus pulposus stem cells, quiescence, cell survival, cell metabolism

1 Introduction

Intervertebral disc degeneration (IDD) is a primary cause of lower back pain and disability, which directly affects the quality of life and work efficiency of the individual, causing a serious social burden (Jin et al., 2020; Chou, 2021; Costăchescu et al., 2022). Serious disc degeneration can lead to a series of degenerative clinical syndromes, such as lumbar disc herniation, spinal stenosis, and spinal instability, which are predominantly treated by surgical methods (Zhao et al., 2019; Wu et al., 2020). Nevertheless, traditional surgery can only decrease the clinical symptoms of IDD but cannot fundamentally correct the degeneration of the disc. Therefore, cell biotherapy for intervertebral disc (IVD) repair has become a research focus in the past decade.

To the best of our knowledge, only few active cells are present in the disc, and the number and function of cells are further decreased during disc degeneration (Roberts et al., 2006; Ma et al., 2019). Therefore, replenishing the functional cells is the most direct approach to restoring disc homeostasis (Sakai and Grad, 2015; Tong et al., 2017). Presently, multiple cell types have been evaluated *in vitro* and *in vivo* and are being used for intradiscal transplantation. Cells used for transplantation include nucleus pulposus cells (NPCs), nucleus pulposus stem cells (NPSCs), and stem cells from other sources (Chen et al., 2016; Kumar et al., 2017; Wang et al., 2018; Ekram et al., 2021; Li et al., 2021). NPSCs are one of the most ideal seed cells because they are derived from NP, which have a phenotype similar to the IVD cells with good proliferative ability (Hu et al., 2018; Du et al., 2021). Nevertheless, how the cells maintain efficient survival after transplanting into the disc is unknown (Sakai and Grad, 2015; Tong et al., 2017). Because the IVD is an avascular organ, the microenvironment of its inner cells is characterized by poor blood supply and nutrient deficiency (ND), and the blood supply is further diminished during the process of IDD (Urban et al., 2004; Roberts et al., 2006; Ma et al., 2019). Therefore, transplanted cells are difficult to keep alive. Consequently, the transplanted cells must first survive in the extreme environment of IVD with poor nutrition and blood supply for cell therapy (Sakai and Grad, 2015; Tong et al., 2017; Yuan et al., 2020; Binch et al., 2021). Moreover, these transplanted cells should maintain favorable bioactivity to produce an extracellular matrix rich in proteoglycan and collagen under the harsh disc environment (Zhang et al., 2019). To conclude, maintaining the survival and biological function of transplanted cells in the harsh degenerated disc microenvironment is important.

Many previous studies have shown that adult stem cells are present in a quiescent state *in vivo*. Quiescence is a state of reversible growth arrest wherein the cells exit the cell cycle and enter the G0 phase, albeit retaining their capacity to divide (Cho et al., 2019; Marescal and Cheeseman, 2020). Once quiescent cells receive activation signals, they can promptly re-enter the cell cycle to start the S-phase and resume proliferation, thereby re-performing biological functions (Rodgers et al., 2014; Goel et al., 2017; Urban and Cheung, 2021). These properties make quiescence play an important role in maintaining stem cell stemness and tissue homeostasis. Research has indicated that stem cells can be induced into quiescence by serum starvation or contact inhibition *in vitro*. Quiescent stem cells can strengthen stemness, resist stress reactions, and improve the tissue repair effect (Wong et al., 2017; Alekseenko et al., 2018; Rumman et al., 2018). Moreover, basal metabolic activity, biosynthesis, and energy requirements are significantly decreased in quiescent stem cells, which favors the adaptive survival of transplanted cells in adverse environments (Ho et al., 2017; Moya et al., 2017; Ferro et al., 2019). Accordingly, we hypothesized that quiescence preconditioning of NPSCs can increase the tolerance of the cells in response to the extreme environment of the degenerated disc after transplantation. We have confirmed the existence of quiescence in NPSCs by serum starvation previously *in vitro* and showed that quiescent NPSCs (Q-NPSCs) can maintain regenerative capacity (Li et al., 2019). Nevertheless, it is unknown whether Q-NPSCs can maintain survival and function under the ND environment for disc repair.

In the present study, we investigated the characteristics of Q-NPSCs and the survival of the cells under the ND condition *in vitro*, and then determined the therapeutic effect of the cells in a rat model of IDD. We also studied the metabolic characteristics of Q-NPSCs through metabolomic analysis and elucidated the potential mechanism of the cells in maintaining homeostasis.

2 Materials and methods

2.1 Isolation and culture of primary rat NPSCs

All animal experiments in this study were approved by the Animal Care and Use Committee of Nanchang University (China) and followed by the Guide for the Care and Use of Laboratory Animals by the National Institutes of Health (NIH). Animals were bred in a natural ventilated room with a dark/light cycle at 20°C–25°C, at *ad libitum* access to water and food.

Primary rat NPSCs were isolated using a low-density culture method, as reported elsewhere (Zhao et al., 2017; Wang et al., 2019; Li et al., 2020). In brief, SD rats were sacrificed by cervical dislocation after inhaling an overdose of isoflurane, and then caudal disc specimens were collected. The NP tissues were separated from the rat coccygeal IVD and washed twice with PBS under sterile conditions. Then, the tissues were digested with 0.2% collagenase type II (Sigma, United States) solution at 37°C for 2 h. After centrifugation at 1000 rpm for 5 min, the cell pellets were cultured in Dulbecco's Modified Eagle Medium/Nutrient Mixture F-12 (DMEM/F12, Gibco, United States) medium supplemented with 10% fetal bovine serum (FBS) and 1% penicillin–streptomycin combination at 37°C under a 5% CO_2 atmosphere. The medium was changed twice a week until sufficient cell colonies were observed, and the cells were digested with 0.25% trypsin-EDTA solution (Gibco) for subculturing. Finally, NPSCs up to the third passage were applied for subsequent experiments.

2.2 Identification of the differentiation capacity of rat NPSCs

The osteogenic, chondrogenic, and adipogenic differentiation capacities of NPSCs were determined by Alizarin red staining, Alcian blue staining, and Oil Red O staining, following the manufacturer's instructions (Cyagen, Guangzhou, China) and the

methods of the previous study (Li et al., 2019). The osteogenic differentiation of NPSCs was induced with osteogenic differentiation medium (RASMX-90021, Cyagen) containing 10% FBS, 1% penicillin-streptomycin, 1% glutamine, 1% β-glycerophosphate, 0.2% ascorbate and 0.01% dexamethasone. After 3 weeks, Alizarin red staining was used to identify mineral deposits. The cells were fixed at room temperature with 4% paraformaldehyde (PFA) for 30 min, and then stained with an Alizarin Red solution for 10 min at room temperature. Then, the cells were washed with PBS and observed microscopically.

Chondrogenic differentiation was induced by a high-density method (Iezaki et al., 2019). NPSCs were suspended to a cell density of 1×10^7 cells per ml. 10 μl were dripped into a the 6-well plate and placed in the incubator for 1.5 h. After that, chondrogenic medium (RASMX-90042, Cyagen) was added for culture, taking care not to destroy the droplet. The medium was changed every 2 days until the sixth day. The cells were fixed with 4% PFA for 10 min, washed twice using PBS, and incubated in Alcian Blue solution for 2 h. Then, the cultures were washed again with PBS and observed by optical microscope.

Adipogenic differentiation was induced with adipogenic medium (RASMX-90031, Cyagen), including induction medium A (containing 10% FBS, 1% penicillin-streptomycin, 1% L-glutamine, 0.2% insulin, 0.1% 3-Isobutyl-1-methylxanthine, 0.1% rosiglitazone and 0.1% dexamethasone) and maintenance medium B (containing 10% FBS, 1% penicillin-streptomycin, 1% L-glutamine and 0.2% insulin). The NPSCs were induced with solution A for 3 days and solution B for 1 day, alternating until lipid-rich droplets appeared. The cells were fixed and then stained with Oil Red O solution for 30 min. After washing with PBS, the culture plates were placed under a microscope for observation.

2.3 Identification of stem cell surface markers

The stem cell specific markers CD73, CD90, CD105, CD34, CD45, and HLA-DR were analyzed by flow cytometry. Briefly, rat NPSCs were digested with 0.25% trypsin and collected. The cells were centrifuged at 300 *g* for 5 min, washed twice with PBS, and finally resuspended in 0.1 ml of PBS. The samples were incubated at room temperature with primary antibodies CD73-PE (Bs-4834R, Bioss, Beijing, China), CD90-PE (Bs-0778R, Bioss), CD105-APC (67075-1-lg, Proteintech, Wuhan, China), CD34-FITC (Bs-0646R, Bioss), CD45-FITC (Bs-4819, Bioss), and HLA-DR-APC (Bs-1198R, Bioss) for 30 min, washed twice with PBS, and then incubated in the dark with secondary antibodies for 30 min After being washed again twice with PBS, they were detected by flow cytometry.

2.4 Induction of quiescence and reactivation in NPSCs

NPSCs (2×10^5) were seeded in a 25-cm^2 cell-culture flask and cultured in a standard medium (DMEM/F12 supplemented with 10% FBS). After 24 h, the cells were used as proliferating NPSCs (P-NPSCs). At this time point, another group of NPSCs were rinsed with PBS and cultured in a low-serum medium (DMEM/F12 supplemented with 0.1% FBS) for 48 h to induce quiescence, as quiescent NPSCs (Q-NPSCs). Next, the medium was changed every 3 days with a low-serum medium, and, on day 7, with the standard medium in order to stimulate the cells. After 24 h, the cells were used as reactivated NPSCs (Re-NPSCs).

2.5 Nutrient-deficient culture conditions

In vitro, the degenerative disc microenvironment was simulated by culturing cells in a glucose-free DMEM without FBS, which was defined as the nutrient deficiency (ND) condition (Liu et al., 2017; Wang et al., 2020). The cell experiments were divided into four groups based on the participating cell types: P-NPSCs (proliferating NPSCs), P-ND-NPSCs (proliferating NPSCs cultured under ND), Q-NPSCs (quiescent NPSCs), and Q-ND-NPSCs (quiescent NPSCs cultured under ND). Quiescent cells were prepared 2 days in advance (Day-2), and the proliferating cells were prepared 1 day in advance (Day-1). On Day 0, the medium for both P-ND and Q-ND was replaced with a glucose-free DMEM without FBS and subsequently cultured without any medium change.

2.6 Cell cycle analysis

The cell cycle of NPSCs was detected by flow cytometry. Briefly, the samples were digested with 0.25% trypsin, collected, and then washed twice with PBS. Then, the cells were fixed in precooled 75% ethanol and stored at −20°C until further use. To analyze the cell cycle, the fixed cells were centrifuged and the ethanol was discarded. Then, the cells were hydrated with PBS for 15 min, and the supernatant was discarded after centrifugation. Then, 1 mL of the DNA staining solution (Multi Sciences, Hangzhou, China) was added and mixed well. The stained cells were incubated in the dark at room temperature for 30 min, followed by flow cytometry analysis.

2.7 Immunofluorescence

The cell slides prepared earlier were fixed in 4% paraformaldehyde for 15 min and then permeated with 0.5% Triton X-100 for another 15 min at room temperature. The cells were then blocked with 10% goat serum for 30 min and incubated with a primary antibody at 4°C overnight. Then, the cells were treated with secondary antibodies in the dark at room temperature for 1 h and counter-stained with DAPI for 5 min. After sealing the slices, the images were observed by fluorescence microscopy and subjected to semi-quantitative analysis using ImageJ.

2.8 Cell proliferation, apoptosis, and survival analysis

The Cell Counting Kit-8 (CCK-8; Solarbio, Beijing) was used to detect the cell viability of NPSCs. In accordance with the above-mentioned methods, NPSCs were seeded into a 96-well plate at the density of 5000 cells/well, and 100 μl of the medium was added to each well. For detection purpose, 10 μl of the CCK-8 solution was added to each well and incubated for 3 h. The optical density (OD) at 450 nm was measured using an enzyme-labeled instrument.

TABLE 1 The histological grading of the disc degeneration.

Cellularity and morphology	Grade
Cellularity of the annulus fibrosus	1. Fibroblasts comprise more than 75% of the cells
	2. Neither fibroblasts nor chondrocytes comprise more than 75% of the cells
	3. Chondrocytes comprise more than 75% of the cells
Morphology of the annulus fibrosus	1. Well-organized collagen lamellae without ruptured or serpentine fibers
	2. Inward bulging, ruptured or serpentine fibers in less than one-third of the annulus
	3. Inward bulging, ruptured or serpentine fibers in more than one-third of the annulus
Border between the annulus fibrosus and nucleus pulposus	1. Normal, without any interruption
	2. Minimal interruption
	3. Moderate or severe interruption
Cellularity of the nucleus pulposus	1. Normal cellularity with stellar-shaped nuclear cells evenly distributed throughout the nucleus
	2. Slight decrease in the number of cells with some clustering
	3. Moderate or severe decrease (>50%) in the number of cells with all the remaining cells clustered and separated by dense areas of proteoglycans
Morphology of the nucleus pulposus	1. Round, comprising at least half of the disc area in mid-sagittal sections
	2. Rounded or irregularly shaped, comprising one-quarter to half of the disc area in mid-sagittal sections
	3. Irregularly shaped, comprising less than one-quarter of the disc area in mid-sagittal sections

The apoptosis of NPSCs was detected using the FITC-Annexin V/PI Kit (UE, Suzhou, China). First, the cells were digested with EDTA-free trypsin solution and then centrifuged, followed by washing twice with pre-cooled PBS. The resultant cells were collected and resuspended with 100 µl of 1× binding buffer, followed by the addition of 5 µl FITC-Annexin V (AV) and 5 µl PI working solution. In addition, AV and PI single-stained cells were prepared for flow compensation regulation. After incubation at room temperature for 15 min, the samples were analyzed by flow cytometry.

The Hoechst 33342/PI Staining Kit (Solarbio) was used to label the living and dead cells. According to the manufacturer's instruction, the cells were treated with a staining buffer and dyed at 4°C for 30 min in the dark. Finally, the images were observed using a fluorescence microscope. Hoechst 33342-positive and PI-negative cells were designated as viable cells, whereas Hoechst 33342-positive and PI-positive cells were designated as dead cells.

Cell survival was determined by performing the Trypan Blue Exclusion Dye assay. Briefly, the cells were digested with trypsin and centrifuged at 1000 rpm for 1 min, and the supernatant was discarded and resuspended in 900 µl of PBS. Then, 100 µl of 0.4% trypan blue (Gibco) solution was added, mixed, and stained for 3 min. A small amount of the cell suspension was absorbed and counted in a blood cell-counting plate. The dead cells were stained blue, while the living cells were unstained. The cell survival rate was expressed as the percentage of viable cells relative to total cells at each time point. In addition, the NPSCs were stained with hematoxylin eosin (HE) dye and observed under a microscope.

2.9 Cell retention study in isolated intervertebral discs

To investigate the survival of NPSCs after implantation into the disc. We constructed a rat IVD organ culture model (Wu et al., 2019; Liao et al., 2021). The tail disc with an intact endplate was isolated from 3-month-old SD rats (300 g) and cultured in DMEM/F12 medium supplemented with 15% FBS and 1% penicillin/streptomycin at 37°C. A solution of 1.5 M NaCl and 0.4 M KCl was added to adjust the osmotic pressure of the medium to 400 mOsm, which is similar to the physiological conditions. NPSCs with a positive GFP expression from GFP transgenic SD rats (donated by Xinqiao Hospital) were employed for tracing. The cell suspension (2 µl) containing 1×10^4 P-NPSCs(GFP+) or Q-NPSCs(GFP+) cells was slowly injected into the disc using a 31G needle, and the injection was kept inserted at the site for about 5 min to prevent any leakage. The culture medium was replaced every 3 days. At each time point, the cultured discs were observed using an animal imaging system (AniView600, BLT, Guangzhou, China), and the fluorescence intensity of each membrane was subsequently quantified.

2.10 Rat IDD model induction and NPSCs implantation

Following anesthesia, the tail was disinfected with iodophor, and a 21G-puncture needle was used to puncture different levels of the tail IVD at a depth of 5 mm. The needle was inserted into the center of the nucleus pulposus through the annulus fibrosus and rotated by 360° and maintained for 30 s. After 2 weeks, the caudal discs of different levels were divided into four groups: Control (not punctured), P-NPSCs (punctured and injected with P-NPSCs(GFP+)), Q-NPSCs (punctured and injected with Q-NPSCs(GFP+), and PBS (punctured and injected with PBS) groups. The injection protocol was performed as described in Section 2.9. The segments were injected with 2 µl cell suspension (containing 1×10^4 cells) or 2 µl PBS.

2.11 Radiographic analysis

X-ray were taken to assess the disc height at 0, 2 and 4 weeks after cell injection. Briefly, the animal was placed in the prone position with the tail straight and the ray perpendicular to the tail. The disc height index (DHI) was calculated according to the method described by Han et al. (Han et al., 2008) to evaluate the disc height. Changes in DHI were normalized to the preoperatively measured

TABLE 2 Primes sequences.

Gene	Forward primer	Reverse primer	Id
PCNA	GCCCTCAAAGACCTCATCAAT	ATCAGCATTATCTTCAGCCCTTA	NM_022381.3
Ki67	CCATTAACAAGAGTGAGGGAGTG	TGAGTGGAGTATTAGGAGGCAAG	XM_006230453.2
Sox9	CACATCTCTCCTAACGCCATCT	GCGGCAGGTATTGGTCAAACTC	NM_080403.2
Acan	AGTGACCCATCTGCTTACCCTG	CTGCATCTATGTCGGAGGTAGTG	XM_039101034.1
Col2a1	GTGTCAAGGGTCACAGAGGTTAC	CGCTCTCACCCTTCACACCT	NM_012929.1
GAPDH	CTGGAGAAACCTGCCAAGTATG	GGTGGAAGAATGGGAGTTGCT	NM_017008.4

DHI and expressed as %DHI (= measured DHI/before acupuncture DHI × 100). All images were measured by three independent observers who were blinded to the experimental design.

2.12 Histological analysis

Two weeks after the cell transplantation, the rats were sacrificed and their caudal disc tissues were assessed. These tissues were fixed in 4% paraformaldehyde, decalcified, and embedded in paraffin. For the immunohistochemistry analysis, the sections were incubated with Collagen-II (1:200, 28459-1-AP, Proteintech) or Aggrecan (1: 200, 13880-1-AP, Proteintech) antibodies. On the other hand, the sections were stained with hematoxylin–eosin (HE), saffron O-fast green (SO), and toluidine blue (TB). The images were then observed under the microscope (Olympus, Tokyo, Japan). The degree of disc degeneration was assessed based on the historical grading of the disc degeneration (Table 1) (Zhou et al., 2018). The control, Q-NPCSs, P-NPSCs and PBS groups each contained six samples and were scored by three independent observers.

2.13 Real-time quantitative PCR

Total RNA was extracted from the cells with TRIzol reagent (Invitrogen, United States) and transcribed into cDNA using a reverse transcription kit (Takara, Japan), which was amplified by using the SYBR Green Master Mix (Takara). Then, the mRNA expression levels of PCNA, Ki67, Sox9, Acan, and Col2a1 were detected by using the Real-time ABI 7900 HT System (Applied Biosystems, CA, United States), using GAPDH as the internal reference. The results of the experiment were calculated using the $2^{-\Delta\Delta CT}$ method. The primers are listed in Table 2.

2.14 Metabolomics analysis

To detect the differences in the metabolic patterns between P-NPSCs and Q-NPSCs, the cells were collected (four samples from each group), and it was ensured that the number of cells in each sample was not less than 1×10^6. The cells were centrifuged and the supernatant was discarded. Then, the wet pellets were flash-frozen under liquid nitrogen for 30 s and then transferred to −80°C for storage until use. Widely targeted/non-target metabolomics experiment was performed at the Biomarker Technologies (Beijing, China) using the following process: after further treatment of the sample with methanol and acetonitrile, metabolomic analysis was performed by using an LC/MS system consisting of Waters Acquity I-class PLUS ultra-high-performance liquid chromatography tandem equipped with the Waters Xevo G2-XS QTOF high-resolution mass spectrometer. The raw data collected using MassLynx V4.2 was processed by the Progenesis QI software for peak extraction, peak alignment, and other data processing operations. The identified compounds were searched for classification and pathway information in the KEGG, HMDB, and lipidmaps databases. According to the grouping information, the difference multiples were calculated and compared, and *t*-test was applied to calculate the difference significance *p*-value of each compound. The R language package ropls was used to perform the orthogonal partial least squares discriminant analysis (OPLS-DA) modeling, and 200-times permutation tests was performed to verify the reliability of the model. The VIP (Variable Importance in Projection) value of the model was calculated through multiple cross-validation to measure the effect of each metabolite expression pattern on the classification of each sample, thus assisting the filtrated metabolites. The method of combining the difference multiple, the *p*-value, and the VIP value of the OPLS-DA model was adopted to screen the differential metabolites. The screening criteria were FC > *p*-value <0.05 and VIP >1. The difference metabolites of the KEGG pathway enrichment significance were calculated using the hypergeometric distribution test.

2.15 Statistical analysis

All experiments were performed in triplicate. The mean ± standard deviation (SD) was applied to present the data. Graphics and statistical analyses were conducted by GraphPad Prism eight software. Student's t-test for two groups and one-way ANOVA with Tukey *post hoc* test for three or more groups were used for group comparisons. $p < 0.05$ was considered to indicate statistical significance.

3 Results

3.1 Characterization of NPSCs

After three passages, the cells were purified; they exhibited a long spindle shape with a uniform morphology and whirlpool arrangement

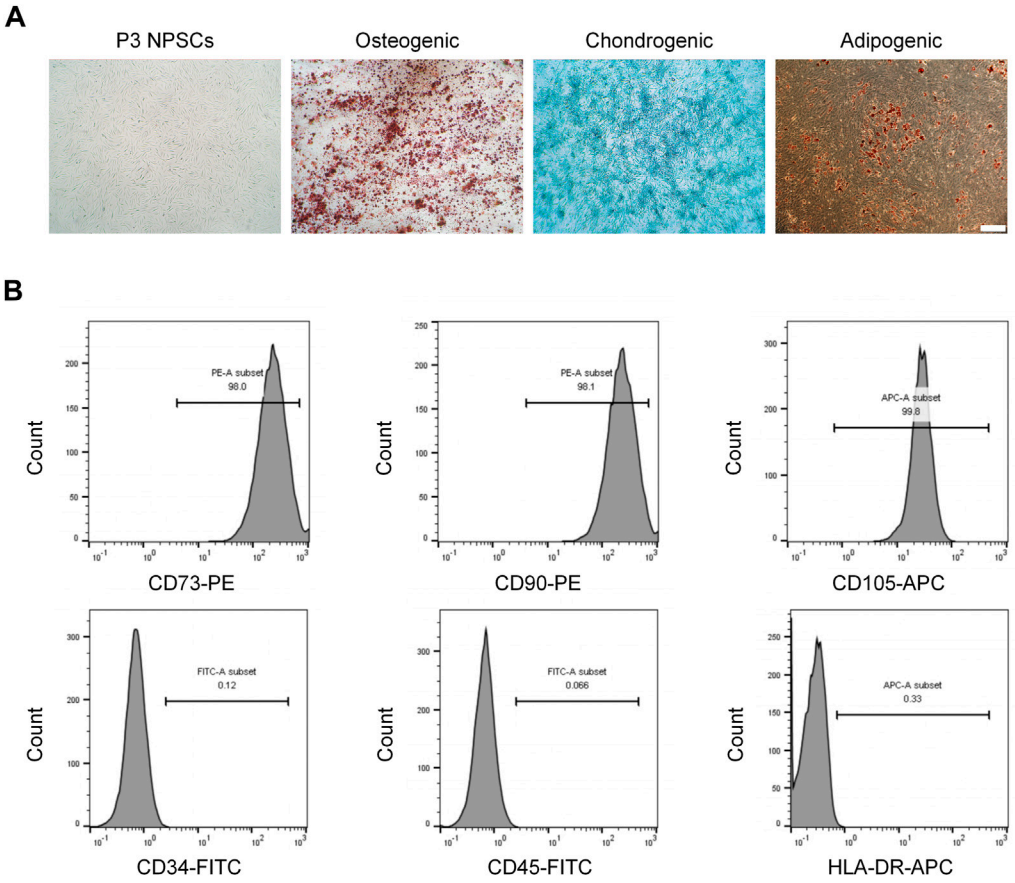

FIGURE 1
Morphological characteristics and identification of nucleus pulposus stem cells (NPSCs). **(A)** P3 NPSCs exhibited a long spindle shape with a uniform morphology and whirlpool arrangement. Osteogenic, chondrogenic, and adipogenic differentiation capacities of NPSCs were identified by Alizarin Red staining, Alcian blue staining, and Oil Red O staining, respectively. **(B)** Cell surface markers of NPSCs were detected by flow cytometry. The NPSCs positively expressed CD73, CD90 and CD105 and negatively expressed CD34, CD45, and HLA-DR.

(Figure 1A). After inducing osteogenic differentiation of the NPSCs, the formation of mineralized nodules was determined by Alizarin red staining. For the chondrogenic differentiation, Alcian blue staining showed a large amount of glycosaminoglycan accumulation in the cells. Oil Red O staining showed many intracellular lipid droplets after adipogenic differentiation (Figure 1A). For the uninduced NPSCs in these stains, no significant positive stains were observed, as demonstrated in the previous study (Li et al., 2019). Furthermore, the expressions of NPSCs surface markers CD73 (+), CD90 (+), CD105 (+) were 98.0%, 98.1%, and 99.8%, respectively, whereas the expressions of CD34 (−), CD45 (−), HLA-DR (−) were 0.12%, 0.07%, and 0.33% respectively, by flow cytometry (Figure 1B). To conclude, these results showed that the NPSCs had higher purity and stemness, which was suitable for the treatment of IVD.

3.2 Quiescent NPSCs sustained favorable potential for proliferation and biological function

The quiescent state of NPSCs was induced by serum starvation (DMEM/F12 medium containing 0.1% FBS) and its characteristics were observed. Compared with the proliferating NPSCs (P-NPSCs), the growth of the quiescent NPSCs (Q-NPSCs) was arrested and the cells gradually shrunk and became smaller. At the same time, the cell morphology gradually changed from a long spindle shape to a round or polygon, and the transparency increased. After 7 days, Q-NPSCs were reactivated with DMEM/F12 medium containing 10% FBS. It can be seen that the cells exit the quiescent state and start to proliferate again. It manifested that the cell morphology gradually expands and recovers the long spindle shape (Figure 2A). According to the CCK-8 assay, Q-NPSCs had low or no growth activity compared with P-NPSCs. However, after reactivation, the NPSCs showed the same growth activity as the P-NPSCs and continued to rise over time (Figure 2B). Flow cytometry was adopted to examine the cell cycle (Figures 2C, D). The percentage of Q-NPSCs in the G0/G1 phase was significantly higher than that of P-NPSCs and reactivated NPSCs (Re-NPSCs). In addition, the Q-NPSCs can maintain pluripotent differentiation potential. In our pervious study (Li et al., 2019), we have observed that the Re-NPSCs can be induced to osteogenic, chondrogenic, and adipogenic differentiation just like the Q-NPSCs. These results showed that serum starvation can induce NPSCs to enter the G0 phase, which was defined as the quiescent

10.3389/fbioe.2023.1073238

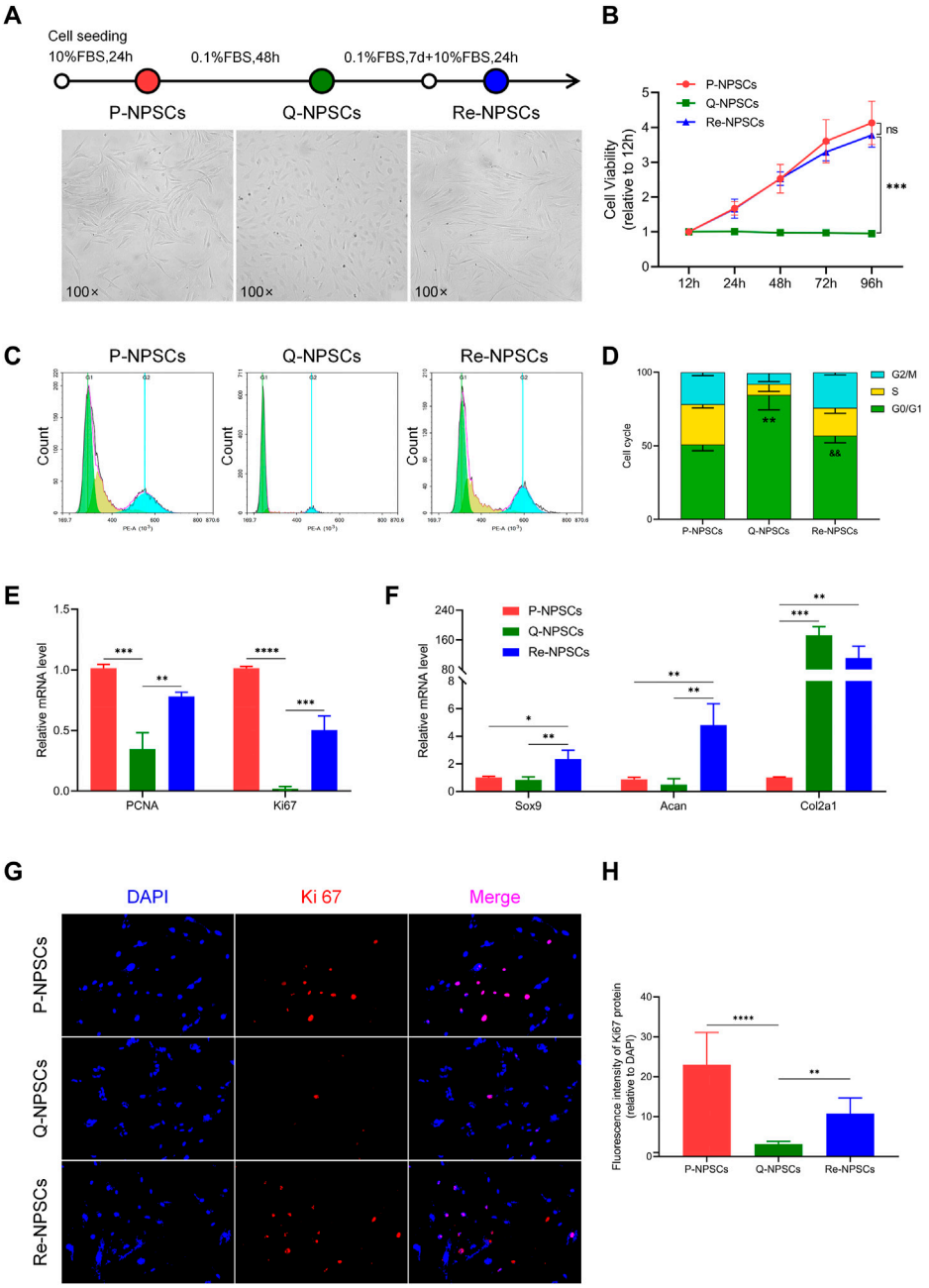

FIGURE 2
Morphological characteristics, proliferative potentials, and biological functions of the NPSCs were analyzed before and after quiescence induction and reactivation. **(A)** The morphology changes of P-NPSCs, Q-NPSCs and Re-NPSCs. **(B)** The cell viability of NPSCs in each group were detected by CCK-8 assay. $^{ns}p > 0.05$, $^{***}p < 0.001$. **(C,D)** The cell cycle of NPSCs in each group were analyzed by flow cytometry and through statistical analysis. $^{**}p < 0.01$, P-NPSCs vs. Q-NPSCs; $^{\&\&}p < 0.01$, Q-NPSCs vs. Re-NPSCs. **(E,F)** The relative mRNA levels of PCNA and Ki67 **(E)** as well as that of Sox9, Acan and Col2a1 **(F)** were analyzed by qRT-PCR. **(G,H)** The protein expression of Ki67 was detected by immunofluorescence **(G)**, followed by quantitative analysis by ImageJ software **(H)**. $^{*}p < 0.05$, $^{**}p < 0.01$, $^{***}p < 0.001$, $^{****}p < 0.0001$. P-NPSCs: proliferating NPSCs; Q-NPSCs: quiescent NPSCs; Re-NPSCs: reactivated NPSCs.

state. After reactivation, the cells re-entered the cell cycle and resumed proliferation.

Moreover, the expression of genes and the levels of proteins were evaluated to determine the biological activity of each group. PCNA and Ki67 are classical markers of cellular proliferation. Compared with P-NPSCs, the mRNA levels of PCNA and Ki67 in Q-NPSCs decreased significantly, and the levels of PCNA and Ki67 increased again in Re-NPSCs (Figure 2E). Furthermore, when compared with P-NPSCs, the protein level of Ki67 was decreased in Q-NPSCs. After reactivation, the protein level of Ki67 was restored (Figures 2G,H). In addition, many chondrogenic genes (Sox9, Acan, and Col2a1) that promote extracellular matrix synthesis were detected. In contrast to P-NPSCs, Sox9 and Acan mRNA expression was slightly downregulated in Q-NPSCs but restored in Re-NPSCs.

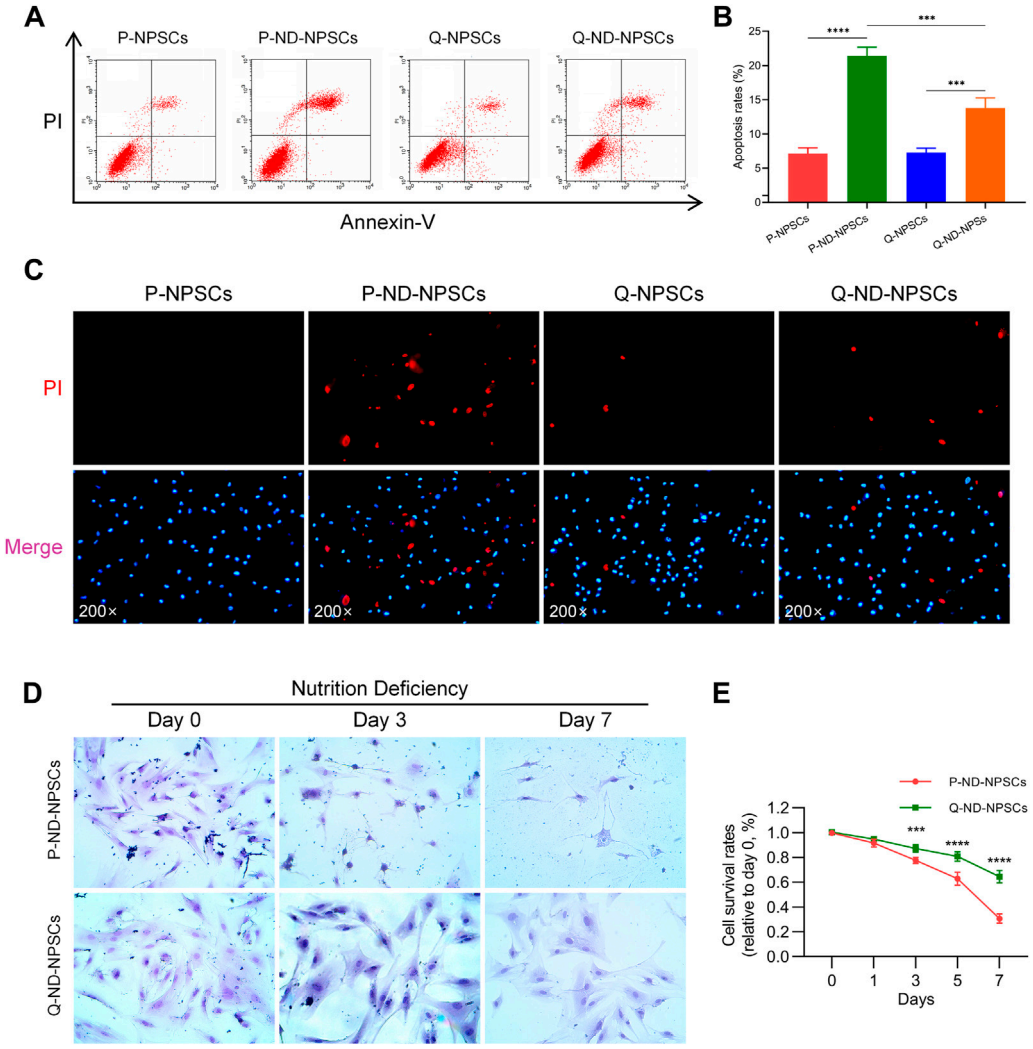

FIGURE 3
The apoptosis and survival of P-NPSCs and Q-NPSCs were analyzed *in vitro* under nutrient deficiency conditions. **(A,B)** The apoptosis of P-NPSCs, P-ND-NPSCs, Q-NPSCs and Q-ND-NPSCs were analyzed by flow cytometry **(A)** and statistical analyses **(B)**. **(C)** The NPSCs in each group were stained with the Hoechst 33342 dye (blue) and PI dye (red). Blue cells without red color signify living cells and red cells signify dead cells. **(D)** To observe the morphology of the surviving cells in each group, the cells were stained with hematoxylin Eosin (HE). **(E)** The survival of P-ND-NPSCs and Q-ND-NPSCs was analyzed by the Trypan Blue Exclusion Dye assay.

However, an interesting observation was that Col2a1 mRNA expression was significantly increased in Q-NPSCs and Re-NPSCs (Figure 2F). These results showed that the proliferation and partial biological activity of NPSCs are temporarily suppressed by quiescence induction but resume or increase immediately after reactivation.

3.3 Quiescence preconditioning favored NPSCs against apoptosis and increase cell survival under nutrient deficiency *in vitro*

To observe the response of proliferating NPSCs (P-NPSCs) and quiescent NPSCs (Q-NPSCs) in response to the nutrient-deficient (ND) environment, flow cytometry analysis was performed to detect cellular apoptosis. Even though quiescence preconditioning by serum starvation led to apoptosis, the apoptosis rate was less than 10% compared with unpreconditioned NPSCs, which was within the acceptable range. The P-NPSCs and Q-NPSCs were then cultured in the ND condition. After 48 h, both P-NPSCs and Q-NPSCs showed a significant increase in apoptosis, whereas Q-NPSCs had lower apoptosis than P-NPSCs (Figures 3A, 3B). Moreover, Hoechst 33342/PI double staining was used to visualize the living and dead cells at this time (Figure 3C). No obvious PI-positive cells were found in the untreated P-NPSCs, whereas a small number of PI-positive cells were seen in the Q-NPSCs. Under the ND culture condition, the number of PI-positive cells in quiescent NPSCs (Q-ND-NPSCs) was significantly lower than in proliferating NPSCs (P-ND-NPSCs). These results demonstrated that quiescence preconditioning can inhibit apoptosis and reduce cell death under the ND condition.

With the progression of nutrient deprivation, more and more P-ND-NPSCs died, and “ghost cells” appeared (Figure 3D). On the

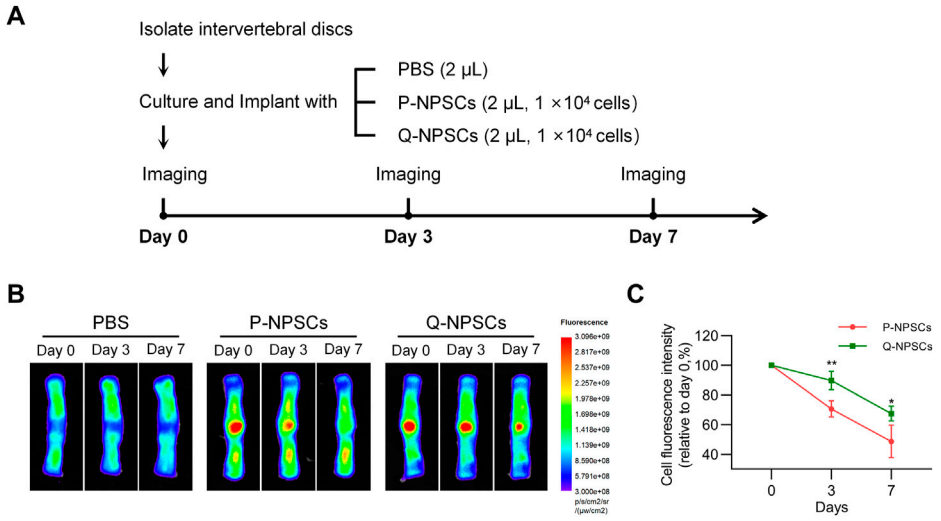

FIGURE 4
The survival of NPSCs after implantation into isolated discs was measured using an animal fluorescence imaging system. **(A)** Grouping and procedure of the cell retention study. **(B,C)** The fluorescence intensity, which indicates the number of surviving cells, was measured at day 0, day 3 and day 7 after injection of P-NPSCs and Q-NPSCs. PBS was implanted as a control. *$p < 0.05$, **$p < 0.01$, ***$p < 0.001$, ****$p < 0.0001$.

contrary, the Q-ND-NPSCs showed almost no morphological changes and less cell death from day 0 to day 7. The results of the trypan blue exclusion experiment showed (Figure 3E) that the cell survival rate of the P-ND-NPSCs continued to decrease significantly, and reached only about 30% on the seventh day, whereas that of the Q-ND-NPSC decreased slowly and remained above 60% on the seventh day. These results showed that quiescence preconditioning increased the tolerance under the ND environment, thereby improving the cell survival rate.

Furthermore, the retention of P-NPSCs and Q-NPSCs after implantation in the disc was determined by *in vitro* imaging analysis. As shown in Figure 4, the fluorescence intensity represented cell retention. The fluorescence cells after implantation of P-NPSCs and Q-NPSCs decreased in the IVD. However, the fluorescence intensity of Q-NPSCs was higher than that of P-NPSCs on the seventh day of implantation. These results suggested that quiescence preconditioning also contributed to the survival of NPSCs in the IVD after implantation.

3.4 Quiescence preconditioning increased the ability of NPSCs to alleviate the intervertebral disc degeneration *in vivo*

To determine the therapeutic effect of Q-NPSCs transplantation on disc degeneration compared with P-NPSCs *in vivo*, a rat model of IDD was established by needle puncture. After 2 weeks, P-NPSCs, Q-NPSCs, and PBS were administered into different segments of intervertebral discs, where PBS was used as the control. The untreated segment was the normal group. We then performed radiographic analysis and histological analysis of each group after transplantation, as shown in Figure 5A.

First, the intervertebral disc height was observed by X-ray after cell injection and evaluated by disc height index (DHI) (Figures 5B, C). Compared with the normal group, DHI decreased after induction of IDD in the PBS, P-NPSCs, and Q-NPSCs groups. The mean DHI continued to decrease in the PBS group. After 2 weeks of cell transplantation, the DHI of the P-NPSCs group and Q-NPSCs group was significantly higher than that of the PBS group. After 4 weeks of cell transplantation, the DHI of the Q-NPSCs group was significantly higher than that of the P-NPSCs group. All these results suggested that NPSCs transplantation can maintain IVD height and quiescence preconditioning can increase this ability.

Four weeks after transplantation, the caudal discs were harvested to assess histological differences between each group. The macroscopic observation of the IVD was evaluated (Figure 5D). The NP and AF in the IVD without acupuncture were distinctly defined. The AF was complete, and the NP tissue was water-rich. In the PBS group, the AF structure was disordered, and the NP area was significantly reduced and replaced by microscopic tissues. Although AF tissues in the P-NPSC and Q-NPSC groups were thicker than those in the PBS group, they were rich in NP tissues, and the boundary between the NP and AF was clear. Notably, the NP area of the Q-NPSC group was larger than that of the P-NPSC group. HE staining (Figure 5E) showed that NP tissues were arranged neatly and evenly in the normal group. In the PBS group, NP tissues were damaged or disappeared and filled with fibrous connective tissues, whereas AF tissues were disordered and lost their concentric circular lamellar structures. The distribution and structures of the NP and ECM in the P-NPSC and Q-NPSC groups were visible; however, the quantity and structure of the ECM in the Q-NPSC group were better than those in the P-NPSC group. S-O staining (Figure 5E) showed that polysaccharide content in the PBS group decreased significantly; thus, the staining of both groups was stronger than that of the PBS group. Furthermore, the staining of the Q-NPSC group was stronger than that of the P-NPSC group. In contrast, toluidine blue staining (Figure 5E) showed that the P-NPSC and Q-NPSC groups showed more NP chondrocytes and positive proteoglycan staining than the PBS group, and the staining intensity

10.3389/fbioe.2023.1073238

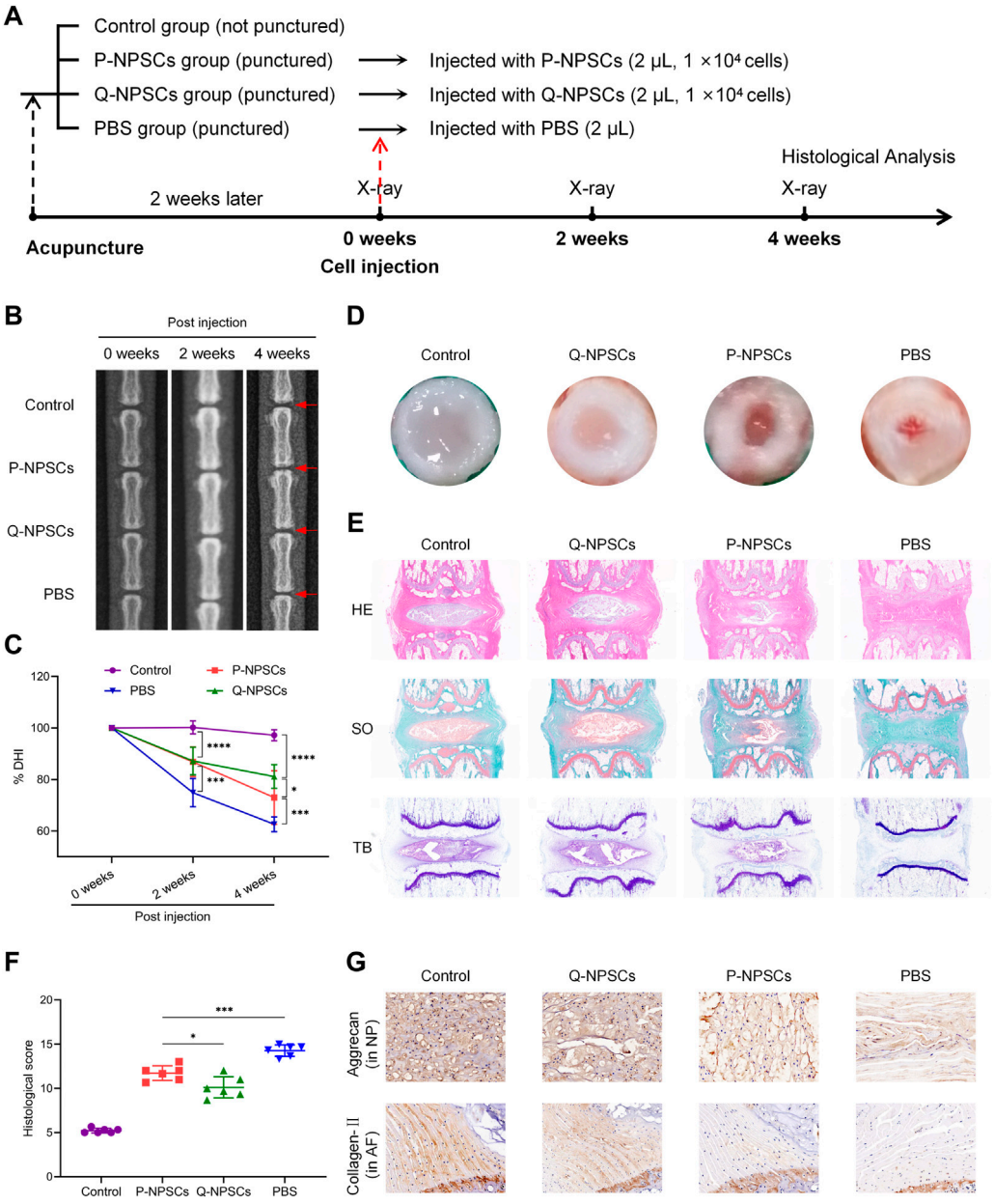

FIGURE 5
The therapeutic effects of P-NPSCs and Q-NPSCs on intervertebral disc degeneration (IDD) were analyzed and compared *in vivo*. **(A)** Groupings and procedures for *in vivo* experiments. **(B)** X-rays were captured to assess the disc height before the puncture, at 2 weeks after the puncture and then at 2 weeks after the cell injection. The red arrows indicate the location of the disc, as well as the locations of the acupuncture and injection cells. **(C)** The disc height index (DHI) was calculated and expressed as %DHI to assess the change in disc height after cell implantation. **(D)** Two weeks after the cell transplantation, the rat caudal disc tissues were assessed. **(E)** The disc sections were stained with hematoxylin eosin (HE), saffron O-fast green (SO), and toluidine blue (TB). **(F)** The degree of disc degeneration was assessed through histological scoring. **(G)** The protein expression of aggrecan in the nucleus pulposus (NP) and collagen-II in the annulus fibrosus (AF) was determined by immunohistochemistry analysis (×100). *$p < 0.05$, ***$p < 0.001$.

of the Q-NPSC group was better than that of the P-NPSC group. Overall, the histological scores were significantly higher in all experimental groups than those in the normal group and were higher in the PBS group than those in the P-NPSC and Q-NPSC groups. The histological scores of the Q-NPSC group were lower than those of the P-NPSC group (Figure 5F). These results indicated that the transplantation of preconditioned quiescent NPSCs might maintain or improve the tissue structure of the IVD with better effects than the transplantation of non-preconditioned proliferating NPSCs.

Immunohistochemical staining showed that collagen-II and aggrecan were present in the normal, P-NPSC, and Q-NPSC groups (Figure 5G). Due to the absence of NP tissues in the PBS group, only small amounts of collagen-II and aggrecan were observed. According to the quantitative analysis, collagen-II and

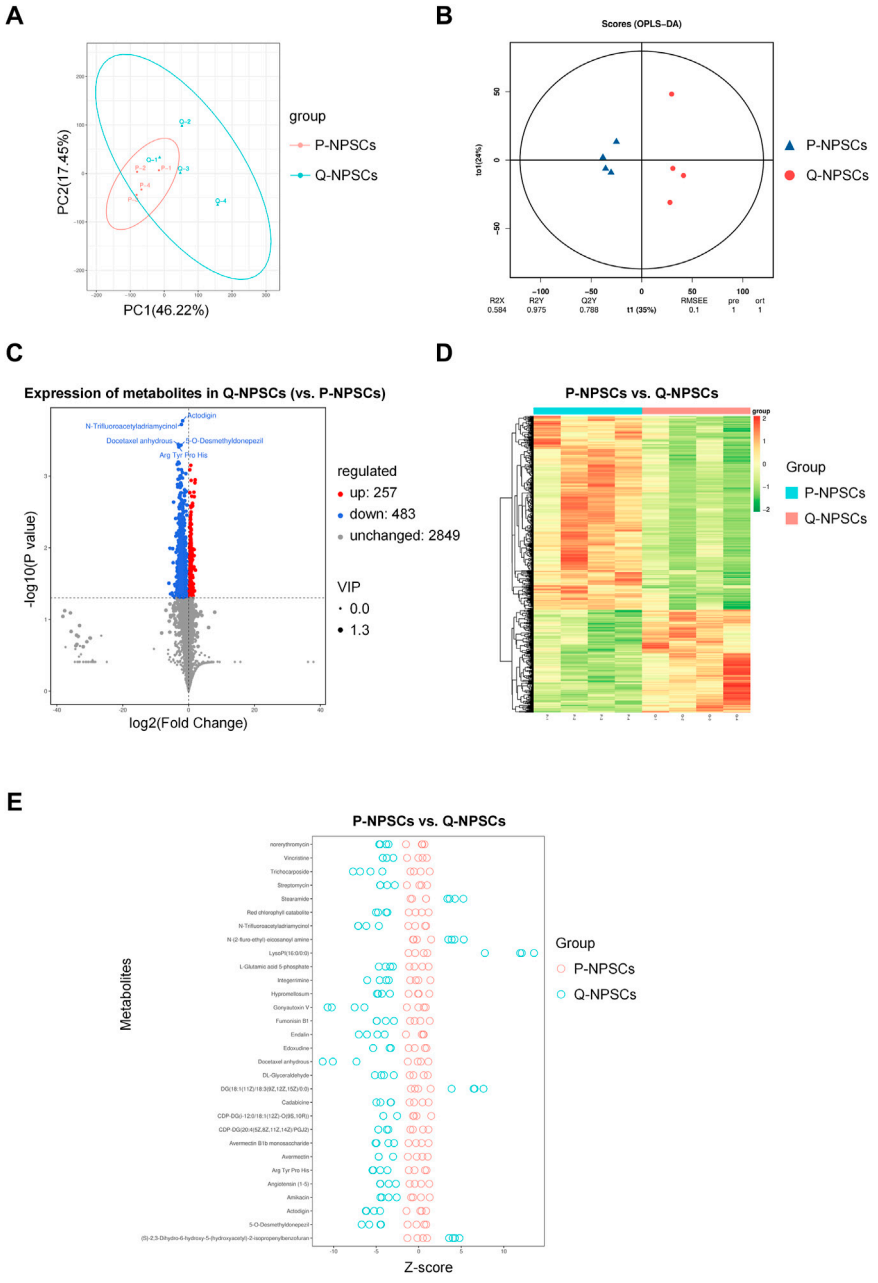

FIGURE 6
The metabolomics analysis of P-NPSCs and Q-NPSCs. **(A)** Principal component analysis (PCA) revealed the metabolic differences between P-NPSCs and Q-NPSCs. **(B)** The permutation test was performed by the orthogonal partial least squares discriminant analysis (OPLS-DA). **(C,D)** The differential metabolites of P-NPSCs and Q-NPSCs were analyzed by cluster analysis and represented by volcano plots **(C)** and heat map **(D)**. The screening criteria were Fold Change (FC) > *p*-value <0.05 and Variable Importance in Projection (VIP) > 1. The scatter size represents the VIP value of the OPLS-DA model. The labeled differential metabolites in the volcano represent the top five differential metabolites ranked by *p*-value. **(E)** The difference deviation in the P-NPSCs and Q-NPSCs were analyzed using the Z-score. A positive value means up, while a negative value means down. The top 30 differential metabolites ranked by *p*-value are shown in **(E)**.

aggrecan levels in the P-NPSC and Q-NPSC groups were significantly higher than those in the PBS group and lower than those in the normal group. The collagen-II and aggrecan levels in the Q-NPSC group were higher than those in the P-NPSC group. These results suggested that the preconditioned quiescent NPSCs maintained ECM production in the degenerate disc.

3.5 Preconditioned quiescent NPSCs adopt an adaptive metabolic pattern

Using the liquid chromatography-quaternary time-of-flight mass spectrometry (LC-QTOF) technology, qualitative and quantitative analyses were performed for metabolomics on the

eight samples of P-NPSCs and Q-NPSCs, and a total of 14,809 peaks were detected (Supplementary Figure S1, Supplementary File S1). A total of 3,589 metabolites were annotated using the online METLIN database and Biomark's self-built library. Principal component analysis (PCA) showed considerable differences between P-NPSCs and Q-NPSCs (Figure 6A, Supplementary File S2). Orthogonal partial least squares discriminant analysis (OPLS-DA) was performed to assess the reliability of the data model. The Q2Y score of the OPLS-DA represents the predictive ability of the model, that is, whether the model can distinguish correct sample groups by metabolic expression. The closer the R2Y and Q2Y of the index are to 1, the more stable and reliable the model is, that is, the model can be used to screen differential metabolites. The model was considered effective when Q2Y > 0.5 and excellent when Q2Y > 0.9. This model has a Q2Y value of 0.788 (Figure 6B). Then 740 differential metabolites were screened out according to Fold Change (FC), *p*-value, and Variable Importance in Projection (VIP) obtained by the OPLS-DA. Differences were considered significant if FC ≥ 1, *p*-value <0.05 and VIP ≥1. Compared with the P-NPSCs, the overall metabolic level of the Q-NPSC group was reduced, with 483 downregulated and 257 upregulated metabolites. The expression levels of differential metabolites in the two groups were represented by volcano and heatmap, as shown in Figures 6C, D and Supplementary File S3 respectively. The Z-score (standard score) value, a value converted based on the quantitative value of metabolites, was used to measure the difference deviation between the experimental and control groups. It should be noted that the Z-scores are calculated based on the mean and standard deviation of the control group (P-NPSCs), in order to center the control group on the axis for easy comparison. A positive value means up, while a negative value means down. The top 30 differential metabolites ranked by *p*-value are shown in Figure 6E (Supplementary File S4).

Next, a pathway enrichment analysis was performed using the KEGG database for these differential metabolites (Figures 7A, 7B, Supplementary Files S5, S6). Considerable differences were observed in the following metabolic pathways: phenylalanine, tyrosine, and tryptophan biosynthesis, plant hormone biosynthesis, cyanoamino acid metabolism, and phenylpropanoid biosynthesis. Then, by analyzing the pathway network map (Figure 7C), it was found that L-tyrosine, L-tryptophan, Serotonin, and L-malic acid were enriched into multiple metabolic pathways, indicating that they play a role in these different pathways. The ROC curves were used to analyze the possibility of these four differential metabolites as specific markers of the quiescent state of NPSCs (Figure 7D). The AUC (area under the curve) is a very useful measure for measuring the ROC curve. It is always between 0.5 and 1.0. The closer the AUC is to 1, the more different the substance is from the control and experimental groups (i.e., a potential biomarker). L-tyrosine, L-tryptophan and L-malic acid have an AUC of 1, and Serotonin has an AUC of 0.875. The boxplots showed that the expressions of L-tyrosine, L-tryptophan, Serotonin, and L-malic acid in Q-NPSCs were significantly lower than those in P-NPSCs. These results showed that the Q-NPSC group showed distinct metabolic patterns that were significantly different from those in the P-NPSC group. Furthermore, it may be possible to find biomarkers for the quiescent state of the NPSCs from a metabolic perspective, and a large sample size is required for verification.

4 Discussion

Stem cell transplantation for IDD treatment is a hot topic in current research. NPSCs have become one of the ideal seed cells because of their unique advantages. However, stem cells used for transplantation are generally in the proliferative phase, which is inconsistent with the quiescence of adult stem cells *in vivo*. Moreover, we have previously confirmed the quiescence of NPSCs *in vitro* (Li et al., 2019). Theoretically, the transplantation of Q-NPSCs would be more suitable for the internal environment of the disc. In addition, quiescent stem cells can resist adverse environments to enhance their survival. Moya et al. showed that preconditioned quiescent human MSCs could survive better *in vitro* under hypoxia and glucose-free conditions (Moya et al., 2017). In view of the special ND microenvironment in the IVD, we hypothesized that the transplantation of Q-NPSCs could better preserve survival and cellular biological functions, facilitating the repair of the degenerated disc. As shown in Figure 8, we tested this hypothesis through *in vivo* and *in vitro* experiments.

First, we successfully isolated NPSCs from rat NP tissues and identified their multilineage differentiation ability and immunophenotypes. As shown in Figure 1, NPSCs have good growth activity, high purity, and strong differentiation ability, and they are highly potential seed cells for repairing IDD. Then we induced these NPSCs to enter the quiescent phase by serum starvation pretreatment for 48 h. As shown in Figure 2, the vast majority of quiescence-inducing NPSCs were in the G0 phase and showed low or no proliferation. The mRNA levels of PCNA and Ki67 were decreased. Compared with the proliferating NPSCs, the mRNA levels of Sox9 and Acan were also decreased in the quiescent NPSCs. Interestingly, Col2a1 mRNA level was significantly increased. The secretion of ECM was increased in quiescent cells, potentially reflecting the preservation of essential physiological functions of the cells in response to harsh environments (Lemons et al., 2010). In addition, we also observed Ki67 level by cellular immunofluorescence. Similar to the mRNA level, Ki67 level was significantly decreased in the Q-NPSCs. However, when the cells were reactivated, the proliferative activity was immediately restored, and the mRNA levels of PCNA, Ki67, Sox9, and Acan were significantly restored or increased, and the mRNA level of Col2a1 was high. Furthermore, Ki67 level was restored in the reactivated NPSCs. These results suggest that Q-NPSCs maintain the potential to proliferate, differentiate, and synthesize ECM and may even perform better after reactivation.

As shown in Figures 2D,E,H, Re-NPSCs outperformed P-NPSCs in the expression of Sox-9, Acan, and Col2a1, and were comparable to P-NPSCs in cell viability, but slightly inferior to P-NPSCs in the expression of PCNA and Ki67 and in the cell cycle. This involves the activation mechanism of quiescent stem cells. Urbán et al. (Urban and Cheung, 2021) suggested that when stem cells enter a deep quiescent state, it takes longer to recover to a proliferative state, which is influenced by various factors. Furthermore, due to the drawbacks of inducing stem cells into a quiescent state by means of serum starvation, it leads to a degree of apoptosis or irreversible senescence (G0) (Marescal and Cheeseman, 2020). These ideas suggest it takes a longer time for stem cells to recover from

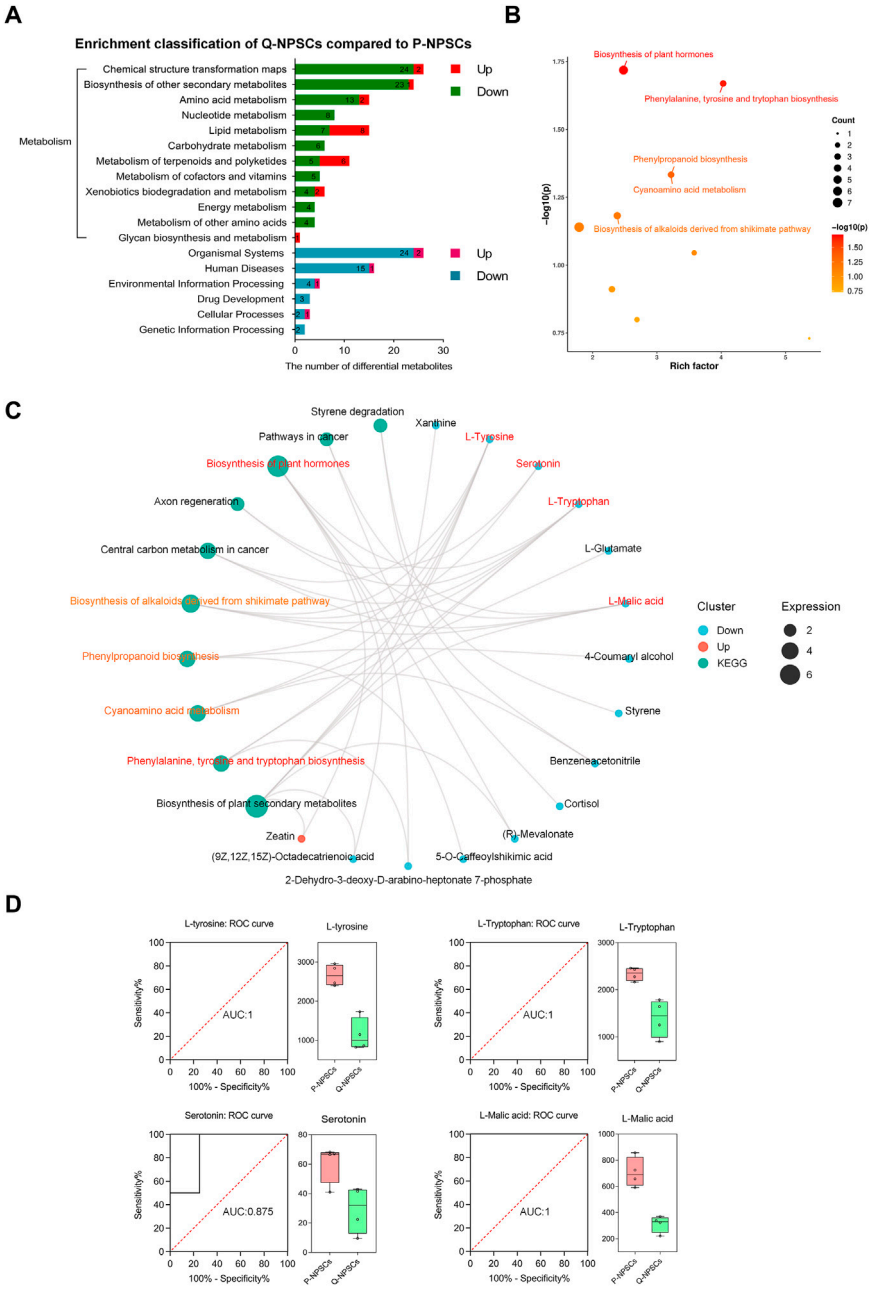

FIGURE 7
The pathway enrichment analysis of differential metabolites between P-NPSCs and Q-NPSCs. **(A)** Metabolic pathway and other pathways were analyzed with reference to the KEGG database. **(B)** Bubble map of the KEGG enrichment factor for differential metabolites. The *X*-axis is the enrichment factor and the *Y*-axis is the *p*-value. The size of the dots represents the number of differential metabolites enriched. The labeled dots are the top five metabolic pathways ranked by *p*-value and were used for the analysis; The unlabeled dots were not used. **(C,D)** Several representative differential metabolites of Q-NPSCs compared to P-NPSCs were obtained by enrichment network diagram **(C)** and analyzed by the receiver operating characteristic (ROC) curves and box plots **(D)**.

quiescence and that some degree of cell loss occurs are well made. This is a problem that researchers are eager to address and look forward to more satisfactory induction methods in the future. In conclusion, our data suggest that NPSCs regain proliferation and biological functions to levels comparable with P-NPSCs. We believe that as technology advances and difficulties are resolved in the future, quiescence preconditioned NPSCs are expected to become a new transplantation strategy for repairing disc degeneration.

Studies have shown that quiescence enables stem cells to withstand harsh environments and reduces cell death (Stuart and Brown, 2006; Alekseenko et al., 2018; Ferro et al., 2019). P- NPSCs and Q-NPSCs were cultured in a serum-free and glucose-free

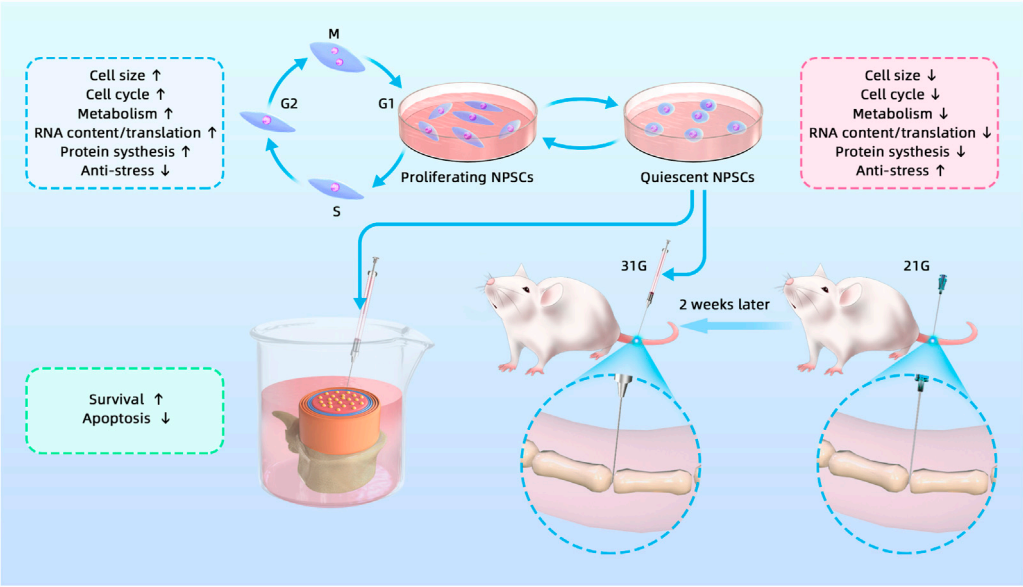

FIGURE 8
Graphical abstract of the study, including *in vivo* and *in vitro* experiments.

environment to investigate their survival under ND conditions *in vitro*. As shown in Figure 3, the results showed that Q-NPSCs showed a higher survival rate and anti-apoptotic ability than P-NPSCs in response to the ND environment. Subsequently, when the two types of NPSCs were implanted into the IVD, a similar phenomenon was observed; the Q-NPSCs survived more, as shown in Figure 4. On the seventh day of cell transplantation, the survival rate of these P-NPSCs decreased to 30%, whereas that of the Q-NPSCs remained above 60%. This result indicates that Q-NPSCs have better tolerance to the ND environment than P-NPSCs, which contributes to cell survival.

Cell therapy of the IVD depends on the survival of transplanted cells and their biological functions (Sakai and Grad, 2015; Tong et al., 2017). In this study, we constructed a rat model of IDD by needle puncture injury. We transplanted quiescent NPSCs, proliferating NPSCs, and PBS into the IVD of the rat IDD model and evaluated the repair efficacy of each group by radiography, histology, and ECM synthesis. The results are shown in Figure 5. The disc segment degeneration was most obvious in PBS injection only. In contrast, the degeneration of the segments transplanted with either quiescent or proliferating NPSCs was significantly improved. However, Q-NPSC transplantation showed lower disc height reduction, lower histological scores, and better ECM synthesis than P-NPSC transplantation. Therefore, quiescence preconditioning can improve the effectiveness of NPSCs in IDD repair.

Although many previous studies have reported cell therapy for IDD, ensuring cell survival after transplantation is difficult. In this study, we present an innovative treatment strategy for the quiescence preconditioning of NPSCs. This approach was experimentally evaluated and successfully demonstrated to improve the survival and repair ability of NPSCs, both *in vitro* and *in vivo*. However, due to the lack of vertical stress on the spine, the rat model of IDD constructed by needle puncture was not completely consistent with the IDD process in humans (Han et al., 2008). Therefore, performing experiments on large animals, such as rhesus monkeys (Zhou et al., 2013), is necessary to verify the repair ability of quiescent NPSCs further.

However, one of the most important questions will be to determine whether engrafted cells survive over the long term and directly contribute to disc formation, or if they survive only transiently, but in a manner that is sufficient to stimulate a repair from within the endogenous environment. According to previous studies (Clouet et al., 2019; Lyu et al., 2019), there must be endogenous cellular repair during disc degeneration. In our study, injected segments significantly delayed the disc degeneration compared to segments without injected cells, indicating that exogenous NPSCs play an important role in repairing intervertebral disc degeneration. This may be one of the shortcomings of this study, and more information is needed for further research.

Based on the above studies, we have confirmed that Q-NPSCs are more tolerant to the harsh environment to maintain survival, but the specific mechanism still needs further exploration. Previous studies have shown that the quiescent state of stem cells is regulated by metabolism (Moya et al., 2017; Theret et al., 2017; Cho et al., 2019; Marescal and Cheeseman, 2020). Moya A et al. reported that quiescence pretreatment causes a protective metabolic adaptation to improve the survival of human MSCs in an ischemic environment (Moya et al., 2017). Theret M et al. showed that AMP-activated protein kinase, the master metabolic regulator of a cell, regulated muscle stem cells returning to quiescence, emphasizing the importance of metabolism in stem cell fate (Theret et al., 2017). Therefore, we examined the metabolic differences between the

quiescent and proliferating NPSCs by metabolomics. The results are shown in Figures 6, 7. The overall metabolic level of the quiescent NPSCs was significantly reduced, including amino acid, nucleotide, carbohydrate, and energy metabolisms. Amino acid metabolism pathways (including tyrosine, tryptophan, and phenylalanine metabolisms) and nucleotide metabolism pathways (including pyrimidine and purine metabolisms) were significantly downregulated, indicating that protein anabolism was reduced, which was consistent with previous reports (Cho et al., 2019; Marescal and Cheeseman, 2020).

Further analysis of the KEGG enrichment network graph revealed several significantly under-expressed metabolites such as L-tyrosine, L-tryptophan, Serotonin, and L-malic acid, which are key metabolites in multiple enrichment pathways. L-Tyrosine is closely related to cell cycle transition (Kaldis, 2007; Jäkel et al., 2012). The cyclin-dependent kinase inhibitor P27 can be phosphorylated on tyrosine, and phosphorylated P27 reduces the ability to inhibit the activity of cyclin-dependent kinases, a mechanism that allows cells to enter the cell cycle from quiescence. In this study, we hypothesized that the low level of tyrosine in the quiescent NPSCs reduced the phosphorylation of P27, improving the stability of P27, thus inhibiting the cell cycle and allowing the NPSCs to remain in the quiescent state. Moreover, tryptophan is an essential amino acid that the body cannot synthesize; it is also an essential precursor in serotonin synthesis, which promotes proliferation (Comai et al., 2020). Thus, with the constant depletion of tryptophan in quiescent NPSCs, cell cycle arrest was induced (Mellor et al., 2003; Oh et al., 2017) and serotonin level was reduced (Fang et al., 2018; Gordeeva and Safandeev, 2021), probably contributing to NPSC quiescence. L-Malic acid is a vital organic acid produced in the metabolic process of organisms and an important intermediate in the tricarboxylic acid cycle and its branch, the glyoxylate cycle. L-Malic acid can quickly pass through the cell membrane and enter mitochondria to participate in energy metabolism directly (Ding et al., 2016); it is also an important component of the malate aspartate shuttle and is important in transporting NADH from the cytosol to mitochondria for ATP production (Scholz et al., 2000; Wu et al., 2011). In the present study, L-malic acid was reduced in the Q-NPSCs, which reduced ATP production.

However, we found that lipid, terpenoid, and polyketide metabolisms were active in the quiescent NPSCs. This is consistent with previously reported results (Lemons et al., 2010). Lipid metabolism is an important and complex biochemical reaction in the body, which refers to the process of digestion, absorption, synthesis, and decomposition of lipids in organisms under the catalysis of numerous enzymes to be processed into products needed by the body to ensure the normal operation of physiological functions and is crucial for life activities (DeBose-Boyd, 2018). Lipids are not only essential for energy supply and storage but they also play an important role as structural components of biofilms (Yao et al., 2019). Thus, ensuring basic lipid metabolism is beneficial for maintaining cellular functions and for stabilizing the membrane structure. In addition, terpenoids and polyketides stabilize cells, resist oxidation, and inhibit proliferation (de Carvalho and da Fonseca, 2006; Kotoku et al., 2017), which need to be further verified in Q-NPSCs.

5 Conclusion

In summary, our findings suggested that the quiescence preconditioning of the NPSCs maintained proliferative potential and cell viability, enhanced survival, and exhibited cellular functions in response to the transition to a harsh, nutrient-deficient environment, thereby facilitating IDD repair. Thus, we hypothesized that the quiescent NPSCs adopted an adaptive metabolic pattern that favored resistance to the metabolic stresses encountered. As this quiescence preconditioning method *via* serum starvation is safe, feasible, and does not require many cells, it can be a suitable strategy for using NPSCs in IDD treatment in the future.

Data availability statement

The datasets presented in this study can be found in online repositories. The names of the repository/repositories and accession number(s) can be found in the article/Supplementary Material.

Ethics statement

The animal study was reviewed and approved by Institutional Animal Care and Use Committee of Nanchang University.

Author contributions

QC, BL and XC contributed to the conception, study design, and final decision of the manuscript. QC and QY contributed to the study design, data collection and analysis, and manuscript writing and revision. CP and RD contributed to the experimental studies and data collection. TW provided the experimental methods and materials. JC, HW, and XZ contributed to the data analysis. BL and XC were the project administrators.

Funding

This study was funded by the Thousand Talents Program of Jiangxi Province (No. JXSQ2019201026), Jiangxi Key Laboratory of Intervertebral Disc Disease (No. 20202BCD42018), National Natural Science Foundation of China (No. 82060403).

Acknowledgments

Thanks to Fanli Chong and Rui Zuo of Xinqiao Hospital for providing rats (GFP+), and thank all other researchers and study participants for their contributions.

Conflict of interest

The authors declare that the research was conducted in the absence of any commercial or financial relationships that could be construed as a potential conflict of interest.

Publisher's note

All claims expressed in this article are solely those of the authors and do not necessarily represent those of their affiliated organizations, or those of the publisher, the editors and the reviewers. Any product that may be evaluated in this article, or claim that may be made by its manufacturer, is not guaranteed or endorsed by the publisher.

Supplementary material

The Supplementary Material for this article can be found online at: https://www.frontiersin.org/articles/10.3389/fbioe.2023.1073238/full#supplementary-material

References

Alekseenko, L. L., Shilina, M. A., Lyublinskaya, O. G., Kornienko, J. S., Anatskaya, O. V., Vinogradov, A. E., et al. (2018). Quiescent human mesenchymal stem cells are more resistant to heat stress than cycling cells. *Stem Cells Int.* 2018, 1–15. doi:10.1155/2018/3753547

Binch, A. L. A., Fitzgerald, J. C., Growney, E. A., and Barry, F. (2021). Cell-based strategies for IVD repair: Clinical progress and translational obstacles. *Nat. Rev. Rheumatol.* 17 (3), 158–175. doi:10.1038/s41584-020-00568-w

Chen, X., Zhu, L., Wu, G., Liang, Z., Yang, L., and Du, Z. (2016). A comparison between nucleus pulposus-derived stem cell transplantation and nucleus pulposus cell transplantation for the treatment of intervertebral disc degeneration in a rabbit model. *Int. J. Surg.* 28, 77–82. doi:10.1016/j.ijsu.2016.02.045

Cho, I. J., Lui, P. P., Obajdin, J., Riccio, F., Stroukov, W., Willis, T. L., et al. (2019). Mechanisms, hallmarks, and implications of stem cell quiescence. *Stem Cell Rep.* 12 (6), 1190–1200. doi:10.1016/j.stemcr.2019.05.012

Chou, R. (2021). Low back pain. *Ann. Intern. Med.* 174 (8), ITC113–ITC128. doi:10.7326/AITC202108170

Clouet, J., Fusellier, M., Camus, A., Le Visage, C., and Guicheux, J. (2019). Intervertebral disc regeneration: From cell therapy to the development of novel bioinspired endogenous repair strategies. *Adv. Drug Deliv. Rev.* 146, 306–324. doi:10.1016/j.addr.2018.04.017

Comai, S., Bertazzo, A., Brughera, M., and Crotti, S. (2020). Tryptophan in health and disease. *Adv. Clin. Chem.* 95, 165–218. doi:10.1016/bs.acc.2019.08.005

Costăchescu, B., Niculescu, A.-G., Teleanu, R. I., Iliescu, B. F., Rădulescu, M., Grumezescu, A. M., et al. (2022). Recent advances in managing spinal intervertebral discs degeneration. *Int. J. Mol. Sci.* 23 (12), 6460. doi:10.3390/ijms23126460

de Carvalho, C. C. C. R., and da Fonseca, M. M. R. (2006). Biotransformation of terpenes. *Biotechnol. Adv.* 24 (2), 134–142. doi:10.1016/j.biotechadv.2005.08.004

DeBose-Boyd, R. A. (2018). Significance and regulation of lipid metabolism. *Seminars Cell & Dev. Biol.* 81, 97. doi:10.1016/j.semcdb.2017.12.003

Ding, S., Yang, Y., and Mei, J. (2016). Protective effects of L-malate against myocardial ischemia/reperfusion injury in rats. *Evidence-based Complementary Altern. Med. ECAM* 2016, 1–9. doi:10.1155/2016/3803657

Du, Y., Wang, Z., Wu, Y., Liu, C., and Zhang, L. (2021). Intervertebral disc stem/progenitor cells: A promising "seed" for intervertebral disc regeneration. *Stem Cells Int.* 2021, 1–12. doi:10.1155/2021/2130727

Ekram, S., Khalid, S., Bashir, I., Salim, A., and Khan, I. (2021). Human umbilical cord-derived mesenchymal stem cells and their chondroprogenitor derivatives reduced pain and inflammation signaling and promote regeneration in a rat intervertebral disc degeneration model. *Mol. Cell. Biochem.* 476 (8), 3191–3205. doi:10.1007/s11010-021-04155-9

Fang, Y., Liu, C., Shu, B., Zhai, M., Deng, C., He, C., et al. (2018). Axis of serotonin -pERK-YAP in liver regeneration. *Life Sci.* 209, 490–497. doi:10.1016/j.lfs.2018.08.047

Ferro, F., Spelat, R., Shaw, G., Duffy, N., Islam, M. N., O'Shea, P. M., et al. (2019). Survival/adaptation of bone marrow-derived mesenchymal stem cells after long-term starvation through selective processes. *Stem Cells* 37 (6), 813–827. doi:10.1002/stem.2998

Goel, A. J., Rieder, M. K., Arnold, H. H., Radice, G. L., and Krauss, R. S. (2017). Niche cadherins control the quiescence-to-activation transition in muscle stem cells. *Cell Rep.* 21 (8), 2236–2250. doi:10.1016/j.celrep.2017.10.102

Gordeeva, O., and Safandeev, V. (2021). 5-Hydroxytryptophan (5-HTP)-induced intracellular syndrome in mouse non-neural embryonic cells is associated with inhibited proliferation and cell death. *Neuropharmacology* 195, 107862. doi:10.1016/j.neuropharm.2019.107862

Han, B., Zhu, K., Li, F.-C., Xiao, Y.-X., Feng, J., Shi, Z.-L., et al. (2008). A simple disc degeneration model induced by percutaneous needle puncture in the rat tail. *Spine* 33 (18), 1925–1934. doi:10.1097/BRS.0b013e31817c64a9

Ho, T. T., Warr, M. R., Adelman, E. R., Lansinger, O. M., Flach, J., Verovskaya, E. V., et al. (2017). Autophagy maintains the metabolism and function of young and old stem cells. *Nature* 543 (7644), 205–210. doi:10.1038/nature21388

Hu, B., He, R., Ma, K., Wang, Z., Cui, M., Hu, H., et al. (2018). Intervertebral disc-derived stem/progenitor cells as a promising cell source for intervertebral disc regeneration. *Stem Cells Int.* 2018, 1–11. doi:10.1155/2018/7412304

Iezaki, T., Fukasawa, K., Yamada, T., Hiraiwa, M., Kaneda, K., and Hinoi, E. (2019). Cartilage induction from mouse mesenchymal stem cells in high-density micromass culture. *Bio-protocol* 9 (1), e3133. doi:10.21769/BioProtoc.3133

Jäkel, H., Peschel, I., Kunze, C., Weinl, C., and Hengst, L. (2012). Regulation of p27*Kip1*by mitogen-induced tyrosine phosphorylation. *Cell CycleGeorget. Tex.)* 11 (10), 1910–1917. doi:10.4161/cc.19957

Jin, Z., Wang, D., Zhang, H., Liang, J., Feng, X., Zhao, J., et al. (2020). Incidence trend of five common musculoskeletal disorders from 1990 to 2017 at the global, regional and national level: Results from the global burden of disease study 2017. *Ann. Rheumatic Dis.* 79 (8), 1014–1022. doi:10.1136/annrheumdis-2020-217050

Kaldis, P. (2007). Another piece of the p27Kip1 puzzle. *Cell* 128 (2), 241–244. doi:10.1016/j.cell.2007.01.006

Kotoku, N., Ishida, R., Matsumoto, H., Arai, M., Toda, K., Setiawan, A., et al. (2017). Biakamides A-D, unique polyketides from a marine sponge, act as selective growth inhibitors of tumor cells adapted to nutrient starvation. *J. Org. Chem.* 82 (3), 1705–1718. doi:10.1021/acs.joc.6b02948

Kumar, H., Ha, D. H., Lee, E. J., Park, J. H., Shim, J. H., Ahn, T. K., et al. (2017). Safety and tolerability of intradiscal implantation of combined autologous adipose-derived mesenchymal stem cells and hyaluronic acid in patients with chronic discogenic low back pain: 1-year follow-up of a phase I study. *Stem Cell Res. Ther.* 8 (1), 262. doi:10.1186/s13287-017-0710-3

Lemons, J. M. S., Feng, X.-J., Bennett, B. D., Legesse-Miller, A., Johnson, E. L., Raitman, I., et al. (2010). Quiescent fibroblasts exhibit high metabolic activity. *PLoS Biol.* 8 (10), e1000514. doi:10.1371/journal.pbio.1000514

Li, B., Sun, C., Sun, J., Yang, M. H., Zuo, R., Liu, C., et al. (2019). Autophagy mediates serum starvation-induced quiescence in nucleus pulposus stem cells by the regulation of P27. *Stem Cell Res. Ther.* 10 (1), 118. doi:10.1186/s13287-019-1219-8

Li, B., Yang, Y., Wang, L., and Liu, G. (2021). Stem cell therapy and exercise for treatment of intervertebral disc degeneration. *Stem Cells Int.* 2021, 1–10. doi:10.1155/2021/7982333

Li, Z., Chen, S., Ma, K., He, R., Xiong, L., Hu, Y., et al. (2020). Comparison of different methods for the isolation and purification of rat nucleus pulposus-derived mesenchymal stem cells. *Connect. Tissue Res.* 61 (5), 426–434. doi:10.1080/03008207.2019.1611793

Liao, Z., Liu, H., Ma, L., Lei, J., Tong, B., Li, G., et al. (2021). Engineering extracellular vesicles restore the impaired cellular uptake and attenuate intervertebral disc degeneration. *ACS Nano* 15 (9), 14709–14724. doi:10.1021/acsnano.1c04514

Liu, J., Yuan, C., Pu, L., and Wang, J. (2017). Nutrient deprivation induces apoptosis of nucleus pulposus cells via activation of the BNIP3/AIF signalling pathway. *Mol. Med. Rep.* 16 (5), 7253–7260. doi:10.3892/mmr.2017.7550

Lyu, F. J., Cheung, K. M., Zheng, Z., Wang, H., Sakai, D., and Leung, V. Y. (2019). IVD progenitor cells: A new horizon for understanding disc homeostasis and repair. *Nat. Rev. Rheumatol.* 15 (2), 102–112. doi:10.1038/s41584-018-0154-x

Ma, K., Chen, S., Li, Z., Deng, X., Huang, D., Xiong, L., et al. (2019). Mechanisms of endogenous repair failure during intervertebral disc degeneration. *Osteoarthr. Cartil.* 27 (1), 41–48. doi:10.1016/j.joca.2018.08.021

Marescal, O., and Cheeseman, I. M. (2020). Cellular mechanisms and regulation of quiescence. *Dev. Cell* 55 (3), 259–271. doi:10.1016/j.devcel.2020.09.029

Mellor, A. L., Munn, D., Chandler, P., Keskin, D., Johnson, T., Marshall, B., et al. (2003). Tryptophan catabolism and T cell responses. *Adv. Exp. Med. Biol.* 527, 27–35. doi:10.1007/978-1-4615-0135-0_3

Moya, A., Larochette, N., Paquet, J., Deschepper, M., Bensidhoum, M., Izzo, V., et al. (2017). Quiescence preconditioned human multipotent stromal cells adopt a metabolic profile favorable for enhanced survival under ischemia. *Stem Cells* 35 (1), 181–196. doi:10.1002/stem.2493

Oh, J. E., Shim, K. Y., Lee, J. I., Choi, S. I., Baik, S. K., and Eom, Y. W. (2017). 1-Methyl-L-tryptophan promotes the apoptosis of hepatic stellate cells arrested by interferon-γ by increasing the expression of IFN-γRβ, IRF-1 and FAS. *Int. J. Mol. Med.* 40 (2), 576–582. doi:10.3892/ijmm.2017.3043

Roberts, S., Evans, H., Trivedi, J., and Menage, J. (2006). Histology and pathology of the human intervertebral disc. *J. Bone Jt. Surg. Am. Volume* 88, 10–14. doi:10.2106/jbjs.f.00019

Rodgers, J. T., King, K. Y., Brett, J. O., Cromie, M. J., Charville, G. W., Maguire, K. K., et al. (2014). mTORC1 controls the adaptive transition of quiescent stem cells from G0 to G(Alert). *Nature* 510 (7505), 393–396. doi:10.1038/nature13255

Rumman, M., Majumder, A., Harkness, L., Venugopal, B., Vinay, M. B., Pillai, M. S., et al. (2018). Induction of quiescence (G0) in bone marrow stromal stem cells enhances their stem cell characteristics. *Stem Cell Res.* 30, 69–80. doi:10.1016/j.scr.2018.05.010

Sakai, D., and Grad, S. (2015). Advancing the cellular and molecular therapy for intervertebral disc disease. *Adv. Drug Deliv. Rev.* 84, 159–171. doi:10.1016/j.addr.2014.06.009

Scholz, T. D., TenEyck, C. J., and Schutte, B. C. (2000). Thyroid hormone regulation of the NADH shuttles in liver and cardiac mitochondria. *J. Mol. Cell. Cardiol.* 32 (1), 1–10. doi:10.1006/jmcc.1999.1047

Stuart, J. A., and Brown, M. F. (2006). Energy, quiescence and the cellular basis of animal life spans. *Comp. Biochem. Physiology. Part A, Mol. Integr. Physiology* 143 (1), 12–23. doi:10.1016/j.cbpa.2005.11.002

Theret, M., Gsaier, L., Schaffer, B., Juban, G., Ben Larbi, S., Weiss-Gayet, M., et al. (2017). AMPKα1-LDH pathway regulates muscle stem cell self-renewal by controlling metabolic homeostasis. *EMBO J.* 36 (13), 1946–1962. doi:10.15252/embj.201695273

Tong, W., Lu, Z., Qin, L., Mauck, R. L., Smith, H. E., Smith, L. J., et al. (2017). Cell therapy for the degenerating intervertebral disc. *Transl. Res.* 181, 49–58. doi:10.1016/j.trsl.2016.11.008

Urban, J. P. G., Smith, S., and Fairbank, J. C. T. (2004). Nutrition of the intervertebral disc. *Spine* 29 (23), 2700–2709. doi:10.1097/01.brs.0000146499.97948.52

Urban, N., and Cheung, T. H. (2021). Stem cell quiescence: The challenging path to activation. *Development* 148 (3), dev165084. doi:10.1242/dev.165084

Wang, F., Nan, L. P., Zhou, S. F., Liu, Y., Wang, Z. Y., Wang, J. C., et al. (2019). Injectable hydrogel combined with nucleus pulposus-derived mesenchymal stem cells for the treatment of degenerative intervertebral disc in rats. *Stem Cells Int.* 2019, 1–17. doi:10.1155/2019/8496025

Wang, W., Wang, Y., Deng, G., Ma, J., Huang, X., Yu, J., et al. (2018). Transplantation of hypoxic-preconditioned bone mesenchymal stem cells retards intervertebral disc degeneration via enhancing implanted cell survival and migration in rats. *Stem Cells Int.* 2018, 1–13. doi:10.1155/2018/7564159

Wang, Y., Yang, Y., Zuo, R., Wu, J., Zhang, C., Li, C., et al. (2020). FOXO3 protects nucleus pulposus cells against apoptosis under nutrient deficiency via autophagy. *Biochem. Biophys. Res. Commun.* 524 (3), 756–763. doi:10.1016/j.bbrc.2020.01.168

Wong, T. Y., Chang, C. H., Yu, C. H., and Huang, L. L. H. (2017). Hyaluronan keeps mesenchymal stem cells quiescent and maintains the differentiation potential over time. *Aging Cell* 16 (3), 451–460. doi:10.1111/acel.12567

Wu, J. L., Wu, Q. P., Peng, Y. P., and Zhang, J. M. (2011). Effects of L-malate on mitochondrial oxidoreductases in liver of aged rats. *Physiological Res.* 60 (2), 329–336. doi:10.33549/physiolres.931986

Wu, P. H., Kim, H. S., and Jang, I. T. (2020). Intervertebral disc diseases part 2: A review of the current diagnostic and treatment strategies for intervertebral disc disease. *Int. J. Mol. Sci.* 21 (6), 2135. doi:10.3390/ijms21062135

Wu, X., Liao, Z., Wang, K., Hua, W., Liu, X., Song, Y., et al. (2019). Targeting the IL-1β/IL-1Ra pathways for the aggregation of human islet amyloid polypeptide in an *ex vivo* organ culture system of the intervertebral disc. *Exp. Mol. Med.* 51 (9), 1–16. doi:10.1038/s12276-019-0310-7

Yao, B.-C., Meng, L.-B., Hao, M.-L., Zhang, Y.-M., Gong, T., and Guo, Z.-G. (2019). Chronic stress: A critical risk factor for atherosclerosis. *J. Int. Med. Res.* 47 (4), 1429–1440. doi:10.1177/0300060519826820

Yuan, J., Jia, J., Wu, T., Liu, X., Hu, S., Zhang, J., et al. (2020). Comprehensive evaluation of differential long non-coding RNA and gene expression in patients with cartilaginous endplate degeneration of cervical vertebra. *Exp. Ther. Med.* 20 (6), 1. doi:10.3892/etm.2020.9390

Zhang, X., Qiao, B., Hu, Z., Ni, W., Guo, S., Luo, G., et al. (2019). BMP9 promotes the extracellular matrix of nucleus pulposus cells via inhibition of the notch signaling pathway. *DNA Cell Biol.* 38 (4), 358–366. doi:10.1089/dna.2018.4478

Zhao, L., Manchikanti, L., Kaye, A. D., and Abd-Elsayed, A. (2019). Treatment of discogenic low back pain: Current treatment strategies and future options-a literature review. *Curr. Pain Headache Rep.* 23 (11), 86. doi:10.1007/s11916-019-0821-x

Zhao, Y., Jia, Z., Huang, S., Wu, Y., Liu, L., Lin, L., et al. (2017). Age-related changes in nucleus pulposus mesenchymal stem cells: An *in vitro* study in rats. *Stem Cells Int.* 2017, 1–13. doi:10.1155/2017/6761572

Zhou, X., Wang, J., Fang, W., Tao, Y., Zhao, T., Xia, K., et al. (2018). Genipin cross-linked type II collagen/chondroitin sulfate composite hydrogel-like cell delivery system induces differentiation of adipose-derived stem cells and regenerates degenerated nucleus pulposus. *Acta Biomater.* 71, 496–509. doi:10.1016/j.actbio.2018.03.019

Zhou, Z., Jiang, B., Zhou, Z., Pan, X., Sun, H., Huang, B., et al. (2013). Intervertebral disk degeneration: T1ρ MR imaging of human and animal models. *Radiology* 268 (2), 492–500. doi:10.1148/radiol.13120874

frontiers | Frontiers in Bioengineering and Biotechnology

TYPE Original Research
PUBLISHED 04 April 2023
DOI 10.3389/fbioe.2023.1076524

OPEN ACCESS

EDITED BY
Yori Endo,
Brigham and Women's Hospital and Harvard Medical School, United States

REVIEWED BY
Carolina Petrillo,
Columbia University Irving Medical Center, United States
Glyn Palmer,
University of Florida, United States

*CORRESPONDENCE
Jörn Stitz,
joern.stitz@th-koeln.de

SPECIALTY SECTION
This article was submitted to Preclinical Cell and Gene Therapy, a section of the journal Frontiers in Bioengineering and Biotechnology

RECEIVED 21 October 2022
ACCEPTED 24 March 2023
PUBLISHED 04 April 2023

CITATION
van Heuvel Y, Schatz S, Hein M, Dogra T, Kazenmaier D, Tschorn N, Genzel Y and Stitz J (2023), Novel suspension retroviral packaging cells generated by transposition using transposase encoding mRNA advance vector yields and enable production in bioreactors.
Front. Bioeng. Biotechnol. 11:1076524.
doi: 10.3389/fbioe.2023.1076524

Novel suspension retroviral packaging cells generated by transposition using transposase encoding mRNA advance vector yields and enable production in bioreactors

Yasemin van Heuvel[1,2], Stefanie Schatz[1,2], Marc Hein[3,4], Tanya Dogra[4], Daniel Kazenmaier[4,5], Natalie Tschorn[1,2], Yvonne Genzel[4] and Jörn Stitz[1]*

[1]Research Group Medical Biotechnology and Bioengineering, Faculty of Applied Natural Sciences, University of Applied Sciences Cologne, Campus Leverkusen, Cologne, Germany, [2]Institute of Technical Chemistry, Gottfried Wilhelm Leibniz University Hannover, Hanover, Germany, [3]Chair of Bioprocess Engineering, Otto-Von-Guericke-University Magdeburg, Magdeburg, Germany, [4]Max Planck Institute for Dynamics of Complex Technical Systems, Bioprocess Engineering, Magdeburg, Germany, [5]Faculty of Biotechnology, University of Applied Sciences Mannheim, Mannheim, Germany

To date, the establishment of high-titer stable viral packaging cells (VPCs) at large scale for gene therapeutic applications is very time- and cost-intensive. Here we report the establishment of three human suspension 293-F-derived ecotropic MLV-based VPCs. The classic stable transfection of an EGFP-expressing transfer vector resulted in a polyclonal VPC pool that facilitated cultivation in shake flasks of 100 mL volumes and yielded high functional titers of more than 1×10^6 transducing units/mL (TU/mL). When the transfer vector was flanked by transposon terminal inverted repeats (TIRs) and upon co-transfection of a plasmid encoding for the transposase, productivities could be slightly elevated to more than 3×10^6 TU/mL. In contrast and using mRNA encoding for the transposase, as a proof of concept, productivities were drastically improved by more than ten-fold exceeding 5×10^7 TU/mL. In addition, these VPC pools were generated within only 3 weeks. The production volume was successfully scaled up to 500 mL employing a stirred-tank bioreactor (STR). We anticipate that the stable transposition of transfer vectors employing transposase transcripts will be of utility for the future establishment of high-yield VPCs producing pseudotype vector particles with a broader host tropism on a large scale.

KEYWORDS

sleeping beauty transposon, mRNA transfection, suspension cell, retroviral vector, murine leukemia virus (MLV), stirred-tank bioreactor, gene therapy, mRNA transfection

Introduction

Retroviral and lentiviral vectors represent more than 25% of all viral vectors used in somatic gene therapy today (Ginn et al., 2018). Retroviral vectors mediate efficient stable gene transfer into a variety of cell types including early progenitor and hematopoietic stem cells. This qualifies these vectors to be the favorite choice for the treatment of inherited monogenic diseases. The

majority of current clinical trials aim at the treatment of adenosine deaminase-deficient severe combined immunodeficiency (ADA-SCID; (Blaese et al., 1995; Aiuti et al., 2002; Gaspar and Thrasher, 2005); X-linked severe immunodeficiency (SCID-X1 (Cavazzana-Calvo et al., 2000; Howe et al., 2008; Hacein-Bey-Abina et al., 2014; Cavazzana et al., 2016); or Wiskott-Aldrich syndrome (WAS (Boztug et al., 2010; Braun et al., 2014; Hacein-Bey Abina et al., 2015; Ferrua et al., 2019)).

Gamma-retroviral vectors based on murine leukemia virus (MLV) can be produced continuously employing stable viral packaging cells (VPCs) expressing the viral structural genes *gag/pol* (packaging construct), *env* (envelope construct) and a transfer vector harboring the gene of interest *in trans* (Maetzig et al., 2011). Most commonly, a transfer vector-free clonal VPC is first generated by screening numerous cell clones for particle production efficiencies (Miller, 1990; Cosset et al., 1995; Morita et al., 2000; Wang et al., 2015). In a second step, the transfer vector of choice is stably transfected followed again by a time-intensive screening of cell clones yielding high-titer vector preparations. To date, mostly adherent VPCs derived from human cell lines are used for clinical grade vector productions hampering the scale-up for preclinical and clinical trials (Coroadinha et al., 2010; Park et al., 2018). In contrast, VPCs that grow in suspension at higher densities as well as in serum-free media allow for viral vector productions in large bioreactors. In pioneering studies, Ghani and colleagues (Ghani et al., 2006; Ghani et al., 2007) established a retroviral packaging cell line derived from a human suspension 293SF cell producing retroviral titers of up to 4×10^7 transducing units per mL (TU/mL) comparable to yields obtained with adherent VPCs. However, a very time-intensive screening needed to be conducted to identify a high-yield transfer vector-positive VPC clone.

We previously reported on the generation of a stable polyclonal VPC using *Sleeping Beauty* (SB)- derived transposon vectors encompassing MLV-derived retroviral vector components, namely, an enhanced green fluorescent protein (EGFP) encoding transfer vector (pSB-LEGFP-N1), a packaging (pSB-Gag/Pol) and an ecotropic envelope construct (pSB-Env) were co-transfected with a transposase expression vector (pSB100X). Within 3 weeks, stable human adherent, as well as suspension VPCs were generated. These VPCs produced MLV-based vectors at high titers efficiently transducing murine-/and hamster cell lines, murine hematopoietic stem and early progenitor cells (HSPCs) as well as cell lines from different donor species recombinant expressing the murine cationic amino acid transporter (mCAT; (Berg et al., 2019; van Heuvel et al., 2021). Here, we describe the establishment of a polyclonal 293-F derived human suspension cell called MuPACK.e in only 3 weeks employing SB- and MLV-based packaging components.

Moreover, we examined whether the time-intensive screening for high-titer cell clones upon introduction of a transfer vector can be omitted. Therefore, we compared three different approaches: MuPACK.e cells were i) stably transfected with the transfer vector plasmid pLEGFP-N1 harboring the reporter genes *egfp* and *neomycin resistance* (*neoR*) - the most commonly used approach. ii) The transfer vector plasmid now encompassing the TIRs of SB flanking the transfer vector cassette (pSB-LEGFP-N1) was co-transfected with the transposase-expression plasmid pSB100X construct. iii) To increase biosafety and to exclude the genomic integration of pSB100X, and thus the potential sustained expression of the transposase possibly resulting in the re-mobilization of vector components, we co-transfected pSB-LEGFP-N1 together with *in vitro* transcribed mRNA encoding the highly active SB100X (Bire et al., 2013; Kebriaei et al., 2017; Tschorn et al., 2022). Subsequently, all 3 cell pools were selected for high transfer vector expression using escalating concentrations of neomycin (G418). Functional and physical vector titers were assessed conducting transduction experiments and vector particle quantification using capsid-specific ELISA and a quantitative reverse transcription PCR (RT qPCR). The most productive VPC established, using transposase transcripts, was further characterized employing enhanced cell densities and larger scale production in an automated stirred-tank bioreactor (STR).

Methods and materials

Cells

Embryonic human kidney suspension FreeStyle™ 293-F cells (Thermo Fisher Scientific, United States) were grown in FreeStyle™ 293 expression medium (Gibco, United States) or Dynamis™ supplemented with 8 mM L-glutamine (for STR, Gibco, United States) or GlutaMAX™ (for shake flasks, Gibco, United States). Cells were cultured at 37 °C, 8% CO_2, and at 137 rpm in shake flasks (Thermo Fisher Scientific, United States) using a Minitron shaker incubator (INFORS HT, Switzerland) with an orbit of 5 cm. The adherent NIH/3T3 murine fibroblast target cells (ATCC CRL-1658) were maintained in Dulbecco's modified Eagle medium high glucose, pyruvate (DMEM; Gibco, Germany), supplemented with 10% fetal bovine serum (FBS; Gibco, United States) at 37°C in a humidified atmosphere at 5% CO_2. Cell number and viability was accessed using a cell counter (anvajo GmbH, Germany).

Plasmids

The MLV-based retroviral transfer vector pLEGFP-N1 (Clontech, United States) harbors the *enhanced green fluorescent protein* (*EGFP*) and the *neomycin resistance* (*neoR*) genes. The generation of the transfer vector, the packaging construct, the envelope construct in transposon vector backbones and the transposase construct was described previously (Berg et al., 2019).

The *SB100X* gene was amplified from pCMV-SB100X (Berg et al., 2019) and inserted into pIVTRup (a gift from Ángel Raya (Addgene plasmid #101362; https://n2t.net/addgene:101362; RRID: Addgene_101362). This plasmid served as a template for PCR amplification using primers containing the T7 promoter and polyT tail sequences respectively. The resulting amplicons were subjected to *in vitro* transcription (IVT) of SB100X-mRNA using HiScribe™ T7 ARCA mRNA Kit (NEB, USA) following the manufacturer's instructions, respectively. After DNase treatment, the mRNA was purified using the Monarch® RNA Cleanup Kit (NEB, United States). RNA purity was confirmed using a Tecan Infinite® and stored in aliquots at −80°C. The final mRNA encompassed the 5′-Cap, the 5′-UTR, the coding sequence of the transposase, the 3′-UTR and the polyA tail (Tschorn et al., 2022).

TABLE 1 Operating bioreactor production parameters.

Parameter	Bioreactor DASGIP® eppendorf
Basal medium	Dynamis™ + 8 mM L-glutamine
Initial working volume	500 mL
Agitation	150 rpm
Agitation direction	Downflow
Air flowrate	3 L/h
Initial dissolved oxygen (DO)	89.7%
Temperature	37 °C
pH	7.09 no active control post inoculation
Initial VCD	0.84×10^6 cells/mL

Establishment of stable ecotropic MLV-based vector packaging cells MuPACK.e

Packaging cells were generated by co-transfection of 3×10^7 293-F cells in 20 mL shake flask cultures with 35.6 µg of pSB-gag/pol, 11.9 µg of pSB-env and 2.5 µg of the transposase construct using polyethylenimine transfection reagent (PEI:DNA mass ratio of 3:1; linear PEI, 1 mg/mL, MW 40,000; Polysciences Inc., United States). 9 mL fresh medium was added 3 hours later and a complete medium exchange was performed on the following day. Two days post-transfection, cells were subjected to 4 µg/mL puromycin and 50 µg/mL hygromycin (both InvivoGen, France). Every passage, the concentration of both antibiotics was escalated to a final concentration of 10 µg/mL puromycin and 200 µg/mL hygromycin resulting in a stable VPC bulk population called MuPACK.e within 21 days.

The subsequent transfections with the respective transfer vectors were performed as described in detail (Bauler et al., 2020). For 30 million cells a total amount of 16.5 µg of pDNA/mRNA was co-transfected. A mass ratio of 1:10 (transposase to transfer vector) for the plasmid-based transposase construct and a mass ratio of 1 to 1 for the mRNA encoding the transposase was used (PEI:DNA mass ratio of 2:1 and PEI:mRNA mass ratio of 4:1; linear PEI, 1 mg/mL, MW 40,000; Polysciences Inc., United States). The mRNA-PEI mixes in this case were always prepared in a separate tube and PEI was diluted directly into the mRNA-medium mixture. VPCs stably expressing a transfer vector were subjected to G418 mediated selection pressure 4 days post-transfection at increasing concentrations of G418 ranging from 50 µg/mL to a final concentration of 200 µg/mL. Two weeks post antibiotic selection with G418, all three antibiotics were added at final concentrations of 10 µg/mL puromycin and 200 µg/mL hygromycin and G418. After 3 weeks, for transposition-based transfection and 2 month for classical plasmid-based transfection, and rigorous selection, cells were expanded and cryo-stocks were made and rigorous selection, cells were expanded and cryo-stocks were prepared.

MLV vector productions in shake flasks and STR

Stable VPCs were seeded at a viable cell density of 2×10^6 cells/mL in 500 mL shake flasks in 100 mL antibiotic-free FreeStyle™ medium or Dynamis™ supplemented with 8 mM GlutaMAX™. After 24 h of production, retroviral vectors were harvested by centrifugation at 100 *g* for 3 min at RT and made cell-free using a PVDF syringe filter with a 0.45 µm pore size (Carl Roth, Germany). Retroviral vector preparations were frozen at −80°C in 1.8 mL aliquots. For high-density VPC cultivations, the stable VPC was seeded at 4×10^6 cells/mL in 250 mL shake flasks in 50 mL Dynamis™ medium supplemented with 8 mM GlutaMAX™ and MLV-based vectors were harvested after 48, 72 and 96 h.

For larger-scale vector production, cultivation in an STR with a 500 mL working volume (DASGIP® Parallel Bioreactor System, Eppendorf AG, Cat. 76DG04CCBB) was performed. The STR was equipped with one inclined blade impeller (three blades, 30°angle, 50 mm diameter) and a macro-sparger. Production parameters are shown in Table 1 Prior to inoculation, the stable VPC MuPACK.e.SB-LEGFP.N1$_{mRNA}$ was thawed and expanded in Dynamis™ medium supplemented with highest concentrations of antibiotics in shake flasks for 2 weeks. When cultures showed viabilities >90% and a density of 2×10^6 cells/mL, cells were centrifuged (300 g, 5 min, RT) and the complete medium was replaced with fresh antibiotic-free Dynamis™ medium. The STR was inoculated with 0.8×10^6 cells/mL and ran at 37°C, $pO_2 \geq 40\%$, controlled pH 7.0 (deadband ±0.3), and 150 rpm for 10 days. During cultivation thirteen independent viral vector harvests (5 mL) were taken from the cultivation vessel, made cell-free by centrifugation (3,000 g, 10 min at 4°C) and stored at −80°C. The STR was operated in batch mode.

Viral vector titration and flow cytometry

To assess the viral vector titers produced by the established VPCs, 1.0×10^5 adherent target NIH/3T3 murine fibroblasts were seeded in 2 mL per well in six-well dishes 1 day prior to transduction (Nunc, Wiesbaden, Germany). Dilutions of 1:1,000 and 1:10,000 and of retroviral vector samples produced in shake flasks in total volumes of 1 mL were added to target cells. The following day, 1 mL of fresh cultivation medium was added to transduced cells. Three days post-transduction, the percentage of EGFP-positive cells was analyzed using flow cytometry (S3e, Bio Rad, United States; FlowJo BD Biosciences, United States) and used to detect gene transduction efficiencies. Vector titers described as transducing units per mL (TU/mL) were calculated as follows: titer = (F %/(100 × V_{mL})) × S × D wherein F% is the percentage of GFP-positive transduced cells, S represents the number of seeded target cells on the day of transduction, D the dilution factor and V_{mL} the volume of viral vector in mL (Fehse et al., 2004).

For the viral vector titration using vectors produced in STR, adherent target cells were seeded in 48-well dishes at 1×10^4 cells/well in 0.5 mL 1 day prior to transduction. The medium was removed and vector containing supernatant samples in different dilutions of 1:10, 1:100 and 1:1,000, respectively, in a total volume of 0.25 mL were added to the target cells. Three days post-transduction, cells were analyzed employing flow cytometry to determine the percentage of EGFP-positive cells. Vector titers were calculated as described previously employing supernatant dilutions resulting in gene transfer efficiencies between 1.0% and 10.0% EGFP-positive cells (Salmon and Trono, 2007).

To detect the fluorescence intensities of the three VPCs or transduced target cells expressing the EGFP expressing transfer vector, 1×10^6 cells were centrifuged at 100 *g* for 5 min and the cell pellet was diluted in 1 mL flow cytometry buffer (phosphate-buffered saline (PBS), pH 7.2, 0.5% bovine serum albumin (BSA) and 2 mM EDTA). Prior to flow cytometry, viability was determined using an anvajo cell counter (anvajo GmbH, Germany). A total of 10,000 gated single cells were subsequently analyzed for EGFP expression.

Quantification of retroviral vectors using an anti MLV p30 immunoassay

To assess the efficiency of viral vector production, total particle concentration (i.e., physical titer) were quantified using a colorimetric MuLV core p30 antigen ELISA kit (Cell Biolabs, Inc. (Cat. VPK-156, United States)). From each cell-free retroviral particle harvest, one sample was used to detect the total p30 concentration. Samples were thawed from −80°C and diluted 1:10,000 in expression medium and assayed in a 96-well plates in duplicate.

Quantification of transfer vector transcripts in vector particles using RT-qPCR

To quantify the viral vector transfer vector RNA (i.e., physical titer), a real-time reverse transcription quantitative PCR (RT-qPCR) was performed. Cell-free and viral vector-containing cell culture supernatant was used for the extraction and purification of vector RNA according to the manufacturer's instructions (NucleoSpin® RNA virus kit; Macherey-Nagel, Germany).

A two-step hot start RT-qPCR with sequence-unrelated tagged primers was used to specifically quantify viral vector EGFP mRNA copies (Kawakami et al., 2011). Briefly, an external calibration curve was generated for the EGFP-encoding sequence by amplifying from the pLEGFP-N1 transfer vector template plasmid using the primers: T7-gag/EGFP for 5′- TAATACGACTCACTATAGGGATGGTGA GCAAGGGC -3′ and T7-gag/EGFP rev 5′- GCTAGCTTCAGC TAGGCATCTTACTTGTACAGCTCGTCC -3'. 300 ng of the amplicons were *in vitro* transcribed to RNA for 2 h at 37°C using TranscriptAid T7 High Yield Transcription Kit (ThermoFisher Scientific, United States). Transcribed RNA standards were treated with 10 vol% DNase (30 min, 37°C) followed by 10 vol% EDTA treatment (15 min, 65°C) and purified using an RNA isolation kit (Macherey Nagel, Germany).

Subsequently, a hot start reverse transcription PCR was performed. Here, 1 µL of each EGFP mRNA sample and of each generated RNA standard (ranging from 5.0E-07 ng to 5.0E+00 ng), 0.5 µL of dNTPs, 6.5 µL of nuclease-free water and 0.5 µL MLV EGFP tagged RT primer (rev 5′- GCTAGCTTCAGCTAGGCATCTTACTTGTACAGCTCG TCCA -3)' was first incubated at 65°C for 5 min and then at 55 °C for 5 min. For cDNA synthesis, 2 µL of 5X RT buffer (Thermo Fisher Scientific, USA), 1.25 µL of nuclease-free water, and 0.25 µL of Maxima H minus reverse transcriptase (Thermo Fisher Scientific, United States) were added and incubated (30 min, 60°C), before the reaction was terminated (5 min, 85°C). The generated cDNA was diluted to 100 µL.

To perform the qPCR, 4 µL diluted cDNA, 5 µL of 2X QuantiNova SYBR green PCR mix (QIAgen, Germany), and 0.5 µL each of 1 µM primers EGFP qPCR for 5′-CTCGCCGACCACTACC -3′ and EGFP tagged qPCR rev 5′-GCTAGCTTCAGCTAGGCATC-3′ were mixed. For the real-time quantification, samples were subjected to initial denaturation (5 min, 95°C), before 40 amplification cycles (10 s, 95°C; 20 s, 62°C) were carried out. The melt curve analysis was between 65°C and 90°C. For absolute quantification, a regression curve analysis was formulated by plotting the CT values of ten-fold diluted RNA standards against the log10 number of the RNA molecules (Frensing et al., 2014).

Detection of replication-competent retroviruses (RCRs): GFP marker rescue assay and reverse transcriptase (RT) assay

To ensure that detected gene transfer efficiencies were purely a result of vector-mediated transduction and not caused by the unintended generation of RCRs originating from the recombination of complementary vector components, GFP marker rescue assays were performed in triplicate as previously described in detail (Cosset et al., 1995; Berg et al., 2019; van Heuvel et al., 2021). In addition, NIH/3T3 target cells were exposed to vector preparations, expanded and supernatant of transduced cells was collected after five and 12 days. Subsequently, samples were examined using a reverse transcriptase (RT) assay with a detection sensitivity of 10 pg RT per 40 µL sample (Colorimetric reverse transcriptase assay, Roche, Switzerland) following the manufacturer's instructions. Supernatants of stable VPCs and NIH/3T3 cells exposed to the supernatant of naïve 293-F cells served as positive controls and negative controls, respectively (data not shown).

Statistics

An unpaired Student's t-test was used to calculate *p* values. *p* values of less than 0.05 were considered statistically significant (*($p \leq 0.05$), **($p \leq 0.01$), ***($p \leq 0.001$), ****($p \leq 0.0001$)). Graphs and statistics were calculated using GraphPad Prism 7 for Windows 10 software (GraphPad Software, Inc. United States).

Results

Generation of stable MuPACK.e based VPCs

The stable polyclonal suspension VPC MuPACK.e based on ecotropic MLV was established as described using the expression cassettes illustrated in Figure 1, namely, the packaging and envelope construct pSB-Gag/Pol and pSB-Env together with the transposase encoding plasmid pSB100X followed by selection using puromycin and hygromycin. Upon transfection with the constructs illustrated in Table 2 namely, i) only with pLEGFP-N1, ii) with pSB-LEGFP-N1 and the transposase construct and iii) with pSB-LEGFP-N1 and the mRNA of SB100X, stable cell pools were established in the presence of escalating concentrations of G418. Cell-free supernatants of the resultant VPCs MuPACK.e.LEGFP-N1,

10.3389/fbioe.2023.1076524

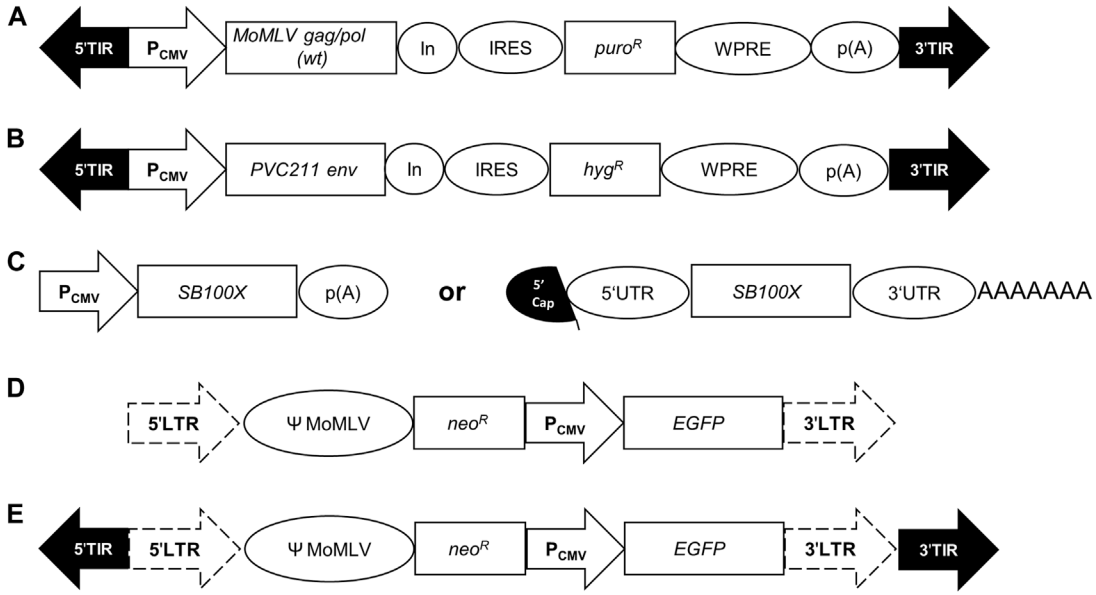

FIGURE 1
Genetic organization of expression cassettes. **(A)** In the packaging construct pSB-Gag/Pol, a CMV promoter/enhancer element (P_{CMV}) drives the expression of the wildtype (wt) Moloney MLV (MoMLV) genes *gag/pol* followed by a synthetic intron (In), an internal ribosome entry site (IRES), a puromycin-resistance gene (*puro*^{R}), the Woodchuck hepatitis virus tripartite posttranscriptional regulatory element (WPRE) and the polyadenylation signal (p(A)) of the bovine growth hormone gene. **(B)** The envelope construct pSB-Env encompasses the human codon-optimized ecotropic envelope gene *env* derived from the Friend MLV molecular clone PVC-211 and the hygromycin-resistance gene (*hyg*^{R}). (**(C)**, left) The transposase construct pSB100X harbors the human codon-optimized gene of the hyper-active *Sleeping Beauty* transposase SB100X. (**(C)**, right) The transcript mRNA-SB100X encompasses the 5′Cap, the 5′UTR, the coding sequence of the transposase *SB100X*, the 3′UTR and a polyA tail (AAAAAAA). **(D)** The transfer vector pLEGFP.N1 encompasses the 5′- and 3′-long terminal repeats (LTRs; dotted arrows) of murine leukemia virus (MLV) flanking the packaging signal Ψ of MoMLV, a neomycin-resistance gene (*neo*^{R}) and a P_{CMV} driven *EGFP* expression. **(E)** The transfer vector pSB-LEGFP.N1 contains the same genetic elements as pLEGFP.N1 but with the flanking 5′- and 3′-terminal inverted repeats (TIRs; black arrows) of *Sleeping Beauty*.

TABLE 2 Overview of plasmids and mRNA employed to generate polyclonal viral packaging cell lines.

VPC:Plasmids, mRNA	MuPACK.e	MuPACK.e. LEGFP-N1	MuPACK.e. SB-LEGFP-N1	MuPACK.e. SB-LEGFP-N1$_{mRNA}$
pSB-Gag/Pol	X	X	X	X
pSB-Env	X	X	X	X
pSB100X	X	X	X	X
mRNA-SB100X	—	—	—	X
pLEGFPN.1	—	X	—	—
pSB-LEGFP.N1	—	—	X	X

MuPACK.e.SB-LEGFP-N1 and MuPACK.e.SB-LEGFP-N1$_{mRNA}$ were harvested and frozen at −80°C. Thawed harvests were subjected to three independent titration experiments conducted in triplicate using murine NIH/3T3 target cells. Transduced cells were analyzed 3 days later for EGFP expression.

Functional titers of generated MLV-based vectors

As depicted in Table 3 MuPACK.e.LEGFP-N1 generated mean vector titers ranging from 9.63×10^5 to 2.16×10^6 TU/mL. Viabilities of the VPC at the time of vector harvests varied between 76% and 85%. With viabilities of always >90%, MuPACK.e.SB-LEGFP-N1 revealed slightly higher titers of 2.17×10^6 to 3.21×10^6 TU/mL. MuPACK.e.SB-LEGFP-N1 showed stable productivity over a period of 2 months in the presence as well as absence of selection pressure (data not shown). The VPC MuPACK.e.SB-LEGFP-N1$_{mRNA}$ showed the by far highest productivity when cells were cultured in FreeStyle™ medium (harvests 1). Titers of 5.12×10^7 TU/mL were detected at VPC viabilities of 80%, respectively.

When the VPC was expanded in Dynamis™ (harvests 2 and 3), known as one of the mediums of choice for batch- and fed-batch cultivation of highly efficient mammalian producer cells, to prepare for cultivation at high densities in an STR or in perfusion cultivation, cell viabilities varied between 73% and

TABLE 3 Functional titers in TU/mL and physical titers in ng/mL (ELISA) of vector particles harvested from the stable VPCs. Frozen-thawed vector preparations harvested from volumes of 100 mL VPC cultures at viable cell densities (VCD) of 4 × 10^6 cells/mL in FreeStyle™ medium in 500 mL shake flasks were titrated in triplicate in NIH/3T3 target cells or measured in a 1:10,000 dilution in an ELISA. In harvests 2 and 3 of VPC MuPACK.e.SB-LEGFP-N1$_{mRNA}$ cells were cultivated in Dynamis™ expression medium. Standard deviations (SD) of mean are indicated.

VPC	Harvest	Viability [%]	Mean titer [TU/mL]	SD	Mean p30 [ng/mL]	SD
MuPACK.e. LEGFP-N1	1	76	9.63×10^5	$\pm 0.35 \times 10^5$	6.38×10^4	$\pm 0.96 \times 10^4$
	2	85	1.26×10^6	$\pm 0.05 \times 10^6$	8.02×10^4	$\pm 1.71 \times 10^4$
	3	85	2.16×10^6	$\pm 0.15 \times 10^6$	1.16×10^5	$\pm 0.22 \times 10^5$
MuPACK.e. SB-LEGFP-N1	1	92	2.17×10^6	$\pm 0.11 \times 10^6$	3.75×10^4	$\pm 1.89 \times 10^4$
	2	90	2.66×10^6	$\pm 0.21 \times 10^6$	5.04×10^4	$\pm 0.17 \times 10^4$
	3	94	3.21×10^6	$\pm 0.32 \times 10^6$	4.24×10^4	$\pm 1.54 \times 10^4$
MuPACK.e. SB-LEGFP-N1$_{mRNA}$	1	80	5.12×10^7	$\pm 0.51 \times 10^7$	7.20×10^4	$\pm 0.78 \times 10^4$
	2	73	2.00×10^7	$\pm 0.05 \times 10^6$	1.86×10^5	$\pm 0.24 \times 10^5$
	3	90	3.10×10^6	$\pm 0.55 \times 10^6$	1.12×10^5	$\pm 0.01 \times 10^5$

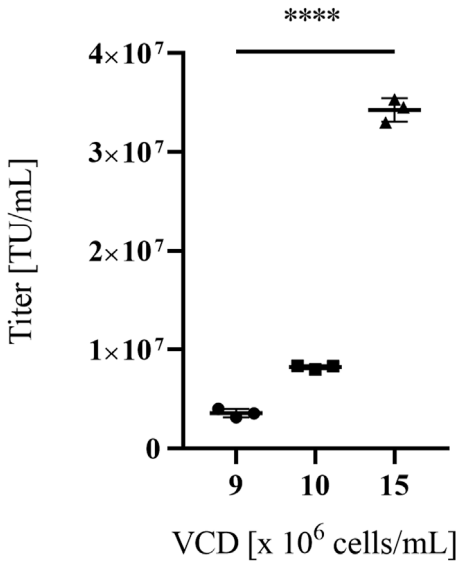

FIGURE 2
Titers of MLV-based vectors in NIH/3T3 target cells of VPC MuPACK.e.SB-LEGFP-N1$_{mRNA}$. Viral vectors were harvested at three different viable packaging cell densities (VCDs) of 9-, 10- and 15 × 10^6 cells/mL. Data shown represent values of technical triplicate experiments ± standard deviation. Statistical significance for all three VPCs with n = 3 was determined to $p \leq 0.0001$(****) using the tailed unpaired Student's t-test.

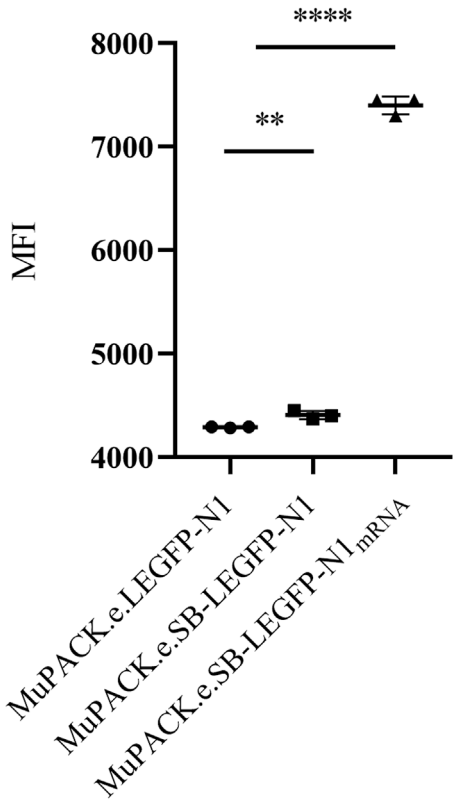

FIGURE 3
Median fluorescent intensities (MFI) of the three VPCs: MuPACK.e.LEGFP-N1, MuPACK.e.SB-LEGFP-N1 and MuPACK.e.SB-LEGFP-N1$_{mRNA}$. Data shown represent measurements in technical triplicates ±standard deviation. Statistical significance between MuPACK.e.SB-LEGFP-N1 and MuPACK.e.SB-LEGFP-N1$_{mRNA}$ based data with n = 3 was determined to $p \leq 0.0001$ (****); between MuPACK.e.LEGFP-N1 and MuPACK.e.SB-LEGFP-N1 was $p \leq 0.01$ (**) using a tailed unpaired Student's t-test.

90% and vector titer productivities of 2.00 × 10^7 TU/mL and 3.10 × 10^6 TU/mL were achieved. For high viable cell density cultivations (VCD), represented in Figure 2, VPCs were cultivated at 50 mL scale and vector particle harvests at VCDs of 9, 10 and 15 × 10^6 cells/mL were titrated in NIH/3T3 cells. VCDs correlated with functional vector titers ranging from 3.58 × 10^6 TU/mL at 9 × 10^6 cells/mL to 3.43 × 10^7 TU/mL at 15 × 10^6 cells/mL in NIH/3T3 cells.

These results were supported by the median fluorescence intensities (MFIs) of the three VPCs detected by flow cytometry and represented in Figure 3. The highest expression of EGFP was detected in MuPACK.e.SB-LEGFP-N1$_{mRNA}$ showing a significantly higher MFI of more than 7,000 compared to

10.3389/fbioe.2023.1076524

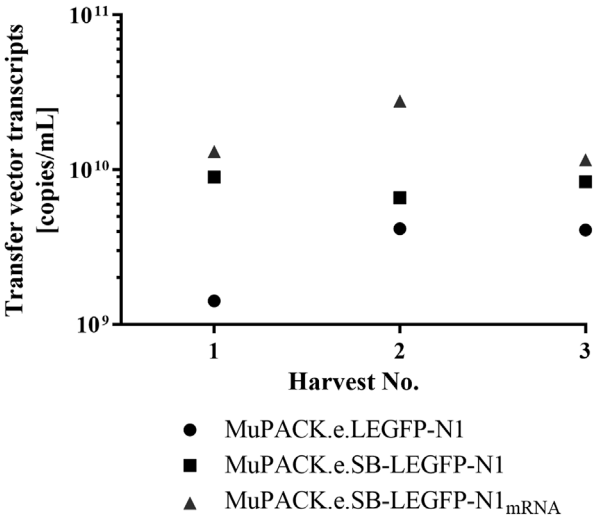

FIGURE 4
Physical titers of transfer vector transcripts in vector particles measured by real-time RT-qPCR. EGFP-specific primers were used to generate amplicons using LEGFP-N1 mRNA packaged in vector particles in each three harvests of the three VPCs (depicted in Table 3). Mean values from assays performed in analytical duplicates are indicated. Dots: MuPACK.e.LEGFP-N1, rectangles: MuPACK.e.SB-LEGFP-N1, triangles: MuPACK.e.SB-LEGFP-$N1_{mRNA}$.

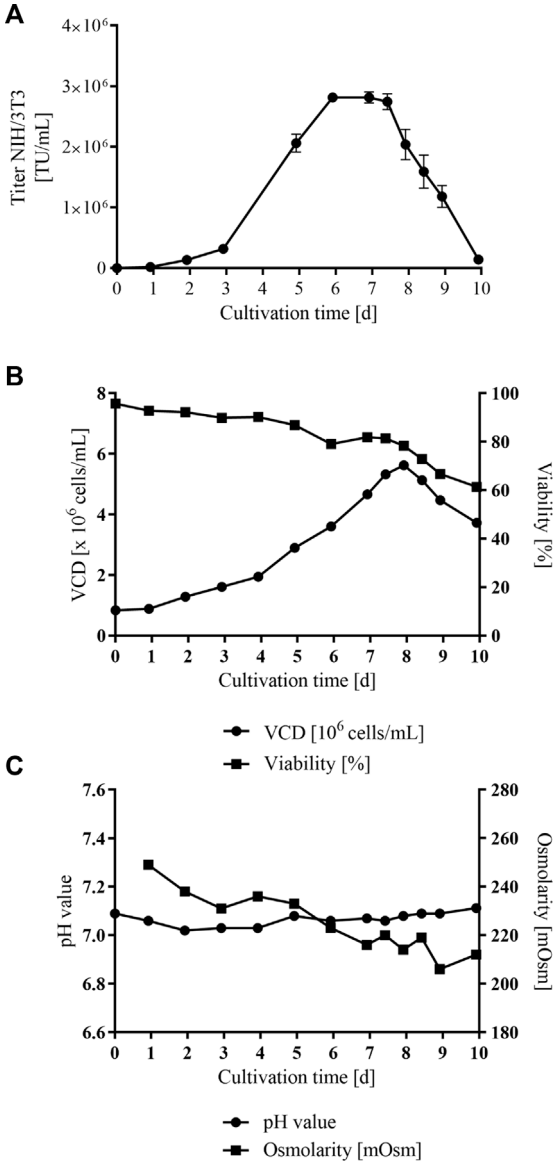

FIGURE 5
Stirred-tank bioreactor vector particle production over 10 days with VPC MuPACK.e.SB-LEGFP-$N1_{mRNA}$. **(A)** NIH/3T3 cells were transduced with cell-free MLV vector containing supernatants harvested at twelve time points. Data points represent average values of technical triplicates, standard deviations are shown as vertical error bars. **(B)** Viable VPC density (VCD) in 1 × 10^6 cells/mL (dots) and cell viability in % (rectangles) during a 10-day STR cultivation. **(C)** pH values (dots) and Osmolarity in mOsm (rectangles) during a 10-day STR cultivation.

the two other VPCs with MFIs between 4,000 and 5,000 ($p \leq 0.0001$).

Physical titer assessment using p30 capsid-specific ELISA

To evaluate the total amount of MLV capsid protein p30 within the three cell-free VPC harvests, a colorimetric ELISA assay was performed, depicted in Table 3. Average p30 concentrations of all three harvests (not shown in Table 3) were for MuPACK.e.LEGFP-N1 8.65 × 10^4 ng/mL (±2.65 × 10^4), for MuPACK.e.SB-LEGFP-N1 4.34 × 10^4 ng/mL (±0.65 × 10^4) and for MuPACK.e.SB-LEGFP-$N1_{mRNA}$ 1.23 × 10^5 ng/mL (±0.58 × 10^5).

Detection of transfer vector transcripts in vector particles using RT-qPCR

The different functional vector titers were likely to result from different transfer vector transcript amounts available for packaging into the vector particles. Thus, RT-qPCR was performed in duplicate using frozen cell-free samples from all VPC vector harvests and EGFP-specific primers. As illustrated in Figure 4, the mean amount of mRNA detected confirmed the trend observed in functional vector titers obtained from all three VPCs. MuPACK.e.SB-LEGFP-$N1_{mRNA}$ (1.16 × 10^{10} to 2.78 × 10^{10} copies/mL) revealed the highest amount of packaged transcripts as compared to MuPACK.e.SB-LEGFP-N1 (6.60 × 10^9 to 8.96 × 10^9 copies/mL), while MuPACK.e.LEGFP-N1 yielded the lowest amounts of encapsidated mRNA (1.42 × 10^9 to 4.16 × 10^9 copies/mL).

Production and functional titer of MLV vectors in STR

To enable vector production at a larger scale, a cultivation in STR was examined with the most productive stable VPC

MuPACK.SB-LEGFP.N1$_{mRNA}$. Cells were cultivated for 10 days in 500 mL Dynamis™ medium supplemented with 8 mM L-glutamine in the absence of antibiotics and medium change as described in detail in materials and methods as well as in Table 1. Figure 5 shows the retroviral vector titers detected in NIH/3T3 cells during a 10 days STR procedure. The VPC culture revealed increasing productivity up to day 6. As illustrated in Figure 5A and at the onset of the culture process, the titers were rather low with about 1×10^5 TU/mL correlating with the low VCD of less than 2×10^6 cells/mL. With increasing VCDs up to 6×10^6 cells/mL (Figure 5B) the transduction-competent particle numbers also increased, generating titers of up to 2.81×10^6 TU/mL in NIH/3T3 cells at day 6. From day 6 to day 7, productivity stayed on a small plateau and from day 7 on, the VCDs continuously decreased to 3.72×10^6 cells/mL resulting in declining titers of 2.04×10^6 TU/mL down to 1.4×10^5 TU/mL at the end of the STR process on day 10. A linear scalability was observed until day 6 of production remaining then on a plateau. From day 8 on and as no medium exchange was performed, the vector production rate, as well as vector titer, dropped in correlation with the decline in VCDs and viability, respectively. While osmolality slightly decreased over time from 249 to 212 mOsm, pH values remained considerably stable around 7.0 (+deadband) throughout the process (Figure 5C).

Discussion

To facilitate high vector yield production in larger scale, stable suspension VPCs are indispensable. In the first step and within only 3 weeks, we established the polyclonal ecotropic MLV-derived suspension VPC MuPACK.e using transposon vector components as previously described and shown in efficient transduction experiments in murine myeloblast-like cells as well as in hematopoietic stem and progenitor cells (Berg et al., 2019; van Heuvel et al., 2021). The establishment of stable high-titer producing VPCs co-expressing the transfer vector of choice is a tedious and time-consuming process. To reduce development times, we compared in a proof-of-concept study three stable gene transfer techniques. In one approach i) the transfer vector plasmid pLEGFP-N1 was simply stably transfected. ii) The transfer vector cassette was flanked by SB-derived TIRs and co-transfected with a transposase plasmid construct pSB100X aiming at the stable transposition of the viral vector component into the VPCs genomes. iii) To exclude the undesired stable transfection of pSB100X and the expression of the transposase over a period of one week, pSB-LEGFP-N1 was co-transfected with mRNA-SB100X.

MuPACK.e.LEGFP-N1 produced vectors at high titers of 9.63×10^5 to 2.16×10^6 TU/mL in NIH/3T3 target cells. These results exceed previously reported ecotropic MLV vector titers. Chan et al. established a human lymphoblast WIL-2 cells-derived suspension VPC using conventional plasmid transfection obtaining 7.5×10^5 TU/mL in NIH/3T3 cells (Chan et al., 2001). MuPACK.e.SB-LEGFP-N1 generated only moderately improved titers between 2.17×10^6 and 3.21×10^6 TU/mL.

MuPACK.e.SB-LEGFP-N1$_{mRNA}$ showed drastically increased productivities reaching vector titers of up to 5.12×10^7 TU/mL when cultivated in 100 mL shake flask volumes at a cell density of 4×10^6 cells/mL in FreeStyle™ or in Dynamis™ medium, respectively. In addition, these results were supported by the physical titers detected using an anti-p30 ELISA. MuPACK.e.SB-LEGFP-N1$_{mRNA}$ showed p30 amounts a power of ten higher than the other two VPCs. Contaminations with RCRs resulting from recombination events of the retroviral vector components were not detected in any of the vector particle preparations conducting a GFP-marker rescue assay and a sensitive RT-detection assay (data not shown).

The high abundance of the transfer vector RNA available for packaging in concert with high level expression of Gag/Pol is a crucial prerequisite for the efficient formation of transduction-competent vector particles (Berg et al., 2019; Sweeney and Vink, 2021). Flow cytometric analysis of the three VPCs revealed different expression levels of EGFP, and thus indicating differences in transfer vector transcript amounts. MuPACK.e.SB-LEGFP-N1$_{mRNA}$ showed a significantly higher MFI compared to the two other VPCs.

Consequently and to assess whether these differences also mirrored the copy number of encapsidated transfer vector mRNA, vector particle harvests from all three VPCs were examined using RT-qPCR. MuPACK.e.SB-LEGFP-N1$_{mRNA}$ showed the highest amount of packaged transfer vector RNA followed by MuPACK.e.SB-LEGFP-N1 and MuPACK.e.LEGFP-N1 confirming the trend observed in functional vector titers. However, the RNA levels were two to three orders of magnitude higher than the functional titers in respective target cells. This gap using two different measurements was previously reported by Geraerts and colleagues 2006 (Geraerts et al., 2006). Transfer vector RNAs detected in the supernatant of the VPCs using qPCR are not necessarily encapsidated (Onafuwa-Nuga et al., 2005; Rulli et al., 2007; Eckwahl et al., 2016).

FreeStyle™ medium limits the VCDs to 4×10^6 cells/mL. We thus conducted a high VPC density experiment in Dynamis™ medium in a 50 mL shake flask scale. VCDs could be elevated to 1.5×10^7 cells/mL reaching titers of up to 3.43×10^7 TU/mL in NIH/3T3 cells. This encouraged us to conduct a first STR pilot cultivation. VPC MuPACK.e.SB-LEGFP-N1$_{mRNA}$ was expanded at larger scale using 500 mL volume STR employing Dynamis™. When the VPC was seeded at a VCD of 0.84×10^6 cells/mL, the maximal cell density peaked at 5.62×10^6 cells/mL along with increasing viability. The highest vector titers of up to 2.81×10^6 TU/mL were obtained on day 6. Osmolality and pH values were moderately decreasing and remained stable, respectively, over the entire cultivation period of 10 days. Viral vector titer and viability decline from day 7 on correlated with the decreasing availability of essential nutrients within the expression medium and with an increase of metabolic degradation products. In addition and observed previously, the amount of cellular proteases may have increased, and thus degraded MLV vector particles (Genzel et al., 2010; Petiot et al., 2011; Hein et al., 2021). Therefore, and to reach productivities of $>1 \times 10^7$ TU/mL in fed-batch approaches, the seed VCD of VPCs should be increased to 2 or 4×10^6 cells/mL allowing the cells to linearly grow to densities of 1.5×10^7 cells/mL or even higher values within the first two or 3 days. Alternatively, fully automated high-density perfusion reactors could be employed, and process parameters would need to be optimized.

Serving as a proof-of-concept, only one VPC pool per transfection technique of the transfer vector was examined here. However, our findings still strongly indicate that the use of

transposon-encoding mRNA is superior to the employment of plasmid-based transposase. Using a ratio of 1:1 (transposase transcript to transfer vector plasmid) instead of a ratio of 1:10 (plasmid-based transposase to transfer vector plasmid) for stable transposition presumably led to a higher availability of active transposases, elevating transposition efficiency. The high amount of transposon-encoding mRNA probably resulted in enhanced copy numbers of SB-LEGFP-N1 per cell genome. Transposase transcripts limit transposase expression to about 18 h Bire et al., 2013). Within this time, a high abundance of transiently co-transfected transposon donor plasmids are available and are likely to facilitate the superior transposition. Using mRNA-based transposase expression appears to avoid overexpression inhibition (OPI) or cytotoxicity observed when plasmid-based transposase constructs are used (Grabundzija et al., 2010; Galla et al., 2011; Bouuaert et al., 2013). OPI is most likely a result of high transposase activity over a period of up to 14 days. A prolonged expression of the transposase could lead to re-mobilization and possibly depletion of packaging and envelope donor expression cassettes resulting in less efficient production of viral vector particles.

To date, larger scale retroviral vector productions are mainly done in cell-factories, packed-bed bioreactors or fixed-bed-bioreactors using adherent VPCs. The cells thus grow on a limited area of the stacked cultivation devices or scaffolds such as beads and microfibers (Merten et al., 2001; Wang et al., 2015; Powers et al., 2020). MLV vectors pseudotyped with the Env proteins of Gibbon ape Leukemia virus (GaLV) with titers ranging from 7.88×10^5 up to 3×10^7 TU/mL could be generated using fixed-bed bioreactors in volumes of 200 mL to 1.4 L, respectively (Merten et al., 2001). Using STRs and perfusion reactors instead, generated MLV vectors pseudotyped with GaLV Env and vesicular stomatitis virus G protein (VSV-G) with titers between 5×10^5 and 3.1×10^7 TU/mL, respectively (Merten et al., 2001; Ghani et al., 2006). The packaging cell line PG13 stably transfected with a transfer vector reached titer of 2×10^6 TU/mL and a *piggy-bac* transposon SIN packaging cell line produced titers of up to 3×10^6 TU/mL. A non-transposon-based amphotropic suspension packaging cell line called 293 GP-A2 produced titers of 4×10^7 TU/mL at a VCD of 12×10^6 cells/mL. However the mean time to develop this stable VPC took several months (reviewed in Park et al., 2018).

Ecotropic MLV vectors, as shown here in our proof-of-concept study, were not yet produced at such titers. We thus anticipate that the VPC MuPACK.e and our approach to rapidly establish VPCs within only 3 weeks using mRNA-based transposase transcripts will foster future viral vector productions at larger scale to facilitate preclinical *ex vivo* gene transfer studies into murine primary cells, respectively. The methodology reported here should also be applicable to SIN-transfer vectors harboring a much lower risk for proto-oncogene insertion sites (Hacein-Bey-Abina et al., 2014; Morgan et al., 2021). Transposon vector utilizing strategies should also prove useful to establish VPCs producing vectors with a broadened host cell range utilizing heterologous envelope proteins stemming from the amphotropic molecular clone MLV 4070Amc or dual tropic 10A1mc (Ghani et al., 2007), GaLV, feline endogenous retrovirus RD114 or VSV-G (Ghani et al., 2006; 2009).

Data availability statement

The raw data supporting the conclusion of this article will be made available by the authors, without undue reservation.

Author contributions

YH: Writing-review and editing, Original draft preparation, Conceptional, Methodology, Formular analysis, Data curation, Visualization. SS: Methodology, Formular analysis, Data curation. MH: Methodology, Visualization, Formular analysis. TD: Methodology, Formular analysis. DK: Methodology. NT: Methodology. YG: Resources, writing-review and editing, Supervision. JS: Conceptional, Resources, writing-review and editing, Supervision, Project administration, Funding acquisition.

Funding

This work was supported by the German Federal Ministry of Education and Research, funding program Forschung an Fachhochschulen, contract number 13FH242PX6 to JS.

Acknowledgments

We would like to thank Nancy Wynserski for her great help to develop the RT-qPCR protocol.

Conflict of interest

The authors declare that the research was conducted in the absence of any commercial or financial relationships that could be construed as a potential conflict of interest.

Publisher's note

All claims expressed in this article are solely those of the authors and do not necessarily represent those of their affiliated organizations, or those of the publisher, the editors and the reviewers. Any product that may be evaluated in this article, or claim that may be made by its manufacturer, is not guaranteed or endorsed by the publisher.

References

Aiuti, A., Slavin, S., Aker, M., Ficara, F., Deola, S., Mortellaro, A., et al. (2002). Correction of ADA-SCID by stem cell gene therapy combined with nonmyeloablative conditioning. *Science* 296, 2410–2413. doi:10.1126/science.1070104

Bauler, M., Roberts, J. K., Wu, C. C., Fan, B., Ferrara, F., Yip, B. H., et al. (2020). Production of lentiviral vectors using suspension cells grown in serum-free media. *Mol. Ther. Methods Clin. Dev.* 17, 58–68. doi:10.1016/j.omtm.2019.11.011

Berg, K., Schäfer, V. N., Bartnicki, N., Eggenschwiler, R., Cantz, T., and Stitz, J. (2019). Rapid establishment of stable retroviral packaging cells and recombinant susceptible target cell lines employing novel transposon vectors derived from Sleeping Beauty. *Virology* 531, 40–47. doi:10.1016/j.virol.2019.02.014

Bire, S., Gosset, D., Jégot, G., Midoux, P., Pichon, C., and Rouleux-Bonnin, F. (2013). Exogenous mRNA delivery and bioavailability in gene transfer mediated by piggyBac transposition. *BMC Biotechnol.* 13, 75. doi:10.1186/1472-6750-13-75

Blaese, R. M., Culver, K. W., Miller, A. D., Carter, C. S., Fleisher, T., Clerici, M., et al. (1995). T lymphocyte-directed gene therapy for ADA-SCID: Initial trial results after 4 years. *Science* 270, 475–480. doi:10.1126/science.270.5235.475

Bouuaert, C. C., Lipkow, K., Andrews, S. S., Liu, D., and Chalmers, R. (2013). The autoregulation of a eukaryotic DNA transposon. *Elife* 2, 006688–e723. doi:10.7554/eLife.00668

Boztug, K., Schmidt, M., Schwarzer, A., Banerjee, P. P., Díez, I. A., Dewey, R. A., et al. (2010). Stem-cell gene therapy for the wiskott–aldrich syndrome. *N. Engl. J. Med.* 363, 1918–1927. doi:10.1056/NEJMoa1003548

Braun, C. J., Boztug, K., Paruzynski, A., Witzel, M., Schwarzer, A., Rothe, M., et al. (2014). Gene therapy for wiskott-aldrich syndrome—long-term efficacy and genotoxicity. *Sci. Transl. Med.* 6, 227ra33. doi:10.1126/scitranslmed.3007280

Cavazzana, M., Six, E., Lagresle-Peyrou, C., André-Schmutz, I., and Hacein-Bey-Abina, S. (2016). Gene therapy for X-linked severe combined immunodeficiency: Where do we stand? *Hum. Gene Ther.* 27, 108–116. doi:10.1089/hum.2015.137

Cavazzana-Calvo, M., Hacein-Bey, S., De Saint Basile, G., Gross, F., Yvon, E., Nusbaum, P., et al. (2000). Gene therapy of human severe combined immunodeficiency (SCID)-X1 disease. *Science* 288, 669–672. doi:10.1126/science.288.5466.669

Chan, L. M. C., Coutelle, C., and Themis, M. (2001). A novel human suspension culture packaging cell line for production of high-titre retroviral vectors. *Gene Ther.* 8, 697–703. doi:10.1038/sj.gt.3301456

Coroadinha, A. S., Gama-Norton, L., Amaral, A. I., Hauser, H., Alves, P. M., and Cruz, P. E. (2010). Production of retroviral vectors: Review. *Curr. Gene Ther.* 10, 456–473. doi:10.2174/156652310793797739

Cosset, F. L., Takeuchi, Y., Battini, J. L., Weiss, R. A., and Collins, M. K. (1995). High-titer packaging cells producing recombinant retroviruses resistant to human serum. *J. Virol.* 69, 7430–7436. doi:10.1128/jvi.69.12.7430-7436.1995

Eckwahl, M. J., Telesnitsky, A., and Wolin, S. L. (2016). Host RNA packaging by retroviruses: A newly synthesized story. *mBio* 7, e02025–e02015. doi:10.1128/mBio.02025-15

Fehse, B., Kustikova, O. S., Bubenheim, M., and Baum, C. (2004). Pois(s)on - it's a question of dose. *Gene Ther.* 11, 879–881. doi:10.1038/sj.gt.3302270

Ferrua, F., Cicalese, M. P., Galimberti, S., Giannelli, S., Dionisio, F., Barzaghi, F., et al. (2019). Lentiviral haemopoietic stem/progenitor cell gene therapy for treatment of wiskott-aldrich syndrome: Interim results of a non-randomised, open-label, phase 1/2 clinical study. *Lancet Haematol.* 6, e239–e253. doi:10.1016/S2352-3026(19)30021-3

Frensing, T., Pflugmacher, A., Bachmann, M., Peschel, B., and Reichl, U. (2014). Impact of defective interfering particles on virus replication and antiviral host response in cell culture-based influenza vaccine production. *Appl. Microbiol. Biotechnol.* 98, 8999–9008. doi:10.1007/s00253-014-5933-y

Galla, M., Schambach, A., Falk, C. S., Maetzig, T., Kuehle, J., Lange, K., et al. (2011). Avoiding cytotoxicity of transposases by dose-controlled mRNA delivery. *Nucleic Acids Res.* 39, 7147–7160. doi:10.1093/nar/gkr384

Gaspar, H. B., and Thrasher, A. J. (2005). Gene therapy for severe combined immunodeficiencies. *Expert Opin. Biol. Ther.* 5, 1175–1182. doi:10.1517/14712598.5.9.1175

Genzel, Y., Dietzsch, C., Rapp, E., Schwarzer, J., and Reichl, U. (2010). MDCK and vero cells for influenza virus vaccine production: A one-to-one comparison up to lab-scale bioreactor cultivation. *Appl. Microbiol. Biotechnol.* 88, 461–475. doi:10.1007/s00253-010-2742-9

Geraerts, M., Willems, S., Baekelandt, V., Debyser, Z., and Gijsbers, R. (2006). Comparison of lentiviral vector titration methods. *BMC Biotechnol.* 6, 34. doi:10.1186/1472-6750-6-34

Ghani, K., Cottin, S., Kamen, A., and Caruso, M. (2007). Generation of a high-titer packaging cell line for the production of retroviral vectors in suspension and serum-free media. *Gene Ther.* 14, 1705–1711. doi:10.1038/sj.gt.3303039

Ghani, K., Garnier, A., Coelho, H., Transfiguracion, J., Trudel, P., and Kamen, A. (2006). Retroviral vector production using suspension-adapted 293GPG cells in a 3L acoustic filter-based perfusion bioreactor. *Biotechnol. Bioeng.* 95, 653–660. doi:10.1002/bit.20947

Ghani, K., Wang, X., de Campos-Lima, P. O., Olszewska, M., Kamen, A., Rivière, I., et al. (2009). Efficient human hematopoietic cell transduction using RD114-and GALV-pseudotyped retroviral vectors produced in suspension and serum-free media. *Hum. Gene Ther.* 20, 966–974. doi:10.1089/hum.2009.001

Ginn, S. L., Amaya, A. K., Alexander, I. E., Edelstein, M., and Abedi, M. R. (2018). Gene therapy clinical trials worldwide to 2017: An update. *J. Gene Med.* 20, e3015–e3051. doi:10.1002/jgm.3015

Grabundzija, I., Irgang, M., Mátés, L., Belay, E., Matrai, J., Gogol-Döring, A., et al. (2010). Comparative analysis of transposable element vector systems in human cells. *Mol. Ther.* 18, 1200–1209. doi:10.1038/mt.2010.47

Hacein-Bey Abina, S., Gaspar, H. B., Blondeau, J., Caccavelli, L., Charrier, S., Buckland, K., et al. (2015). Outcomes following gene therapy in patients with severe wiskott-aldrich syndrome. *JAMA* 313, 1550–1563. doi:10.1001/jama.2015.3253

Hacein-Bey-Abina, S., Pai, S.-Y., Gaspar, H. B., Armant, M., Berry, C. C., Blanche, S., et al. (2014). A modified γ-retrovirus vector for X-linked severe combined immunodeficiency. *N. Engl. J. Med.* 371, 1407–1417. doi:10.1056/NEJMoa1404588

Hein, M. D., Chawla, A., Cattaneo, M., Kupke, S. Y., Genzel, Y., and Reichl, U. (2021). Cell culture–based production of defective interfering influenza A virus particles in perfusion mode using an alternating tangential flow filtration system. *Appl. Microbiol. Biotechnol.* 105, 7251–7264. doi:10.1007/s00253-021-11561-y

Howe, S. J., Mansour, M. R., Schwarzwaelder, K., Bartholomae, C., Hubank, M., Kempski, H., et al. (2008). Insertional mutagenesis combined with acquired somatic mutations causes leukemogenesis following gene therapy of SCID-X1 patients. *J. Clin. Investigation* 118, 3143–3150. doi:10.1172/JCI35798

Kawakami, E., Watanabe, T., Fujii, K., Goto, H., Watanabe, S., Noda, T., et al. (2011). Strand-specific real-time RT-PCR for distinguishing influenza vRNA, cRNA, and mRNA. *J. Virol. Methods* 173, 1–6. doi:10.1016/j.jviromet.2010.12.014

Kebriaei, P., Izsvák, Z., Narayanavari, S. A., Singh, H., and Ivics, Z. (2017). Gene therapy with the sleeping beauty transposon system. *Trends Genet.* 33, 852–870. doi:10.1016/j.tig.2017.08.008

Maetzig, T., Galla, M., Baum, C., and Schambach, A. (2011). Gammaretroviral vectors: Biology, technology and application. *Viruses* 3, 677–713. doi:10.3390/v3060677

Merten, O. W., Cruz, P. E., Rochette, C., Geny-Fiamma, C., Bouquet, C., Gonçalves, D., et al. (2001). Comparison of different bioreactor systems for the production of high titer retroviral vectors. *Biotechnol. Prog.* 17, 326–335. doi:10.1021/bp000162z

Miller, A. D. (1990). Retrovirus P a c k a g i n g Cells. *Hum. Gene Ther.* 14, 5–14. doi:10.1089/hum.1990.1.1-5

Morgan, M. A., Galla, M., Grez, M., Fehse, B., and Schambach, A. (2021). Retroviral gene therapy in Germany with a view on previous experience and future perspectives. *Gene Ther.* 28, 494–512. doi:10.1038/s41434-021-00237-x

Morita, S., Kojima, T., and Kitamura, T. (2000). Plat-E: An efficient and stable system for transient packaging of retroviruses. *Gene Ther.* 7, 1063–1066. doi:10.1038/sj.gt.3301206

Onafuwa-Nuga, A. A., King, S. R., and Telesnitsky, A. (2005). Nonrandom packaging of host RNAs in Moloney murine leukemia virus. *J. Virol.* 79, 13528–13537. doi:10.1128/jvi.79.21.13528-13537.2005

Park, J., Inwood, S., Kruthiventi, S., Jenkins, J., Shiloach, J., and Betenbaugh, M. (2018). Progressing from transient to stable packaging cell lines for continuous production of lentiviral and gammaretroviral vectors. *Curr. Opin. Chem. Eng.* 22, 128–137. doi:10.1016/j.coche.2018.09.007

Petiot, E., Jacob, D., Lanthier, S., Lohr, V., Ansorge, S., and Kamen, A. A. (2011). Metabolic and Kinetic analyses of influenza production in perfusion HEK293 cell culture. *BMC Biotechnol.* 11, 84. doi:10.1186/1472-6750-11-84

Powers, A. D., Drury, J. E., Hoehamer, C. F., Lockey, T. D., and Meagher, M. M. (2020). Lentiviral vector production from a stable packaging cell line using a packed bed bioreactor. *Mol. Ther. Methods Clin. Dev.* 19, 1–13. doi:10.1016/j.omtm.2020.08.010

Rulli, S. J., Hibbert, C. S., Mirro, J., Pederson, T., Biswal, S., and Rein, A. (2007). Selective and nonselective packaging of cellular RNAs in retrovirus particles. *J. Virol.* 81, 6623–6631. doi:10.1128/jvi.02833-06

Salmon, P., and Trono, D. (2007). Production and titration of lentiviral vectors. *Curr. Protoc. Hum. Genet.* 54, 10–24. doi:10.1002/0471142905.hg1210s54

Sweeney, N. P., and Vink, C. A. (2021). The impact of lentiviral vector genome size and producer cell genomic to gag-pol mRNA ratios on packaging efficiency and titre. *Mol. Ther. Methods Clin. Dev.* 21, 574–584. doi:10.1016/j.omtm.2021.04.007

Tschorn, N., van Heuvel, Y., and Stitz, J. (2022). Transgene expression and transposition efficiency of two-component sleeping beauty transposon vector systems utilizing plasmid or mRNA encoding the transposase. *Mol. Biotechnol.*, doi:10.1007/s12033-022-00642-6

van Heuvel, Y., Berg, K., Hirch, T., Winn, K., Modlich, U., and Stitz, J. (2021). Establishment of a novel stable human suspension packaging cell line producing ecotropic retroviral MLV(PVC-211) vectors efficiently transducing murine hematopoietic stem and progenitor cells. *J. Virol. Methods* 297, 114243. doi:10.1016/j.jviromet.2021.114243

Wang, X., Olszewska, M., Qu, J., Wasielewska, T., Bartido, S., Hermetet, G., et al. (2015). Large-scale clinical-grade retroviral vector production in a fixed-bed bioreactor. *J. Immunother.* 38, 127–135. doi:10.1097/CJI.0000000000000072

frontiers | Frontiers in Bioengineering and Biotechnology

TYPE Review
PUBLISHED 13 April 2023
DOI 10.3389/fbioe.2023.1143866

OPEN ACCESS

EDITED BY
Yori Endo,
Brigham and Women's Hospital and Harvard Medical School, United States

REVIEWED BY
Kui Zhang,
The University of Chicago, United States
Shenghui Lan,
Shanghai Eighth People's Hospital, China
Yuan Xiong,
Huazhong University of Science and Technology, China

*CORRESPONDENCE
Le Wang,
lwang1232022@163.com
Zeming Liu,
6myt@163.com

†These authors have contributed equally to this work

RECEIVED 13 January 2023
ACCEPTED 06 April 2023
PUBLISHED 13 April 2023

CITATION
Luo X, Zhu S, Li J, Zeng N, Wang H, Wu Y, Wang L and Liu Z (2023), Potential genetic therapies based on m6A methylation for skin regeneration: Wound healing and scars/keloids.
Front. Bioeng. Biotechnol. 11:1143866.
doi: 10.3389/fbioe.2023.1143866

Potential genetic therapies based on m6A methylation for skin regeneration: Wound healing and scars/keloids

Xiao Luo[1†], Shu Zhu[2†], Jia Li[1†], Ning Zeng[1], Haiping Wang[1], Yiping Wu[1], Le Wang[3*] and Zeming Liu[1*]

[1]Department of Plastic and Cosmetic Surgery, Tongji Hospital, Tongji Medical College, Huazhong University of Science and Technology, Wuhan, China, [2]Department of Medical Ultrasound, Tongji Hospital, Tongji Medical College, Huazhong University of Science and Technology, Wuhan, China, [3]Department of Nephrology, Tongji Hospital, Tongji Medical College, Huazhong University of Science and Technology, Wuhan, Hubei, China

Skin wound healing is a complex and multistage process, where any abnormalities at any stage can result in the accumulation of non-functional fibrotic tissue, leading to the formation of skin scars. Epigenetic modifications play a crucial role in regulating gene expression, inhibiting cell fate determination, and responding to environmental stimuli. m6A methylation is the most common post-transcriptional modification of eukaryotic mRNAs and long non-coding RNAs. However, it remains unclear how RNA methylation controls cell fate in different physiological environments. This review aims to discuss the current understanding of the regulatory pathways of RNA methylation in skin wound healing and their therapeutic implications with a focus on the specific mechanisms involved.

KEYWORDS

m6A methylation, skin regeneration, wound healing, scars, keloids

1 Introduction

As the protective barrier of the body, the skin is often exposed to potential causes of injury that stimulate wound healing (Zeng et al., 2021). The healing of a normal tissue wound after injury is a complex multistage process that involves hemostasis, inflammation, proliferation, and remodeling (Amjadian et al., 2022; Yu et al., 2022). It is important to note that abnormalities in any of these stages can result in the accumulation of non-functional fibrotic tissue, leading to the formation of skin scars (Amini-Nik et al., 2018; Hu et al., 2018).

A pathological scar is formed in the process of wound healing and is a proliferative disease of skin connective tissue. Keloids are one of the most common pathologic scars that

Abbreviations: lncRNAs, long non-coding RNAs; ALKBH5, AlkB homolog 5; meRIP-seq, methylated RNA immunoprecipitation sequencing; miCLIP-seq; single nucleotide mapping of m6A; SAM, S-adenosine methionine; METTL3, methyltransferase-like 3; METTL14, methyltransferase-like 14; WTAP, Wilms' tumor 1-associated protein; RBM15, RNA-binding motif protein 15; VIRMA, Vir-like m6A methyltransferase associated; ZC3H13, Zinc finger CCCH domain-containing protein 13; HNRNPC, heterogeneous nuclear ribonucleoproteins C; VEGF-C, vascular endothelial growth factor C; ECM, extracellular matrix; TGF-β1, transforming growth factor beta 1.

occur in people of color. Keloids typically present as a bulge extending beyond the original wound, nodular hyperplasia, and a hard, red, benign mass with itching, pain, and discomfort (Jones et al., 2017; Xie et al., 2022). Excessive skin scarring, hypertrophy, or keloids pose significant challenges for patients and physicians, as they can result in serious health problems, such as contracture, functional and aesthetic issues, and complications such as pain, thickness, and itching. These problems have a significant negative impact on the physical, mental health, and social quality of life of patients and lead to high medical costs (Goel and Shrivastava, 2010). Therefore, treatment for reducing skin scarring is necessary to improve the recovery of patients.

The pathogenesis of keloids is complex and involves wound tension, genetic factors, immune changes, and programmed cell death, among other factors (Wolfram et al., 2009; Hsu et al., 2017a; Limandjaja et al., 2020; Zhang et al., 2020; Macarak et al., 2021). Keloid formation is closely related to tumor-related genes (Ekstein et al., 2021), and keloids are considered benign fibrogenic skin tumors that possess many cancer-like features, such as uncontrolled proliferation, a lack of spontaneous recovery, and high recurrence rates (Atiyeh et al., 2005). Increasing evidence suggests that the interaction among various promoting or inhibiting factors in the tumor could explain the aggressive clinical behavior of keloids. The most similar genotypes and phenotypes between keloids and cancers are cell energy sources, epigenetic methylation signatures, and epithelial–mesenchymal transformation behavior (Tan et al., 2019).

2 Treatment of skin regeneration

2.1 Wound healing

The research into the wound healing process has a rich history and is rapidly evolving. In addition to traditional therapies, novel treatment options have emerged, such as growth factors, skin substitutes, cytokine stimulants, cytokine inhibitors, matrix metalloproteinase inhibitors, gene and stem therapies, extracellular matrix therapies, angiogenic stimulants, and nanopreparation therapies (Patel et al., 2019; Qian et al., 2020; Matoori et al., 2021).

2.2 Scars or keloids

Scarring and keloid formation can be prevented and treated with a variety of strategies, including pressure, silicone gels, corticosteroids, lasers, and surgery. Pressure suits restrict blood flow to the scar area reducing oxygen supply, increasing collagenase activity, and reducing adhesion between collagen fibers. Stress therapy also regulates the secretion of fibrocytokines and growth factors. Silicone gels mainly increase the temperature and hydration of the blocked scar. Corticosteroids inhibit inflammation, increase the vasoconstriction of the scar, reduce collagen and glycosaminoglycan production, and decrease fibroblast proliferation. Skin grafts are effective, however, they are limited by the availability of skin, graft tissue rejection, infection, and the prevention of wound overtension (Marshall et al., 2018).

As a result, traditional treatments lack specificity, and there is no evidence to support their absolute efficacy. Even with the best treatments, traumatic scarring is inevitable, and current treatments can only reduce scarring (Ekstein et al., 2021). Therefore, it is necessary to establish new methods to prevent or reduce dermal fibrosis by optimizing the wound healing process. This requires a better understanding of the mechanisms, key regulators, and risk factors associated with wound healing (Chen et al., 2021). Recently, epigenetic changes such as DNA methylation, histone modification, and non-coding RNAs (e.g., microRNAs and long non-coding RNAs [lncRNAs]), have been recognized as promising approaches for scar management. lncRNAs, in particular, offer new potential for targeted therapy to improve traditional and combination therapies.

3 Epigenetic inheritance

Epigenetic modifications refer to changes in the gene expression that occur without altering the underlying DNA sequence. These modifications can be passed down from one generation to another and can be influenced by environmental factors such as diet, stress, and exposure to toxins. Epigenetic modifications play a crucial role in development, differentiation, and disease. Dysregulation of epigenetic modifications can lead to a range of disorders, including cancer, neurological disorders, and cardiovascular disease. Understanding epigenetic modifications can provide insight into disease mechanisms and potential targets for therapeutic intervention.

Epigenetic modifications including DNA deposition and histone modifications are well-established mechanisms that regulate gene expression to suppress cell fate determination and the response to environmental stimuli. DNA methylation involves the addition of a methyl group to a cytosine residue in DNA, which can result in the suppression of gene expression. Histone modification involves the addition or removal of chemical groups to histone proteins, which can affect the way that DNA is packaged and therefore impact gene expression. However, the role of transcriptional modifications (RNA) in gene expression regulation is only beginning to be revealed (Hwang et al., 2017; Livneh et al., 2020). mRNA is not just an intermediate molecule, but also an important regulator of gene expression. The process of post-transcriptional regulation of RNA involves a variety of mechanisms, both cis- and trans-acting, that are essential for controlling gene expression programs that determine cell function and fate. These mechanisms include alternative splicing, RNA editing, mRNA stability, and translation initiation, among others. Importantly, these mechanisms can be rapidly and dynamically regulated in response to changes in the cellular environment, allowing for precise control of gene expression in the face of changing conditions (Vu et al., 2019).

3.1 N6-methyladenosine (m6A)

m6A methylation, a prevalent post-transcriptional modification of eukaryotic mRNAs and lncRNAs, has garnered increasing attention in recent years (Wang et al., 2018). RNA methylation of transcripts was first discovered in the 1970s when a poly(A)

sequence was found at the 3′end of mRNA (Desrosiers et al., 1974). However, the methylation site of m6A methylation remained in an early stage of characterization until the recent discovery of fat mass and obesity-associated protein (FTO) (Jia et al., 2011) and AlkB homolog 5 (ALKBH5) as erasers of m6A methylation (Zheng et al., 2013). These findings revealed that this modification could directly control gene expression. With the development of m6A-specific antibodies and several next-generation sequencing techniques, such as m6A sequencing (methylated RNA immunoprecipitation sequencing, meRIP-seq (Dominissini et al., 2012)), and single-nucleotide mapping of m6A methylation (miCLIP-seq (Linder et al., 2015)), the m6A modification of specific mRNAs can now be analyzed in the entire transcriptome.

m6A methylation is a widely distributed and dynamically regulated modification in the transcriptome, whose understanding is primarily focused on its "readers" and "writers." m6A writers are methyltransferases that catalyze the transfer of methyl groups from S-adenosine methionine (SAM) to adenosine at N-6 a). The m6A "writer" complex mainly includes methyltransferase-like 3 (METTL3), METTL14, Wilms' tumor 1-associated protein (WTAP), RNA-binding motif protein 15 (RBM15), Vir-like m6A methyltransferase associated (VIRMA)/KIAA1429, and zinc finger CCCH domain-containing protein 13 (ZC3H13) (Uddin et al., 2021), Among them, METTL3 and its homolog METTL14 form stable heterodimers and exhibit methyltransferase activity. Whereas WTAP was later identified as another component of the mammalian methyltransferase complex (Liu et al., 2021b; Oerum et al., 2021; Guo et al., 2022; Huang et al., 2022). RBM15 and its paramotifs, including RBM15B, KIAA1429, HAKAI, and ZC3H13, have also been reported in recent years, with different important functions such as recruitment and catalysis (Patil et al., 2016; Yue et al., 2018).

"Erasers" of m6A methylation refers to enzymes that can remove or reverse the addition of a methyl group to an adenosine base in RNA molecules. These enzymes are also known as demethylases (Edupuganti et al., 2017). There are several known erasers of m6A methylation, including FTO (Fat Mass and Obesity-associated protein) and ALKBH5 (AlkB Homolog 5) (Zheng et al., 2013). These enzymes belong to the family of alpha-ketoglutarate-dependent dioxygenases and use molecular oxygen to oxidize the methyl group of m6A, which is then removed as formaldehyde. FTO is a member of the AlkB family of non-heme iron and 2-oxoglutarate-dependent dioxygenases. It was the first identified m6A demethylase, and has been shown to be involved in regulating a variety of physiological processes, including adipogenesis, energy metabolism, and circadian rhythm. ALKBH5 is another m6A demethylase that has been shown to regulate RNA metabolism, including RNA splicing, translation, and decay. ALKBH5 is also involved in the regulation of various cellular processes, including cell differentiation and proliferation. (Wei et al., 2018). Future research could lead to the discovery of novel m6A demethylases and alternative mechanisms that mediate m6A modification removal and m6A-labeled transcriptional clearance.

The biological function of m6A modification is primarily mediated through the specific recognition and binding of readers, which are responsible for the diverse effects of m6A methylation on gene expression (Huang et al., 2020; Zhang et al., 2021b). These effects include the regulation of RNA splicing, output, decay, stabilization, and translation (Wang et al., 2014; Alarcon et al., 2015; Spitale et al., 2015; Xiao et al., 2016; Roundtree et al., 2017b; Slobodin et al., 2017). A major reader of m6A methylation is the protein family containing the YTH domain, including YTHDF1, YTHDF2, YTHD3, YTHDC1, and YTHDC2 (Luo and Tong, 2014). For instance, YTHDF1 has been found to enhance translation by binding to translation primers and ribosomes (Wang et al., 2014). In addition, the insulin-like growth factor 2 mRNA-binding protein (IGF2BP) protein family includes IGF2BP1/2/3, comprising reported readers of m6A methylation (Huang et al., 2018). Moreover, heterogeneous nuclear ribonucleoproteins C (HNRNPC) and G (HNRNPG) are considered "indirect" readers of m6A methylation because they preferentially bind to the RNA structural "switches" induced by m6A modification (Hsu et al., 2017b; Zong et al., 2021; Chen et al., 2022). For example, HNRNPC is an important physiological modulator of 3′-untranslated region processing and miRNA maturation and acts as a reader protein during m6A modification. It recognizes m6A modification groups and mediates the selective splicing of mRNA precursors (Gruber et al., 2018). Thus, RNA methylation is dynamically controlled by writers, readers, erasers, and other proteins that might affect these regulators (Figure 1). Although RNA methylation is recognized to play a crucial role in gene expression regulation and many cellular processes (Roundtree et al., 2017a; Meyer and Jaffrey, 2017; Huang et al., 2020; Livneh et al., 2020), how it controls cell fate in different physiological environments remains unclear. In skin regeneration, epigenetic modifications are essential for the proper activation and maintenance of stem cells responsible for tissue regeneration. Epigenetic changes also play a role in the differentiation of keratinocyte and fibroblast. This review aims to discuss the current understanding of the regulatory pathways of RNA methylation in skin wound healing and their therapeutic implications.

3.2 Role of m6A methylation in wound healing

During the wound healing process, various cellular and molecular events are activated, including the regulation of gene expression through RNA modifications such as m6A methylation. The relationship between wound healing and epigenetic inheritance is complicated and unclear (Mi et al., 2020; Zhi et al., 2021). Several studies have demonstrated that m6A methylation can affect wound healing by regulating the expression of genes involved in various cellular processes, such as proliferation, differentiation, and migration of cells (Table 1). Zhou et al. identified adipose-derived stem cells (ADSCs) via flow cytometry and tested their pluripotency in terms of differentiation into adipocytes and bone. Based on this, ADSCs were found to accelerate LEC proliferation, migration, and lymphangiogenesis through the METTL3 pathway and regulate vascular endothelial growth factor C (VEGF-C) expression and VEGF-C-mediated lymphatic angiogenesis through the METTL3/IGF2BP2-m6A pathway, thus promoting the repair of diabetic foot ulcer (DFU) wounds. The modification of ADSCs by METTL3-mediated VEGF-C m6A methylation could be a promising therapeutic strategy for promoting DFU wound healing (Zhou et al., 2021).

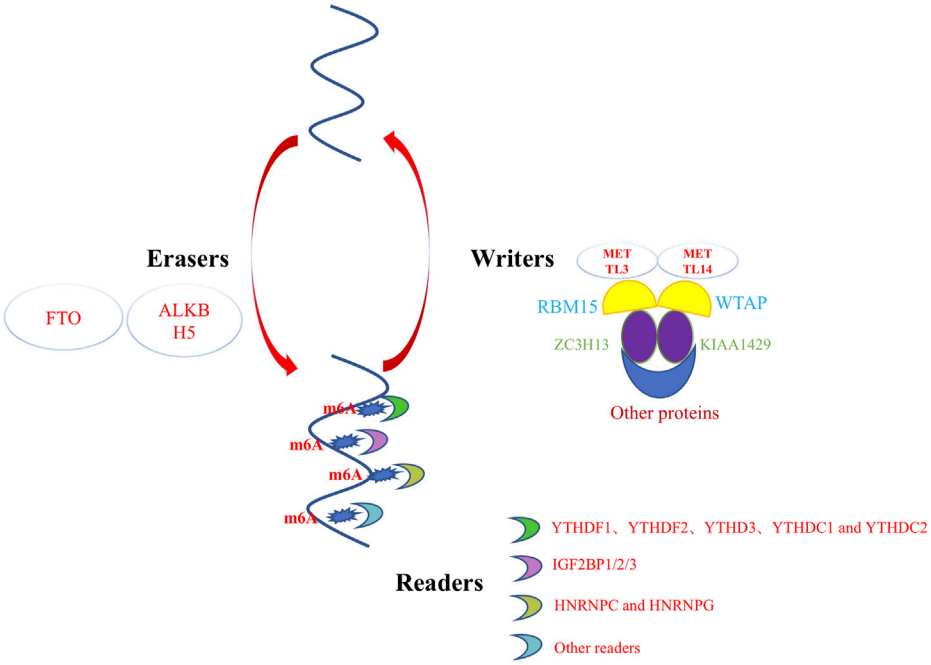

FIGURE 1
m6A methylation is dynamic regulated by writers, erasers, and readers.

TABLE 1 Current research progresses of m6A methylation in wound healing, hypertrophic scars, and keloids.

Authors	Year	PMID	m6A protein	Type	Acting cell	Target molecule	Positive and negative effects	Type of disease
Zhi et al	2021	34753397	IGF2BP2	Reader	keratinocyte:HaCaT cell	heparanase (HPSE)	upregulation	Wound healing
Wu et al	2016	27513293	IGF2BP3	Reader	keratinocyte:HaCaT cell	let-7b	downregulation	Wound healing
Zhou et al	2021	34773968	METTL3	Writer	lymphatic endothelial cell (LEC)	VEGF-C	upregulation	Wound healing
Lee et al	2021	33729590	Mettl14	Writer	epidermal progenitor cells	Pvt1	upregulation	Wound repair
Liang et al	2021	34657574	YTHDC1	Reader	keratinocyte cells	SQSTM1	upregulation	Wound healing
Xie et al	2021	36760238	FTO	Eraser	fibroblasts	COL1A1	upregulation	Keloid
Liu et al	2021	34727293	METTL3	Writer	Tenon's capsule fibroblasts	Smad3	upregulation	Glaucoma

Impaired physiological functions of keratinocytes induced by a high-glucose environment lead to delayed healing of diabetic wounds (Hu and Lan, 2016). In a study of diabetic skin wound healing by Liang et al., m6A RNA modification and the regulation of autophagy were found to play a key role in diabetic skin wound healing. The m6A reader protein YTHDC1 (YTH domain 1), which interacts with autophagy receptor *SQSTM1* mRNA, is downregulated in keratinocytes in both acute and chronic hyperglycemia. The knockdown of YTHDC1 affects keratinocyte biological functions, including an increased apoptosis rate and impaired wound-healing ability. Further studies found that YTHDC1 regulates autophagy in diabetic keratinocytes by regulating the stability of *SQSTM1* nuclear mRNA, ultimately affecting diabetic skin wound healing functions (Liang et al., 2022). Overall, the evidence suggests that m6A methylation plays an important role in regulating gene expression and cellular processes involved in wound healing, making it a promising target for future therapeutic interventions.

3.3 m6A methylation and hypertrophic scars

Hypertrophic scars (HSs) frequently arise following burns and trauma, posing a formidable challenge in the field of wound repair and plastic surgery. Conventional methods, such as surgery, radiotherapy, and hormone therapy, have proven insufficient in achieving complete HS remission, particularly in regions susceptible to HS recurrence (Jaloux et al., 2017), Current studies generally

support the pathological features of HSs, including abnormal inflammation, excessive proliferation and differentiation of fibroblasts, increased angiogenesis, and excessive deposition of extracellular matrix (ECM); however, the causative factors and molecular mechanisms underlying the unremitting collagen synthesis in HSs remain indeterminate (Keane et al., 2018; Roderfeld, 2018; Zhang et al., 2021a). Whether m6A methylation, as a mechanism of targeting abnormal epigenetic modification, can serve as a new target and mechanism for fibrotic diseases and provide a new therapeutic strategy for the treatment of skin fibrosis remains to be determined.

Liu et al. (2021a) conducted a study to investigate the mechanism of m6A modification in HSs and normal skin tissues. The study employed m6A methylation and RNA sequencing, followed by bioinformatics analysis, immunoprecipitation of m6A-related RNA, real-time quantitative polymerase chain reaction verification, and other methods. The presence of 14,791 new m6A methylation peaks in HS samples was accompanied by the disappearance of 7,835 peaks. Unique m6A-related genes in HS were associated with fibrosis-related pathways, and differentially expressed mRNA transcripts were identified in HS samples with hypermethylated or hypomethylated m6A methylation peaks. The m6A transcriptome map of human HS helped to elucidate the possible mechanism underlying m6A-mediated gene expression regulation (Liu et al., 2021b).

Furthermore, Liu et al. (2021b) reported the m6A methylation mechanism of scar formation caused by human Tenon's fibroblasts (HTFs). First, they isolated and identified primary HTFs and found that transforming growth factor beta 1 (TGF-β1) enhanced cell viability and proliferation and ECM deposition in HTFs. Subsequently, TGF-β1 was found to increase the number of m6A methylation events and promote the expression of an m6A "reader." The study further revealed that the downregulation of METTL3 inhibited the TGF-β1-induced promotion of cell viability and proliferation and ECM deposition in HTFs. The results indicated that METTL3 can indeed regulate the expression of Smad3, playing a critical role in the regulation of TGF-β1-induced HTFs and providing new theoretical strategies for regulating scar formation based on METTL3 (Liu et al., 2021b).

3.4 m6A methylation and keloids

The emergence of a public database of collaborative studies has made a vast amount of gene expression data from RNA sequencing available not only for tumor tissues, but also for keloid-associated tissues. This provides great convenience for exploring and identifying gene expression differences in keloid tissue analysis. For example, tumor suppressor genes, such as p53, p16, Fas, and p27, were found to lose their inhibitory effect on fibroblast proliferation after mutations (Tan et al., 2019). Moreover, the overexpression of c-MYC and c-FOS promotes fibroblast proliferation and inhibits apoptosis (He et al., 2017).

Recently, Xie et al. (2022) collected and integrated keloid-related sequencing results from public datasets (GSE44270 and GSE145725) to establish a new keloid risk diagnosis model, extracted m6A-related genes from the literature, and compared their expression matrices between high-risk and low-risk groups to explore differences in m6A methylation. It was found that ALKBH5, FTO, and HNRNPA2B1 were highly expressed, while YTHDF2 was lowly expressed in the high-risk keloid group (Xie et al., 2022). This study provides an idea for treatment planning based on clinical risk grouping.

Furthermore, Lin et al. (2022) investigated the overall m6A-modified RNA pattern and the possible mechanism of keloid pathogenesis (Lin et al., 2022). They collected 14 pairs of normal skin and keloid tissues and found that WTAP and METTL3 protein expression was higher in keloid tissues than in normal tissues. MeRIP and RNA sequencing and bioenrichment analysis revealed 21,020 unique m6A methylation peaks and 6,573 unique m6A-related gene transcripts in keloid samples. In normal tissues, 4,028 unique m6A methylation peaks were found, including 779 m6A-related modified genes. Subsequent functional verification also showed that the m6A-methylated genes and the differentially upregulated genes between the two tissues were mainly related to the Wnt signaling pathway. These findings directly confirmed that keloid fibroblasts were in a state of m6A methylation activation and that the high expression of the Wnt/β-catenin pathway in skin fibroblasts, modified and activated via m6A methylation, might promote the occurrence of keloid.

4 Conclusions and perspectives

Wound healing is a complex biological process involving a series of molecular events to promote skin regeneration. However, abnormal wound healing can lead to the formation of thick, painful, and itchy scars, which can cause aesthetic and functional complications. Therefore, it is crucial to develop more effective and targeted treatments to prevent the deposition of excess fibrous tissue. This can be achieved through a correct understanding of the regulatory mechanisms of wound healing and scar formation.

Given the significant role of genetic and epigenetic differences in physiological or pathological wound repair, we emphasize the critical role of m6A epigenetic changes in regulating the switch during wound healing. Regulatory epigenetic molecules are considered promising therapeutic tools for scar management. However, their exact roles need to be further explored in terms of unexpected genetic disorders.

In conclusion, recent studies have suggested that RNA methylation is a major pathway regulating skin wound healing. This finding highlights the therapeutic potential of genetic and epigenetic approaches for optimizing wound healing and scar management. However, the precise function of m6A methylation in regulating skin wound healing at the cellular level and its potential mechanism in regulating gene expression after transcription require further investigation. Whereas it is exciting to explore RNA methylation as a promising avenue from a therapeutic perspective, translation of these new findings to the clinic remains an urgent challenge. Successful application of these emerging strategies will require advances in existing tools and technologies for the discovery, delivery, and control of genetic and epigenetic regulation, which can help overcome associated challenges and provide a new approach to wound healing management.

Author contributions

All authors contributed to the design of the study and writing of the manuscript. XL, SZ, and JL performed the research, XL, HW, YW, and ZN. wrote the main manuscript text and prepared the figures. LW and ZL. revised the article critically for important intellectual content and provided final approval of the version to be submitted. All authors reviewed the manuscript.

Funding

This study was supported by financial support from the National Natural Science Foundation of China (grant number: 82202461) and Hubei Provincial Natural Science Foundation of China (2022CFB233).

Conflict of interest

The authors declare that the research was conducted in the absence of any commercial or financial relationships that could be construed as a potential conflict of interest.

The reviewer YX declared a shared affiliation with the authors to the handling editor at the time of review.

Publisher's note

References

Alarcon, C. R., Lee, H., Goodarzi, H., Halberg, N., and Tavazoie, S. F. (2015). N6-methyladenosine marks primary microRNAs for processing. *Nature* 519, 482–485. doi:10.1038/nature14281

Amini-Nik, S., Yousuf, Y., and Jeschke, M. G. (2018). Scar management in burn injuries using drug delivery and molecular signaling: Current treatments and future directions. *Adv. Drug Deliv. Rev.* 123, 135–154. doi:10.1016/j.addr.2017.07.017

Amjadian, S., Moradi, S., and Mohammadi, P. (2022). The emerging therapeutic targets for scar management: Genetic and epigenetic landscapes. *Skin. Pharmacol. Physiol.* 35, 247–265. doi:10.1159/000524990

Atiyeh, B. S., Costagliola, M., and Hayek, S. N. (2005). Keloid or hypertrophic scar: The controversy: Review of the literature. *Ann. Plast. Surg.* 54, 676–680. doi:10.1097/01.sap.0000164538.72375.93

Chen, D., Cheung, H., Lau, H. C., Yu, J., and Wong, C. C. (2022). N(6)-Methyladenosine RNA-binding protein YTHDF1 in gastrointestinal cancers: Function, molecular mechanism and clinical implication. *Cancers (Basel)* 14, 3489. doi:10.3390/cancers14143489

Chen, H., Hou, K., Wu, Y., and Liu, Z. (2021). Use of adipose stem cells against hypertrophic scarring or keloid. *Front. Cell Dev. Biol.* 9, 823694. doi:10.3389/fcell.2021.823694

Desrosiers, R., Friderici, K., and Rottman, F. (1974). Identification of methylated nucleosides in messenger RNA from Novikoff hepatoma cells. *Proc. Natl. Acad. Sci. U. S. A.* 71, 3971–3975. doi:10.1073/pnas.71.10.3971

Dominissini, D., Moshitch-Moshkovitz, S., Schwartz, S., Salmon-Divon, M., Ungar, L., Osenberg, S., et al. (2012). Topology of the human and mouse m6A RNA methylomes revealed by m6A-seq. *Nature* 485, 201–206. doi:10.1038/nature11112

Edupuganti, R. R., Geiger, S., Lindeboom, R. G. H., Shi, H., Hsu, P. J., Lu, Z., et al. (2017). N(6)-methyladenosine (m(6)A) recruits and repels proteins to regulate mRNA homeostasis. *Nat. Struct. Mol. Biol.* 24, 870–878. doi:10.1038/nsmb.3462

Ekstein, S. F., Wyles, S. P., Moran, S. L., and Meves, A. (2021). Keloids: A review of therapeutic management. *Int. J. Dermatol* 60, 661–671. doi:10.1111/ijd.15159

Goel, A., and Shrivastava, P. (2010). Post-burn scars and scar contractures. *Indian J. Plast. Surg.* 43, S63–S71. doi:10.4103/0970-0358.70724

Gruber, A. J., Schmidt, R., Ghosh, S., Martin, G., Gruber, A. R., Van Nimwegen, E., et al. (2018). Discovery of physiological and cancer-related regulators of 3' UTR processing with KAPAC. *Genome Biol.* 19, 44. doi:10.1186/s13059-018-1415-3

Guo, S., Zhao, C., Fang, L., Xu, W., Dalia, S., Glass, J., et al. (2022). The m(6)A methyltransferase WTAP plays a key role in the development of diffuse large B-cell lymphoma via regulating the m(6)A modification of catenin beta 1. *Ann. Transl. Med.* 10, 779. doi:10.21037/atm-22-3027

He, Y., Deng, Z., Alghamdi, M., Lu, L., Fear, M. W., and He, L. (2017). From genetics to epigenetics: New insights into keloid scarring. *Cell Prolif.* 50, e12326. doi:10.1111/cpr.12326

Hsu, K. C., Luan, C. W., and Tsai, Y. W. (2017a). Review of silicone gel sheeting and silicone gel for the prevention of hypertrophic scars and keloids. *Wounds.* 29, 154–158.

Hsu, P. J., Zhu, Y., Ma, H., Guo, Y., Shi, X., Liu, Y., et al. (2017b). Ythdc2 is an N(6)-methyladenosine binding protein that regulates mammalian spermatogenesis. *Cell Res.* 27, 1115–1127. doi:10.1038/cr.2017.99

Hu, M. S., Borrelli, M. R., Hong, W. X., Malhotra, S., Cheung, A. T. M., Ransom, R. C., et al. (2018). Embryonic skin development and repair. *Organogenesis* 14, 46–63. doi:10.1080/15476278.2017.1421882

Hu, S. C., and Lan, C. E. (2016). High-glucose environment disturbs the physiologic functions of keratinocytes: Focusing on diabetic wound healing. *J. Dermatol Sci.* 84, 121–127. doi:10.1016/j.jdermsci.2016.07.008

Huang, H., Weng, H., and Chen, J. (2020). The biogenesis and precise control of RNA m(6)A methylation. *Trends Genet.* 36, 44–52. doi:10.1016/j.tig.2019.10.011

Huang, H., Weng, H., Sun, W., Qin, X., Shi, H., Wu, H., et al. (2018). Recognition of RNA N(6)-methyladenosine by IGF2BP proteins enhances mRNA stability and translation. *Nat. Cell Biol.* 20, 285–295. doi:10.1038/s41556-018-0045-z

Huang, Q., Mo, J., Liao, Z., Chen, X., and Zhang, B. (2022). The RNA m(6)A writer WTAP in diseases: Structure, roles, and mechanisms. *Cell Death Dis.* 13, 852. doi:10.1038/s41419-022-05268-9

Hwang, J. Y., Aromolaran, K. A., and Zukin, R. S. (2017). The emerging field of epigenetics in neurodegeneration and neuroprotection. *Nat. Rev. Neurosci.* 18, 347–361. doi:10.1038/nrn.2017.46

Jaloux, C., Bertrand, B., Degardin, N., Casanova, D., Kerfant, N., and Philandrianos, C. (2017). Keloid scars (part II): Treatment and prevention. *Ann. Chir. Plast. Esthet.* 62, 87–96. doi:10.1016/j.anplas.2016.04.006

Jia, G., Fu, Y., Zhao, X., Dai, Q., Zheng, G., Yang, Y., et al. (2011). N6-methyladenosine in nuclear RNA is a major substrate of the obesity-associated FTO. *Nat. Chem. Biol.* 7, 885–887. doi:10.1038/nchembio.687

Jones, M. E., Mclane, J., Adenegan, R., Lee, J., and Ganzer, C. A. (2017). Advancing keloid treatment: A novel multimodal approach to ear keloids. *Dermatol Surg.* 43, 1164–1169. doi:10.1097/dss.0000000000001145

Keane, T. J., Horejs, C. M., and Stevens, M. M. (2018). Scarring vs. functional healing: Matrix-based strategies to regulate tissue repair. *Adv. Drug Deliv. Rev.* 129, 407–419. doi:10.1016/j.addr.2018.02.002

Liang, D., Lin, W. J., Ren, M., Qiu, J., Yang, C., Wang, X., et al. (2022). m(6)A reader YTHDC1 modulates autophagy by targeting SQSTM1 in diabetic skin. *Autophagy* 18, 1318–1337. doi:10.1080/15548627.2021.1974175

Limandjaja, G. C., Niessen, F. B., Scheper, R. J., and Gibbs, S. (2020). The keloid disorder: Heterogeneity, histopathology, mechanisms and models. *Front. Cell Dev. Biol.* 8, 360. doi:10.3389/fcell.2020.00360

Lin, C. X., Chen, Z. J., Peng, Q. L., Xiang, K. R., Xiao, D. Q., Chen, R. X., et al. (2022). The m(6)A-methylated mRNA pattern and the activation of the Wnt signaling pathway under the hyper-m(6)A-modifying condition in the keloid. *Front. Cell Dev. Biol.* 10, 947337. doi:10.3389/fcell.2022.947337

Linder, B., Grozhik, A. V., Olarerin-George, A. O., Meydan, C., Mason, C. E., and Jaffrey, S. R. (2015). Single-nucleotide-resolution mapping of m6A and m6Am throughout the transcriptome. *Nat. Methods* 12, 767–772. doi:10.1038/nmeth.3453

Liu, S. Y., Wu, J. J., Chen, Z. H., Zou, M. L., Teng, Y. Y., Zhang, K. W., et al. (2021a). The m(6)A RNA modification modulates gene expression and fibrosis-related pathways in hypertrophic scar. *Front. Cell Dev. Biol.* 9, 748703. doi:10.3389/fcell.2021.748703

Liu, Y., Gu, C., Li, X., Wang, T., and Yu, L. (2021b). Involvement of METTL3/m6Adenosine and TGFβ/Smad3 signaling on Tenon's fibroblasts and in a rabbit model of glaucoma surgery. *J. Mol. Histol.* 52, 1129–1144. doi:10.1007/s10735-021-10028-8

Livneh, I., Moshitch-Moshkovitz, S., Amariglio, N., Rechavi, G., and Dominissini, D. (2020). The m(6)A epitranscriptome: Transcriptome plasticity in brain development and function. *Nat. Rev. Neurosci.* 21, 36–51. doi:10.1038/s41583-019-0244-z

Luo, S., and Tong, L. (2014). Molecular basis for the recognition of methylated adenines in RNA by the eukaryotic YTH domain. *Proc. Natl. Acad. Sci. U. S. A.* 111, 13834–13839. doi:10.1073/pnas.1412742111

Macarak, E. J., Wermuth, P. J., Rosenbloom, J., and Uitto, J. (2021). Keloid disorder: Fibroblast differentiation and gene expression profile in fibrotic skin diseases. *Exp. Dermatol* 30, 132–145. doi:10.1111/exd.14243

Marshall, C. D., Hu, M. S., Leavitt, T., Barnes, L. A., Lorenz, H. P., and Longaker, M. T. (2018). Cutaneous scarring: Basic science, current treatments, and future directions. *Adv. Wound Care (New Rochelle)* 7, 29–45. doi:10.1089/wound.2016.0696

Matoori, S., Veves, A., and Mooney, D. J. (2021). Advanced bandages for diabetic wound healing. *Sci. Transl. Med.* 13, eabe4839. doi:10.1126/scitranslmed.abe4839

Meyer, K. D., and Jaffrey, S. R. (2017). Rethinking m(6)A readers, writers, and erasers. *Annu. Rev. Cell Dev. Biol.* 33, 319–342. doi:10.1146/annurev-cellbio-100616-060758

Mi, B., Xiong, Y., Yan, C., Chen, L., Xue, H., Panayi, A. C., et al. (2020). Methyltransferase-like 3-mediated N6-methyladenosine modification of miR-7212-5p drives osteoblast differentiation and fracture healing. *J. Cell Mol. Med.* 24, 6385–6396. doi:10.1111/jcmm.15284

Oerum, S., Meynier, V., Catala, M., and Tisne, C. (2021). A comprehensive review of m6A/m6Am RNA methyltransferase structures. *Nucleic Acids Res.* 49, 7239–7255. doi:10.1093/nar/gkab378

Patel, S., Srivastava, S., Singh, M. R., and Singh, D. (2019). Mechanistic insight into diabetic wounds: Pathogenesis, molecular targets and treatment strategies to pace wound healing. *Biomed. Pharmacother.* 112, 108615. doi:10.1016/j.biopha.2019.108615

Patil, D. P., Chen, C. K., Pickering, B. F., Chow, A., Jackson, C., Guttman, M., et al. (2016). m(6)A RNA methylation promotes XIST-mediated transcriptional repression. *Nature* 537, 369–373. doi:10.1038/nature19342

Qian, Z., Wang, H., Bai, Y., Wang, Y., Tao, L., Wei, Y., et al. (2020). Improving chronic diabetic wound healing through an injectable and self-healing hydrogel with platelet-rich plasma release. *ACS Appl. Mater Interfaces* 12, 55659–55674. doi:10.1021/acsami.0c17142

Roderfeld, M. (2018). Matrix metalloproteinase functions in hepatic injury and fibrosis. *Matrix Biol.* 68-69, 452–462. doi:10.1016/j.matbio.2017.11.011

Roundtree, I. A., Evans, M. E., Pan, T., and He, C. (2017a). Dynamic RNA modifications in gene expression regulation. *Cell* 169, 1187–1200. doi:10.1016/j.cell.2017.05.045

Roundtree, I. A., Luo, G. Z., Zhang, Z., Wang, X., Zhou, T., Cui, Y., et al. (2017b). YTHDC1 mediates nuclear export of N(6)-methyladenosine methylated mRNAs. *Elife* 6, e31311. doi:10.7554/elife.31311

Slobodin, B., Han, R., Calderone, V., Vrielink, J., Loayza-Puch, F., Elkon, R., et al. (2017). Transcription impacts the efficiency of mRNA translation via Co-transcriptional N6-adenosine methylation. *Cell* 169, 326–337.e12. doi:10.1016/j.cell.2017.03.031

Spitale, R. C., Flynn, R. A., Zhang, Q. C., Crisalli, P., Lee, B., Jung, J. W., et al. (2015). Structural imprints *in vivo* decode RNA regulatory mechanisms. *Nature* 519, 486–490. doi:10.1038/nature14263

Tan, S., Khumalo, N., and Bayat, A. (2019). Understanding keloid pathobiology from a quasi-neoplastic perspective: Less of a scar and more of a chronic inflammatory disease with cancer-like tendencies. *Front. Immunol.* 10, 1810. doi:10.3389/fimmu.2019.01810

Uddin, M. B., Wang, Z., and Yang, C. (2021). The m(6)A RNA methylation regulates oncogenic signaling pathways driving cell malignant transformation and carcinogenesis. *Mol. Cancer* 20, 61. doi:10.1186/s12943-021-01356-0

Vu, L. P., Cheng, Y., and Kharas, M. G. (2019). The biology of m(6)A RNA methylation in normal and malignant hematopoiesis. *Cancer Discov.* 9, 25–33. doi:10.1158/2159-8290.cd-18-0959

Wang, S., Chai, P., Jia, R., and Jia, R. (2018). Novel insights on m(6)A RNA methylation in tumorigenesis: A double-edged sword. *Mol. Cancer* 17, 101. doi:10.1186/s12943-018-0847-4

Wang, X., Lu, Z., Gomez, A., Hon, G. C., Yue, Y., Han, D., et al. (2014). N6-methyladenosine-dependent regulation of messenger RNA stability. *Nature* 505, 117–120. doi:10.1038/nature12730

Wei, J., Liu, F., Lu, Z., Fei, Q., Ai, Y., He, P. C., et al. (2018). Differential m(6)A, m(6)Am, and m(1)A demethylation mediated by FTO in the cell nucleus and cytoplasm. *Mol. Cell* 71, 973–985.e5. doi:10.1016/j.molcel.2018.08.011

Wolfram, D., Tzankov, A., Pulzl, P., and Piza-Katzer, H. (2009). Hypertrophic scars and keloids--a review of their pathophysiology, risk factors, and therapeutic management. *Dermatol Surg.* 35, 171–181. doi:10.1111/j.1524-4725.2008.34406.x

Xiao, W., Adhikari, S., Dahal, U., Chen, Y. S., Hao, Y. J., Sun, B. F., et al. (2016). Nuclear m(6)A reader YTHDC1 regulates mRNA splicing. *Mol. Cell* 61, 925–519. doi:10.1016/j.molcel.2016.03.004

Xie, J., Zhang, X., Zhang, K., Wu, C., Yao, G., Shi, J., et al. (2022). Construction and validation of the diagnostic model of keloid based on weighted gene co-expression network analysis (WGCNA) and differential expression analysis. *J. Plast. Surg. Hand Surg.* 57, 163–171. doi:10.1080/2000656x.2021.2024557

Yu, H., Wang, Y., Wang, D., Yi, Y., Liu, Z., Wu, M., et al. (2022). Landscape of the epigenetic regulation in wound healing. *Front. Physiol.* 13, 949498. doi:10.3389/fphys.2022.949498

Yue, Y., Liu, J., Cui, X., Cao, J., Luo, G., Zhang, Z., et al. (2018). VIRMA mediates preferential m(6)A mRNA methylation in 3'UTR and near stop codon and associates with alternative polyadenylation. *Cell Discov.* 4, 10. doi:10.1038/s41421-018-0019-0

Zeng, N., Chen, H., Wu, Y., and Liu, Z. (2021). Adipose stem cell-based treatments for wound healing. *Front. Cell Dev. Biol.* 9, 821652. doi:10.3389/fcell.2021.821652

Zhang, J., Zheng, Y., Lee, J., Hua, J., Li, S., Panchamukhi, A., et al. (2021a). A pulsatile release platform based on photo-induced imine-crosslinking hydrogel promotes scarless wound healing. *Nat. Commun.* 12, 1670. doi:10.1038/s41467-021-21964-0

Zhang, T., Wang, X. F., Wang, Z. C., Lou, D., Fang, Q. Q., Hu, Y. Y., et al. (2020). Current potential therapeutic strategies targeting the TGF-β/Smad signaling pathway to attenuate keloid and hypertrophic scar formation. *Biomed. Pharmacother.* 129, 110287. doi:10.1016/j.biopha.2020.110287

Zhang, Y., Chen, W., Zheng, X., Guo, Y., Cao, J., Zhang, Y., et al. (2021b). Regulatory role and mechanism of m(6)A RNA modification in human metabolic diseases. *Mol. Ther. Oncolytics* 22, 52–63. doi:10.1016/j.omto.2021.05.003

Zheng, G., Dahl, J. A., Niu, Y., Fedorcsak, P., Huang, C. M., Li, C. J., et al. (2013). ALKBH5 is a mammalian RNA demethylase that impacts RNA metabolism and mouse fertility. *Mol. Cell* 49, 18–29. doi:10.1016/j.molcel.2012.10.015

Zhi, S., Li, J., Kong, X., Xie, X., Zhang, Q., and Fang, G. (2021). Insulin-like growth factor 2 mRNA binding protein 2 regulates proliferation, migration, and angiogenesis of keratinocytes by modulating heparanase stability. *Bioengineered* 12, 11267–11276. doi:10.1080/21655979.2021.2002495

Zhou, J., Wei, T., and He, Z. (2021). ADSCs enhance VEGFR3-mediated lymphangiogenesis via METTL3-mediated VEGF-C m(6)A modification to improve wound healing of diabetic foot ulcers. *Mol. Med.* 27, 146. doi:10.1186/s10020-021-00406-z

Zong, X., Xiao, X., Shen, B., Jiang, Q., Wang, H., Lu, Z., et al. (2021). The N6-methyladenosine RNA-binding protein YTHDF1 modulates the translation of TRAF6 to mediate the intestinal immune response. *Nucleic Acids Res.* 49, 5537–5552. doi:10.1093/nar/gkab343

frontiers | Frontiers in Bioengineering and Biotechnology

TYPE Original Research
PUBLISHED 12 May 2023
DOI 10.3389/fbioe.2023.1164252

OPEN ACCESS

EDITED BY
Jingfeng Li,
Wuhan University, China

REVIEWED BY
Daqian Wan,
Tongji Hospital Affiliated to Tongji University, China
Xiangyu Chu,
Huazhong University of Science and Technology, China
Fuqiang Gao,
China-Japan Friendship Hospital, China

*CORRESPONDENCE
Jiang Peng,
pengjiang301@126.com
Hua Tian,
tianhua@bjmu.edu.cn

†These authors have contributed equally to this work and share first authorship

RECEIVED 12 February 2023
ACCEPTED 25 April 2023
PUBLISHED 12 May 2023

CITATION
Wang C, Wang P, Li F, Li Y, Zhao M, Feng H, Meng H, Li J, Shi P, Peng J and Tian H (2023), Adenovirus-associated anti-miRNA-214 regulates bone metabolism and prevents local osteoporosis in rats.
Front. Bioeng. Biotechnol. 11:1164252.
doi: 10.3389/fbioe.2023.1164252

Adenovirus-associated anti-miRNA-214 regulates bone metabolism and prevents local osteoporosis in rats

Cheng Wang[1†], Peng Wang[2†], Feng Li[1†], Yang Li[1], Minwei Zhao[1], Hui Feng[1], Haoye Meng[2], Junyang Li[3,4], Peng Shi[4], Jiang Peng[2*] and Hua Tian[1*]

[1]Peking University Third Hospital, Department of Orthopaedics, Engineering Research Center of Bone and Joint Precision Medicine, Ministry of Education, Beijing Key Laboratory of Spinal Disease Research, Beijing, China, [2]Institute of Orthopaedics, Beijing Key Laboratory of Regenerative Medicine in Orthopedics, Key Laboratory of Musculoskeletal Trauma & War Injuries PLA, The Fourth Medical Center of the General Hospital of People's Liberation Army, Beijing, China, [3]Department of Electronic Engineering, Ocean University of China, Qingdao, China, [4]Centre for Robotics and Automation, Shenzhen Research Institute of City University of Hong Kong, Shenzhen, China

Objective: We investigated the expression of miRNA-214 in human osteoporotic bone tissue and tested the utility of adeno-associated virus (AAV) expressing a miRNA-214 inhibitor in terms of preventing local osteoporosis of the femoral condyle in a rat model of osteoporosis.

Methods: (1) Femoral heads of patients who underwent hip replacements at our hospital because of femoral neck fractures were collected and divided into osteoporosis and non-osteoporosis groups based on preoperative bone mineral density data. MiRNA-214 expression was detected in bone tissues exhibiting obvious bone microstructural changes in the two groups. (2) A total of 144 SD female rats were divided into four groups: the Control, Model, Negative control (Model + AAV), and Experimental (Model + anti-miRNA-214) groups. AAV-anti-miRNA-214 was injected locally into the rat femoral condyles; we explored whether this prevented or treated local osteoporosis.

Results: (1) MiRNA-214 expression in the human femoral head was significantly increased in the osteoporosis group. (2) Compared to the Model and Model + AAV groups, the bone mineral density (BMD) and femoral condyle bone volume/tissue volume (BV/TV) ratio in the Model + anti-miRNA-214 group were significantly higher; in addition, the number (TB.N) and thickness (TB.Th) of the trabecular bones were increased (all $p < 0.05$). MiRNA-214 expression in the femoral condyles of the Model + anti-miRNA-214 group was significantly higher than that in the other groups. The expression levels of the osteogenesis-related genes *Alp*, *Bglap*, and *Col1α1* increased, while those of the osteoclast-related genes *NFATc1*, *Acp5*, *Ctsk*, *Mmp9*, and *Clcn7* decreased.

Conclusion: AAV-anti-miRNA-214 promoted osteoblast activity and inhibited osteoclast activity in the femoral condyles of osteoporotic rats, improving bone metabolism and slowing osteoporosis progression.

KEYWORDS

osteoporosis, bone metabolism, miRNA-214, osteoblast activity, osteoclast activity

1 Introduction

Osteoporosis is a common orthopedic disease of middle-aged and elderly individuals. The common clinical features include systemic bone mass reduction and destruction of the bone microstructure. The incidence of osteoporosis has increased in recent years (Johnston and Dagar, 2020). However, osteoporosis awareness is low. Moreover, disease onset is insidious, and in early stages, patients are often asymptomatic, or the symptoms are very mild. Thus, the condition is often not detected. Serious osteoporosis can cause back and leg pain, spinal deformities, and even fractures that seriously compromise the quality of life, shorten life expectancy, and impose heavy burdens on societies and families (LeBoff et al., 2022). There is an urgent need to reduce the incidence of osteoporosis, inhibit bone mass reductions, prevent declines in mechanical strength, and reduce the fracture rate (Arceo-Mendoza and Camacho, 2021). Osteoporosis is a complex disease. It is believed that an imbalance between bone formation and resorption is the principal cause. Thus, if bone metabolism could be regulated via human intervention, natural osteoporosis progression might be prevented and the condition adequately treated.

We previously found that the expression of miRNA-214 was significantly higher in a mouse model of bone loss induced by tail suspension than in the control group, and it correlated negatively with the bone expression levels of ALP and OCN (Sun et al., 2016). Microarray analysis showed that in mature osteoclasts, the expression of miRNA-214 was most significantly affected. We confirmed that miRNA-214 targeted ATF4 to inhibit osteoblast activity and PTEN/PI3K/Akt to promote osteoclast activity (Zhao et al., 2015). Might miRNA-214 serve as an early diagnostic marker of osteoporosis and as a useful therapeutic target?

We collected femoral head samples from patients with femoral neck fractures after they underwent hip replacements and divided the samples into osteoporosis and non-osteoporosis groups by reference to preoperative dual-energy X-ray bone density screening. We measured miRNA-214 expression levels in the bone tissue. We also sought a drug that effectively (bidirectionally) regulated bone metabolism. We tested anti-miRNA-214 (an inhibitor of miRNA-214), which promotes osteogenesis and inhibits osteoclast action. We used this model to treat rat osteoporosis and explored the mechanism in play. We sought new directions toward the treatment of local osteoporosis.

2 Methods

2.1 Clinical sample collection and analysis

Twelve femoral head samples from twelve patients with femoral neck fractures undergoing hip replacements were collected.

Patients subjected to dual-energy X-ray tests prior to hip replacement ($T \geq -1.0$ normal, $-1.0 > T > -2.5$ osteopenia, and $T \leq -2.5$ osteoporosis) were included. To enhance rigor and reflect the real-world situation, patients with T values ≤ -3 formed the osteoporosis group, and those with T values ≥ -1.5 formed the non-osteoporosis group. There were six patients in each group, aged 65–75 years, without systemic or local infection. There were no hip diseases, such as hip osteoarthritis, osteonecrosis of the femoral head, or developmental dysplasia of the hip.

The exclusion criteria were any tumor, diabetes, hyperthyroidism, severe liver or kidney disease, and/or severe rheumatic immune disease. Patients with excessive smoking, alcohol, substance abuse, or mental illness were excluded.

2.2 Detection of miRNA-214 in the clinical samples

We subjected the clinical samples to high-resolution microcomputed tomography (CT) and then measured the miRNA-214 levels in the internal bone tissues. We sought a correlation between a change in the bone microstructure and the local miRNA-214 expression level.

2.3 Preparation and evaluation of adeno-associated virus (AAV)-anti-miRNA-214

The inhibitor of miRNA-214 (anti-miRNA-214) lost activity rapidly in aqueous solutions. Systemic application is compromised by pH and humidity, and the material may exert unknown effects on other organs and systems. Local puncture/fractional administration does not ensure the accuracy of release. AAV has become the most promising gene therapy tool known. The safety profile is good, and its expression persists in the long term (Li and Samulski, 2020; Large et al., 2021). The type of AAV used was 9, which is called AAV9, and the concentration was 10^{13} vg/ml. Based on our previous research, we synthesized AAV-anti-miRNA-214-expressing green fluorescent protein (GFP) to facilitate tracking. We previously synthesized AAV-anti-miRNA-214 and functionally evaluated the material at the cellular level. We found that 30 μL is an excellent measurement (Wang et al., 2019).

2.4 The animal model of osteoporosis

A total of 144 3-month-old female SD rats were randomly divided into four groups: 1. Control, 2. Model, 3. Model + Negative control (Model + AAV), and 4. Model + AAV-anti-miRNA-214 (Model + anti-miRNA-214). The Control group received no treatment, and the Model group underwent only bilateral ovariectomy (OVX). In the Model + AAV group, 30 μL of an AAV suspension was injected into the right lateral femoral condyle at the time of the bilateral OVX; in the Model + AAV-anti-miRNA-214 group, 30 μl of an AAV-anti-miRNA-214 suspension was injected into the right lateral femoral condyle at the time of the OVX. The animal study was reviewed and approved by the Peking University Third Hospital Medical Science Research Ethics Committee.

Osteoporosis was triggered by the OVX. After the rats were anesthetized, the skin was prepared, and the operative area was disinfected with iodophor and a sterile towel spread. With each rat prone, the skin and muscle were dissected longitudinally 1 cm from the right side of the spine and 1 cm below the costal margin. After blunt dissection, pink cauliflower-shaped ovaries were evident when the cellulite was removed. The ovaries and oviducts were excised, ligated near the uterus, and the wounds were closed.

Drug injection: The skin of the right knee was cut and exposed layer-by-layer to the bone surface of the lateral femoral condyle. An empty syringe (500 μl) was used to puncture the bone. This was replaced by a brand-new syringe, and 30 μl of an AAV or AAV-anti-miRNA-214 suspension was slowly injected. The syringe was held in place for 5 min and then removed. Then, the wound was closed. The right femoral condyles were collected 4, 8 weeks after the OVX and subjected to micro-CT, fluorescence microscopy, and pathological evaluation. MiRNA-214 expression and osteoblast and osteoclast activity levels were assayed in the 8-week samples.

2.5 Bone microstructural analysis

2.5.1 Micro-CT, X-ray imaging, and bone morphometric analysis

At 4 and 8 weeks after the OVX, the right femoral condyles were harvested, subjected to X-ray imaging, and then detected by micro-CT using standard settings: resolution 27 × 27 × 27 μm, scan current 450 mA, scan voltage 80 kV, and scan time 88 min. The 8-week samples were subjected to three-dimensional reconstruction. We delineated the region of interest (ROI) within the femoral condyle. The axial surface of the epiphyseal plate served as the baseline. Overall, 50 scan layers were selected for both sides (100 in total), and the epiphyseal plate contour was delineated at 10-layer intervals. Each ROI avoided cortical bone, instead prioritizing cancellous bone. Bone morphometric analysis was performed 4 and 8 weeks after the OVX. We evaluated the BMD, bone volume/tissue volume (BV/TV), and trabecular number (Tb.N), thickness (Tb.Th), and spacing (Tb.sp).

2.5.2 AAV transfection evaluation and pathological examination

At 4, 8 weeks after the OVX, the rats in each group were sacrificed via the induction of deep anesthesia. The right femoral condyles were collected, embedded in a tissue-freezing medium, cut into frozen sections, and stained with 4′,6-diamidino-2-phenylindole hydrochloride (DAPI) for 5 min. Fluorescence microscopy was employed to assess the viral transfection status.

The samples were fixed in 4% (v/v) paraformaldehyde for 2 days, decalcified with 10% (w/v) ethylene diamine tetra-acetic acid, subjected to gradient dehydration and paraffin embedding, cut into 7-μm-thick sections, and subjected to hematoxylin–eosin (HE) staining.

2.6 MiRNA-214 expression and osteoblast and osteoclast activities

At 8 weeks after the OVX, fresh femoral condyles were collected for PCR to measure the expression levels of miRNA-214, the osteoblast activity-related genes *Alp*, *Bglap*, and *Col1α1*, and the osteoclast activity-related genes *NFATc1*, *Acp5*, *Ctsk*, *Mmp9*, and *Clcn7*.

2.7 Statistical analysis

All statistical analyses were performed with SPSS ver. 20.0 statistical software; an analysis of variance was used to compare among-group data. All results are presented as the means ± standard deviations (SDs), and $p < 0.05$ was considered statistically significant.

3. Results

3.1 MiRNA-214 expression in human osteoporosis samples

We used the micro-CT data to select areas with obvious changes in bone microstructure and subjected samples from these areas to PCR. MiRNA-214 expression in the osteoporotic bone tissue was significantly increased (compared to normal tissue); the difference was significant ($p < 0.05$) (Figure 1).

3.2 Bone microstructure morphometry in osteoporotic rats

The 4- and 8-week X-rays showed that the femoral condyles of the Control group exhibited uniform bone density and good structural integrity. The femoral condyle bone density decreased gradually over time in the Model and Model + AAV groups. The differences became more significant over time. However, this was not the case for the Model + anti-miRNA-214 group, and better bone mineral density was maintained in the femoral condyle (similar to the Control group) (Figure 2).

The micro-CT three-dimensional reconstructions showed that the femoral condyle microstructures of different groups differed significantly 8 weeks after the OVX. In the Control group, the trabecular bone structure was continuous and evenly distributed. In the Model and Model + AAV groups, the bone density decreased gradually, the number of trabeculae fell, and most trabecular bone continuity was lost over time. In the Model + anti-miRNA-214 group, the high bone mineral density was preserved, and the trabecular bone structure was basically intact (without obvious osteoporosis) (Figure 3).

The bone morphometry results showed that compared to what was observed in the Model + anti-miRNA-214 group, the BMD and BV/TV of the Model and Model + AAV groups were significantly decreased (both $p < 0.05$). The trabecular number and thickness were also decreased, and the spacing was increased. These differences were statistically significant (all $p < 0.05$) (Figure 4).

3.3 AAV transfection evaluation

The Control and Model groups showed only blue fluorescence at 4 and 8 weeks after the OVX; there was no green fluorescence. However, blue and green fluorescence was apparent in the Model + AAV and Model + anti-miRNA-214 groups; the signals were stronger at 8 weeks. Thus, the AAV virus infected the femoral condyles and replicated extensively (Figure 5).

3.4 Bone histological assessment

The rats were sacrificed 4 and 8 weeks after the OVX, and the condylar paraffin sections were HE-stained. The bone trabeculae of

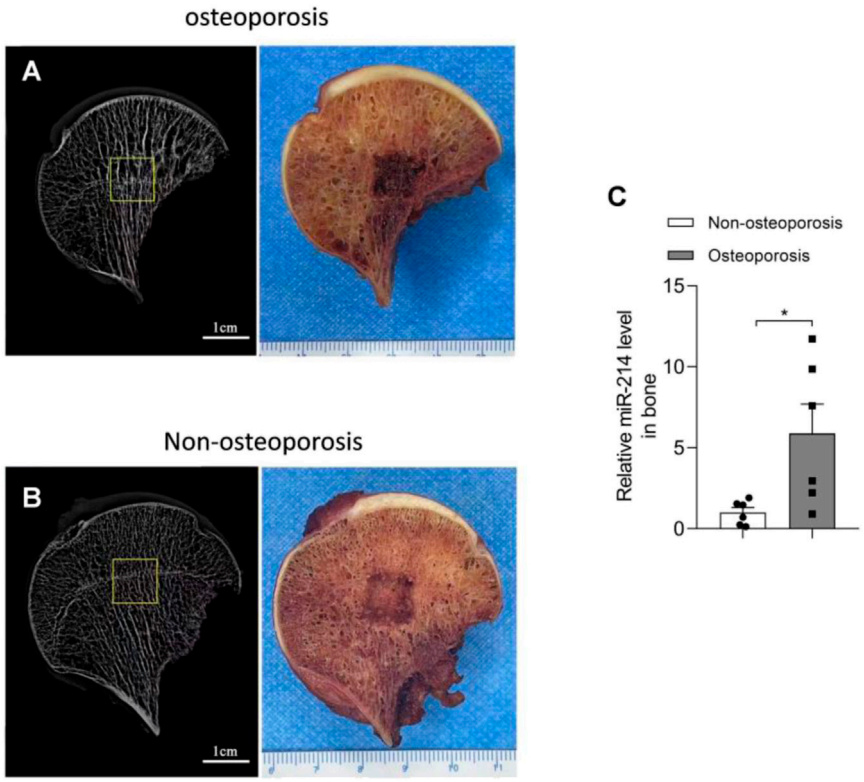

FIGURE 1
Micro-CT results and miRNA-214 expression levels in femoral head samples from both groups. **(A)** Bone microstructure of femoral head samples from the osteoporosis group and a schematic of the affected region. **(B)** Bone microstructure of femoral head samples from the osteoporosis group and a schematic of the affected region. **(C)** MiRNA-214 expression in osteoporotic tissue was significantly higher than that in non-osteoporotic tissue. For both groups, n = 6. All data are means ± SDs (*p<0.05).

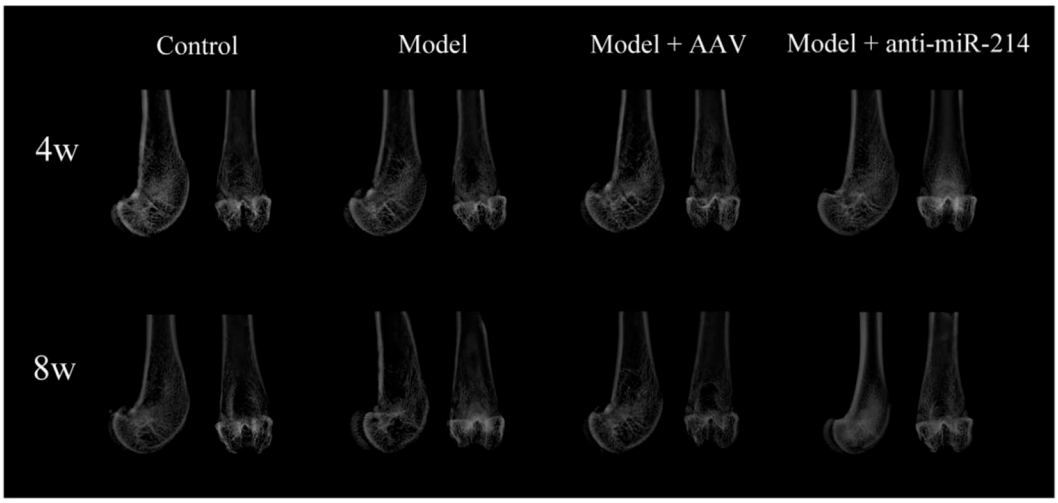

FIGURE 2
X-ray imaging performed at 4 and 8 weeks after OVX. Anteroposterior and lateral radiographs of the femoral condyles of the various groups.

the Control group were orderly and intact, and the osteocyte density was uniform. In the Model and Model + AAV groups, the bone trabecular number and density decreased, the continuities of some trabeculae were interrupted, the number of bone lacunae gradually increased, and the number of osteocytes gradually decreased over time. However, the trabeculae of the Model + anti-miRNA-

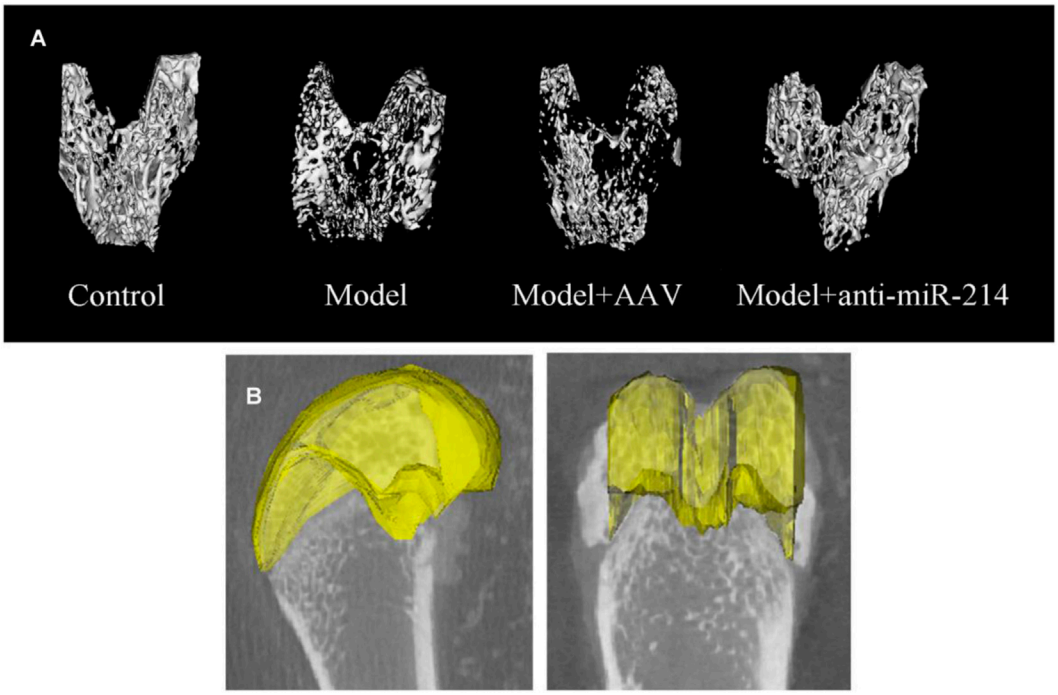

FIGURE 3
(A) Condylar micro-CT three-dimensional reconstructions at 8 weeks after OVX for rats in different groups. **(B)** Selection of an ROI. The axial surface of the epiphyseal plate served as the baseline. Overall, 50 scan layers were selected from either side (100 in total), and the epiphyseal plate contours were determined at 10-layer intervals.

214 group were orderly, and the number of trabeculae and the osteocyte density were similar to those of the Control group (Figure 6).

3.5 Expression of miRNA-214 and genes related to osteoblast and osteoclast activity

MiRNA-214 levels were detected via PCR. At 8 weeks after the OVX, the miRNA-214 levels in the Model and Model + AAV groups increased, and there was no significant difference in the expression of miRNA-214 in the Model + anti-miRNA-214 group compared with the Control group (Figure 7A). At 8 weeks after the OVX (compared to the Control group), the expression of the osteoblast activity-related genes *Alp*, *Bglap*, and *Col1α1* was significantly decreased in the Model and Model + AAV groups but not in the Model + anti-miRNA-214 group. The expression levels of the osteoclast activity-related genes *NFATc1*, *Acp5*, *Ctsk*, *Mmp9*, and *Clcn7* were significantly increased in the Model and Model + AAV groups, but the levels in the Model + anti-miRNA-214 and Control groups did not significantly differ (Figures 7B,C).

4 Discussion

The prevention of osteoporosis would improve bone growth and development, maintain bone quality and mass, and prevent age-related bone loss, falls, and fractures (Munoz et al., 2020). Treatments include basic lifestyle adjustments and bone health supplements. Anti-osteoporosis drugs include vitamin D3, salmon calcitonin, calcitriol, and bisphosphonates (Kanis et al., 2019). However, no drug bidirectionally and efficiently regulates osteogenic and osteoclastic processes. Moreover, some treatments have side effects (mandibular osteonecrosis and renal toxicity) (Fink et al., 2019). Thus, a new approach is needed. Osteoporosis is a systemic metabolic disease; few studies have focused on the prevention and treatment of local osteoporosis. In fact, most patients with osteoporosis do not see a doctor prior to an osteoporotic fracture. Clinically, most such fracture sites are in the hip, spine, or distal radius. If the osteoporosis screening intensity of the high-risk age group were increased, might local anti-osteoporosis treatment of sites prone to fracture be of assistance? Can we reduce the incidence of osteoporotic fractures?

MiRNAs regulate the proliferation, differentiation, and functional activity of various bone cells, playing roles from embryonic bone development to adult bone reconstruction (Kabekkodu et al., 2018; Tafrihi and Hasheminasab, 2019). Lin et al. (Lin et al., 2019) found significantly higher expression of miRNA-338 clusters in postmenopausal patients with osteoporosis than in those without osteoporosis, and they described an estrogen-dependent Runx2/Sox4/miR-338 positive feedback loop regulating osteoblast differentiation. More importantly, the inhibition of miRNA-338 expression delayed the progression of postmenopausal osteoporosis. Hu et al. (Hu et al., 2011) found that miR-2861 targeted Hdac5, a factor inhibiting the transcription of *RUNX2* (which mediates bone formation), and found that

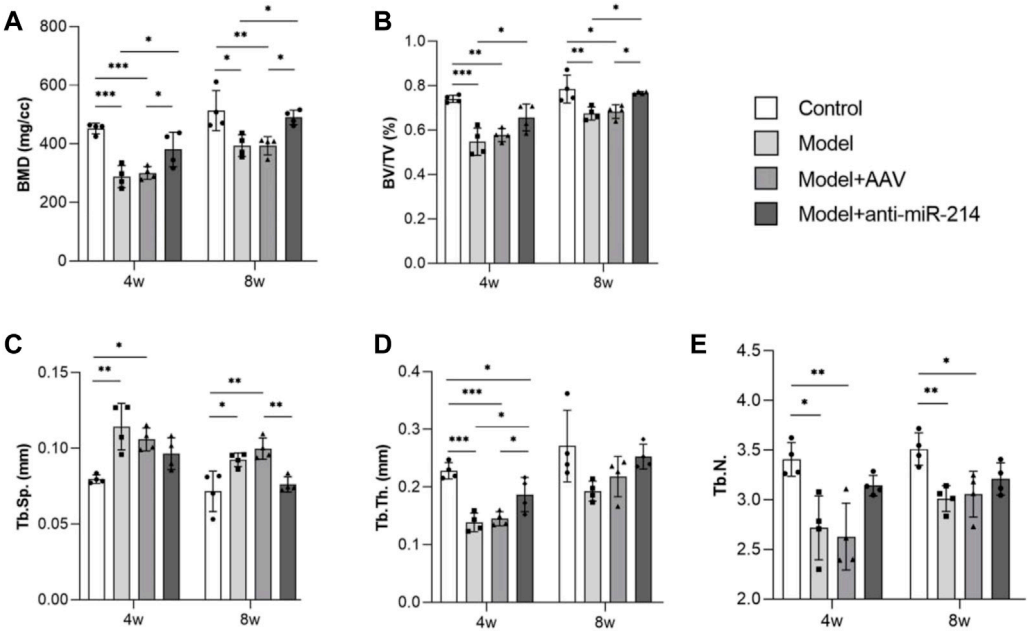

FIGURE 4
Bone morphometric analyses at different times (BMD, BV/TV, Tb.N, Tb.Th, and Tb.sp data). For each group, n = 6. All data are means ± SDs. (*p<0.05; **p<0.01; ***p<0.001)

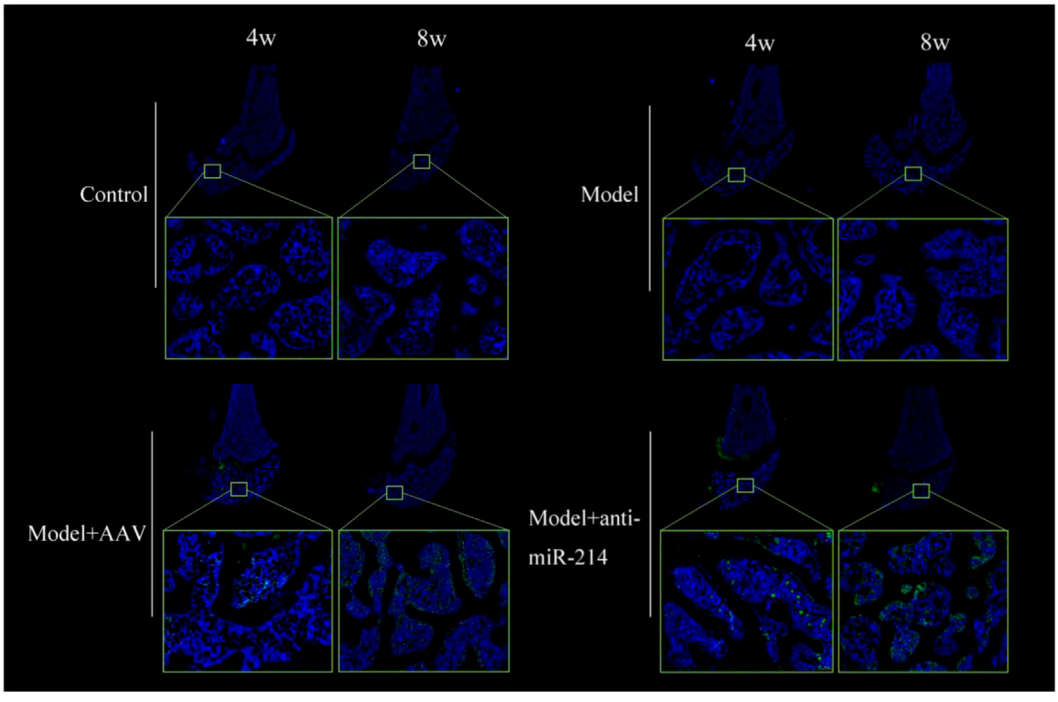

FIGURE 5
Fluorescence images of frozen femoral condyle sections at 4 and 8 weeks after OVX. Blue and green fluorescent signals were evident in the Model + AAV and Model + anti-miRNA-214 groups; the signals were stronger at 8 weeks.

miRNA-3960 targeted Hoxa2 (a repressor of Runx2) to promote osteoblast differentiation. Zhao et al. (Zhao et al., 2021) found that miR-483-5p was upregulated and SATB2 was downregulated in clinical patients with osteoporosis. After mechanistic research, they recognized that miR-483-5p contributed to the pathogenesis of osteoporosis by inhibiting SATB2 and activating the PI3K/AKT

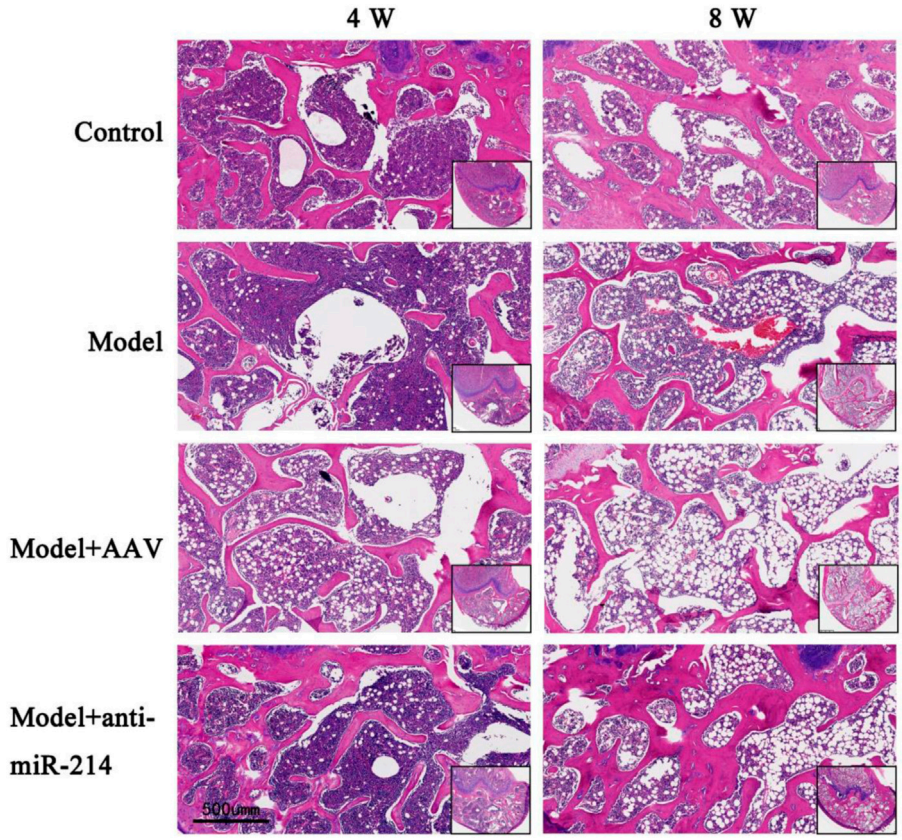

FIGURE 6
Condylar HE staining of the Control, Model, Model + AAV-AAV, and Model + AAV-anti-miRNA-214 groups 4 and 8 weeks after OVX.

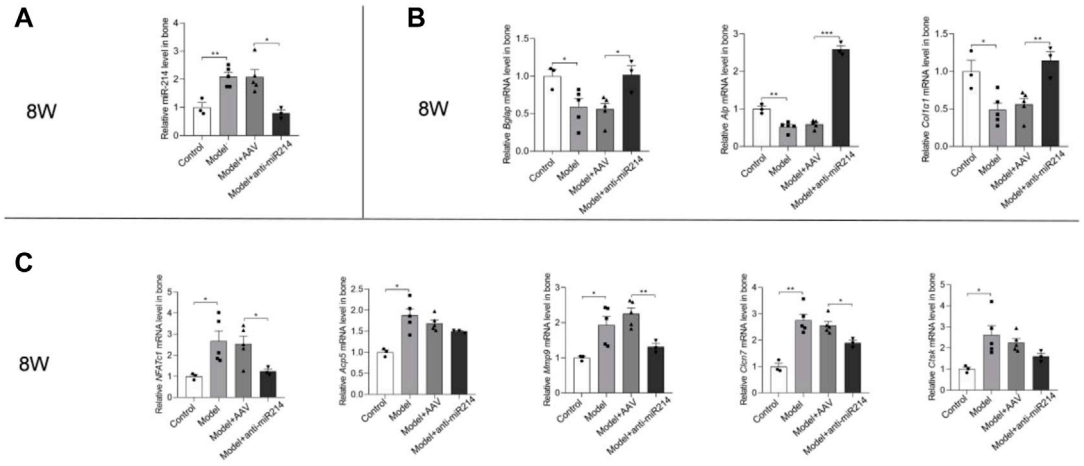

FIGURE 7
(A) Quantitative real-time PCR analyses of the miRNA-214 levels in rat femoral condyles 8 weeks after OVX. **(B)** Expression levels of the osteoblast-associated genes *Alp, Bglap, and Col1α1*. **(C)** Expression levels of the *NFATc1*, *Acp5*, *Ctsk*, *Mmp9*, and *Clcn7* genes. For each group, $n = 6$. All data are means ± SDs (*$p<0.05$; **$p<0.01$; ***$p<0.001$).

pathway. Yu et al. (Yu et al., 2020) also conducted similar research on osteoporosis. After analyzing microarray data and careful verification, they found that patients with osteoporosis had higher miR-16-5p and lower VEGFA levels. Experiments with stem cells have shown that miR-16-5p suppresses osteogenesis by inhibiting VEGFA expression. Wang et al. (Wang et al., 2013)

previously confirmed that miRNA-214 targeted ATF4 in osteoblasts, inhibiting cellular activity.

MiRNAs also play important roles in the regulation of osteoclast differentiation and function (Inoue et al., 2019; Lozano et al., 2019). The Krzeszinski team (Krzeszinski et al., 2014) found that the gene encoding transforming growth factor-β-induced factor 2, a direct target of miR-34a, played a role in promoting bone resorption. As a key osteoclast suppressor, miR-34a may serve as a therapeutic target in patients with osteoporosis and metastatic bone cancer. Sugatani et al. (Sugatani et al., 2011) found that miRNA-21 expression was regulated by various transcription factors (especially c-Fos) during RANKL-induced osteoclast differentiation. Rankl-induced c-Fos upregulated miRNA-21 and then downregulated the expression of programmed cell death protein 4 (PDCD4). This constitutes a c-Fos/miR-21/PDCD4 positive feedback loop that regulates osteoclast function. Our preliminary data show that miRNA-214 slows the inhibition of PI3K/AKT by PTEN, activates the downstream signaling pathway of osteoclasts, and enhances osteoclast activity (Zhao et al., 2015).

We previously performed a detailed analysis of femoral heads with osteonecrosis. Obvious local changes in bone metabolism were apparent. In necrotic areas, osteoclast activity was significantly enhanced, and osteoblast activity was weakened. However, the opposite result was found in sclerotic regions. Therefore, we used an AAV expressing the GFP reporter gene and an inhibitor of miRNA-214 to treat femoral head osteonecrosis in rats. The drug effectively regulated osteoblast and osteoclast activities and prevented osteonecrotic collapse (Wang et al., 2019). Here, we found that the internal bone microstructure of human osteoporotic samples exhibited obvious changes. MiRNA-214 expression was significantly upregulated in osteoporotic tissue, and this was negatively correlated with the expression of genes of osteoblast and osteoclast activities. Thus, miRNA-214 may play a regulatory role in the pathogenesis of osteoporosis.

We thus used AAV-anti-miRNA-214 to locally regulate osteogenic and osteoclastic processes; we sought to change or even reverse osteoporosis. After the OVX, condylar osteoporosis gradually developed in the Control rats, and the miRNA-214 level in the bone increased significantly, suggesting that miRNA-214 is associated with osteoporotic pathogenesis. After the OVX, condylar osteoporosis gradually developed in the rats of the Model and Model + AAV groups, and the bone expression of miRNA-214 increased significantly. Again, these findings suggest that miRNA-214 is associated with osteoporotic pathogenesis. The rats in the Model + anti-miRNA-214 group received AAV-anti-miRNA-214 injections into the right femoral condyles; there was no significant local bone loss. The structural continuity of the trabeculae was ensured, and the trabecular number and thickness did not significantly decrease. Compared to the Model + AAV and Model groups, the expression levels of the osteoblast activity-related genes *Alp*, *Bglap*, and *Col1α1* increased significantly, and those of the osteoclast activity-related genes *NFATc1*, *Acp5*, *Ctsk*, *Mmp9*, and *Clcn7* decreased significantly. These findings suggest that AAV-anti-miRNA-214 prevents osteoporosis via effective bidirectional regulation of bone metabolism, promoting osteoblasts but inhibiting osteoclast activity, reducing bone loss, and effectively delaying osteoporotic pathology.

We have created a new direction toward the early diagnosis, prevention, and treatment of osteoporosis. Molecular markers of early osteoporosis should be further screened and verified because they may aid diagnosis. It is also important to seek drugs that effectively balance osteogenesis and osteoclast function, improve the bone microenvironment, and (when given early) prevent osteoporosis occurrence/development. When treating patients, it is possible to target the sites prone to osteoporotic fractures. Local interventions will enhance the bone masses of the hip, distal radius, spine, and other sites, avoiding osteoporotic fractures caused by falls.

Data availability statement

The original contributions presented in the study are included in the article/supplementary material, further inquiries can be directed to the corresponding authors.

Ethics statement

The animal study was reviewed and approved by Peking University Third Hospital Medical Science Research Ethics Committee.

Author Contributions

HT and JP contributed to conception and design of the study; CW, PW, and FL drafted the manuscript; HYM, JYL, YL, HF, and MWZ acquired and analysed data; PS, HT, and JP revised the manuscript critically. All authors read and approved the final manuscript.

Funding

This work was funded by the National Natural Science Foundation of China (82001481, U20A20194), the Key Clinical Projects of Peking University Third Hospital (No.BYSYZD2019037), and the Bethune Charitable Foundation (G-X-2019-1107-8).

Conflict of interest

The authors declare that the research was conducted in the absence of any commercial or financial relationships that could be construed as a potential conflict of interest.

Publisher's note

References

Arceo-Mendoza, R. M., and Camacho, P. M. (2021). Postmenopausal osteoporosis: Latest guidelines. *Endocrinol. Metab. Clin. North Am.* 50, 167–178. doi:10.1016/j.ecl.2021.03.009

Fink, H. A., MacDonald, R., Forte, M. L., Rosebush, C. E., Ensrud, K. E., Schousboe, J. T., et al. (2019). Long-term drug therapy and drug discontinuations and holidays for osteoporosis fracture prevention: A systematic review. *Ann. Intern Med.* 171, 37–50. doi:10.7326/m19-0533

Hu, R., Liu, W., Li, H., Yang, L., Chen, C., Xia, Z. Y., et al. (2011). A Runx2/miR-3960/miR-2861 regulatory feedback loop during mouse osteoblast differentiation. *J. Biol. Chem.* 286, 12328–12339. doi:10.1074/jbc.m110.176099

Inoue, K., Nakano, S., and Zhao, B. (2019). Osteoclastic microRNAs and their translational potential in skeletal diseases. *Semin. Immunopathol.* 41, 573–582. doi:10.1007/s00281-019-00761-4

Kanis, J. A., Cooper, C., Rizzoli, R., Reginster, J. Y., and Scientific, C. *Advisory Board of the European Society for*, Economic, O. Aspects of, the, A. Committees of Scientific, and F. National Societies of the International Osteoporosis, European guidance for the diagnosis and management of osteoporosis in postmenopausal women. *Osteoporos. Int.* 30 (2019) 3–44.

Johnston, C. B., and Dagar, M. (2020). Osteoporosis in older adults. *Med. Clin. North Am.* 104, 873–884. doi:10.1016/j.mcna.2020.06.004

Kabekkodu, S. P., Shukla, V., Varghese, V. K., Chakrabarty, S., and Satyamoorthy, K. (2018). Clustered miRNAs and their role in biological functions and diseases. *Biol. Rev. Camb Philos. Soc.* 93, 1955–1986. doi:10.1111/brv.12428

Krzeszinski, J. Y., Wei, W., Huynh, H., Jin, Z., Wang, X., Chang, T. C., et al. (2014). Retracted article: miR-34a blocks osteoporosis and bone metastasis by inhibiting osteoclastogenesis and Tgif2. *Nature* 512, 431–435. doi:10.1038/nature13375

Large, E. E., Silveria, M. A., Zane, G. M., Weerakoon, O., and Chapman, M. S. (2021). Adeno-associated virus (AAV) gene delivery: Dissecting molecular interactions upon cell entry. *Viruses* 13, 1336. doi:10.3390/v13071336

LeBoff, M. S., Greenspan, S. L., Insogna, K. L., Lewiecki, E. M., Saag, K. G., Singer, A. J., et al. (2022). The clinician's guide to prevention and treatment of osteoporosis. *Osteoporos. Int.* 33, 2049–2102. doi:10.1007/s00198-021-05900-y

Li, C., and Samulski, R. J. (2020). Engineering adeno-associated virus vectors for gene therapy. *Nat. Rev. Genet.* 21, 255–272. doi:10.1038/s41576-019-0205-4

Lin, C., Yu, S., Jin, R., Xiao, Y., Pan, M., Pei, F., et al. (2019). Circulating miR-338 cluster activities on osteoblast differentiation: Potential diagnostic and therapeutic targets for postmenopausal osteoporosis. *Theranostics* 9, 3780–3797. doi:10.7150/thno.34493

Lozano, C., Duroux-Richard, I., Firat, H., Schordan, E., and Apparailly, F. (2019). MicroRNAs: Key regulators to understand osteoclast differentiation? *Front. Immunol.* 10, 375. doi:10.3389/fimmu.2019.00375

Munoz, M., Robinson, K., and Shibli-Rahhal, A. (2020). Bone health and osteoporosis prevention and treatment. *Clin. Obstet. Gynecol.* 63, 770–787. doi:10.1097/grf.0000000000000572

Sugatani, T., Vacher, J., and Hruska, K. A. (2011). A microRNA expression signature of osteoclastogenesis. *Blood* 117, 3648–3657. doi:10.1182/blood-2010-10-311415

Sun, W., Zhao, C., Li, Y., Wang, L., Nie, G., Peng, J., et al. (2016). Osteoclast-derived microRNA-containing exosomes selectively inhibit osteoblast activity. *Cell Discov.* 2, 16015. doi:10.1038/celldisc.2016.15

Tafrihi, M., and Hasheminasab, E. (2019). MiRNAs: Biology, biogenesis, their web-based tools, and databases. *Microrna* 8, 4–27. doi:10.2174/2211536607666180827111633

Wang, C., Sun, W., Ling, S., Wang, Y., Wang, X., Meng, H., et al. (2019). AAV-Anti-miR-214 prevents collapse of the femoral head in osteonecrosis by regulating osteoblast and osteoclast activities. *Mol. Ther. Nucleic Acids* 18, 841–850. doi:10.1016/j.omtn.2019.09.030

Wang, X., Guo, B., Li, Q., Peng, J., Yang, Z., Wang, A., et al. (2013). miR-214 targets ATF4 to inhibit bone formation. *Nat. Med.* 19, 93–100. doi:10.1038/nm.3026

Yu, T., You, X., Zhou, H., He, W., Li, Z., Li, B., et al. (2020). MiR-16-5p regulates postmenopausal osteoporosis by directly targeting VEGFA. *Aging (Albany NY)* 12, 9500–9514. doi:10.18632/aging.103223

Zhao, C., Sun, W., Zhang, P., Ling, S., Li, Y., Zhao, D., et al. (2015). miR-214 promotes osteoclastogenesis by targeting Pten/PI3k/Akt pathway. *RNA Biol.* 12, 343–353. doi:10.1080/15476286.2015.1017205

Zhao, F., Xu, Y., Ouyang, Y., Wen, Z., Zheng, G., Wan, T., et al. (2021). Silencing of miR-483-5p alleviates postmenopausal osteoporosis by targeting SATB2 and PI3K/AKT pathway. *Aging (Albany NY)* 13, 6945–6956. doi:10.18632/aging.202552

frontiers | Frontiers in Bioengineering and Biotechnology

TYPE Brief Research Report
PUBLISHED 17 July 2023
DOI 10.3389/fbioe.2023.1150892

OPEN ACCESS

EDITED BY
Jingfeng Li,
Wuhan University, China

REVIEWED BY
Majid Jabir,
University of Technology, Iraq
Tommy Michel Alain,
University of Ottawa, Canada

*CORRESPONDENCE
Almohanad A. Alkayyal,
aalkayyal@ut.edu.sa
Ahmad Bakur Mahmoud,
abamahmoud@taibahu.edu.sa

RECEIVED 25 January 2023
ACCEPTED 03 July 2023
PUBLISHED 17 July 2023

CITATION
Alkayyal AA, Darwish M, Ajina R, Alabbas SY, Alotaibi MA, Alsofyani A, Bokhamseen M, Hakami M, Albaradie OA, Moglan AM, Hala S, Alsahafi AF, Zakri S, Almuzaini A, Alsharari K, Kaboha F, Taher MY, Zein HS, Alroqi F and Mahmoud AB (2023), Repurposing the oncolytic virus VSVΔ51M as a COVID-19 vaccine.
Front. Bioeng. Biotechnol. 11:1150892.
doi: 10.3389/fbioe.2023.1150892

Repurposing the oncolytic virus VSVΔ51M as a COVID-19 vaccine

Almohanad A. Alkayyal[1,2]*, Manar Darwish[2], Reham Ajina[2,3], Saleh Y. Alabbas[2], Mohammed A. Alotaibi[2], Abeer Alsofyani[4,5], Maha Bokhamseen[2], Maumonah Hakami[2], Omar A. Albaradie[2,6], Abdulaziz M. Moglan[2,6], Sharif Hala[5,7], Abdullah Faisal Alsahafi[5,7], Samer Zakri[5,7], Adnan Almuzaini[8], Khamis Alsharari[8], Feras Kaboha[8], Mustafa Y. Taher[9], Haggag S. Zein[2,10], Fayhan Alroqi[2,11,12] and Ahmad Bakur Mahmoud[9,13,14]*

[1]Department of Medical Laboratory Technology, Faculty of Applied Medical Sciences, University of Tabuk, Tabuk, Saudi Arabia, [2]Immunology Research Program, King Abdullah International Medical Research Center, Riyadh, Saudi Arabia, [3]Department of Clinical Laboratory Sciences, College of Applied Medical Sciences, King Saud Bin Abdulaziz University for Health Sciences, Riyadh, Saudi Arabia, [4]Department of Cellular Therapy and Cancer Research, King Abdullah International Medical Research Center, Jeddah, Saudi Arabia, [5]King Saud Bin Abdulaziz University for Health Sciences, Ministry of National Guard Health Affairs, Jeddah, Saudi Arabia, [6]College of Medicine, King Saud Bin Abdulaziz University for Health Sciences, Jeddah, Saudi Arabia, [7]Infectious Disease Research Department, King Abdullah International Medical Research Centre, Ministry of National Guard Health Affairs, Jeddah, Saudi Arabia, [8]Experimental Medicine Department, King Abdullah International Medical Research Centre, Jeddah, Saudi Arabia, [9]College of Applied Medical Sciences, Taibah University, Madinah, Saudi Arabia, [10]Department of Microbiology and Immunology, Dalhousie University, Halifax, NS, Canada, [11]Department of Immunology, Ministry of the National Guard—Health Affairs, Riyadh, Saudi Arabia, [12]King Saud Bin Abdulaziz University for Health Sciences, Riyadh, Saudi Arabia, [13]Strategic Research and Innovation Laboratories, Taibah University, Madinah, Saudi Arabia, [14]Immunology Research Program, King Abdullah International Medical Research Center, Jeddah, Saudi Arabia

The coronavirus disease 2019 (COVID-19) pandemic imposes an urgent and continued need for the development of safe and cost-effective vaccines to induce preventive responses for limiting major outbreaks around the world. To combat severe acute respiratory syndrome coronavirus 2 (SARS-CoV-2), we repurposed the VSVΔ51M oncolytic virus platform to express the spike receptor-binding domain (RBD) antigen. In this study, we report the development and characterization of the VSVΔ51M-RBD vaccine. Our findings demonstrate successful expression of the RBD gene by the VSVΔ51M-RBD virus, inducing anti-RBD responses without attenuating the virus. Moreover, the VSVΔ51M-RBD vaccine exhibited safety, immunogenicity, and the potential to serve as a safe and effective alternative or complementary platform to current COVID-19 vaccines.

KEYWORDS

COVID-19 pandemic, oncolytic virus, repurposing oncolytic virus, VSVΔ51M-RBD vaccine, SARS-CoV2 vaccine

Introduction

Severe acute respiratory syndrome coronavirus 2 (SARS-CoV-2) emerged in Wuhan, the capital of Hubei Province in China, and rapidly caused a pandemic in 2020. Despite the efforts made to contain the spread of this virus, as of 20 January 2023, there have been over 663 million confirmed cases and over 6.7 million deaths reported globally (WHO, 2023). The urgent need for an effective vaccine led to an unprecedented effort to develop and test

multiple vaccine candidates. Currently, there are at least 21 COVID-19 vaccines approved globally for emergency use (Rahman et al., 2022). These vaccines have been developed using different platforms, including inactivated, live attenuated, protein subunit, virus-like particle (VLP), viral vector, DNA, and RNA platforms. Although they have some similarities in activating immune responses against SARS-CoV-2, they also possess some differences in their immunogenicity and efficacy profiles (Frederiksen et al., 2020; Rahman et al., 2022).

SARS-CoV-2 is classified into the Coronaviridae family, which is characterized by an enveloped structure with a positive-sense single-stranded RNA (+ssRNA) genome. The viral genome encodes four structural proteins, known as the spike (S), envelope (E), membrane (M), and nucleocapsid (N) proteins (Wang et al., 2020). The S protein facilitates viral entry into cells through the receptor angiotensin-converting enzyme 2 (ACE2) expressed in various cell types, including epithelial cells of the respiratory system (Salamanna et al., 2020). Hence, vaccinating against the S protein generates neutralizing antibodies and abrogates SARS-CoV-2 entry, making the S protein one of the most favorable targets in COVID-19 vaccine designs (Dai and Gao, 2021).

Oncolytic viruses (OVs) are a new class of therapeutics that can selectively infect and replicate in tumor cells, with the primary objective being the direct lysis of cancer cells. Infection with an OV results in a profound inflammatory reaction within the tumor, initiating innate and adaptive antitumor immune responses. Therefore, OV administration is a promising cancer treatment strategy (Kaufman et al., 2015). The recombinant vesicular stomatitis virus (VSV) vaccine platform has been widely used to combat several viral outbreaks, including those caused by Nipah (Foster et al., 2022; de Wit et al., 2023), Lassa (Safronetz et al., 2015; Cross et al., 2020), and Ebola (Henao-Restrepo et al., 2017) viruses. VSVΔ51M is a VSV variant with deletion of methionine (M) 51 in the matrix gene. The deletion of this amino acid results in an impairment in the ability of the virus to block the antiviral interferon (IFN) response in normal tissues, increasing the safety profile of this variant (Stojdl et al., 2003; Wu et al., 2008). In our previous study (Alkayyal et al., 2023), we found that VSVΔ51M encoding the SARS-CoV-2 RBD had a significantly larger viral plaque surface area and higher viral titers than the parental virus, subsequently improving the viral spreading capacity. Moreover, we demonstrated that the presence of the SARS-CoV-2 RBD in the VSVΔ51M genome enhanced VSVΔ51M oncolytic activity *in vitro*. These findings suggest that our VSVΔ51M-RBD platform may have therapeutic potential as a vaccine for COVID-19.

Here, we report that utilizing the oncolytic VSVΔ51M-RBD platform generated an anti-RBD humoral response *in vivo*, with a potentially good safety profile. Therefore, this vaccine warrants further preclinical and clinical investigation.

Material and methods

Construction of VSVΔ51M-RBD vaccine

The VSVΔ51M-RBDvirus was created as described previously (Alkayyal et al., 2023). Briefly, codon-optimized RBD gene, containing the amino acid region (319–541aa) of the full Spike gene of the SARS-CoV-2 (2019-nCoV), from the RBD expression plasmid (Sino Biological Inc., Beijing, China, cat# VG40592-UT) was inserted into a plasmid encoding the VSVΔ51M antigenome plasmid. The insertion was between the G and L genes, and primers used for this insertion as follows: Forward 5′-TGGAAAGTAAGC TAGCTGTATGAAAAAAACTCATCAACAGCCATCATGAGG GTCCAACCA-3′ and Reverse: 5′-GAAGAATCTGGCTAGCTC AGAAGTTCACACACTTGTTC-3’. These primers were designed to be compatible with the In-Fusion® HD Cloning Kit (Takara Bio Inc., United States of America, cat# 638910). Both viruses were rescued in A549 cell line by infecting them with vaccinia virus expressing T7 polymerase and subsequently transfecting using Lipofectamine 2000 with 2 mg of VSVΔ51M-RBD DNA plasmid together with plasmids encoding for VSV N, P and L (1, 1.25, 0.25 mg, respectively). The rescued virus was passaged and plaque purified, amplified and titrated on VERO cells.

Cell lines and media

A549 human lung carcinoma and VERO cell lines were generous gifts from Mr. Suhail Melibary (King Abdulaziz University Hospital, Jeddah, Saudi Arabia). Both were cultured in Dulbecco's Modified Eagle Medium (DMEM, Gibco) containing 10% fetal bovine serum (FBS), 2 mM L-glutamine, 1 mM sodium pyruvate, 100 units/mL penicillin and 100 µg/mL of streptomycin. Cells were maintained in humidified incubators at 37°C and 5% CO^2 (Al-Musawi et al., 2020; Ibrahim et al., 2021).

Propagation and purification of VSVΔ51M and VSVΔ51M-RBD viruses

VERO cells were infected with either VSVΔ51M or VSVΔ51M-RBD (MOI = 1). Post 24 h of infection, media was harvested with 20 mM EDTA, and centrifuged at 500 RCF for 10 min. The supernatant was filtered through a 0.22 µm pore size sterile filter and centrifuged at 21,000 RCF for 1 h and 30 min 4°C. Pellet was resuspended in 1x PBS. 20% sucrose was added to the virus and centrifuged at 41,000 RCF for 1 h and 30 min 4°C. Pellet was resuspended in 1x PBS. The virus was aliquoted and stored at −80°C.

Virus titration and plaque assay

VERO cells were seeded in 12-well plates and infected by VSVΔ51M-RBD 10x serial dilutions (10^2—10^{10}). After 1 h of incubation in a 37°C/5% CO^2 incubator, agarose media (2:1 of 15% FBS DMEM media: 3% agarose) replaced the virus media. Post 24 h incubation at 37°C/5% CO^2 incubator, media was removed and wells were covered by methanol—acetic acid fixative solution (3:1) for another 24 h at room temperature (RT). Agar was then removed and wells were rinsed with water. Wells were stained with Coomassie Blue (1mL/well) for 1 h RT. Finally, wells were rinsed with water and set to dry. Viral titers were calculated by means of the number of plaques in accordance with the viral dilution factor.

Mice vaccination

For immune response studies, C57BL/6 or BALB/c female mice (6–10 weeks old) were vaccinated via the indicated route with the VSVΔ51M-RBD vaccine or the parental vector for two doses, 2 weeks apart. The blood from individual mice was collected from the submandibular vein. After clotting of blood at room temperature, samples were centrifuged and serum was obtained. Serum samples were stored at 4°C until further analysis.

For different routes study, Immunizations were performed through; Intraperitoneal (IP), Intradermal (ID), Intravenous (IV), subcutaneous (SC), and intramuscular (IM) at 2×10^8 PFU/mL. Two weeks after the boost immunization, blood samples were collected.

For the dose escalation study, Immunizations were performed intramuscularly on the hind leg. Mice were vaccinated once with either 5×10^7, 1×10^8, 5×10^8 or 1×10^9 PFU/mL. Two weeks after immunization, blood samples were collected.

Western blot analysis

VERO cells were infected with VSVΔ51M or VSVΔ51M-RBD viruses at a multiplicity of infection (MOI) of 1. At 24 h post-infection, cells were collected and centrifuged at 500 *g* for 5 min. VSVΔ51M- and VSVΔ51M-RBD-infected cells were lysed in RIPA lysis buffer (Thermo Scientific) with protease inhibitor. Fifty μg of total proteins were loaded and separated on 8% SDS-PAGE. Proteins were transferred to nitrocellulose membranes, blocked with 5% skimmed milk for 1 h at room temperature then incubated with the primary antibody against SARS-CoV-2 RBD overnight at 4°C. Membranes were washed three times with 1x PBS-Tween for 5 min each and incubated with IRDye labeled secondary antibodies for 1 h at room temperature. After a series of washes (3 × 5 min), the protein bands were then visualized using an Odyssey Infrared Imaging System (LI-COR Biosciences). β-actin expression was used as an endogenous control for Western blotting. The primary antibodies used in Western blot experiments were as follows: SARS-CoV-2 (2019-nCoV) spike antibody, Mouse Mab (Sino Biological Inc., Beijing, China, cat# 40591-MM42, 1:1000), and monoclonal anti-β-actin (Abcam, United States of America 1:1000).

RNA extraction for RT-qPCR analysis

VERO cells grown in a 12-well plate were infected with VSVΔ51M or VSVΔ51M-RBD, (MOI = 1) for 24 h in a 37°C/5% CO^2 incubator. In each well, 500 μL of TRIzol Reagent (life technologies) were added to the cells. Samples were collected and stored at −80°C. On the day of RNA extraction, 200 μL of chloroform was added to each sample, incubated for 3 min, then centrifuged at 12,000 g for 10 min at 4°C. The clear aqueous top phase was recovered in a clean tube containing 500 μL of isopropanol. The tube was mixed by inversion and incubated at room temperature for 10 min. Samples were then centrifuged at 12,000 g for 10 min at 4°C, and the supernatant was discarded. The pellet was washed with 500 μL of 75% ethanol, vortexed, then centrifuged at 7,500 g for 5 min at 4°C and the supernatant was discarded. The pellet was dried at room temperature for 10 min and RNA was resuspended in 20 μL of RNase-free water and stored at—80°C until further analysis. The expression of the RBD was assessed using Quantifast SYBR Green RT-PCR (cat# 204156) relative to the GAPDH gene. The RBD gene was detected using the following primer pair: RBD Forward Primer (5′-GGAGTGAGC CCAACCAAACT-3′) and RBD Reverse Primer (5′-GGGGCAATC TGTCTCACCTC-3′). For the GAPDH gene, the primer pair used was: GAPDH Forward Primer (5′-TAAATTGAGCCCGCAGCC TCCC-3′) and GAPDH Reverse Primer (5′-GACCAAATCCGT TGACTCCGACCT-3′). Negative controls were included using nuclease-free water. The reactions were performed on a QuantStudio 5 Real-Time PCR system (Applied Biosystems) (Al-Shammari et al., 2020).

The detection of the RBD protein-specific IgG by indirect ELISA

SARS-CoV-2 spike RBD protein-specific IgG levels in mouse sera were determined by indirect ELISA. 96-well ELISA plates were coated with 1ug/mL SARS-Cov-2 Spike RBD recombinant protein (Sino Biological Inc., Beijing, China, cat# 40592-VNAH) overnight at 4°C. Plates were then washed with PBST, Phosphate Buffer Saline with 0.05% tween-20, (SIGMA) three times. Plates were then blocked with a BSA blocking buffer (PBST with 3% BSA (SIGMA)), for 2 h at room temperature (RT). Ten-fold serial diluted serum samples, starting with a 1:10 dilution, were incubated in the blocking buffer for 1 h at 37°C and then washed three times with PBST. Bound IgG was detected using HRP-conjugated goat anti-mouse IgG (at 1:2000) (EMD Millipore Corporation, Billerica, MA, United States of America cat# AP308P). Following a 1 h incubation at 37°C, washed plates were developed with 100 μL of the peroxidase substrate TMB (3,3′,5,5’ Tetramethylbenzidine) liquid substrate system for ELISA (SIGMA, United States of America, cat# 34021) for 20 min at RT. The reaction was quenched with 1N HCl (hydrochloric acid). Absorbance was read at 450 nm using an ELISA plate reader.

Statistical analysis

All statistical analyses were performed using GraphPad Prism 9.0 software. Student’s t-test, one-way ANOVA with Tukey’s multiple comparisons test, and Dunnett’s multiple comparisons test were used as appropriate to determine statistical significance, with a cutoff of $p = 0.05$. The data are presented as mean ± SD (Bahjat et al., 2021).

Results

Development of the VSVΔ51M-RBD vaccine

To generate a VSVΔ51M-RBD vaccine candidate, the RBD coding sequence of SARS-CoV-2 was inserted into the VSVΔ51M genome between the glycoprotein (G) and polymerase (L) genes (Figure 1A). To confirm RBD expression by the rescued VSVΔ51M-RBD vaccine, we infected VERO cells with either VSVΔ51M or

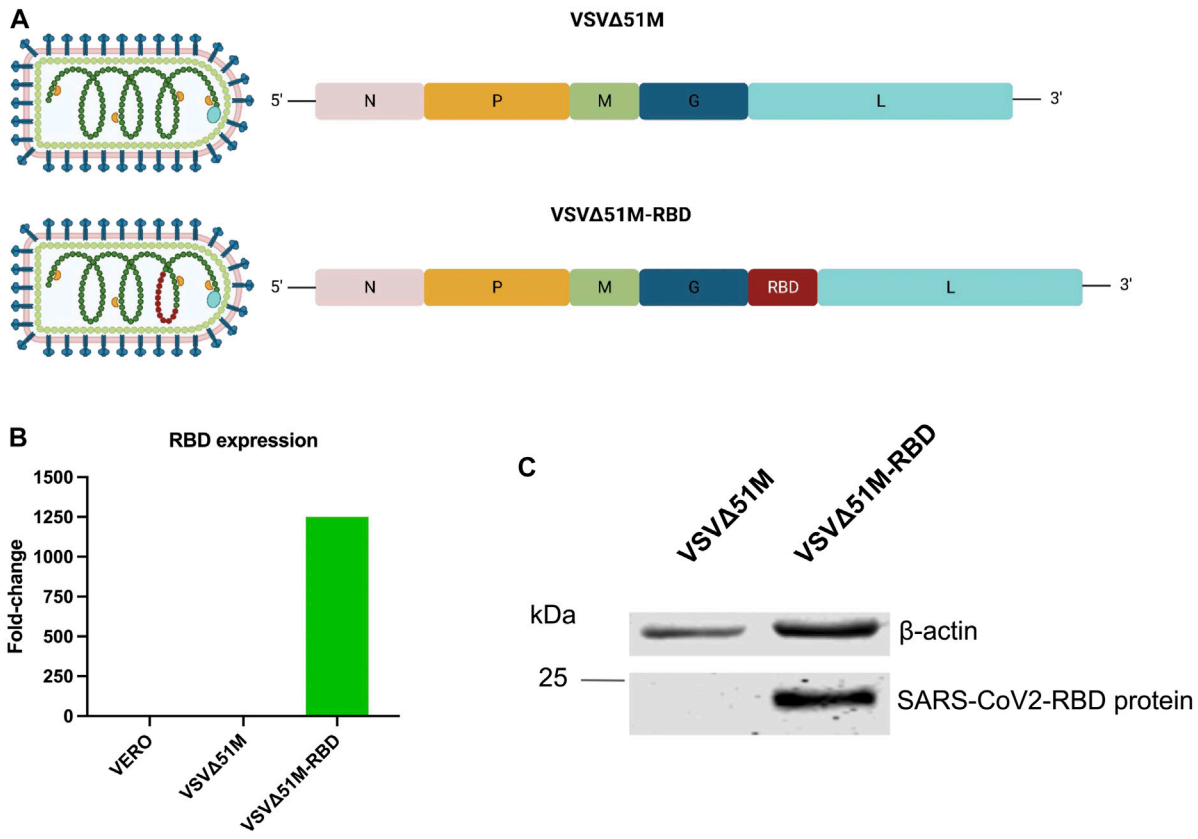

FIGURE 1
Generation of SARS-CoV-2 (2019-nCoV) Spike RBD VSVΔ51M viral vaccine. **(A)** schematic diagram of the VSVΔ51M-RBD viral genome highlighting the location of the SARS-CoV2 RBD insertion site. **(B)** RNA expression levels of RBD normalized to GAPDH in VERO - VSVΔ51M-RBD–or VSVΔ51M-infected cells, in comparison to uninfected VERO cells n = 1. **(C)** Protein expression levels of RBD in lysates of VSVΔ51M-RBD infected VERO cells in comparison to VSVΔ51M infected VERO cells. A band representing RBD ~25 kDa was detected in VSVΔ51M-RBD, while no band was observed in the VSVΔ51M control. Figure 1A was created with BioRender.com under license agreement number NQ24WIY7X0.

VSV-Δ5M1-RBD and evaluated the expression level of the RBD gene in the infected cells by using qRT–PCR. Indeed, the expression level of the RBD gene produced by VSV-Δ5M1-RBD (in terms of the RBD gene copy number) exhibited an approximately 1250-fold increase, but this was not the case for uninfected VERO cells or VSVΔ51M infected cells, in which the RBD gene signal was not detectable (Figure 1B). To further evaluate the expression of the RBD at the protein level, we performed a Western blot analysis of VERO cells infected with either VSVΔ51M or VSV-Δ5M1-RBD. As expected, we were able to detect RBD protein expression in the VSV-Δ5M1-RBD-infected cells, with a band at ~25 kDa corresponding to the size of the inserted RBD gene, suggesting that the generated vaccine could infect and express the RBD protein (Figure 1C).

The VSVΔ51M-RBD virus retains its cytotoxicity and viral fitness

To confirm the retained cytotoxicity of VSVΔ51M-RBD, we infected a VERO cell monolayer with VSVΔ51M-RBD at a multiplicity of infection (MOI) of 1 and evaluated the cytopathic effect (CPE) of the virus at different time points. Images of VSVΔ51M-RBD-infected VERO cells acquired at 8, 24 and 48 h post-infection (hpi) indicated that the CPE increased with time, suggesting that the cytotoxicity of the VSVΔ51M-RBD virus was retained (Figure 2A). To determine if the insertion of the SARS-CoV-2 RBD gene into the VSVΔ51M genome attenuated viral cytotoxic activity, a single-step growth curve was generated by infecting VERO cells with either VSVΔ51M or VSVΔ51M-RBD and evaluating viral production at 6, 12, 24, 36, 48, and 72 h post-infection. As expected, the production rates of both viruses increased gradually from 6 to 12 h and plateaued at 24 h (Figure 2B). Interestingly, VSVΔ51M-RBD resulted in significantly higher viral titers at 12, 24 and 36 h post-infection ($p < 0.05$, $^{**}p < 0.005$, and $^{***}p < 0.0005$, respectively). Collectively, these observations suggest that the insertion of the SARS-CoV-2 RBD gene into the VSVΔ51M genome did not attenuate VSVΔ51M viral cytotoxicity or fitness.

The VSVΔ51M-RBD vaccine is safe and immunogenic

To evaluate the immunogenicity of our COVID-19 vaccine candidate, we first wanted to determine the best route of vaccination for inducing an anti-RBD response. We vaccinated

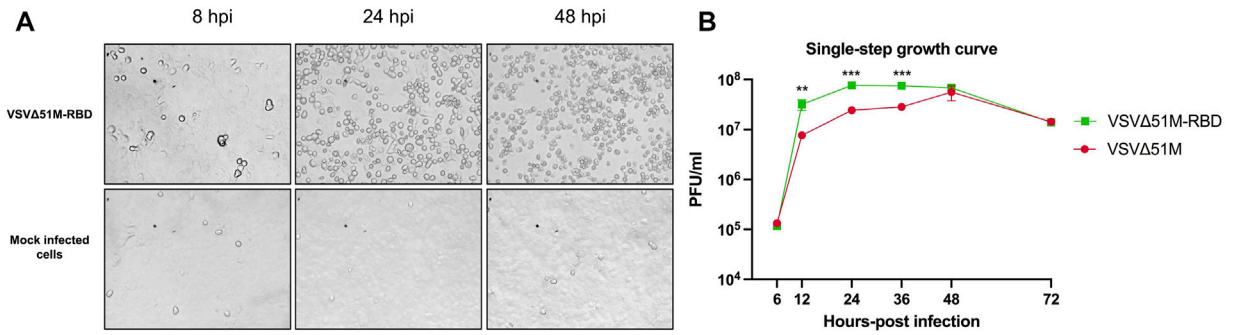

FIGURE 2
Characterization of VSVΔ51M-RBD. VERO cells were infected with VSVΔ51M-RBD at an (MOI = 1). **(A)** Images were captured at 8-, 24- and 48-h post-infection (hpi) using a phase-contrast microscope (data are represented at ×20 magnification). **(B)** Single-step growth kinetics of VSVΔ51M and VSVΔ51M-RBD. VERO cells were infected with the recombinant VSV viruses (MOI = 3) and virus titers were measured at the indicated time points post-infection by plaque assay. $p < 0.05$, $^{**}p < 0.005$, $^{***}p < 0.0005$ by *t*-test.

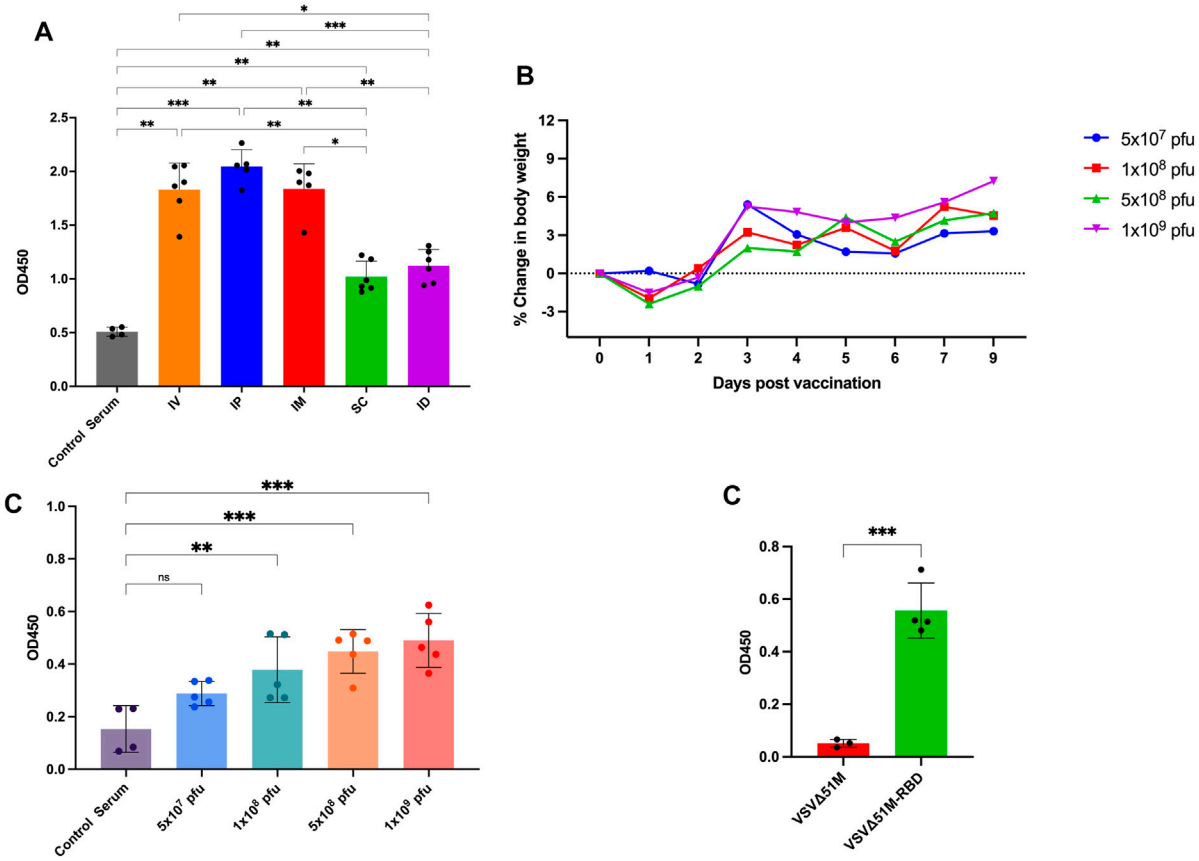

FIGURE 3
Immunogenicity of VSVΔ51M-RBD in mice. **(A)** Humoral immune responses were assessed by RBD-specific ELISA for administering the vaccine through different routes; IP, IM, IV, ID, SQ in C57BL/6 mice at week 2 post-immunization **(B)** Average body weight of vaccinated mice with different doses; 5×10^7, 1×10^8, 5×10^8 or 1×10^9 PFU/mL, in a dose escalation manner. After vaccination, mice were weighed daily. Percent body weight per group was calculated compared to body weight at the time of vaccination. **(C)** The corresponding humoral immune responses for different doses; 5×10^7, 1×10^8, 5×10^8 or 1×10^9 PFU/mL at week 2 post-immunization **(D)**. The detection of RBD antibodies in VSVΔ51M-RBD vaccinated Balb/c mice. Serum was collected from all animals 2 weeks post booster immunization. IgG titers were determined by ELISA against the recombinant VSVΔ51MRBD. N = three to five biologically independent animals per group. Error bars indicate as ± SD. $p < 0.05$, $^{**}p < 0.005$, $^{***}p < 0.0005$, by one-way ANOVA with Tukey's multiple comparisons test for panel A, Dunnett's multiple comparisons test for panel C, and a Student's t-test for panel D.

naive C57BL/6 mice with the VSVΔ51M-RBD vaccine twice (a priming dose on Day −14 and a booster dose on Day 0) using five different routes (IP, intraperitoneal; ID, intradermal; IV, intravenous; SC, subcutaneous; and IM, intramuscular) (Figure 3A). Two weeks after the booster vaccination, we found that the serum anti-RBD level was detectable for all vaccinated routes but to a greater extent when mice were vaccinated via the IP, IM, or IV route compared to the SC and ID routes, and these increases were statistically significant (IP vs. SC, IP vs. ID, IP vs. Control Serum, IM vs. SC, IM vs. ID, IM vs. Control Serum, SC vs. IV, SC vs. Control Serum, ID vs. IV, ID vs. Control Serum, IV vs. Control Serum. This observation suggests that the VSVΔ51M-RBD vaccine is immunogenic. Hence, we selected the IM route for subsequent experiments due to its ease of testing in the clinical development stage.

Next, we performed a dose escalation experiment to evaluate whether the VSVΔ51M-RBD vaccine could be tolerated in doses that have been reported to be tolerable in mice (Kim et al., 2022). Based on our observation of the anti-RBD response induced by IM vaccination with VSVΔ51M-RBD, we vaccinated naive mice with a single dose of VSVΔ51M-RBD administered intramuscularly at different doses (5×10^7, 1×10^8, 5×10^8 and 1×10^9 PFU). As expected, the mice vaccinated with 1×10^8, 5×10^8 or 1×10^9 PFU experienced flu-like symptoms, and transient weight loss was observed 24 hours after vaccine administration but rebounded beginning at 48 hours (Figure 3B). Concomitantly, the levels of anti-RBD antibodies in the serum of the vaccinated mice were assessed at week two after vaccination and were correlated with the vaccination dose (Figure 3C). The levels of anti-RBD antibodies induced by the 1×10^8, 5×10^8 and 1×10^9 PFU doses were significantly higher compared to serum from unvaccinated. Furthermore, we wanted to assess whether this immunogenicity could be replicated in another mouse strain. Therefore, we vaccinated BALB/C mice with 2×10^8 PFU/mL VSVΔ51M or VSVΔ51M-RBD administered IM. As shown in Figure 3E, this vaccination approach resulted in a significantly higher serum anti-RBD level than the injection of the VSVΔ51M virus at 2 weeks after the booster vaccination (p-value <0.005). Taken together, these results provide supportive evidence that the VSVΔ51M-RBD vaccine is safe and immunogenic *in vivo* when tested in mice.

Discussion

The goal of this study was to repurpose the oncolytic virus VSVΔ51M for COVID-19 vaccination. Here, we generated a VSVΔ51M-RBD vaccine candidate by inserting the RBD coding sequence of SARS-CoV-2 into the VSVΔ51M genome. Then, by comparing VSVΔ51M-RBD to the parental VSVΔ51M virus, we determined that the SARS-CoV-2 RBD gene did not negatively attenuate VSVΔ51M viral cytotoxicity or fitness. Additionally, we demonstrated that the VSVΔ51M-RBD vaccine was safe and immunogenic *in vivo*.

The VSVΔ51M-RBD vaccine has unique advantageous characteristics. The VSV vaccine platform can generate a rapid and effective immune response, and it is suitable for efficient large-scale virus production (Patel et al., 2015; Fathi et al., 2019). Therefore, it has been clinically used and preclinically investigated to combat several viral outbreaks, including the SARS-CoV-2 pandemic (Dieterle et al., 2020; Yahalom-Ronen et al., 2020; Kim et al., 2022). In this study, we employed an attenuated VSV strain, VSVΔ51M, which harbors the deletion of methionine (M) 51. This genetic alteration makes the VSVΔ51M variant more sensitive to the interferon (IFN) response (Stojdl et al., 2003; Wu et al., 2008). Hence, VSVΔ51M not only retains the advantages of VSV but is also much safer than wild-type VSV. Hence, VSVΔ51M not only retains the advantages of VSV but is also much safer than wild-type VSV. Additionally, the insertion of the SARS-CoV-2 RBD gene into the VSVΔ51M genome significantly improved the viral replication capacity (Alkayyal et al., 2023). This novel observation has been employed when utilizing VSVΔ51M-RBD as an anticancer agent with a better therapeutic index than the parental VSVΔ51M virus owing to its enhanced replication and spreading in cancer cells. Moreover, previous studies have shown that the spike protein of SARS-CoV-2, particularly the S1 region containing the receptor-binding domain (RBD), can interfere with and downregulate the production and signaling pathway of type I interferon (IFN-I) by suppressing the phosphorylation and nuclear translocation of STAT1 and disrupt its interaction with JAK1 (Zhang et al., 2021). However, in our study, we found that the insertion and expression of the RBD antigen in the VSVΔ51M platform did not negatively impact viral replication probably owing to its interstice interferon sensitivity. The VSVΔ51M-RBD virus retained its cytotoxicity and viral fitness, indicating that the presence of the RBD gene did not attenuate the virus.

VSVΔ51M-RBD is potentially an effective booster vector for adenovirus-based COVID-19 vaccines. There are currently four different adenovirus-based COVID-19 vaccines approved for emergency use. These vaccines are Janssen Ad26.COV2.S, Oxford/AstraZeneca ChAdOx1 nCoV-19 (AZD1222), Sputnik V Gam-COVID-Vac and Convidecia Ad5-nCoV. However, adenovirus-based vaccines typically require a booster immunization to enhance the duration and potency of the adenovirus-elicited immune responses (Bridle et al., 2013). In alignment with our strategy for developing rhabdovirus-based COVID-19 vaccines, there is compelling evidence in the literature suggesting that rhabdoviruses, including VSV (Bridle et al., 2013) and Maraba virus (Pol et al., 2019), can further improve the quantity and quality of T cells when used as booster vaccines with adenovirus-based priming vectors. Given that the VSVΔ51M-RBD vaccine is a rhabdovirus, it is likely that heterologous immunization mediated by boosting with our VSVΔ51M-RBD viral vector after priming with an adenovirus-based vaccine could be an efficient booster strategy for COVID-19 vaccination. The heterologous prime-boost approach has been investigated in the context of COVID-19 vaccination before by utilizing an adenovirus-based vaccine (ChAdOx1 nCoV-19) priming immunization with an mRNA (BNT162b2) booster vaccination, which revealed that this vaccination strategy elicits potent humoral and cellular immunity against prevalent SARS-CoV-2 variants (Gross et al., 2022). Given the limited access to the biosafety level 3 (BSL-3) containment facilities required to handle SARS-CoV-2 safely, we were not able to conduct efficacy studies for the VSVΔ51M-RBD vaccine. Nonetheless, the use of the VSVΔ51M-RBD vaccine did not lead to serious side effects and was

able to elicit a humoral immune response, which might provide protective immunity against SARS-CoV-2. These findings warrant further investigation and potential translation into the clinical trial setting.

Data availability statement

The raw data supporting the conclusion of this article will be made available by the authors, without undue reservation.

Ethics statement

The animal study was reviewed and approved by Institutional Animal Care and Use Committee (IACUC), King Abdullah International Medical Research Centre, Riyadh, Saudi Arabia under IACUC approval number EXO-RYD-22-419837-1645.

Author contributions

AAA and AM contributed to the conception and design of the study. AAA, AM, MD, SA, MA, AdA, KA, and FK performed the *in vivo* experiments. AAA, AM, MD, MA, MB, MH, AbA, SZ, OA, AM, and SA performed experiments and statistical analysis. AAA, AM, and RA wrote the first draft of the manuscript. MD, SH, SZ, MT, HZ, AbA and FA wrote sections of the manuscript. All authors contributed to the arti-cle and approved the submitted version.

Funding

The authors extend their appreciation to King Abdullah International Medical Research Centre, Riyadh, Saudi Arabia for funding this study through project number (RC20/210/R) and the Deanship of Scientific Research at the University of Tabuk for funding this work through project number (0191-1441-S).

Conflict of interest

The authors declare that the research was conducted in the absence of any commercial or financial relationships that could be construed as a potential conflict of interest.

Publisher's note

All claims expressed in this article are solely those of the authors and do not necessarily represent those of their affiliated organizations, or those of the publisher, the editors and the reviewers. Any product that may be evaluated in this article, or claim that may be made by its manufacturer, is not guaranteed or endorsed by the publisher.

References

Al-Musawi, S., Albukhaty, S., Al-Karagoly, H., Sulaiman, G. M., Jabir, M. S., and Naderi-Manesh, H. (2020). Dextran-coated superparamagnetic nanoparticles modified with folate for targeted drug delivery of camptothecin. *Adv. Nat. Sci. Nanosci. Nanotechnol.* 11 (4), 045009. doi:10.1088/2043-6254/abc75b

Al-Shammari, A. M., Al-Saadi, H., Al-Shammari, S. M., and Jabir, M. S. (2020). Galangin enhances gold nanoparticles as anti-tumor agents against ovarian cancer cells. *AIP Conf. Proc.* 2213 (1), 020206. doi:10.1063/5.0000162

Alkayyal, A. A., Ajina, R., Cacciabue, M., Alkayyal, A. A., Saeedi, N. H., Hussain Alshehry, T., et al. (2023). SARS-CoV-2 RBD protein enhances the oncolytic activity of the vesicular stomatitis virus. *Front. Immunol.* 14, 1082191. doi:10.3389/fimmu.2023.1082191

Bahjat, H. H., Ismail, R. A., Sulaiman, G., and Jabir, M. S. (2021). Magnetic field-assisted laser ablation of titanium dioxide nanoparticles in water for anti-bacterial applications. *J. Inorg. Organomet. Polym. Mater.* 31, 3649–3656. doi:10.1007/s10904-021-01973-8

Bridle, B. W., Clouthier, D., Zhang, L., Pol, J., Chen, L., Lichty, B. D., et al. (2013). Oncolytic vesicular stomatitis virus quantitatively and qualitatively improves primary CD8(+) T-cell responses to anticancer vaccines. *Oncoimmunology* 2 (8), e26013. doi:10.4161/onci.26013

Cross, R. W., Xu, R., Matassov, D., Hamm, S., Latham, T. E., Gerardi, C. S., et al. (2020). Quadrivalent VesiculoVax vaccine protects nonhuman primates from viral-induced hemorrhagic fever and death. *J. Clin. Invest.* 130 (1), 539–551. doi:10.1172/jci131958

Dai, L., and Gao, G. F. (2021). Viral targets for vaccines against COVID-19. *Nat. Rev. Immunol.* 21 (2), 73–82. doi:10.1038/s41577-020-00480-0

de Wit, E., Feldmann, F., Cronin, J., Goldin, K., Mercado-Hernandez, R., Williamson, B. N., et al. (2023). Distinct VSV-based Nipah virus vaccines expressing either glycoprotein G or fusion protein F provide homologous and heterologous protection in a nonhuman primate model. *EBioMedicine* 87, 104405. doi:10.1016/j.ebiom.2022.104405

Dieterle, M. E., Haslwanter, D., Bortz, R. H., 3rd, Wirchnianski, A. S., Lasso, G., Vergnolle, O., et al. (2020). A replication-competent vesicular stomatitis virus for studies of SARS-CoV-2 spike-mediated cell entry and its inhibition. *Cell Host Microbe* 28 (3), 486–496.e6. doi:10.1016/j.chom.2020.06.020

Fathi, A., Dahlke, C., and Addo, M. M. (2019). Recombinant vesicular stomatitis virus vector vaccines for WHO blueprint priority pathogens. *Hum. Vaccin Immunother.* 15 (10), 2269–2285. doi:10.1080/21645515.2019.1649532

Foster, S. L., Woolsey, C., Borisevich, V., Agans, K. N., Prasad, A. N., Deer, D. J., et al. (2022). A recombinant VSV-vectored vaccine rapidly protects nonhuman primates against lethal Nipah virus disease. *Proc. Natl. Acad. Sci. U. S. A.* 119 (12), e2200065119. doi:10.1073/pnas.2200065119

Frederiksen, L. S. F., Zhang, Y., Foged, C., and Thakur, A. (2020). The long road toward COVID-19 herd immunity: Vaccine platform technologies and mass immunization strategies. *Front. Immunol.* 11, 1817. doi:10.3389/fimmu.2020.01817

Gross, R., Zanoni, M., Seidel, A., Conzelmann, C., Gilg, A., Krnavek, D., et al. (2022). Heterologous ChAdOx1 nCoV-19 and BNT162b2 prime-boost vaccination elicits potent neutralizing antibody responses and T cell reactivity against prevalent SARS-CoV-2 variants. *EBioMedicine* 75, 103761. doi:10.1016/j.ebiom.2021.103761

Henao-Restrepo, A. M., Camacho, A., Longini, I. M., Watson, C. H., Edmunds, W. J., Egger, M., et al. (2017). Efficacy and effectiveness of an rVSV-vectored vaccine in preventing Ebola virus disease: Final results from the Guinea ring vaccination, open-label, cluster-randomised trial (Ebola Ca suffit!). *Lancet* 389 (10068), 505–518. doi:10.1016/s0140-6736(16)32621-6

Ibrahim, A. A., Kareem, M. M., Al-Noor, T. H., Al-Muhimeed, T., AlObaid, A. A., Albukhaty, S., et al. (2021). Pt(II)-Thiocarbohydrazone complex as cytotoxic agent and apoptosis inducer in caov-3 and HT-29 cells through the P53 and caspase-8 pathways. *Pharm. (Basel)* 14 (6), 509. doi:10.3390/ph14060509

Kaufman, H. L., Kohlhapp, F. J., and Zloza, A. (2015). Oncolytic viruses: A new class of immunotherapy drugs. *Nat. Rev. Drug Discov.* 14, 642–662. doi:10.1038/nrd4663

Kim, G. N., Choi, J. A., Wu, K., Saeedian, N., Yang, E., Park, H., et al. (2022). Correction: A vesicular stomatitis virus-based prime-boost vaccination strategy induces potent and protective neutralizing antibodies against SARS-CoV-2. *PLoS Pathog.* 18 (11), e1011000. doi:10.1371/journal.ppat.1011000

Patel, M. R., and Kratzke, R. A. (2015). "Genetic engineering of oncolytic viruses for cancer therapy," in *Techniques and approaches*. Editors J. Laurence and M. Franklin (Amsterdam, Netherlands: Elsevier Inc: Academic Press), 261–279.

Pol, J. G., Acuna, S. A., Yadollahi, B., Tang, N., Stephenson, K. B., Atherton, M. J., et al. (2019). Preclinical evaluation of a MAGE-A3 vaccination utilizing the oncolytic Maraba

virus currently in first-in-human trials. *Oncoimmunology* 8 (1), e1512329. doi:10.1080/2162402x.2018.1512329

Rahman, M. M., Masum, M. H. U., Wajed, S., and Talukder, A. (2022). A comprehensive review on COVID-19 vaccines: Development, effectiveness, adverse effects, distribution and challenges. *Virus Dis.* 33 (1), 1–22. doi:10.1007/s13337-022-00755-1

Safronetz, D., Mire, C., Rosenke, K., Feldmann, F., Haddock, E., Geisbert, T., et al. (2015). A recombinant vesicular stomatitis virus-based Lassa fever vaccine protects Guinea pigs and macaques against challenge with geographically and genetically distinct Lassa viruses. *PLoS Negl. Trop. Dis.* 9 (4), e0003736. doi:10.1371/journal.pntd.0003736

Salamanna, F., Maglio, M., Landini, M. P., and Fini, M. (2020). Body localization of ACE-2: On the trail of the keyhole of SARS-CoV-2. *Front. Med. (Lausanne)* 7, 594495. doi:10.3389/fmed.2020.594495

Stojdl, D. F., Lichty, B. D., tenOever, B. R., Paterson, J. M., Power, A. T., Knowles, S., et al. (2003). VSV strains with defects in their ability to shutdown innate immunity are potent systemic anti-cancer agents. *Cancer Cell* 4 (4), 263–275. doi:10.1016/s1535-6108(03)00241-1

Wang, M. Y., Zhao, R., Gao, L. J., Gao, X. F., Wang, D. P., and Cao, J. M. (2020). SARS-CoV-2: Structure, biology, and structure-based therapeutics development. *Front. Cell Infect. Microbiol.* 10, 587269. doi:10.3389/fcimb.2020.587269

WHO (2023). WHO coronavirus disease (COVID-19) dashboard: WHO. Available at: https://covid19.who.int/.

Wu, L., Huang, T. G., Meseck, M., Altomonte, J., Ebert, O., Shinozaki, K., et al. (2008). rVSV(M Delta 51)-M3 is an effective and safe oncolytic virus for cancer therapy. *Hum. Gene Ther.* 19 (6), 635–647. doi:10.1089/hum.2007.163

Yahalom-Ronen, Y., Tamir, H., Melamed, S., Politi, B., Shifman, O., Achdout, H., et al. (2020). A single dose of recombinant VSV-ΔG-spike vaccine provides protection against SARS-CoV-2 challenge. *Nat. Commun.* 11 (1), 6402. doi:10.1038/s41467-020-20228-7

Zhang, Q., Chen, Z., Huang, C., Sun, J., Xue, M., Feng, T., et al. (2021). Severe acute respiratory syndrome coronavirus 2 (SARS-CoV-2) membrane (M) and spike (S) proteins antagonize host type I interferon response. *Front. Cell Infect. Microbiol.* 11, 766922. doi:10.3389/fcimb.2021.766922

Frontiers in
Bioengineering and Biotechnology

Accelerates the development of therapies, devices, and technologies to improve our lives

A multidisciplinary journal that accelerates the development of biological therapies, devices, processes and technologies to improve our lives by bridging the gap between discoveries and their application.

Discover the latest Research Topics

See more →

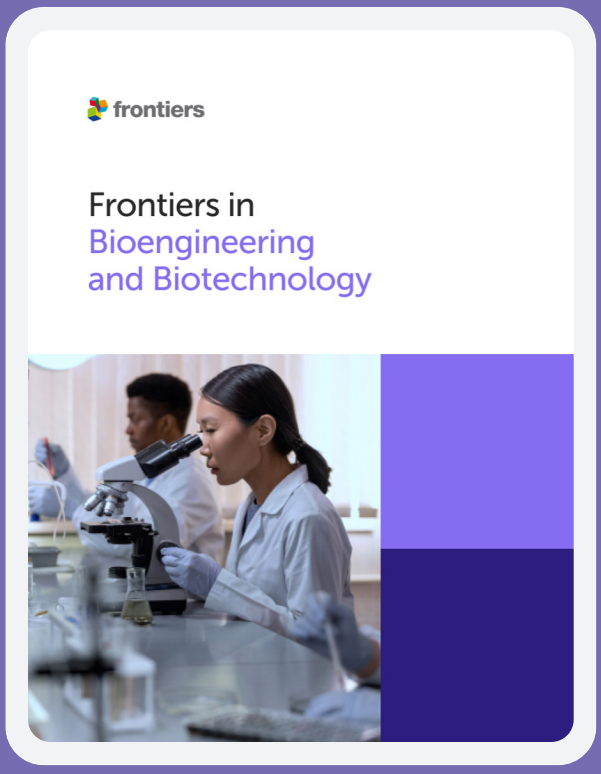

Frontiers

Avenue du Tribunal-Fédéral 34
1005 Lausanne, Switzerland
frontiersin.org

Contact us

+41 (0)21 510 17 00
frontiersin.org/about/contact